NBS SPECIAL PUBLICATION 554

U.S. DEPARTMENT OF COMMERCE/National Bureau of Standards

Proceedings of a Conference on Neutrons from Electron Medical Accelerators

NATIONAL BUREAU OF STANDARDS

The National Bureau of Standards[1] was established by an act of Congress on March 3, 1901. The Bureau's overall goal is to strengthen and advance the Nation's science and technology and facilitate their effective application for public benefit. To this end, the Bureau conducts research and provides: (1) a basis for the Nation's physical measurement system, (2) scientific and technological services for industry and government, (3) a technical basis for equity in trade, and (4) technical services to promote public safety. The Bureau's technical work is performed by the National Measurement Laboratory, the National Engineering Laboratory, and the Institute for Computer Sciences and Technology.

THE NATIONAL MEASUREMENT LABORATORY provides the national system of physical and chemical and materials measurement; coordinates the system with measurement systems of other nations and furnishes essential services leading to accurate and uniform physical and chemical measurement throughout the Nation's scientific community, industry, and commerce; conducts materials research leading to improved methods of measurement, standards, and data on the properties of materials needed by industry, commerce, educational institutions, and Government; provides advisory and research services to other Government agencies; develops, produces, and distributes Standard Reference Materials; and provides calibration services. The Laboratory consists of the following centers:

Absolute Physical Quantities[2] — Radiation Research — Thermodynamics and Molecular Science — Analytical Chemistry — Materials Science.

THE NATIONAL ENGINEERING LABORATORY provides technology and technical services to the public and private sectors to address national needs and to solve national problems; conducts research in engineering and applied science in support of these efforts; builds and maintains competence in the necessary disciplines required to carry out this research and technical service; develops engineering data and measurement capabilities; provides engineering measurement traceability services; develops test methods and proposes engineering standards and code changes; develops and proposes new engineering practices; and develops and improves mechanisms to transfer results of its research to the ultimate user. The Laboratory consists of the following centers:

Applied Mathematics — Electronics and Electrical Engineering[2] — Mechanical Engineering and Process Technology[2] — Building Technology — Fire Research — Consumer Product Technology — Field Methods.

THE INSTITUTE FOR COMPUTER SCIENCES AND TECHNOLOGY conducts research and provides scientific and technical services to aid Federal agencies in the selection, acquisition, application, and use of computer technology to improve effectiveness and economy in Government operations in accordance with Public Law 89-306 (40 U.S.C. 759), relevant Executive Orders, and other directives; carries out this mission by managing the Federal Information Processing Standards Program, developing Federal ADP standards guidelines, and managing Federal participation in ADP voluntary standardization activities; provides scientific and technological advisory services and assistance to Federal agencies; and provides the technical foundation for computer-related policies of the Federal Government. The Institute consists of the following centers:

Programming Science and Technology — Computer Systems Engineering.

[1]Headquarters and Laboratories at Gaithersburg, MD, unless otherwise noted; mailing address Washington, DC 20234.
[2]Some divisions within the center are located at Boulder, CO 80303.

Proceedings of a Conference on Neutrons from Electron Medical Accelerators

Proceedings of a Conference held at the National Bureau of Standards, Gaithersburg, Maryland, April 9-10, 1979

Edited by:

H.T. Heaton, II

National Measurement Laboratory
National Bureau of Standards
Washington, DC 20234

R. Jacobs

Bureau of Radiological Health
Food and Drug Administration
Rockville, Maryland 20857

Sponsored in part by:

Bureau of Radiological Health
Food and Drug Administration
U.S. Department of Health,
Education, and Welfare

With cooperation from:
American Association of
Physicists in Medicine

U.S. DEPARTMENT OF COMMERCE, Juanita M. Kreps, Secretary

Luther H. Hodges, Jr., Under Secretary

Jordan J. Baruch, Assistant Secretary for Science and Technology

NATIONAL BUREAU OF STANDARDS, Ernest Ambler, Director

Issued September 1979

Library of Congress Catalog Card Number: 79-600133

National Bureau of Standards Special Publication 554
Nat. Bur. Stand. (U.S.), Spec. Publ. 554, 172 pages (Sept. 1979)
CODEN: XNBSAV

U.S. GOVERNMENT PRINTING OFFICE
WASHINGTON: 1979

For sale by the Superintendent of Documents, U.S. Government Printing Office, Washington, D.C. 20402
Stock No. 003–003–02115–6 Price $4.75
(Add 25 percent additional for other than U.S. mailing)

PREFACE

These are the proceedings of the Conference on Neutrons from Electron Medical Accelerators held April 9-10, 1979 at the National Bureau of Standards, Gaithersburg, Maryland. When medical accelerators such as betatrons, microtrons and electron linear accelerators are operated at energies above about 10 MeV, neutrons can be produced by photonuclear interactions with machine components such as collimators, beam flatteners, etc. The purpose of this conference was to acquaint members of the scientific, radiotherapy, regulatory, and accelerator manufacturing communities with the latest state-of-the-art information concerning this neutron production.

The program opened with a keynote address which was followed by five invited paper sessions. These sessions were concerned with the uses of high energy beams in radiotherapy; the existing regulations, their interpretation and application; the biological effects of neutrons and the appropriate quality factors to use in evaluating the hazard associated with a given electron accelerator; the characteristics of neutron radiation from existing accelerators, the instrumentation, measurement and calculational techniques available for determining the neutron spectral fluence and dose in both the primary as well as the leakage beams; and finally what shielding and design techniques can be employed to reduce the neutron production to a minimum. The conference closed with a summary session which was recorded and is reproduced in full in these proceedings for those interested in comments and review of the full conference.

In order to achieve broad and even coverage of the field, papers were presented by invitation only although attendance at the conference was open to anyone. In spite of the highly specific topic of the conference there were 208 registrants with 22 participants from 8 foreign countries.

The papers are printed in the proceedings as they were received from the authors and in the order in which they were presented in the sessions. For convenience we have preserved the conference notation for the sessions. To speed the publication of the proceedings, all papers were submitted by the authors in camera-ready form. We are greatly indebted to the authors and all those who assisted in the preparation of the manuscripts. Their efforts have made it possible to get the proceedings in print much more rapidly than would otherwise be the case.

When commercial equipment, instruments and materials are mentioned or identified in this proceedings it is intended only to adequately specify experimental procedure. In no case does such identification imply recommendation or endorsement by the National Bureau of Standards, nor does it imply that the material or equipment identified is necessarily the best available for the purpose.

The Editors gratefully acknowledge the assistance of the National Bureau of Standards Office of Technical Publications in the preparation of these proceedings and of Mrs. Kathy Stang of the National Measurement Laboratory and Miss Jo Ann Lorden of the Public Information Division for help in the arrangements for the conference, and the excellent secretarial assistance of Mrs. Karen Fritz and Mrs. Joan Donahue.

H. Thompson Heaton, II
National Bureau of Standards

Robert Jacobs
Bureau of Radiological Health

ABSTRACT

These proceedings are the compilation of 18 papers presented at the Conference on Neutrons from Electron Medical Accelerators held in Gaithersburg, MD on April 9 and 10, 1979. The topics addressed include: properties of high energy beams for radiotherapy, regulations, biological interpretation, physical measurements and calculations, and neutron reduction techniques..

Key words: Dosimetry, high energy radiotherapy beams, leakage, measurement techniques, medical accelerators, neutrons, relative biological effe standards, shielding techniques.

TABLE OF CONTENTS

CONFERENCE PERSONNEL

Conference Co-Chairmen

J. E. Leiss
National Bureau of Standards

J. C. Villforth
Bureau of Radiological Health

Program Committee

L. M. Bates
American Association of Physicists in Medicine

R. S. Caswell
National Bureau of Standards

J. A. Devanney
Bureau of Radiological Health

E. G. Fuller
National Bureau of Standards

H. T. Heaton, II
National Bureau of Standards

G. R. Holeman
Yale University

R. Jacobs
Bureau of Radiological Health

J. S. Laughlin
Memorial Sloan-Kettering Cancer Center

R. C. McCall
Stanford Linear Accelerator Center

J. McDonald
Memorial Sloan-Kettering Cancer Center

C. S. Nunan
Varian

R. Schneider
Bureau of Radiological Health

R. J. Schultz
Yale University

W. P. Swanson
Stanford Linear Accelerator Center

UNWANTED NEUTRON CONTRIBUTION TO MEGAVOLTAGE X-RAY AND ELECTRON THERAPY

J.S. Laughlin, A. Reid, L. Zeitz, & J. Ding
Memorial Sloan-Kettering Cancer Center
New York, N.Y. 10021

The significance of megavoltage x-ray and electron therapy and their development is briefly outlined and illustrative plans presented. Early and recent measurements of photoneutron fluence present in the x-ray beam, and outside the x-ray beam but also incident on a patient, have been reviewed. The variation of incident neutron production with x-ray energy, as well as that of the dose in the patient due to internally produced photoneutrons, has been estimated.

(Accelerators; betatrons; electrons; megavoltage; neutrons; therapy; x-rays)

Introduction

I appreciate very much the privilege of speaking at the initiation of this important conference on neutrons from medical accelerators. This conference has attracted participation by most, if not all, of the experts in this field and it is likely that the work to be reported here will lead to a resolution of this problem. We are all concerned with the problem which confronts those employing high-energy x-rays and electrons for treatment: that of the proper evaluation of the role of the associated neutron contamination. Before adding my comments on the inherent neutron additive to megavoltage therapy, I should like to review something of the frame of reference of this problem.

Not only were the radiations with which we are concerned originally discovered in physical laboratories, but their continuing development in an optimum manner appropriate to medical application has been paced by physical developments. The most useful x-ray energies for diagnostic purposes were achieved early and by the time of World War I, and thereafter, x-rays with peak energies ranging from 30 to 150 kiloelectronvolts were readily available. Although there was recognition that higher energies were necessary in the megaelectron voltage range for optimum treatment application, the appropriate energies were not achieved until after World War II.

My own involvement was at this point. I had the opportunity to work with Professor D.W. Kerst, developer of the betatron, and Dr. Henry Quastler, therapeutic radiologist at the University of Illinois. Our group, with the leadership of Kerst and Quastler, first employed high-energy x-rays, those from a 20 MeV betatron, for treatment of cancer in 1948[1]. The early measurements and experience with betatron x-rays was rapidly added to by H.E. Johns and other workers in the immediately ensuing years[2,3]. In 1951, H.E. Johns initiated Cobalt-60 beam therapy which became the most prevalent methodology for megavoltage therapy[4]. Also in 1951, Dr. Roger Harvey and I initiated high-energy electron beam (6 to 24 MeV) therapy[5] at the University of Illinois College of Medicine. This had required me to spend the previous year or so, in addition to getting betatron x-ray therapy started, in developing methods of collimation, monitoring, dosimetry and treatment planning for high-energy electrons, as well as on improvements in beam extraction. Linear accelerators were soon also developed and applied to both electron and x-ray therapy[6,7] Accordingly, within the decade immediately following the second World War, megavoltage x-ray and electron beam therapy were fully launched with their many advantages and a few problems, with one of which we are concerned today.

Early Neutron Measurements for Megavoltage Therapy

Neutrons are produced by photodisintegration in the target of an accelerator as well as in the differential filter and collimator arrangement. These neutrons will be incident on the patient as a contaminant in the primary x-ray beam and will also reach the patient through the shielding. Neutrons are also produced by photodisintegration within the patient, and much lower energy neutrons are ambient in the radiation room. My early measurements with respect to this problem were published but I will review a few aspects of them which are relevant to our problem. At that time I employed two methods of measurement, one a gated boron trifluoride (BF_3) counter within a specially designed paraffin cave (Figure 1), and also threshold detectors in the form of rhodium foils with and without cadmium enclosures for thermal neutron detection. For fast-neutron detection the foils were used inside a moderator. In the latter case, a cadmium envelope around the entire moderator was sometimes employed. A radium-beryllium (Ra-Be) standard neutron source calibrated at the Argonne Laboratory was used for calibration purposes. The results were published in 1951[8]. They were carried out for three different field sizes in addition to a 1-centimeter-diameter field, with these conclusions:

1. The neutrons incident on the patient were produced primarily in the target with lesser amounts in the filter and collimator arrangement.

2. The primary neutron energies from the betatron were lower than those from the radium-beryllium source as determined by absorption measurements (Figure 2).

3. The concrete walls of the room moderated the neutrons giving rise to a slow neutron ambience.

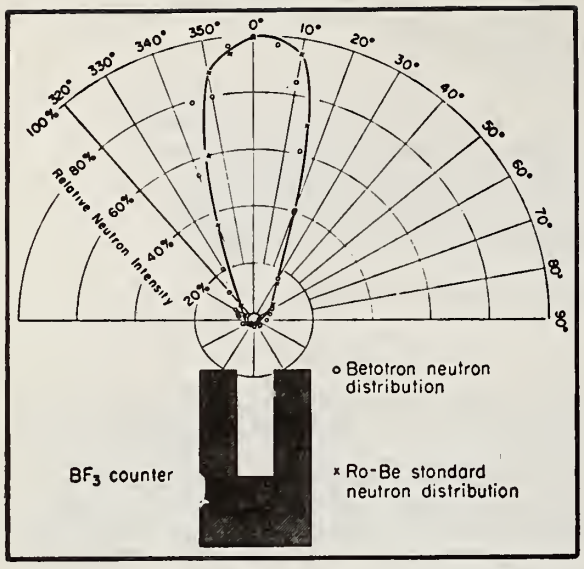

Figure 1. Horizontal cross section of BF_3 counter in paraffin directional geometry. Plot shows relative number of neutrons approaching survey position horizontally. Ra-Be measurements were made with standard at same distance from the counter as the betatron target[8]

4. Fast neutrons in the beam produced a dose in the patient's body. (The values of fast neutron fluence in the x-ray beam are given in Figure 14.) Outside in the primary x-ray beam the neutron level fell off but not as rapidly as the x-ray beam. The dose due to neutrons incident on the patient outside the primary x-ray beam was about half the neutron dose in the x-ray beam.

5. The average dose throughout the patient produced by absorption of photoneutrons generated in the patient was estimated on the basis of body constituents, photodisintegration cross sections as a function of bremsstrahlung energy, and simplifying geometrical assumptions. For the three different field sizes, the average photoneutron dose ranged from about 0.05×10^{-4} to 0.4×10^{-4} rad, per rad in the x-ray beam. This was less, by an order of magnitude, than the dose produced in the body immediately outside the incident x-ray beam by incident fast neutrons, and much less than the scattered x-ray dose internally in the patient. Accordingly, the internal neutron dose was considered to be clinically permissible.

6. The slow and thermal energy neutrons from the shielding and walls were determined to be negligible.

7. With electrons, for which the cross section for electrodisintegration had been measured to be less than that for photodisintegration by a factor of 400[9], measurement at a position just outside an electron beam indicated that the neutron flux was only 6% of that present with an x-ray beam at the same dose rate.

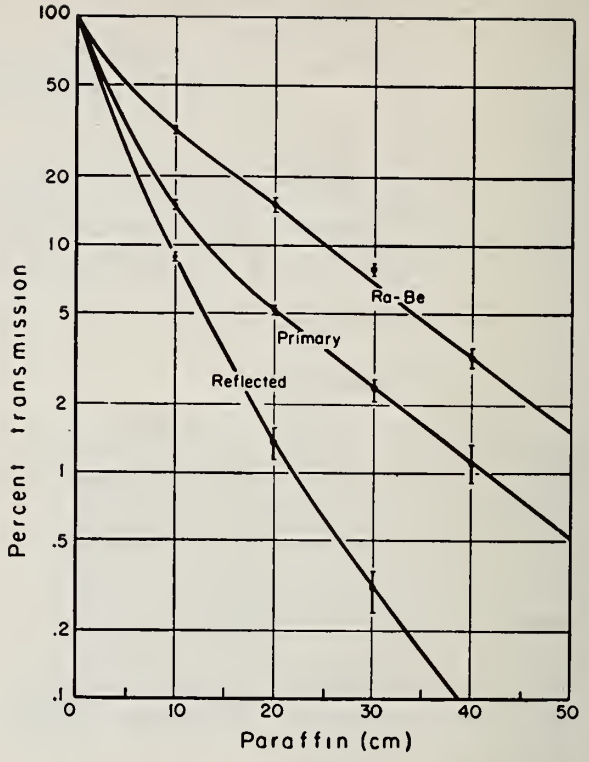

Figure 2. Absorption of neutrons for mixed Ra-Be source compared with that of primaries from betatron, and of those reflected from walls[8].

Since 1951 there have been many more measurements, most carried out with improved technology. It is naturally gratifying that subsequent measurements have essentially confirmed the measurements carried out in my laboratory at that time and also that the conclusions reached then appear to be still justifiable. Before reviewing some of the measurements in the literature I should like to say something about the science of high-energy x-ray and electron beam treatment planning against the background of which this neutron problem must be viewed.

Megavoltage X-ray and Electron Beam Treatment

Specific cases will illustrate advantages of megavoltage x-rays and electrons. These cases were supplied by Ann Reid of our treatment planning group.

1. Liposarcoma, post-surgery. This patient received 4000 rad of 10 MV x-rays in 20 fractions over 30 days using two lateral arcs of uneven weighting and with uncommon centers separated by 7 cms. The resulting dose distribution is shown in Figure 3. The required target volume was unusual both in shape and extent and because the margins were indefinite clinically. This plan not only offered good coverage of the tentative target volume, but also had the advantage of a slower fall-off of dose outside this area than would have been offered by a fixed field technique. For this large volume the moving beams offered the

further advantage of spreading the dose and resulting in better clinical tolerance of the course of radiation therapy than a plan using only four fixed fields.

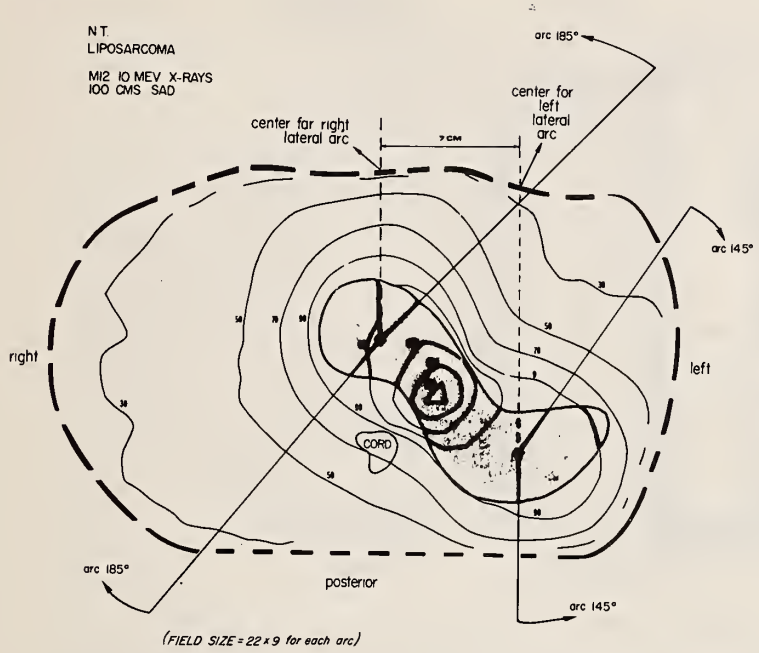

Figure 3. Patient treated for liposarcoma using a waving beam technique with 10 MV X-rays.

2. Recurrent adenocarcinoma of the right antrum, post surgery. Extensive recurrent disease necessitated a large treatment volume. The 6 MeV linear accelerator unit was used to take advantage of its sharp penumbral characteristics in cutting off the dose to the left eye. However, due to the infiltration of the disease, a high skin dose was required and so bolus was necessary. The technique used was a heavily weighted anterior field contributing all the dose in the anterior region and two wedged fields of lower weighting coming in behind the eyes to compensate both for the falling anterior field pattern and boost the dose in the posterior region of the target volume. The resulting dose distribution (Figure 4) shows good uniformity throughout the target volume and a dose of about 4% to the left eye.

3. Mesothelioma. The problem was to produce the required dose over a large irregularly shaped volume while still keeping the lung dose under tolerance limits. This was achieved by combining 6 MeV x-ray fields with 10 MeV electron beams. The technique is simple, but the positioning of the blocks critical. The individual dose distributions for the two modalities are shown. Approximately 3800 rad were delivered with opposing fields with 6 MV x-rays (Figure 5) with the areas overlaying the lung blocked out. These shielded areas were then treated with 10 MeV electrons to a dose of about 3500 rad (Figure 6). Both x-ray and electron fields were treated on the same day. The resulting dose distribution is shown in Figure 7. The large volume received from 3000 to 4000 rad with small hot spots of 6000 rad at the junction while the lung dose was kept under 2000 rad.

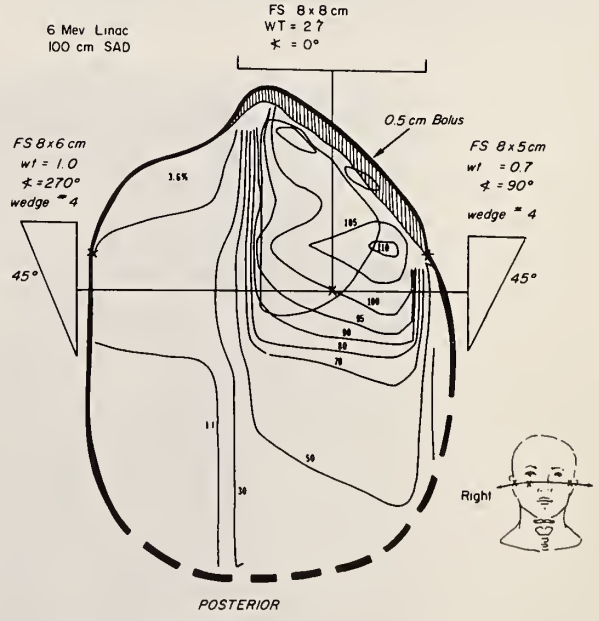

Figure 4. Patient treated for carcinoma of the right antrum using 6 MV X-rays.

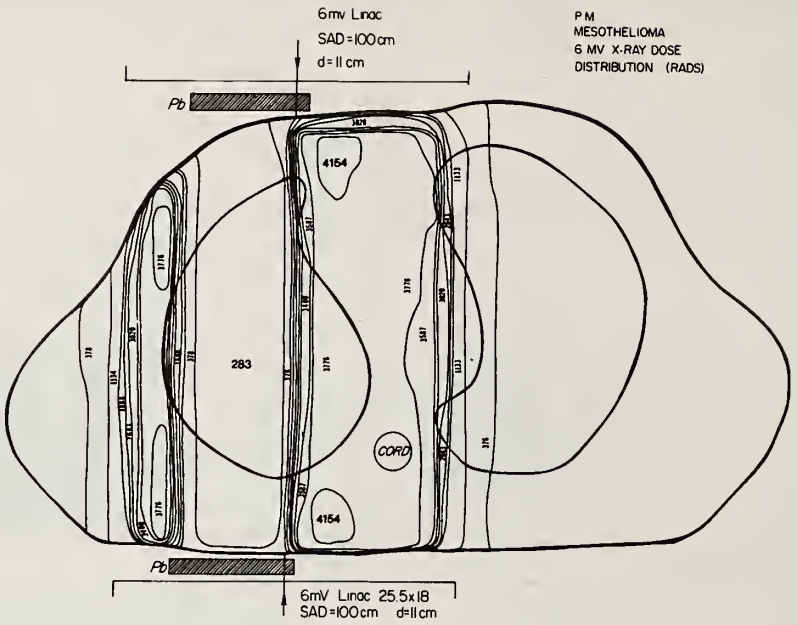

Figure 5. 6 MV X-ray distribution for patient treated for mesothelioma.

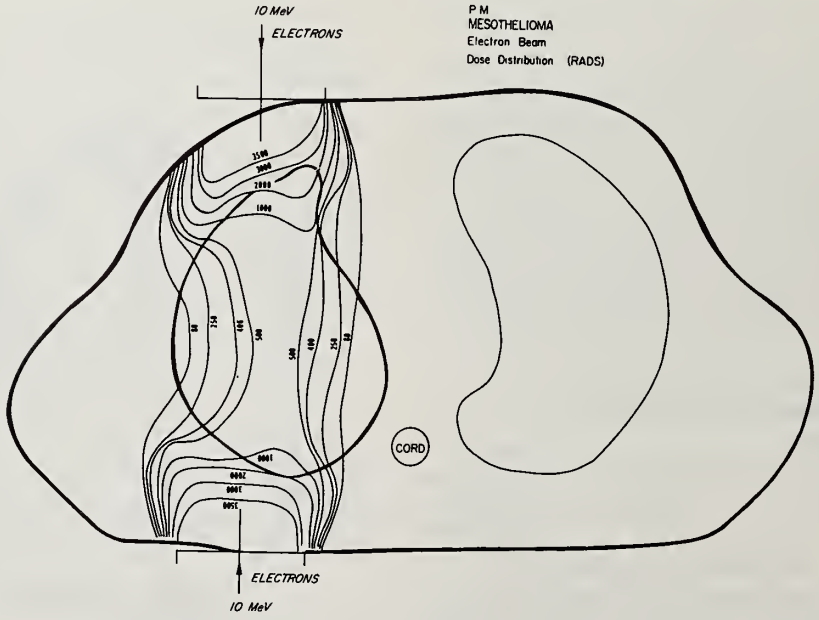

Figure 6. 10 MeV electron distribution for same patient as in Figure 5.

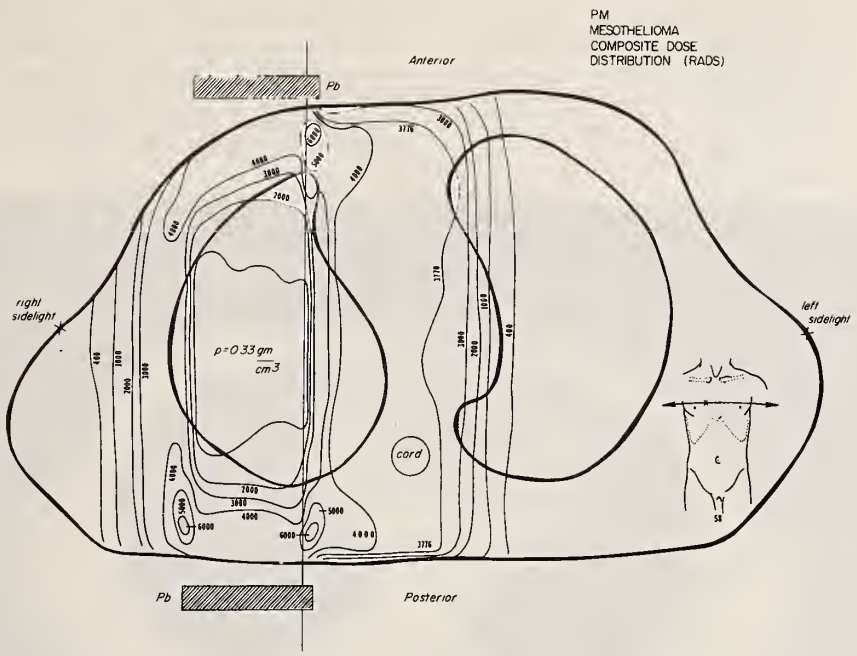

Figure 7. Dose distributions of Figures 5 and 6 combined to show final treatment plan for this mesothelioma.

4. Osteogenic sarcoma. The difficulty in this case was that the required dose for tumor control was 6000 rad while the tolerance dose to the cord is 4000 rad, and the tumor was wrapped around three sides of the cord. The solution lay in the use of a gravity-oriented block of the shape shown in Figure 8 and a 360° rotation with Co-60 gamma rays. The block is small and its placement critical. Computerized axial tomograph (CAT) scans were done with markers indicating both patient alignment for treatment and the outline of the shadow of the block on the skin when positioned

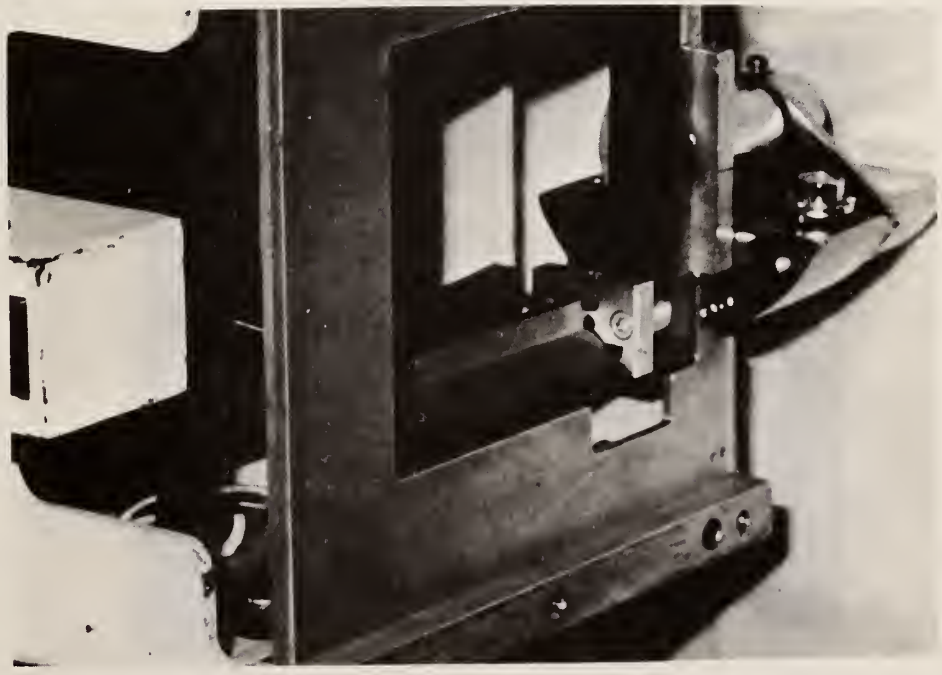

Figure 8. Gravity orientated tungsten block used to shield spinal cord in patient with osteosarcoma.

(Figure 9). The scan allowed clear confirmation of patient and block alignment as well as the final treatment plan involving inhomogeneity corrections (Figure 10) and the final treatment plan incorporating phantom measurement corrections for scattering into the shadow of the block (Figure 11).

5. Chest wall. For chest wall recurrences in post-mastectomy breast carcinoma patients, electron beam therapy is frequently used. Treatment planning incorporating corrections for changing absorption patterns in lung has been done by hand (Figure 12). Computer models for electron beam therapy treatment planning have been developed and incorporated with CAT information to

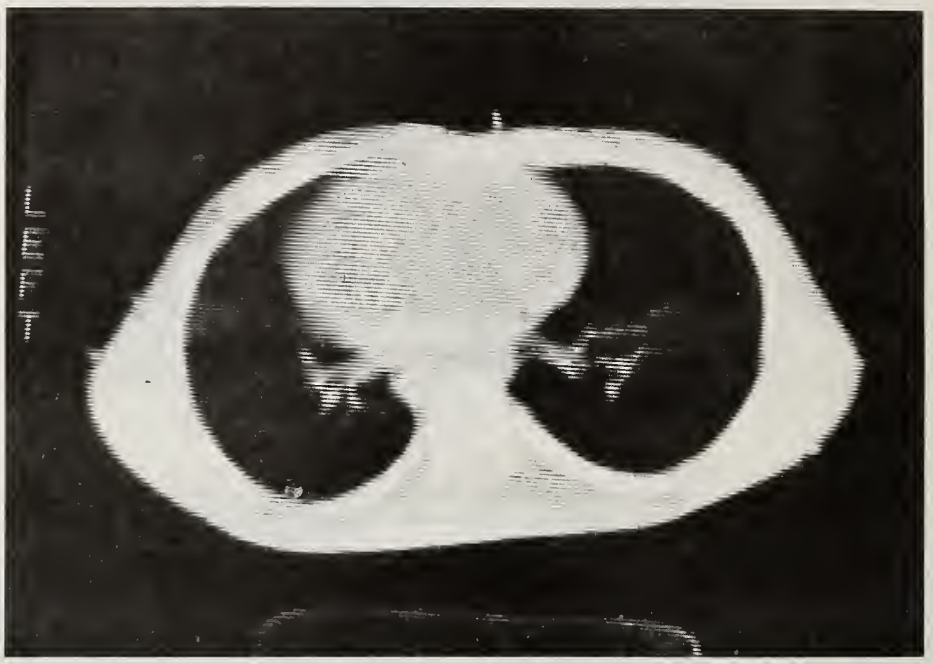

Figure 9. CAT scan with markers verifying block and spinal cord alignment with patient in treatment position.

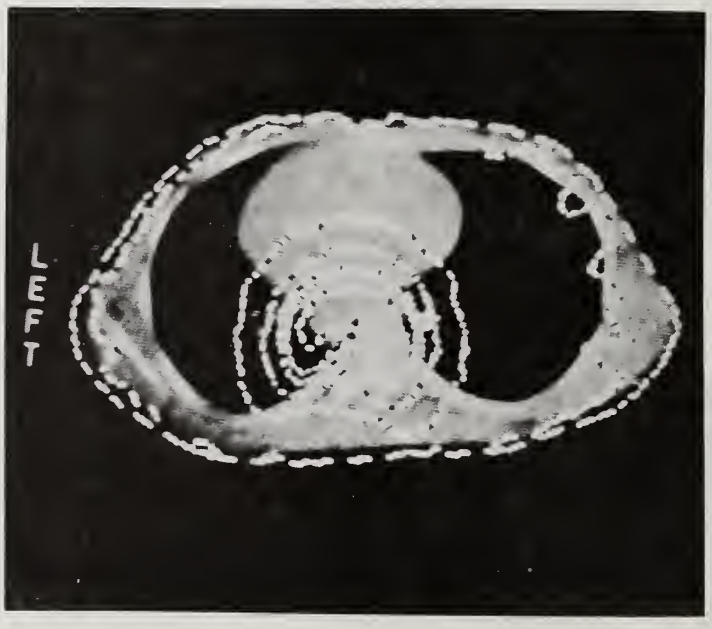

Figure 10. Computerized dose distribution for osteogenic sarcoma.

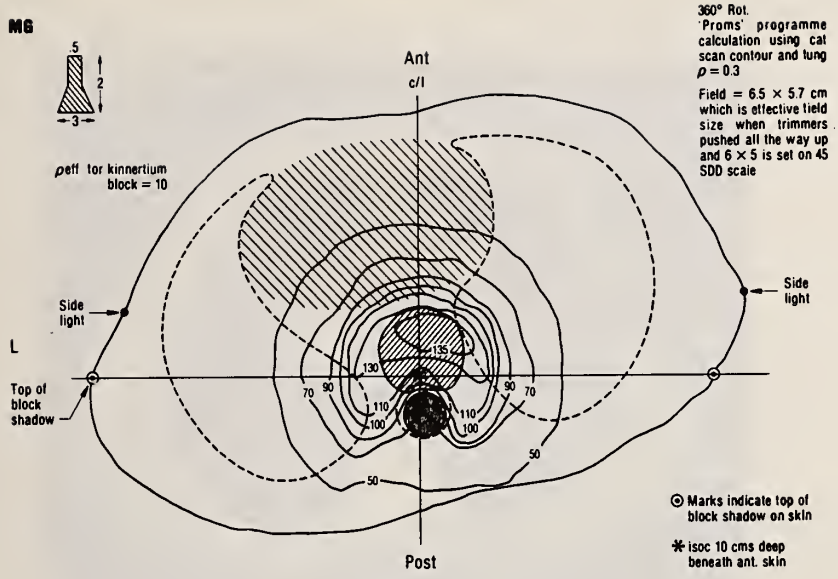

Figure 11. Final dose distribution incorporating inhomogeneity and scatter contributions for patient with osteogenic sarcoma.

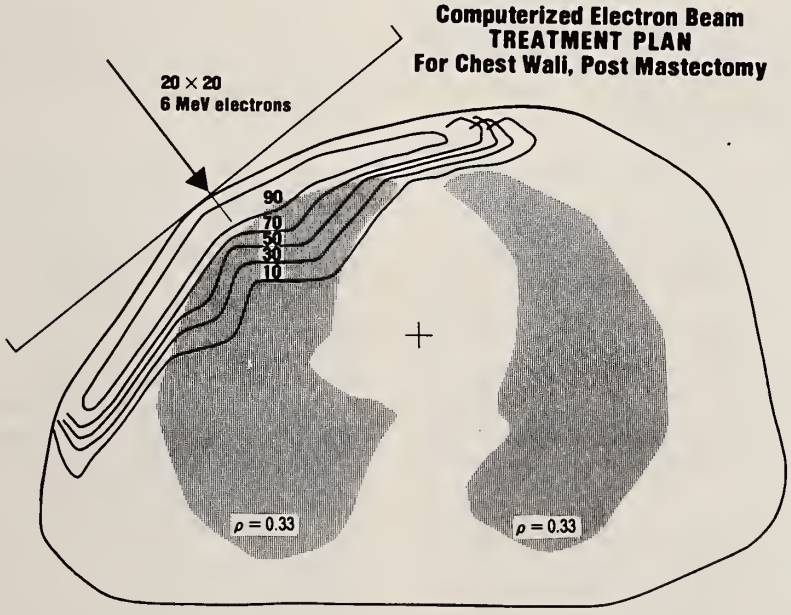

Figure 12. Hand calculated dose distribution for treatment of chest wall recurrence in breast cancer post mastectomy.

correct for inhomogeneities so that such distribution and displays as (Figure 13) shown are available.

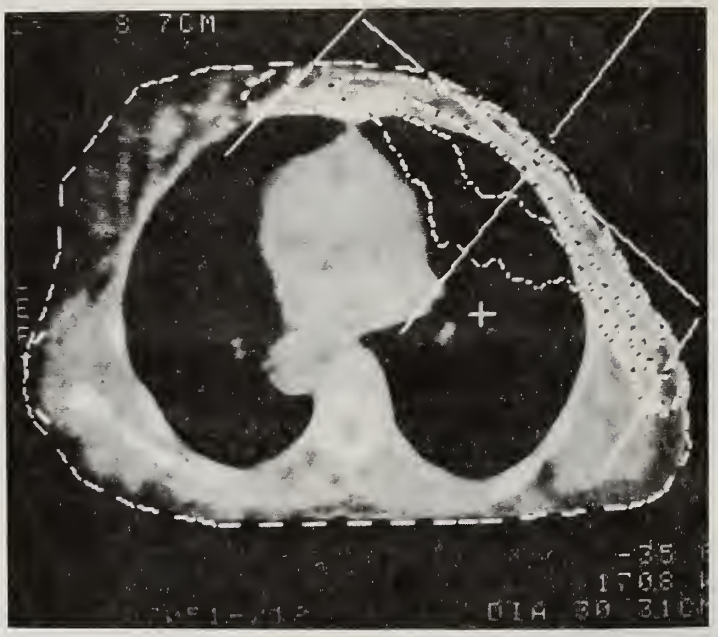

Figure 13. Computerized dose distribution utilizing CAT data for same patient as in Figure 12.

Neutron Measurements in Megavoltage Therapy

In the limited time it is possible to comment on only a part of the recent literature[10-23] Of course, the results to be presented by other investigators may change, and will certainly add to our information on pertinent dose levels.

Measurements were reported in 1972 by Axton and Bardell[10] which were carried out with a 35 MeV Brown Boveri betatron and a 16 MeV Mullard linear accelerator. Gold foils were employed in polythene spherical moderators, and calibrated at two different neutron energies with the National Physical Laboratory Van de Graaff accelerator using the $^{7}Li(p,n)^{7}Be$ reaction. The measured levels were somewhat high with respect to most other investigators which may be partially explained on the basis of the large field size (25 cm. by 25 cm.) employed and also possible photonuclear reactions in the moderator. Measurements have been reported by McGinley, et.al.[11] with a 10 MeV Varian Clinac-18 linear accelerator, a 25 MeV Allis-Chalmers betatron, and a 45 MeV Brown Boveri betatron. For fast neutrons they employed a bare indium foil in a cubic water-filled container, and the fission neutron spectrum of californim-252 was used for calibration. For thermal neutrons they used the indium foils with and without a cadmium shield. A plutonium-beryllium neutron source housed in a paraffin moderator was used for calibration purposes. As would be expected, since the threshold for photodisintegration in copper is 9.9 MeV, the neutron values measured for an x-ray energy of 10 MeV were very low. In fact, the neutron fluence in the beam was lower than that outside the beam. These and their other measurements are shown in Figure 14. Measurements with a 25 MeV Shimadzu betatron were reported by Fox and McAllister[12] in 1977. They employed the neutron-proton reaction in aluminum for fast neutrons. They determined the primary target to be the major source of neutrons and that a large beam flattener contributed approximately 15% of the neutrons. Their measurements are shown in Figure 14. Measurements with a Philips linear accelerator operated at 18 MeV were reported by Gur et.al.[13] in 1978. Their fast neutron measurement technology was similar to that employed by Fox and McAllister. Indium foils were used for thermal measurements. The experiments were repeated for three different field sizes. Neutron fluence was found in their case to be independent of field size. The slow neutrons accounted for only about 1.5% and 5% of the total neutron dose in rads inside and outside the treatment fields, respectively.

Measurements with the 25 MeV Sagittaire were reported by Price, Nath and Holeman[14] in 1978. They employed phosphorus-31 for both thermal and fast neutrons. In the case of the fast neutrons they relied on the reaction $^{31}P(n,p)^{31}S$, which has a half life of 2.62 hours and a beta particle

with a maximum energy of 1.48 MeV. For thermal neutron detection they relied on the reaction $^{31}P(n,\gamma)^{32}P$ with a resulting half life of 14.3 days and a beta particle with a maximum energy of 1.71 MeV. The beta activity was counted using a liquid scintillation spectrometer. Phosphorus was used in the form of P_2O_5 powder placed in a small vial. All other activation products were shown to have either very short half lives or to be stable, except for the two desired radionuclides ^{31}Si and ^{32}P. They had demonstrated that the photon sensitivity was less than 4%, which makes these threshold detectors particularly attractive.

Measurements were reported by Wilenzick et.al.[15] in 1973 with a 25 MeV Sagittaire Linear Accelerator and a 19 MeV Siemens betatron. They employed both fission fragment track detectors and silicon diode detectors. The fission fragment detectors consisted of a thin uranium foil in contact with a disk of Lexan polycarbonate plastic. Calibration was carried out with a californium-252 source. The sensitivity of this detector appeared to be linear with a neutron dose between 4 and 300 rad. Because of the appreciable cross section for photofission, neutron measurements could not be made in the primary x-ray beam with the track detectors. The silicon diode detectors consisted of a p-i-n structure produced by diffusion of boron and phosphorus atoms into high ohmic monocrystalline silicon. The change in forward voltage was measured by applying a constant current of 25 mA before and after exposure to neutrons and observing the potentials. The increase in voltage was determined to be a non-linear function of the neutron dose. Neutron flux measurements outside of the beam with the track detectors are somewhat larger than those obtained with the silicon diodes, possibly due to underestimation of the photofission correction. Also, it appears that diodes are particularly sensitive to electrons and photons so that they cannot be reliably employed in an x-ray beam. In 1978 McCall and Jenkins[16] carried out a study of the photon and electron response of silicon diode neutron detectors. A Varian Clinac-35 accelerator was used from which the electron beam could be extracted as well as the x-ray beam. They made a comprehensive study of the response of silicon diodes, silicon disks as well as moderated indium foil detectors. Their measurements quantitatively defined the photosensitivity of silicon diodes.

Shown in Figure 14 are measured fast neutron fluences obtained with threshold detectors plotted as a function of the accelerator energy. The numbers are identified with the references in the caption and results are given for both betatrons and linear accelerators with measurements made of neutron fluence in and outside of the primary x-ray beam. Considering the differences in field sizes, measurement techniques and correction factors employed, the spread of measurements is not surprising. Also, differences in spectra of the calibration sources can account for some of the spread. An important conclusion which is suggested by this distribution is that the magnitude of the neutron fluence, either in or outside the primary x-ray

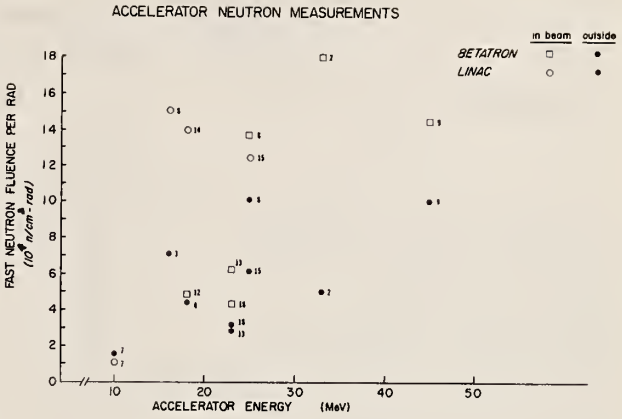

Figure 14. Fast neutron fluence measurement vs accelerator energies. Measurements numbered (2,3): reference 10; (7,8,9): 11; (12,13): 12; (14): 13; (15): 14; and (18): 8

beam, does not increase appreciably with x-ray energy. Measurements of the neutron flux in the primary x-ray beam as a function of field size are plotted in Figure 15. As indicated, two investigators found field size dependence for their collimator arrangements whereas two other installations did not have such a dependence.

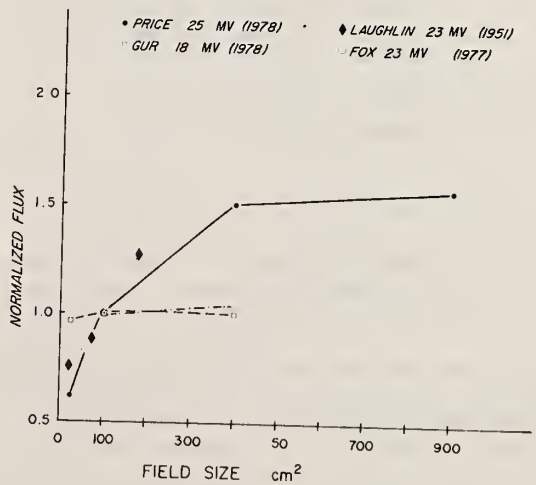

Figure 15. Fast neutron fluence in x-ray beam as a function of field size. Normalized at 100 cm^2.

Table 1

Ratio of Fast Neutron Fluence in Primary

X-Ray Beam to that Outside

Investigator/Year/Machine (ref.)	Fast Neutron Fluence in beam / out of beam	Distance Outside Edge of Field cm
K. Lofgren (1970) Betatron (17)	2.8	0-7
Axton (1972) Betatron (10)	3.6	27.5
Axton (1972) Linac (10)	2.1	27.5
Wilenzick (1973) Betatron (15)	4 3	5
Wilenzick (1973) Linac (15)	6.4	5
McGinley (1976) Linac (11)	0.7	5
McGinley (1976) Betatron (11)	1.4	5
McGinley (1976) Betatron (11)	1.4	5
Fox (1977) Betatron (12)	2.1	5
Gur (1978) Linac (13)	3.2	5
Price (1978) Linac (14)	2.0	5
Stranden (1977) Betatron (19)	2.1	50
Laughlin (1951) Betatron (8)	1.5	12.5

In Table 1 ratios, as determined on different machines, of the neutron fluence in the x-ray beam to the neutron fluence incident on the patient but outside the x-ray beam are tabulated. The values determined by threshold detector methods range from 1.4 to 3.6. This degree of difference can be readily explained on the basis of different collimator arrangements, differential filter size, etc. Higher ratios are obtained with the use of silicon diode detectors but the authors have indicated that photon sensitivity of the detectors was not appreciated. Chaudri, et.al.[22] in an abstract indicated measurements carried out with a betatron at energies of 15, 20, 25 and 30 MeV. Their observed neutron fluence increased rapidly with energy but appeared comparable to other results reviewed here. Relevant to the consideration of x-ray dose internally scattered are the measurements of Rawlinson and Johns[26]. They showed by phantom measurements that the scattered x-ray energy exceeded the leakage x-ray energy by factors ranging from 5 to 20 for different situations.

An associated problem to patient exposure is that of personnel exposure. This problem has been recently discussed by Schulz[21] who emphasizes that the RBE for carcinogenic effects obtained from analysis of atomic bomb data from Japan ranges between factors of 30 to 60[27,28]. This consideration increases the significance of the problem of measuring low level amounts of neutron fluence in the presence of low level x-rays and electrons, including areas outside the treatment room. Schulz has designed an ionization chamber filled alternately with argon or propane which does appear to provide an improvement in the method of measurement of low level neutron exposure.

Calculated Neutron Production

Since most of the measurements of neutron fluence were with accelerators in the 20 MeV range, it appeared important as well as interesting to inquire into the situation with even higher energy x-rays. As indicated in Figure 14, there are a few data at higher energies and these do not suggest any particular increase in neutron fluence incident on the patient. A possibly more important problem is whether or not the neutron dose due to photoneutrons produced within the patient, which appeared to be at acceptable levels at 20 MeV, might increase to unacceptable levels at higher energies. The important assumptions were that the target thickness is in all cases equal to the mean range of the electrons,and that all of the photons in the bremsstrahlung spectrum could interact with all of the nuclei present in one target thickness. The number of x-rays produced in the target was estimated on the basis of the Kramers equation[23]. A numerical integration over the appropriate energy region of the product of the cross sections[24] for photoneutron production and the number of x-ray photons gave the number of photoneutrons produced in the target. The values of the thresholds and cross section dependence on energy were taken from the "Atlas of Photoneutron Cross Sections Obtained with Monoenergetic Photons" by B.L. Berman[24]. On this basis, the ratio of the total number of photoneutrons to x-ray energy produced in a tungsten target was obtained and is plotted in Figure 16. The calculations for platinum and gold gave closely similar results. Calculations carried out for copper indicated a lower yield by a factor of at least three. The calculated production of neutrons in the target rises from a low level at 10

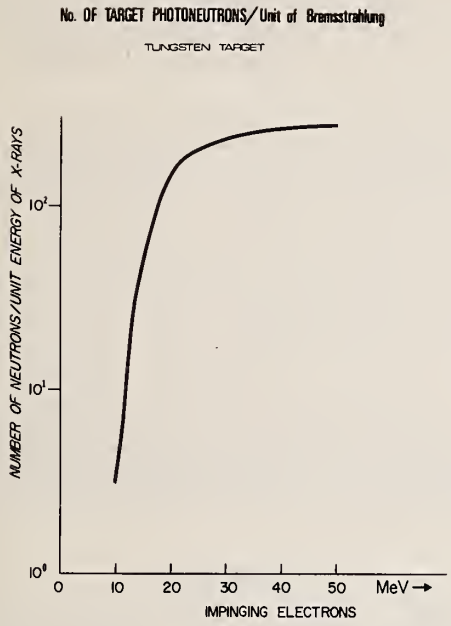

Figure 16. Photoneutron production in the accelerator target as a function of energy of the impinging electrons.

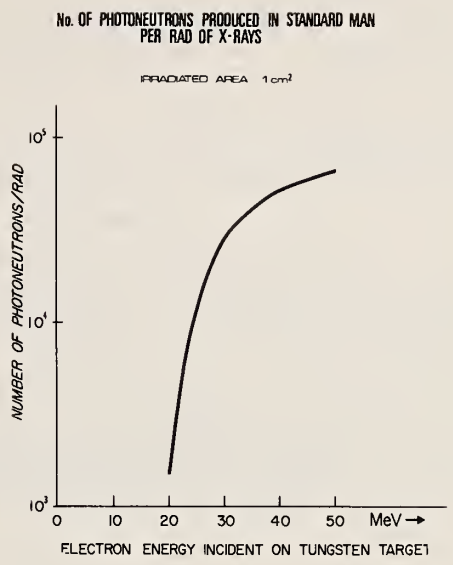

Figure 17. Photoneutron production within the patient.

MeV; increases by a factor of 50 in going from 10 MeV to 20 MeV; and by a factor of less than 2 from 20 MeV up to 30 MeV. On this basis we would not expect the shielding problem for accelerators to increase substantially above 30 MeV, neglecting the slightly higher average energy of the photoneutrons produced.

This contrasts with the situation for the photoneutrons produced within the patient as shown in Figure 17. We estimated the number of photoneutrons produced and the x-ray energy absorbed per gram of tissue in a defined volume of a standard man. The average dose produced in that standard man by the absorption of these photoneutrons was calculated on the basis of the following assumptions:

1. The man was a rectangular parallelepiped 12 cm deep in the direction of the x-ray beam with a length of 152 cm and a width of 38 cm, amounting to a volume of 70,000 cubic cm.

2. The nuclei contributing appreciably to photoneutron production reactions are oxygen (7.44 grams/cm^2), carbon (2.77 grams/cm^2), nitrogen (0.31 grams/cm^2), calcium (0.17 grams/cm^2), and additionally hydrogen (1.12 grams/cm^2) for the absorbed dose calculation. The absorption of neutrons from the irradiated region to the most distal corner of the phantom man was estimated on the basis of known cross sections[29]. It was assumed that this fraction applied to all of the neutron production which overestimates the amount of neutron energy absorbed in the man. All of the difference between the energy of the incident photon and the threshold energy is transferred to the photoneutrons.

In Figure 17 it is indicated that the production of photoneutrons in the patient increases between 20 MeV and 30 MeV by a factor of 20 and is still increasing more gradually at energies above that. When converted into the average dose produced within the patient on the assumptions given above, we have for a 200 square centimeter field with a 20 MV x-ray beam an average dose throughout the man of about 5×10^{-8} rad, increasing to 2×10^{-6} at 30 MV, to 5×10^{-6} at 40 MV, and to 8×10^{-6} rad at 50 MV. Values just outside the periphery of the x-ray beam are somewhat higher and dose levels at the extremities of the man are somewhat lower. These calculations come from a comprehensive analysis (in preparation, 31) of the distribution of high LET dose produced throughout the patient's body during megavoltage x-ray treatment. These values are less than those estimated in my earlier calculations, which, however, assumed the total absorption of all of the neutrons. An important conclusion is that despite this dramatic increase in the internally produced neutron dose as a function of energy, it is still substantially less than that due to the internally scattered x-ray dose.

Horsley, Johns and Haslam[30] estimated the total energy absorption by human tissue for the major nuclear reactions caused by high energy x-rays, including that for photoneutrons. They assumed all of this energy was absorbed in the irradiated region. This is acceptable for the charged particle reactions, but only a small proportion of the photoneutrons are locally absorbed,

most being absorbed elsewhere in the body or escaping. For this reason, their estimate of 0.3 - 0.6% additional energy absorbed in the irradiated region is somewhat high. Our estimate for photoneutron production for 30 MV x-rays, converted to the energy in the fluence of neutrons produced in the irradiated volume per rad delivered, is about a factor of 2 less than that calculated by Horsley, et.al.,[29] for 28 MV. In our calculations, use was made of the cross section profiles from the Berman Atlas[24]. These differed considerably, at least for the $^{16}(\gamma,\eta)^{15}0$ reaction, from the profiles used by Horsley, et.al.,[30]. When the cross section profile of Berman[24] was replaced by that employed by Horsley, et.al.,[30] calculations showed an increase of 1.5 in the number of photoneutrons produced by the oxygen reaction. Since the oxygen present contributes about 70% of the photoneutrons produced in man, this difference in the cross section employed would account for most of the factor of 2 elevation of the Horsley, et.al.,[30] estimate.

It is also essential to consider the quality factor to be employed for neutron equivalent dose calculations. In order to obtain a biological neutron equivalent dose it is important to know the RBE of neutrons for cell killing. The RBE values obtained in our laboratory for lethality with HeLa cells in a fast neutron field, whose dose average LET was about 50 KeV/μm, went from 2 at high doses to about 3.5 at low doses[32]. Similar results were obtained by Broerse, et.al.[33] and by Hall, et.al.[34]. This has also been examined recently in a paper by Slater and Chu[24] who have emphasized the consequence of a changing modifying factor (QF) in the computation of dose equivalent in rem. It should be kept in mind that higher values are in going to lower doses or dose rates res... because the reference radiation has a shoulder in its dose response as contrasted with heavy particle radiation, such as neutrons, in which the extrapolation number is closer to unity.

Summary

1. The important physically based advantage of megavoltage photon and electron treatment has been illustrated, and the historical development of this technology briefly reviewed.

2. Measurements of neutron fluences from various accelerators have been reviewed. With allowance for differences in machine geometries, accelerator operating parameters, measurement technologies, the results are in fair agreement.

3. It is recommended that basic measurement data be reported separately before conversion factors such as quality factor are applied. Such factors are functions of energy and are not applied in a uniform manner by different investigators. Availability of data before folding in such factors facilitates interpretation.

4. Values of fluence or absorbed dose produced in a patient's body by either incident neutrons or internally generated neutrons are substantially less than that due to scattered x-rays. In the opinion of the author, a leakage rate greater than 0.1% appears reasonable, even if it is on an equivalent dose basis and includes a reasonable quality factor.

5. Calculations based on a simple model indicate that the incident neutron fluence per unit x-ray intensity should not increase markedly above 30 MeV x-ray energy. Measured values are not in disagreement with this prediction.

6. Calculations also indicate that the internally produced photo neutron dose will still increase appreciably above 30 MeV before leveling off.

In conclusion, with the participation of those present and the data to be presented, I am sure we can look forward to a stimulating and useful meeting. The National Bureau of Standards and the Bureau of Radiological Health should be congratulated on organizing this timely and important conference.

References

(1) Quastler, H., Adams, G.D., Almy, G.M., Dancoff, S.M., Hanson, A.O., Kerst, D.W., Koch, H.W., Lanzl, L.H., Laughlin, J.S., Reisen, D.E., Robinson, C.S., Austin, V.T., Kerley, T.G., Lanzl, E.F., McClure, G.Y., Thompson, E.A., and Skaggs, L.S. Technique for application of the betatron to medical therapy. American Journal of Roentgenology, 61: 591-625 (1949).

(2) Johns, H.E., Darby, E.K., Haslam, R.N.H., Katz, L., Harrington, E.L. Depth dose data and isodose distributions for radiation from a 22 MeV betatron. American Journal of Roentgenology, 62: 257-268 (1949).

(3) Laughlin, J.S., and Davies, W.D. Procedure in dose distribution measurement of 25 MeV x-rays. Science, 11: 514-516 (1950).

(4) Johns, H.E., Bates, L.M., and Watson, T.A. 1000 Curie cobalt units for radiation therapy. British Journal of Radiology, 25: 296-318 (1952).

(5) Laughlin, J.S., Harvey, R.A., Haas, L.L., Lindsay, J.E., and Beattie, J.S. Physical aspects of rotation therapy with the betatron, Part I. American Journal of Roentgenology, 65: 947-951 (1951).

(6) Miller, C.W. Travelling-wave linear accelerator for x-ray therapy. Nature, 171: 297 (1953).

(7) Greene, D., Nelson, K.A. Performance of a linear accelerator in clinical service. Instrumental & Technical Notes, 33: 336-338 (1960)

(8)

Laughlin, J.S. Physical considerations in the use of a 23-MeV medical betatron. Nucleonics, 8: 5-16 (1951).

(9)

Skaggs, L.S., Laughlin, J.S., Hanson, A.O., and Orlin, J.S. Electrodisintegration of Cu^{63}, Ag^{107}, Ag^{109}. Physical Review, 73: 420 (1948).

(10)

Axton, E.J., Bardell, A.G. Neutron production from electron accelerators used for medical purposes. Physics in Medicine and Biology, 17: 293-298 (1972).

(11)

McGinley, P.H., Wood, M., Mills, M., Rodriquez, R. Dose levels due to neutrons in the vicinity of high-energy medical accelerators. Medical Physics, 3: 397-402 (1976).

(12)

Fox, J.G., McAllister, J.D. Fast neutrons from a 25-MeV betatron. Medical Physics, 4: 387-396 (1977).

(13)

Gur, D., Rosen, J.C., Bukovitz, A.G., and Gill, A.W. Fast and slow neutrons in an 18-MV photon beam from a Philips SL/75-20 linear accelerator. Medical Physics, 5: 221-222 (1978).

(14)

Price, K.W., Nath, R., and Holeman, G.R. Fast and thermal neutron profiles for a 25-MV x-ray beam. Medical Physics, 5: 285-289 (1978).

(15)

Wilenzick, R.M., Almond, P.R., Oliver, G.D., and DeAlmeida, C.E. Measurement of fast neutrons produced by high-energy x-ray beams of medical electron accelerators. Physics in Medicine and Biology, 18: 396-408 (1973).

(16)

McCall, R.C., and Jenkins, T.M., and Oliver, G.D. Photon and electron response of silicon-diode neutron detectors. Medical Physics, 5: 37-41 (1978).

(17)

Löfgren, K., and Spring, E. Neutron radiation produced by the 32 MeV roentgen beam of a medical betatron. Acta Radiologica, 9: 247-256 (1970).

(18)

Deye, J.A., Young, F.C. Neutron production from a 10 MV medical linac. Physics in Medicine and Biology, 22: 90-94 (1977).

(19)

Stranden, E. Neutron doses to patients in high energy x-ray therapy. Physics in Medicine and Biology, 22: 1011-1013 (1977).

(20)

Ernst, W. and Ovadia, J. Contaminant dose from incident neutrons associated with 22.5-MeV x-rays from a betatron. Radiology, 66: 105-106 (1956).

(21)

Schulz, R. Argon/propane ionization-chamber dosimetry for mixed x-ray/neutron fields. Medical Physics, 5: 525-531 (1978).

(22)

Chaudri, M.A., Allen, P., Millar, M., Muirhead, E., Rouse, J., Spicer, B. Absolute determination of the neutron flux produced by the interaction of high energy Bremsstrahlung with tissue. Abstract, private communication.

(23)

Sproull, W.T. X-Rays in Practice, Chapter 3, The continuous x-ray spectrum, pp. 20-44. McGraw-Hill, New York (1946).

(24)

Berman, B.L. Atlas of photoneutron cross sections obtained with monoenergetic photons, Preprint UCRL-78482, Dec. 30, 1976. (Original references are cited by Berman in Atlas.)

(25)

Slater, J.M., Chu, W.T. A comment on the leakage radiation regulations of high energy radiotherapy machines. Private Communication.

(26)

Rawlinson, J.A., Johns, H.E. Letter to the Editor. Medical Physics, 4: 456-457 (1977).

(27)

Rossi, H.H., and Mays, C.W. Leukemia risk from neutrons. Health Physics, 34: 353-360 (1978).

(28)

Ishimaru, T., Otake, M., and Ichimaru, M. Dose-response relationship of neutrons and x-rays to leukemia incidence among atomic bomb survivors in Hiroshima and Nagasaki by type of leukemia, 1950-1971. Radiation Research, 77: 377-394 (1979).

(29)

Stehn, J.R., Goldberg, M.D., Magurno, B.A., and Wiener-Chasman, R. Neutron cross sections, Vol. I, Z = 1 Fo 20, BNL 325, Second Edition, Supplement No. 2 (1964).

(30)

Horsley, R.J., Johns, H.E., and Haslam, R.N.H. Energy absorption in human tissue by nuclear processes with high-energy x-rays. Nucleonics, 11: 28-31 (1953).

(31)

Zeitz, L., and Laughlin, J.S. High LET dose distribution produced by megavoltage x-ray treatment (in preparation).

(32)

Zeitz, L., Canada, T.R., Djordjevic, B., Dymbort, G., Freeman, R., McDonald, J.C., O'Neil, J., and Laughlin, J.S. A biological determination of the variation of fast-neutron field quality with depth, RBE, and OER. Radiation Research, 63: 211-225 (1975).

(33)

Broerse, J.J. RBE values of fast neutrons for damage to organized tissues in experimental animals. In: Radiation Research Biomedical, Chemical and Physical Perspectives. Eds. O.F. Nygaard, H.J. Adlar, and W.K. Sinclair, Academic Press, New York, p. 1073 (1975).

(34)

Hall, E.J., Novak, J.K., and Marino, S.A. Comparative radiobiological measurements with two high-energy cyclotron-produced neutron beams presently used in radiotherapy. British Journal of Radiology, 47: 882-887 (1974).

ADVANTAGES AND PROPERTIES OF HIGH ENERGY PHOTON BEAMS

H.E. Johns
Ontario Cancer Institute, 500 Sherbourne Street,
Toronto, Ontario, Canada M4X 1K9

A brief history of the development of high energy machines - cobalt 60 units, betatrons and linacs is presented. The properties and advantages of these machines are discussed. The large increase in cure rate resulting from the use of these machines in the treatment of cancer of the cervix is presented. Instead of worrying about neutrons, we should be dealing with the properties of these beams. They should be designed to give as small an entrance dose as possible and the peak dose should be placed as far below the skin as possible. These parameters are much more important than neutron leakage. Ways of improving these beams by altering the flattening filter and other components are described. Problems arising from the use of very large half body fields are discussed. With very large fields, surface doses become large and the buildup properties of the beam disappear. Ways of improving these fields are dealt with. It is suggested that regulatory agencies should be more concerned with beam improvements than with neutron leakage which is not a problem. The hope is expressed that with CT scanning and the possible improvements in beam direction and dose calculations, a further dramatic increase in cure rate will result.

(betatrons; cobalt units; dose buildup; linacs; patient survival)

Introduction

This is a conference on neutrons from electron medical accelerators and according to the prospectus for the meeting, we have been asked to study "the shielding and design techniques which can be employed to reduce the neutron production to a minimum". I object to this statement since I am only interested in reducing neutrons to a minimum provided that in doing so we do not interfere with some of the other properties of the beam. We and the regulatory agencies should be interested in optimizing the beam for radiotherapy not merely in reducing neutrons to a minimum. In this session I intend to discuss some of the properties and advantages of high energy photon beams. This will be followed by Dr. Powers, who will talk about the use of high energy x-rays in cancer cure and finally, we will hear a discussion by Alan Rawlinson on scattered radiation relative to leakage radiation. I hope this session will show that neutron production is not a problem.

Some 30 years ago when I first became involved in using the betatron for medical purposes, we were, of course, aware of the fact that with high energy photons one could produce (γ,n), (γ,p) and (γ,α) reactions in tissue[1]. After a radiation treatment patients were (and are) radioactive, and it is relatively easy to measure this activity with a geiger counter. The question immediately arises: Is the energy absorbed in these processes important in comparison with that from the conventional ionization and excitation of molecules? We showed that for 20 MeV bremsstrahlung the energy absorbed by these processes was about .3% of the total. Since this type of interaction gives rise to high LET particles, the biological effect could be 10 times as high or contribute 3% of the biological effect. Thirty years ago, we decided this would not be a problem, and to my knowledge, it never has been. Similar findings were made by Laughlin in 1951[2], and more recently by Chaudhri in Melbourne[3].

Properties of High Energy Photon Beams

Now, let us return to the main problem - the useful properties of high energy photon beams in cancer therapy. Figure 1 shows three isodose patterns from 200 kV radiation (left) cobalt 60 radiation (centre) and betatron radiation (right).

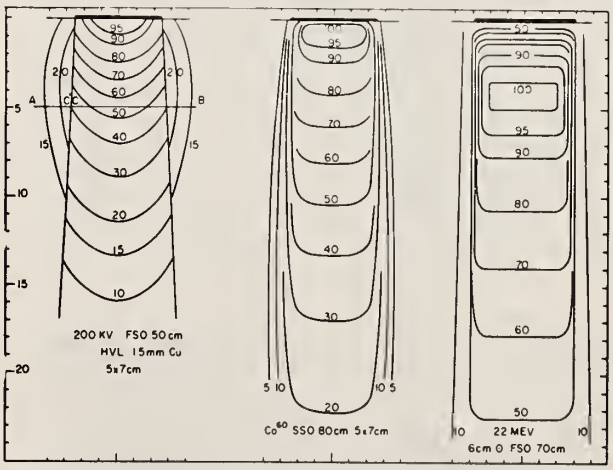

Fig. 1. Isodose distributions for 200 kV, Co-60, and 22 MeV betatron radiation.

Today, we have available all three types of radiations and radiations with intermediate properties. It is useful to acquire some perspective in this matter. At the end of World War II, most cancer centres had 200 kV x-ray equipment, and a few had 400 kV units, and a very few had 1 MeV

Van de Graaff generators.

200 kV radiation is really completely unsuitable for most types of radiotherapy. The dose on the surface is 100% and this falls to about 25% at a depth of 10 cm. With such radiation it is almost impossible to deliver a tumorcidal dose to a tumour near the centre of the body without producing intolerable skin reactions. In fact, in those days, radiotherapists did not even attempt to treat an obese person. Attempts were made in the Scandanavian countries to increase the tumor dose relative to skin dose through rotation therapy, but with only limited success.

All of this was changed when betatrons came on the scene. The first betatron to be used in cancer therapy was at Urbana, Illinois, under the direction of Dr. Donald Kerst. He, with a group of young enthusiastic physicists, including such people as Laughlin, Adams, Skags, Skaggs, Lanzl, and others, used the betatron to treat one of their graduate students suffering from a brain tumor[5]. Figure 1 is worth examining in detail, to see what had really happened as a result of this invention.

The surface dose from a betatron is now nearly zero, and with proper design the maximum dose is at a depth of 5 cm and the 10 cm depth dose is some 80%. The radiotherapist now has a beam which can be used to concentrate radiation in the tumor and save normal tissues surrounding it. Betatrons were developed rapidly by our group in Saskatchewan[6], and by Laughlin[2,4,5], working in Chicago.

Two years later, cobalt 60 came along. Figure 1 shows that it has many desirable properties, the surface dose is very small, the maximum dose is about 5 mm below the skin and the 10 cm depth dose is about 50%[7,8]. Now, cobalt units do not produce as good a radiation distribution as the betatron, but they are, of course, very much simpler to operate. During the next 20 years cobalt units were placed in operation in all parts of the world, and were the main tool of radiotherapy. In recent years, they have been challenged by linacs, which can give much higher dose rates and can operate in the range from 3 MeV up to 20 MeV (Co-60 is equivalent to a 3 MeV linac) and can give very large fields.

Can we, from the vantage point of 1979, look back and see whether or not these technical developments have increased the cure rate? Dr. Bush, Director of our Institute, has looked at treatment results in two periods of time in Ontario. The period from 1935-1944, before the introduction of Cobalt 60 and the periods 1958-1960 and 1960-1969, after the introduction of cobalt units and betatrons. Figure 2 shows percentage survival of cancer of the cervix for these two periods of time. You can see that the final slope of the survival curve for low energy radiation is always greater than the slope of the normal population, so that in actual fact, patients were never cured by this type of radiation. Figure 2 shows that after the introduction of high energy radiotherapy, the survival is much greater and the final survival curve parallels the normal survival curve. Today, patients are actually cured by radiotherapy. Dr. Bush has done a cost benefit analysis on this problem, and has shown that if a woman's life is worth $205 a year, the whole of the high energy radiotherapy program can be paid for by the extra years of life given to the many women with cancer of the cervix. There can be no doubt today then, that high energy radiotherapy has had a major impact on cancer and we as physicists may take some of the credit. I am sure our next speaker, Dr. Powers, will also discuss this increased cure rate resulting from the use of high energy radiation.

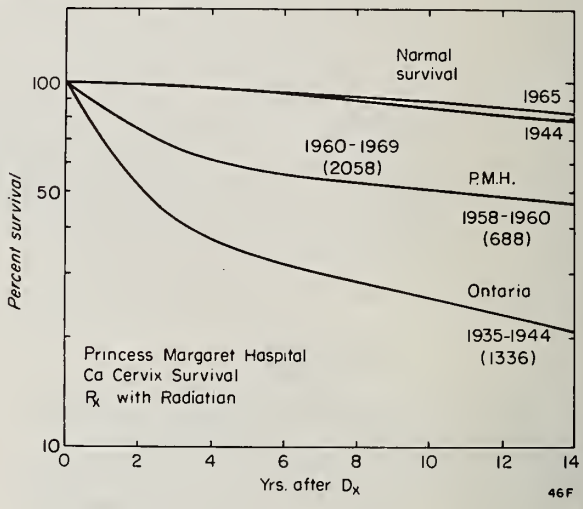

Fig. 2. Cure rate for cancer of the cervix in the era before and after the introduction of high energy radiation (Co-60, betatron or linac radiation) due to Bush[9].

Cobalt 60 Versus Betatron Radiation

During the last 30 years, there has been a continual improvement of cobalt units, linear accelerators and betatrons in the energy range 4-30 MeV, and the user today is forced to try and decide which machine should be purchased. Should it be a cobalt unit, a linac at 4 MeV, or 6 MeV, or 10 MeV, or should it be a higher energy linac or betatron in the 18-25 MeV range? Cobalt units are gradually being replaced by linacs - often for the wrong reasons (they are supposed to be a health hazard), while betatrons with their low output and small field sizes are gradually being replaced by linacs. Now, what photon energy is best? To my knowledge, there is only one controlled study which seriously attempts to answer this question. This is a study performed in our Institute by Dr. W.W. Allt[10], who carried out a random study on patients with advanced cancer of the cervix. He treated half the patients with our best technique using cobalt 60 and the other half using betatron radiation. Figure 3 shows the distribution obtained by these two machines. You can see that the dose in the region of the tumour can be made uniform and can be made to cover about the same area from both machines, but the dose in the regions near the skin are much higher with cobalt 60 than with betatron radiation.

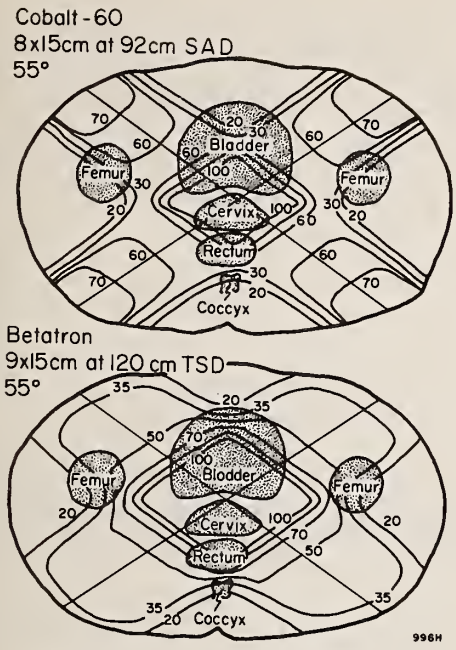

Fig. 3. Dose distributions in the controlled clinical study by Allt in the treatment of cancer of the cervix. Upper Co-60, lower betatron.

This random study suffered from a number of problems since there were differences in the number of fields per day, and the way patients were placed in the two beams. There were also differences in the absolute dosimetry of the two systems since this was in an era when it was exceedingly difficult to perform an absolute calibration of the betatron beam. In spite of these reservations, the differences in clinical results were spectacular, as shown in Figure 4. This figure is based on the original work of Allt[10], but updated by Bush[9], to cover a longer period of time following treatment. The figure shows that we get a gain in the 14 year survival from about 23% to 41%. The graph also shows that both beams in fact give cures since their final slopes are equivalent to the survival curves for normal populations.

The question arises then, why did we do better with high energy beam than with cobalt 60? This is a question which cannot be answered unequivocally, but I believe the differences in results are mainly due to the quite different dose patterns for the same dose to the tumor volume; the high energy beam deposits much less radiation in the normal tissue in the region between the skin and the tumour.

What Photon Energy Is Best?

We now turn to the vexing problem as to what photon energy is best. We know from our clinical experiment that our betatron operating in the photon mode at 22 MeV gave much better results than Co-60, but we do not know what clinical results would have been achieved had we used a

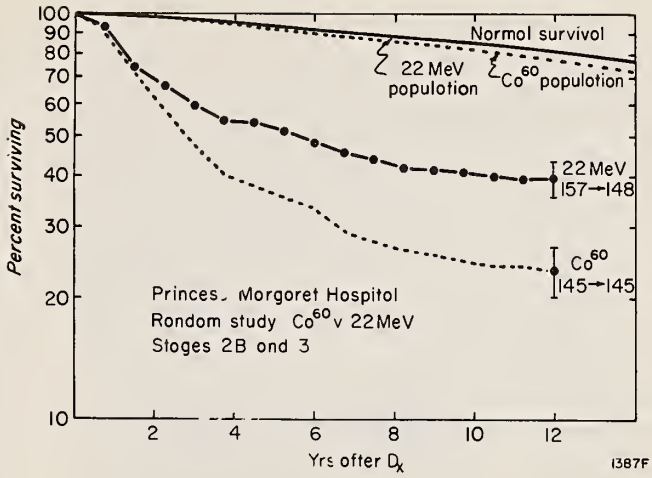

Fig. 4. Survival data for cancer of the cervix for the clinical random study by Allt[10], updated by Bush[9] to longer survival times.

10 MeV linac or an 8 MeV linac or a 6 MeV linac. This question can probably not be answered unequivocally, since it would be unethical to carry out such a clinical experiment today. In an attempt to answer this question we show Figure 5, which is the dose distribution when two opposing fields are applied to a patient 25 cm thick. The distribution obtained in our clinical study realiy involved two of these distributions nearly at right angles to one another. The graph shows that with 25 MeV radiation the dose rises from a small

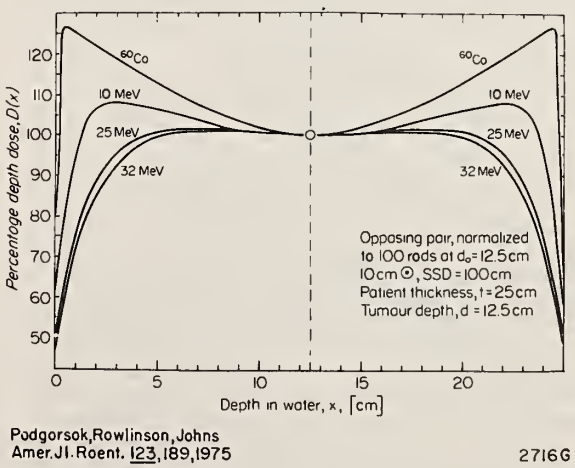

Fig. 5. Dose distribution for opposing pairs of fields treating a patient 25 cm thick. Distributions are given for cobalt 60, 10 MeV, 25 MeV, and 32 MeV beams. Data by Podgorsak, Rawlinson and Johns[11].

value at the skin surface to reach a constant value from a depth of 5 to 20 cm. In contrast, the cobalt beam contributes considerably more radiation to the region immediately under the skin surface, while 10 MeV is about half way between

the two. This would then suggest that 25 MeV is better than 10, which in turn is better than cobalt 60. It should be noted that increasing the photon energy above 25 MeV produces a minimal effect, and suggests that nothing is to be gained from a dose distribution point of view by using radiation of energy greater than 25 MeV. When one also realizes that the flattening of a high energy beam becomes increasingly more difficult as the energy is raised, and since the higher the energy the greater the neutron yield from the collimating system, there seems to be a good argument against using energy much above 25 MeV. We believe then, that a linac operating in the photon mode should operate in 20-25 MeV and that this is the optimum energy for the treatment of deep seated tumors. Because of this belief we are installing such machines in the six government operating clinics in the Ontario Cancer Treatment and Research Foundation. Lower energy machines such as Co-60 are still very useful for more superficial tumors such as those of the head and neck, and for much of the paliative work of a clinic.

Are linacs and Betatrons of the Same Energy Equivalent?

About 10 years ago, when we realized the clinical advantage of using a betatron over a cobalt unit, it was necessary to purchase a new therapy machine. We therefore looked for an accelerator which would have the distribution of a betatron but which would be capable of irradiating large fields at high output. We purchased a 35 M Varian linac. In the photon mode, this machine operates at 25 MeV. Much to our surprise, we found that it was equivalent to our betatron operating at 16 MeV, as illustrated in Figure 6[11]. Detailed investigations showed that the inferior dose distribution was mainly due to the use of a high atomic number flattening filter. We found that by using a lower atomic number target of aluminum and an aluminum flattening filter, the dose distribution could be made equivalent to that of the betatron as illustrated in Figure 7. The main factor responsible for the differences in the dose distribution is the material used in the flattening filter. The differences are due to the way the absorption coefficient varies with photon energy for materials of high, medium and low atomic number (see Fig. 8). Because pair production increases with increase in photon energy above the threshold at 1 MeV, high energy photons are more easily stopped in a material such as lead than are low energy ones. If a high atomic number material like lead or tungsten is used as the filter, it will preferentially remove the high energy photons from the beam. It would seem rather foolish to go to the trouble of producing high energy photons and then remove them by the flattening filter. These ideas were thoroughly discussed years ago[2,6], when betatrons were first put into operation. The reason for the use of high Z filters is the difficulty of getting the large filter of low Z material in the limited space which is available in the head of a linac. It is for this reason that manufacturers of linacs have refused to build flattening filters of the proper material. I am delighted to note, however that in the last year, Varian has investigated this problem and has shown how its old Clinac,

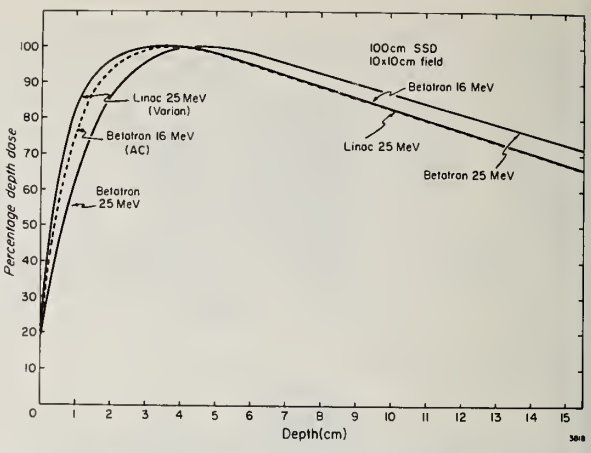

Fig. 6. Depth dose distribution for a betatron at 25 MeV and a betatron at 16 MeV. Taken from Podgorsak, Rawlinson and Johns[11].

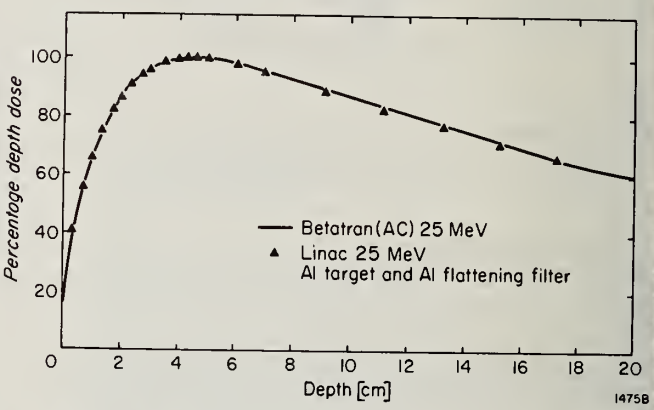

Fig. 7. Dose distribution for 25 MeV linac using an aluminum target and aluminum flattening filter compared to an Allis Chalmers Betatron both operating at 25 MeV. Data from reference 11.

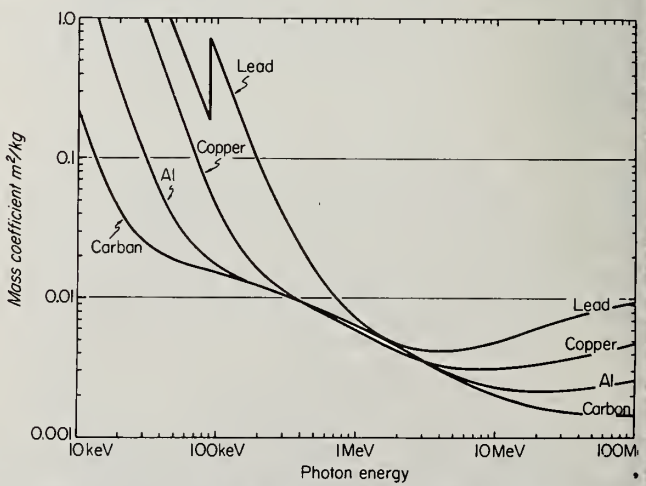

Fig. 8. Total attenuation coefficient in metres squared/kg for carbon, aluminum, copper, and lead as a function of photon energy.

such as the one we have in Toronto, can be improved to look like a betatron through the use of a medium atomic number filter. This is illustrated in Figure 9, taken from the work of McCall, McIntyre and Turnbull[13].

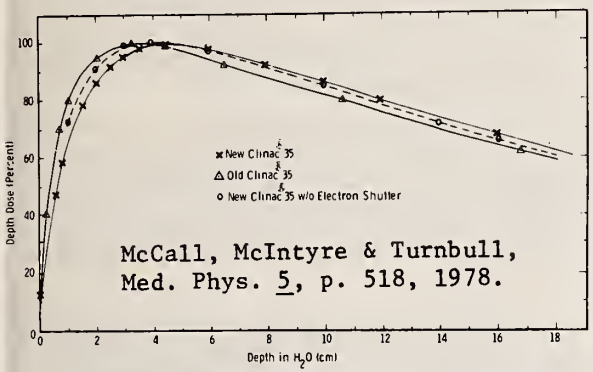

The depth dose curves for the old and new designs of the Clinac 35. The energy was 25 MeV, SSD of 100 cm, and 10 × 10-cm fields.

Fig. 9. Depth dose data for the old and new design of Varian Clinac 35[13].

Possible New Design for Linac Head

In designing the head, space is at a premium and it is very difficult to include in the design a flattening filter made of aluminum, or aluminum oxide or some other low atomic number material. We have studied this problem for the last year and Figures 10a and 10b show a possible way of overcoming this problem. Figure 10a shows the conventional way of putting all the components which are required into a linear accelerator head. Figure 10b shows how one can place the adjustable collimator in one plane and in this way save enough space so that a full size flattening filter of aluminum may be used. We are developing this collimator for use on our 35 MeV Varian linac. With it we hope that the depth dose distribution from the linear accelerator will be equivalent to our betatron. In my opinion, these problems which I have discussed are more important than designing a head with minimum leakage for neutrons. We really want a high energy photon beam which gives practically no dose on the surface of the skin and gives its maximum dose as far below the surface as possible.

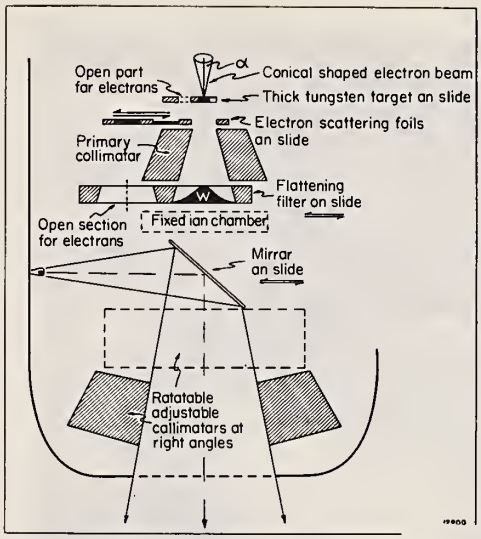

Fig. 10a. Schematic diagram to show the arrangement of the components in a conventional linac head.

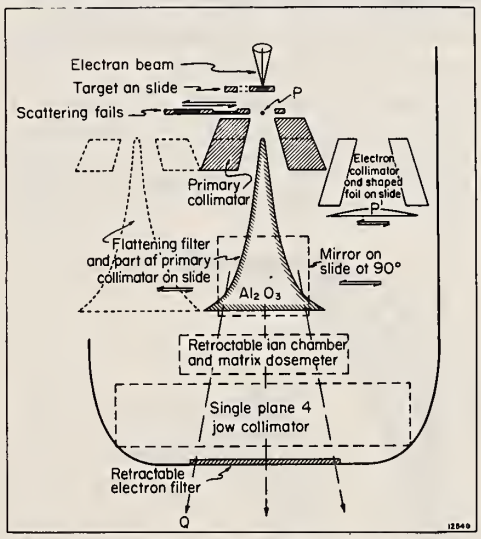

Fig. 10b. Schematic diagram showing arrangement of components to take an aluminum oxide flattening filter. The space is acquired by designing the collimator so that the four components move in one place on the surface of the spheres rather than in two planes in the conventional system.

Electron Contamination

Thirty years ago, the main emphasis in radiotherapy was in obtaining very small precisely determined fields. In recent years, radiotherapists have turned more and more to larger fields. An extreme example of this is illustrated in Fig. 11 and shows a cobalt 60 unit, which we have designed to treat half the body of the patient at one time[14]. This gives a very large field of 60 x 150 cm. In the head is a flattening filter to give a uniform dose in the midplane of a patient lying under this machine. This machine was developed for Dr. Fitzpatrick and Dr. Rider[15,16], who have now treated over 500 patients with half body irradiation. The patient is treated by two opposing pairs of fields, over half their body to a dose of about 800 rads in as short a time as possible, to avoid radiation sickness. Patients are then returned to the hospital about a month later, and the other half of their body is treated in the same manner. This has proved to be a good way to treat patients with multiple metastases, and some of our patients are alive five years after their first treatment. This is an example of an exceedingly large field, but very large fields are also being used in treating Hodgkins disease. When large fields are used the beam is often very badly contaminated with electrons. Figure 12 shows some curves taken with cobalt 60 and the effect of these low energy

Fig. 11. Photograph of half body irradiation at the Ontario Cancer Institute.

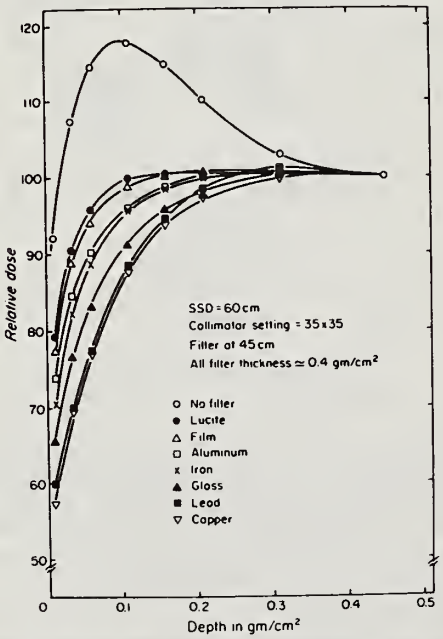

Fig. 12. Relative dose as a function of depth for a large field setting for a cobalt-60 unit. Curves are shown for different electron filters.[17]

electrons which completely destroy the build-up characteristics of the beam. I believe that agencies such as the Bureau of Radiation Health, and the manufacturers should spend far more effort in finding ways to remove the electrons from the beam so that pure photon beams may be used to treat patients than to worry unnecessarily about neutrons which may be present in the beam.

Problems for the Future

1. Removal of electron contamination

I believe we need to find ways to reduce electron contamination in high energy photon beams, especially for large fields. I would like to see some imaginative research using perhaps high magnetic fields, which might be switched on to remove these electrons from the beam.

2. Higher precision in dose delivery

With the introduction of CT scanning in many radiotherapy centres, we now have a method of assuring very accurate beam direction. In addition, the possibility of doing very precise dose calculations now exist. More careful work in this field is reqired.

Another aspect of the problem of precise dose delivery involves calibration procedures for high energy (6-25 MeV) machines. For years, these have been performed using a dosemeter calibrated at Co-60 energies but used at the higher energy. The user measures the "exposure" using the calibrated dosemeter and then multiplies the reading so obtained by agreed on factors, C_λ for photons and C_E for electrons (ICRU). He then applies numerous correction factors which are not universally accepted and are not accurately known to estimate the dose. This is an unsatisfactory situation since today we could do much better using a direct calibration of the machine, using a calorimeter. Laughlin's[19] group have long been involved in recommending such a procedure. Calorimeters of two types have been developed - those using tissue equivalent plastic (TEP) and those using pure graphite. With pure graphite Domen[18] at NBS has developed a beautiful system allowing a dose determination in graphite to 0.1%. The TEP calorimeter is of less precision because of the unknown amount of energy which produces chemical change in the plastic and so does not appear as heat.

The next step in dose calibration is more difficult. We require a transfer instrument (probably an ion chamber) which can measure the ratio of the dose in graphite (or TEP) to the dose in a water or tissue phantom at some reference point. Such a transfer instrument would be calibrated at the standardization laboratory in grays/meter reading in water (or tissue) using the calorimeter and then used in the field. Development of the best type of transfer instrument and the appropriate correction factors is required to enable us to go from the dose in a graphite (or TEP) calorimeter to the dose at a suitable reference point in the users water or tissue-like phantom.

I believe that if we solve some of the problems which I have summarized, that in ten yearts, we will find that we have made another leap forward in increasing the cure rate. To do this, however, we must pay a great deal of attention to detail, we must find ways to improve our beams and improve the precision with which the beams are administered to the patient. We should not become lost in regulatory arguments concerning allowed neutron fluxes. The important problem is the improvement of the beams for high energy machines.

References

[1] Energy absorption in human tissue by nuclear processes with high energy x-rays. R.J. Horsley, H.E. Johns and R.N.H. Haslam. Nucleonics 11, No. 2, 28-31 (1953).

[2] Use of a 23 MeV medical betatron. J.S. Laughlin. Nucleonics 8, No. 4, 5-16,(1951).

[3] Absolute determination of neutron flux produced by the interaction of high energy bremsstrahlung with tissue. M.A. Chaudhri, M. Pion, E. Miller, E. Muirhead, J. Rouse and B. Spicer. A.A.P.M. Workshop. Electron Linear Accelerators in Radiotherapy Workship, (1978).

[4] Techniques for application of the betatron to medical therapy. G.D. Adams, G.M. Almy, S.M. Dancoff, A.O. Hanson, D.W. Kerst, H.W. Koch, E.F. Lanzl, L.H. Lanzl, J.S. Laughlin, H. Quastler, D.E. Riesen, C.S. Robinson and L.S. Skaggs. Am. J. Roentgen. 60, No. 2, 153-157,(1948).

[5] Techniques for application of the betatron to medical therapy with report of one case. H. Quastler, G.D. Adams, G.M. Almy, S.M. Dancoff, A.O. Hanson, D.W. Kerst, H.W. Koch, L.H. Lanzl, J.S. Laughlin, D.E. Riesen, C.S. Robinson, Jr., V.T. Austin, T.G. Kerley, E. F. Lanzl, G.Y. McClure, E.A. Thomson, L.S. Skaggs. Am. J. Roentgen. 61, No. 5, 591-625, (1949).

[6] Depth dose data and isodose distributions for radiation from a 22 MeV betatron. H.E. Johns, E.K. Darby, R.N.H. Haslam, L. Katz, and E.L. Harrington. Am. J. Roentgen 62, 257,(1949).

[7] 1000 Curie cobalt unit for radiation therapy. I. The Saskatchewan Cobalt 60 Unit. H.E. Johns, L.M. Bates and T.A. Watson. Br. Jl. Radiol. 25, 296-302,(1952)

[8] II. Depth dose data and diaphragm design for the Saskatchewan 1000 curie cobalt unit. H.E. Johns, E.R. Epp, D.V. Cormack and S.O. Fedoruk. Br. Jl. Radiol. 25, 302-308 (1952).

[9] Malignancies of the overy, uterus and cervix. R.S. Bush. Edward Arnold Publishers, London, England,(1979).

[10] Supervoltage radiation treatment in advanced cancer of the uterine cervix. A preliminary report. W.E.C. Allt. Can. Med. Ass. J. 100 792-797 (1969).

[11] X-ray depth doses from linear accelerators in the energy range from 10 to 32 MeV. E.B. Podgorsak, J.A. Rawlinson and H.E. Johns. Am. J. Roentgen. 123, 182-191, (1975).

[12] Percentage depth dose for high energy x-ray beams in radiotherapy. J.A. Rawlinson, and H.E. Johns. Am. J. Roentgen. 118, 4, 919-922, (1973).

[13] Improvement of linear accelerator depth-dose curves. Richard C McCall, Raymond D. McIntyre, and William G. Turnbull, Med. Phys. 5, No. 6, 518-524 (1978).

[14] Cobalt-60 therapy unit for large field irradiation. H.E. Johns, W.D. Rider, H. Aget, P.M.K. Leunt, and H.P. Webb. In Press, Medical Physics. (1979).

[15] Half-body radiotherapy. Peter J. Fitzpatrick and W.D. Rider. Int. J. Radiation Oncology Biol. Phys. 1, 197-207, (1976).

[16] Half-body radiotherapy of advanced cancer. P.J. Fitzpatrick, and W.D. Rider. J. Can. Assn. Radiol. 27, No.2, 75-79, (1976).

[17] Use of electron filters to improve the buildup characteristics of large fields from Cobalt-60 beams. P.M.K. Leung, and H.E. Johns. Med. Phys. 4, No. 5, 441-444, (1977).

[18] A heat-loss compensated calorimeter: Theory, Design and Performance. S.R. Domen, and P.J. Lamperti. J. of Res. of the NBS A - Physics and Chemistry 78A, p. 595, No. 5, (1975).

[19] Calorimetric and ionometric dosimetry for cyclotron produced fast neutrons. J.C. McDonald, M.I. Chang, and J.S. Laughlin. Proc. 3rd Symposium on Neutron Dosimetry in Biol. and Med. (Ed. Burger, G., and Ebert, H.G.).

NBS SP 554 (1979)

USE OF HIGH ENERGY X RAYS IN CANCER CURE

W. E. Powers
Wayne State University School of Medicine
Detroit, MI 48201

The speaker did not submit either an abstract or written version of his talk for inclusion in the proceedings of this conference. For further information, contact the speaker directly.

SCATTERED RADIATION RELATIVE TO LEAKAGE RADIATION IN HIGH ENERGY X-RAY BEAMS

J. A. Rawlinson
Physics Division
Ontario Cancer Institute
Toronto, Ontario CANADA M4X 1K9

It has been common practice recently to limit the neutron leakage reaching the patient outside the useful beam to 0.1% in rems of the dose on the central axis. This value appears to be based on earlier recommendations regarding X-ray leakage. It is shown by comparison to the dose received by the patient due to photon scatter that this value is unnecessarily low.

(Dose, leakage, medical accelerator, neutrons, scatter, X-rays)

One of the purposes of this conference will be to consider the risk to the patient as a result of stray neutron radiation received by those parts of the patient outside the useful treatment beam. To reduce this risk to an acceptable level we must set limits to the maximum neutron leakage produced by medical electron accelerators. The purpose of this paper is to present some ideas which will help provide a more rational basis than hitherto for setting such neutron leakage levels.

Up to now the thinking about neutron leakage levels has been guided largely by earlier recommendations concerning X-ray leakage levels. For X-ray leakage present day regulatory practice appears to stem from the recommendations of ICRP Committee IV[1], recommendations made over 25 years ago. This committee specified that the radiation leakage through the permanent housing of X-ray therapy equipment should not exceed 0.1% of the dose rate on the central axis of the useful beam. At that time the recommendation was intended to apply to X-rays only. Equipment of the period could meet the requirement without undue difficulty. There was no problem.

More recently, however, in the case of high energy medical electron accelerators, the same 0.1% leakage requirement has been interpreted[2] as including neutrons as well as X-rays, with the leakage being expressed as a dose equivalent (in rems or sieverts). It is here that the problem arises for recent measurements have suggested that the neutron leakage in rems from present-day medical accelerators operating at high energies (20 MV and above) usually exceeds 0.1% and is typically 0.2%-0.5%[3-5]. Equipment manufacturers claim that considerable changes might be required in the design of medical accelerators if the new leakage requirement was to be met. Furthermore it is possible that such changes would seriously compromise the usefulness of these accelerators for their intended purpose, radiation therapy. We will hear more on these issues during the remainder of this conference.

In view of this debate it seems timely to reconsider the criteria on which to base leakage requirements. Does the original 0.1% leakage value for X-ray leakage really bear close scrutiny? It appears to us that, in fact, this value is rather lower than it need be.

To understand this, it must be borne in mind that a patient undergoing radiation therapy receives stray radiation not only from machine leakage but also by scattering from the useful beam. This situation is depicted in Figure 1. The scatter arises from the patient himself and also from the surfaces of the treatment room. The former component is absolutely unavoidable; it is an accepted consequence of his radiation treatment. The latter component, also, we can in practice do very little about. The two components together in effect form a lower limit to the dose received by the patient outside the useful beam. It seems unnecessary, therefore, to limit leakage radiation (whether it be X-rays or neutrons) to doses or dose equivalents much below those that the patient inevitably receives from scattered photon radiation.

The question then is, what is the magnitude of the scattered radiation in normal radiation therapy practice? Figure 1 illustrates how this can be determined. If a close-fitting insert of say 3 tenth value layers is fitted into the collimation system, we measure just the leakage radiation. If this value is subtracted from the dose measured for an open beam of the same field size, then we obtain the contribution due to scatter (or more precisely the component of the stray radiation arising from the useful beam).

Our measurements indicate that in normal radiation therapy practice the stray radiation due to scatter is much greater than presently allowed leakage radiation. Figure 2 shows the measured dose due to photon scatter received at points along the longitudinal axis of a long unit-density phantom of 20 x 30-cm^2 cross-section irradiated by a 30 x 30-cm^2 beam of 25-MV X-rays and a 30 x 30-cm^2 beam of ^{60}Co γ rays. The irradiation geometry is shown in the inset of the figure. Each point on the plot is the difference between the dose obtained with the collimator jaws open and the dose obtained with the useful beam blocked off. Measurements at points greater than 5 cm from the geometric edge were taken with a 3-cm^3 ion chamber in a Presdwood phantom; all other points were obtained with a 0.6-cm^3 ion chamber in a water phantom. The dashed curve in Figure 2

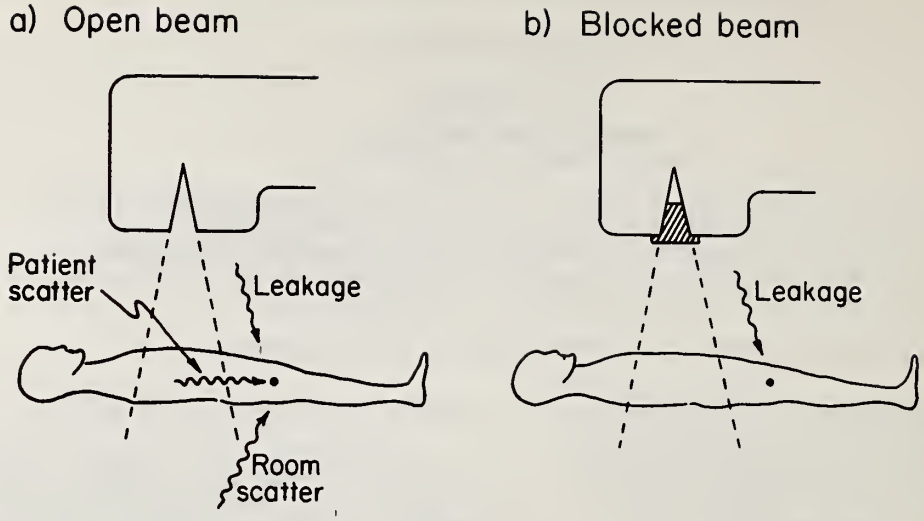

Figure 1 - Schematic illustration depicting the sources of stray radiation reaching a point in a patient outside the useful treatment beam. The stray radiation due to scatter can be obtained by subtracting the dose measured in b) from that measured in a).

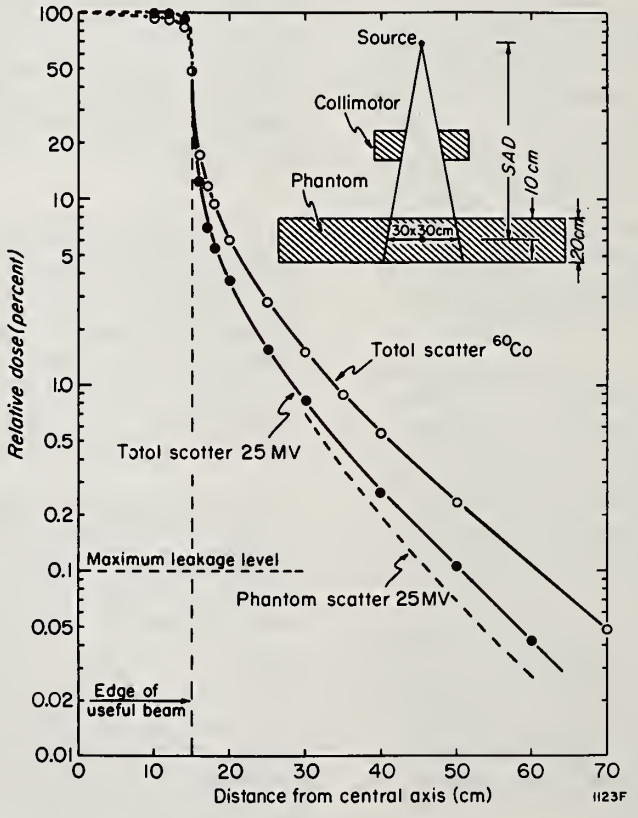

Figure 2 - Dose due to photon scatter along the longitudinal axis at depth 10 cm in a phantom irradiated by a 30 x 30-cm^2 beam. Open circles: ^{60}Co 80 cm SAD; closed circles: 25-MV X-rays 100 cm SAD. Doses are normalized to 100% on the central axis of the useful beam at depth 10 cm.

ENERGY IMPARTED TO A PHANTOM OF 20 x 30 CM^2 CROSS-SECTION AND MASS 70 KG FOR AN ABSORBED DOSE OF ONE GRAY DELIVERED TO THE CENTRE OF THE PHANTOM

	25 Mv x-rays (Varian Clinac-35) 30 x 30 cm^2 beam 100 cm SAD	^{60}Co γ-rays (AECL Theratron 780) 30 x 30 cm^2 beam 80 cm SAD
Energy Imparted within useful beam	16.2 joule	15.8 joule
Energy Imparted beyond useful beam due to scatter	1.39 joule	1.69 joule
Energy Imparted beyond useful beam due to 0.1% leakage	0.052 joule	0.061 joule
Ratio of scatter to leakage	27 : 1	28 : 1

1147F

Table 1

shows the contribution of the scatter arising from the phantom. It was separated from the total scatter using the method described by Karzmark[6].

It is evident from the figure that the scatter dose exceeds the allowed leakage dose up to a considerable distance from the central axis - approximately 50 cm for the 25-MV beam and 60 cm for the ^{60}Co beam. In any other irradiation condition, of course, the value will be greater or lesser depending primarily on the volume of medium irradiated.

An alternative way of assessing the relative importance of scatter and leakage is to compare the relative energy imparted to the phantom (integral dose) outside the useful beam. This calculation has been performed for the irradiation parameters of Fig. 2 and the results are shown in Table 1. In this table the useful beam is considered to be the volume bounded by the geometric edges of the beam and the edges of the phantom. Calculations within the useful beam and to 5 cm beyond the geometric edge were obtained by summation of dose values calculated at 1-cm intervals through the phantom. The dose values were calculated using the treatment-planning computer algorithms of Cunningham[7,8] with machine parameters selected to fit the experimental data. Calculations beyond 5 cm from the beam edge were made by direct summation of experimental scatter-dose values measured at 5-cm intervals through the phantom. For the leakage calculation it was assumed that the leakage dose was constant and equal to 0.1% of the dose on the central axis of a 10 x 10-cm^2 field at the depth of dose maximum.

It is seen from the table that the energy imparted outside the useful beam due to scatter is more than 20 times greater than the energy due to leakage. This is true for both the 25-MV beam and the ^{60}Co beam and therefore presumably for energies in between. The ratio will of course be less for smaller beams. Yet, even for a small beam (10 x 10 cm^2) directed at one end of the phantom, similar calculations show that the scatter energy imparted is more than five times greater than the allowed leakage. In short, in conventional radiation therapy practice, patient dose from scattered radiation is much larger than that from leakage.

It can be concluded from this that existing maximum leakage levels could be increased substantially. If it is indeed true that there are real difficulties in having present equipment meet the 0.1% leakage requirements than we would recommend that the leakage requirements be relaxed somewhat (by perhaps a factor of 5). No significant additional risk to the patient would result.

References

[1] Report of Committee IV (1953-1959) on Protection Against Electromagnetic Radiation Above 3 MeV and Electrons, Neutrons and

Protons. ICRP Publ. No. 4 (Pergamon, Oxford, 1964).

[2] Suggested State Regulations for Control of Radiation Section F9 - X-Ray and Electron Therapy Systems (1 MeV and above), revised draft (U.S. DHEW, Washington, DC. 1976).

[3] E. J. Axton and A. G. Bardell, Phys. Med. Biol. 17, 293 (1972).

[4] R. M. Wilenzick, P. R. Almond, G. D. Oliver, and C. E. DeAlmeida, Phys. Med. Biol. 18, 396 (1973).

[5] G. D. Oliver, J. A. Rawlinson, and R. Cox, AAPM Q. Bull., p. 97 (June 1973) (abstract).

[6] C. J. Karzmark and T. Capone, Br. J. Radiol. 41, 222 (1968).

[7] J. R. Cunningham, Phys. Med. Biol. 17, 42 (1972).

[8] J. R. Cunningham, Phys. Can. 25, 23 (1969) (abstract).

INTERNATIONAL STANDARDS FOR MEDICAL ACCELERATORS

G R Higson

Department of Health & Social Security
London, England

The International Electro-technical Commission is engaged in a major programme for the development of standards for medical electrical equipment. A standard for the radiation safety of electron medical accelerators will soon be published. The main features of this standard are described and some of the background to them is discussed.

(Accelerators; IEC; interlocks; leakage; radiation; safety; standards)

Introduction

The International Electro-technical Commission (IEC) is the major international standardisation body for electrical equipment. It was formed in 1906 and has since become the electrical counterpart of the International Organisation for Standardisation (ISO) and 41 countries are members.

In 1968 a Technical Committee (IEC TC 62) on Electrical Equipment in Medical Practice was created "to prepare international recommendations concerning the manufacture, installation and application of electrical equipment in medical practice". This Committee now covers a wide variety of medical electrical equipment through 4 sub-committees and 24 working groups.

Working Group 1 of Sub-Committee 62C (Beam Teletherapy and Particle Accelerators) started work in 1972 and was given as its first task the production of a comprehensive standard covering all aspects of medical electron accelerators, their accessories and buildings. Work is in hand on 4 parts of this comprehensive standard: General Requirements; Radiation Safety; Electrical and Mechanical Safety, and Performance. Parts 1 and 2 are now in the final processes of publication and I hope will become available towards the end of this year. It has taken a long time to produce this standard but it must be remembered that the protocol of the IEC depends not only on reaching agreement in committee but on obtaining a concensus of agreement from the member countries and the document containing Parts 1 and 2 has been circulated to National Committees 3 times: In 1974 as a draft for discussion;[1] in 1975 as a draft for views on its acceptability;[2] and in 1976 for voting under the Six Months Rule[3] and in 1977 some modifications to the final document were circulated for voting under the Two Months Procedure[4].

In discussing the radiation safety requirements specified in this document it is important to emphasise that it does not attempt to desoribe the optimum conditions of an accelerator for giving radiotherapy treatment. This description is contained in Part 4 - Performance - which is currently in draft. Rather it describes certain essential safety provisions and such levels of performance beyond which the equipment is positively unsafe.

Dose Monitoring

There must be two independent dose monitoring systems either of which will shut down the accelerator when a pre-set value is reached. Both the dose monitoring systems must work correctly and consistently at dose rates up to twice the maximum specified for the equipment. If that level is reached a separate dose rate monitoring system must shut down the equipment. In the event of a mains power failure information about the dose given must be held for at least twenty minutes in such a way that it can be retrieved.

Some rather crude checking of the dose distribution is required by a system which will stop the irradiation if the measured distribution changes by more than 20% as such a change will indicate a major failure e g in the beam control system or in the filtering.

If irradiation is stopped for any reason other than the primary dose monitoring system reaching the pre-set value, then a warning signal must be given at the control panel. If, as will be expected, the irradiation is stopped by the primary system working correctly, then the other dose monitoring system must be checked for correct functioning before the next treatment can be started.

A timer may be fitted as an optional back-up to the dose monitoring systems but, if it is, it must comply with requirements analogous to those for the dose monitoring systems.

Radiation Type

If the accelerator is capable of both electron and X-ray treatment then the radiation type must be selected at the control panel before irradiation is possible. If actions have to be carried out in the treatment room (e g replacing a target by a scattering foil) in order to change the radiation type, then radiation must be

prevented if the actions at the control panel and in the treatment room do not agree and furthermore no display of the selected type must be given until all these selection operations have been completed and are in agreement.

Selection of Other Operating Conditions

There are analogous provisions for the selection of energy, stationary or moving-beam therapy, field flattening or beam scattering filters, wedge filters and applicators. Specific requirements are added according to the particular operating condition e g systems to check that filters are properly inserted in the equipment, that the equipment moves during moving-beam therapy and remains stationary during stationary-beam therapy and that the electron beam energy does not vary by more than 20% from the selected value.

In the case of scanned-beam accelerators the scanning control signals must be monitored to ensure that they remain within the manufacturer's specified limits.

This combination of checking and interlock systems has been criticised for its complexity and the corresponding increased cost of accelerators but, in fact, almost all of these systems are in use to varying degrees on accelerators being used today and the IEC document is regarded by its originators as simply combining the best features of existing equipment rather than as breaking new ground.

Contamination of the Treatment Beam

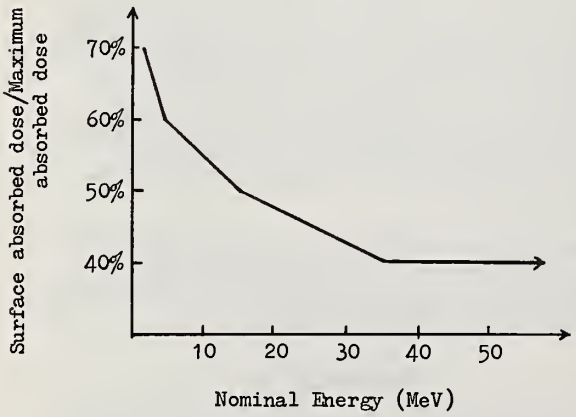

Figure 1: Limits of absorbed dose at the surface during X-irradiation

Permissible limits of contamination of an X-ray beam by electrons and an electron beam by X-rays are shown in Figures 1 and 2. These figures

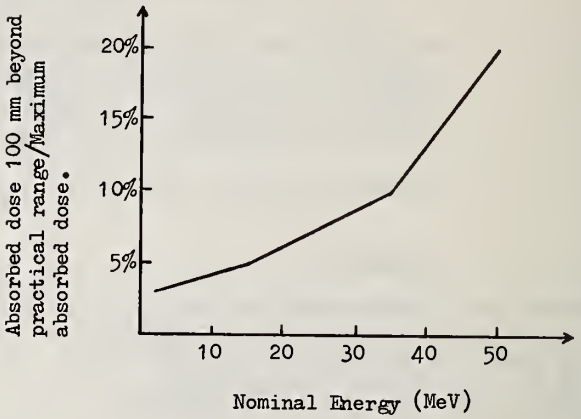

Figure 2: Limits of stray X-radiation during electron irradiation

were originally derived from the German standard DIN 6847[5] and the limits for X-ray contamination of an electron beam agree with that standard. Those for electron contamination of an X-ray beam are more severe than DIN 6847. No limit is set for neutron contamination of an X-ray beam but the manufacturer is required to measure it and to declare the level to the purchaser.

Leakage Radiation

When we first considered the subject of leakage radiation we turned naturally to ICRP 15 with the intention of simply referring to the levels quoted in that document. However, consideration of ICRP 15 led to the conclusion that that document was rather inappropriate for modern accelerators capable of large field sizes. Eventually a more complex specification was produced which is largely based on the idea of giving special care to the unwanted radiation arising over a plane of 2 metres radius in which the patient might be found and relaxing a little outside this area.

The permissible leakage through the diaphragms may be 2% of the Central Axis Dose - as permitted by ICRP 15 - for equipment with a maximum field size up to 22 x 22 cms. For accelerators with maximum field sizes larger than this the permissible leakage through the diaphragms is reduced in accordance with a formula which keeps the leakage dose-area product constant. The effect of this is shown in Figure 3 and it will be seen, for instance, that an accelerator capable of a maximum field of 40 x 40 cms must have diaphragms which permit leakage no more than 0.6% of the Central Axis Dose.

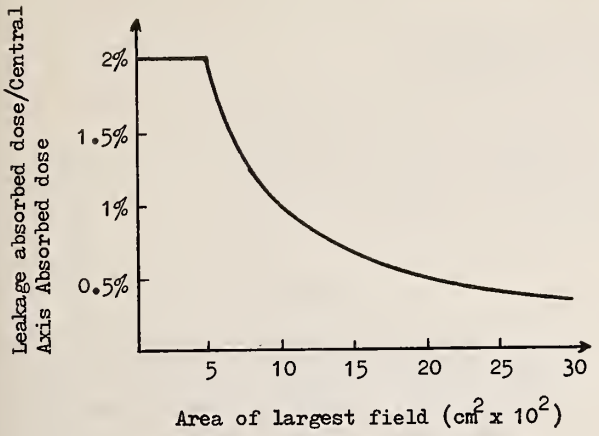

Figure 3: Leakage radiation through beam limiting devices

The structure outside the diaphragms must not allow leakage radiation over the 2 metre radius "patient plane" to exceed an average of 0.1% (ICRP value) of the Central Axis Dose although individual areas up to 100 cm^2 may rise to 0.2%. In the area outside the "patient plane" leakage radiation must be restricted to 0.5% of the Central Axis Dose at 1 metre from the path of the electron beam. Although this leakage level represents a considerable relaxation on ICRP 15 the disposition of the protected region introduces an important new concept.

The logic of this approach is that in the area outside the patient plane, the main consideration is the protection of persons outside the treatment room. This relaxation of the ICRP figure requires the addition of a few inches of concrete to the treatment room walls and is considered to be more cost-effective than building more absorption into the accelerator structure.

These concepts, and figures, have been discussed with the ICRP Committee 3 during the years of development of the IEC standard. No objections have been raised by ICRP although that must not be taken as implying that the ICRP are in any way supporting the values given in the IEC standard. ICRP are now preparing to revise ICRP Publications numbers 15 and 22 and it is our hope that there will be no clash between ICRP recommendations and IEC standards.

Neutron Leakage

The setting of standards for neutron leakage posed particular difficulties both because of the absence of authoritative recommendations and the shortage of reliable data about the characteristics of existing accelerators. It was uncertain whether the 0.1% limit suggested in ICRP 15 was intended to apply to accelerators and whether it was intended to include a neutron component but paragraph 1.3.5 of ICRP 15 states "in the application of new techniques or equipment, e g neutron therapy, this requirement may not be practicable". The Committee were inclined to interpret this as less than mandatory but, in attempting to keep as close as possible to ICRP recommendations, the first draft standard contained the requirements that neutron leakage "should not exceed 0.01% (of the Central Axis Dose at the same distance) and shall not exceed 0.02%". (These figures are in rads).

When this draft was circulated comments were received from many National Committees, including the USA, that the limit of 0.02% was impractical. The results of Axton and Bardell[6] and Wilenzick et al[7] showed that neutron leakage doses could vary from 0.015 - 0.08% of the Central Axis Dose. Figures of the same order were later published by other workers. Consideration of these results led eventually to the present formulation that over the 2 metre radius patient plane the average dose for neutron leakage shall not exceed 0.02% of the Central Axis Dose at the same distance and the maximum dose in the patient plane shall not exceed 0.05% thus allowing for the relatively high values at the edge of the useful field. This formulation calls for all accelerators to achieve the performance currently achieved by the best available accelerators but no logical argument could be found for requesting a lower value of leakage. An average leakage of 0.02% implies that a patient receiving a therapy dose of 6,000 rads would experience a whole body neutron dose of 1.2 rads, or 12 rems assuming an RBE of 10. This value can hardly be considered as excessive for a patient undergoing therapy treatment and consideration of the practical difficulties in patient treatment that would result from the addition of sufficient neutron shielding to reduce these values significantly led the Committee to confirm these values which were accepted in the last circulation of the document to National Committees.

In our view there is no case for pressing for more severe standards than these in the present state of knowledge. If all accelerators to be produced in future can meet all the requirements contained in this standard the already very small risks to patients resulting from treatment by radiotherapy equipment will be reduced yet further without making severe demands on new technology or novelty in design. Almost every feature called for in this standard has been shown to be practicable at reasonable cost and the aim of incorporating all the best features currently available on individual machines on all accelerators is regarded as a cost-effective approach to improving the quality of electrical equipment used in medicine.

References

(1) Medical Electron Accelerators in the Range 1 - 50 MeV. Section One: General. Section Two: Safety Requirements for Equipment (Manufacturer). 62C (Secretariat)3. International Electro-technical Commission, Geneva (June 1974).

(2) Medical Electron Accelerators in the Range 1 - 50 MeV. Section One: General. Section Two: Safety Requirements for Equipment (Manufacturer). 62C (Secretariat)7. International Electro-technical Commission, Geneva (September 1975).

(3) Medical Electron Accelerators in the Range 1 - 50 MeV. Section One: General. Section Two: Safety Requirements for Equipment (Manufacturer). 62C (Central Office)4. International Electro-technical Commission, Geneva (November 1976).

(4) Amendments to Document 62C (Central Office)4: Medical Electron Accelerators in the Range 1 - 50 MeV. Section One: General. Section Two: Safety Requirements for Equipment (Manufacturer), 62C (Central Office)8. International Electro-technical Commission, Geneva (May 1978).

(5) Draft Revision of DIN 6847, Medical Electron Accelerators: Radiation Protection Rules for Manufacturers. Deutches Institut fur Normung, Berlin, (1975).

(6) Neutron Protection from Electron Accelerators used for Medical Purposes. E J Axton and A G Bardell. Phys Med Biol 17, 293 (1972).

(7) Measurement of Fast Neutrons Produced by High Energy X-ray beams of Medical Electron Accelerators. R M Wilenzick, P R Almond, G D Oliver and C E De Almeida. Phys Med Biol 18, 3, 396-408 (1973).

STATE REGULATIONS FOR MEDICAL ACCELERATORS

C.H. Smith
Oklahoma State Department of Health
Oklahoma City, Oklahoma 73152

The "Suggested State Regulations for the Control of Radiation" includes a section regarding medical accelerators. The provisions of that section are reviewed.

(Regulations, SSRCR, Accelerators, Leakage Radiation, State)

Introduction

State radiation control agencies have a need for comprehensive regulations regarding the use of ionizing radiation. Those regulations need to cover all types of radiation sources and be compatible with regulations of federal agencies functioning in radiation control.

These regulations also need to be reasonably uniform from state to state to allow industry to function on a national scale.

The "Suggested State Regulations for the Control of Radiation" (SSRCR) are written to be used by the individual state agencies when radiation control regulations are being promulgated.

The Suggested State Regulations for the Control of Radiation does contain a section regarding medical accelerators which will be used by many state radiation control programs as the basis of constructing regulations regarding medical accelerators which will be effective in their jurisdiction.

Background of the SSRCR

State radiation statutory authority is generally written to cover all sources of ionizing radiation. This wide authority is not duplicated at the federal level. To be utilized as a model the SSRCR must cover all sources except those over which the NRC retains authority even in "agreement states", e.g. nuclear power plants, be compatible with existing regulations of several federal agencies, and recommendations of nationally or internationally recognized authorities.

The SSRCR can serve only as a reference when state agencies are writing or revamping their regulations. Program goals, legal requirements, and fiscal restrictions within an individual state make it such that there may never be an absolutely uniform set of regulations regarding ionizing radiation across the United States. However, the difficulty of writing regulations is such, that individual authorities will probably prefer to use or shape the model regulations for their own state regulations. But no state authority is obligated to adopt any portion of the SSRCR.

Currently the various parts of the SSRCR which regard different types of radiation sources or particular uses of radiation sources are written or updated by working groups, appointed by the Conference of Radiation Program Directors from members of that conference. Federal representatives also serve on each working group.

The current 1978 edition has just been published and was prepared by the Conference of Radiation Control Program Directors, the FDA/Bureau of Radiological Health, the U.S. Nuclear Regulatory Commission, and the Environmental Protection Agency, and the Public Health Service.

The SSRCR was first published in 1962 by the Council of State Governments with the assistance of the U.S. Public Health Service and the U.S. Atomic Energy Commission.

The original version was intended to provide for the control of all sources of radiation and did include a part regarding the use of x-rays in the healing arts.

The SSRCR was updated in 1964 and 1966 to maintain compatibility with the U.S. Atomic Energy Commission regulations. The 1970 edition among other changes, modified the part regarding the use of x-ray in the healing arts to reflect recommendations made by the NCRP Report #33.

The 1974 edition of the SSRCR included new parts regarding instruction to workers, analytical x-ray equipment, and particle accelerators. A rationale for changes was added as part of the format. The part regarding the use of x-rays in the healing arts was given a total rewrite.

One of the reasons for that rewrite was the federal diagnostic x-ray standard which was published in 1972. Section 360F of PL 90-602, The Radiation Control Health and Safety Act of 1968, requires that if a standard has been established by the federal government regarding electronic product radiation that "no state or political subdivision of a state shall have any authority either to establish or to continue in effect any standard which is applicable to the same aspect of performance of such product and which is not identical to the federal standard."

The 1978 edition of the SSRCR which should be generally available shortly, includes a section directed toward medical accelerators and a rewritten section regarding lower energy therapy units.

Accelerator Regulations

The original version of the SSRCR contained a section which stated requirements for therapeutic x-ray installations. This section was maintained in later editions with few changes. The requirements stated were largely directed toward the 250 kVp units which were being replaced by the cobalt teletherapy units in radiation therapy applications at that time.

With the emergence of the high energy accelerator units it became apparent that the requirements as written in 1962 needed revision to provide adequate safety measures for accelerators.

When the working group assigned responsibility for writing the portion of the SSRCR assembled its materials and references, the existence of an excellent document, which was still in draft form, produced by the International Electrotechnical Commission was noted. That document, as well as recommendations made by the National Council on Radiation Protection and Measurements, the American Association of Physicists in Medicine and individual comments, were used as the basis of the SSRCR section regarding medical accelerators.

The final version of the SSRCR accelerator requirements differentiates between new equipment and existing equipment using a date included in the definitions. The date was given a special notation indicating to the reviewing agency that the implications of including the SSRCR date within their regulations should be carefully considered.

The SSRCR accelerator regulations, if adopted and placed into effect by an individual state, may require a given amount of backfitting on accelerators. During the construction of the model, consideration was given to the cost and practicality of providing a particular safety feature on an accelerator where that safety feature was not part of the original accelerator design versus the additional safety which would be provided by the feature.

Provisions of SSRCR Accelerator Regulations

Leakage Radiation to the Patient Area.

It became apparent very early in the groups discussions that any criteria written regarding accelerator leakage radiation was going to be controversial. Many conflicting opinions regarding leakage radiation were received by the group during the time that the model was being written.

The provision regarding leakage radiation is stated in terms of new equipment (defined as equipment manufactured after August 1, 1980) and existing equipment (defined as equipment manufactured on or before August 1, 1980.)

The requirement for new equipment is stated as 0.1% of the useful beam in the patient plane outside of the useful beam and includes the neutron component as part of the leakage radiation.

It was recognized that some currently produced high energy accelerators cannot meet that standard, but the group was of the opinion that a more lenient standard could not be stated until the ICRP or the NCRP took such a position. It was concluded that the 0.1% criteria as stated in ICRP Report Number 15, 1969, should be retained for new equipment.

The requirement for existing equipment is stated as 0.1% of the useful beam but excluded the neutron component from being considered as part of the leakage radiation.

The criterias are stated in terms of rems rather than rads. Another part of the SSRCR contains a conversion table for neutron flux equivalents. That table is identical to that found in 10CFR Part 20 of the Nuclear Regulatory Commission Regulations.

The patient plane concept which is utilized wao taken from the IEC draft.

Leakage Radiation Outside the Patient Area

The criteria stated in this section of 0.1% of the useful beam for x-ray leakage and 0.5% for neutron leakage can be met by current units and the figures are included to give a base facility shielding design.

A criteria of 2% transmission through the beam limiting device is stated. Previous versions of the SSRCR had stated 5%. The ICRP Committee 3 noted the inadequacy of the 5% criteria.

Beam Monitors. The requirement is written in of new equipment and existing equipment. New equipment is required to have two useful beam monitoring systems. Existing equipment is required to have one monitoring system.

Termination of Irradiation by the Dose Monitoring System. The requirement is similar to IEC recommendations but differs in that a secondary system is required to terminate irradiation when 102% of the pre-set dose monitor units has been reached rather than 115%.

Timer. A timer is required for both new and existing units. It differs from the IEC draft where a timer is suggested but not required.

Absorbed Dose Rate. Parallels IEC draft recommendations. A portion of the last IEC draft regarding a device to terminate irradiation if the dose rate exceeds 10 times maximum was not incorporated.

Surveys. A review of all new or significantly revised facilities is required to be performed by a qualified expert.

Other Requirements. Many parrallel and are similar in language to the IEC draft requirements. These include requirements for filters, beam quality, beam symmetry, selection of display of dose monitor units, termination of radiation, interruption switches, termination switches, selection of radiation type, selection of treatment mode, location of focal spot and beam orientation, and system checking facilities.

Calibrations. Semi-annual calibrations are required and are to be performed by or under the direct supervision of a qualified expert using instrumentation traceable to a national standard.

Spot Checks. The spot check procedures are required to be developed by a qualified expert but not necessarily performed by that person. The procedures must state the time intervals at which the spot checks must be performed.

Operating Procedures.

Compliance and Enforcement

The model does specify some conditions under which some measurements will be made, but in general, the method of demonstrating compliance is left to the registrant.

The language used permits the use of manufacturer furnished data to demonstrate compliance with some measurements which may be difficult to perform at an individual facility, e.g. neutron leakage to the patient plane.

Administrative procedures will vary from state to state regarding inspection frequency and records to be maintained for an individual facility. The facility may be asked to submit plans prior to initiating installation or may be asked to demonstrate compliance to all parts of that states regulations prior to initiating patient treatment.

Future Accelerator Regulations

The format of the SSRCR and the procedures which have been arranged will allow a frequent updating of the model. Comments which you may have regarding any provision of the SSRCR, particularly the portion regarding accelerators, may place such comment with the FDA/Bureau of Radiological Health, Rockville, Maryland 20857.

If the FDA/Bureau of Radiological Health does place into effect regulations regarding accelerators it may require that the current SSRCR provisions be revised, if requirements regarding the same aspect of performance are stated which are significantly different from those stated in the SSRCR.

NBS SP 554 (1979)

THE RBE OF NEUTRONS

Harald H. Rossi
Radiological Research Laboratory
Department of Radiology
Cancer Center/Institute of Cancer Research
Columbia University College of Physicians & Surgeons
New York, New York 10032

The RBE of neutrons is not only a function of energy but more importantly a function of absorbed dose. A combination of experimental and theoretical findings permits at least a fair estimate of the dependence of neutron RBE on both of these factors. It would appear that in radiotherapy with high voltage electron accelerators neutrons have a minimal biological effect on the treatment volume but that they may be an important and perhaps a biologically dominant factor in leakage radiation.

(Neutrons, radiotherapy, RBE)

In efforts to obtain a better insight into the action of ionizing radiations, biological systems have very often been irradiated under varying conditions. Perhaps the most important physical aspects altered in such experiments have been the temporal and the spatial distributions of radiation energy. Obviously the interpretation of the results obtained requires an understanding of the physical change involved. This is rather trivial in the case of temporal changes but far from simple in the case of the spatial ones. In fact some theories of the biological action of radiation have been proposed that imply impossible energy distributions in the irradiated cell.

The principal factor in considerations relating to spatial energy distributions in irradiated tissues is the difference between the absorbed dose, D, i.e., the average value of the quotient of energy and the mass in which it is deposited, and the specific energy, z, which is the actual value of this quotient in regions of specified dimensions. If these regions and/or the absorbed dose are so large that the dose is imparted by many charged particles the difference between z and D is small. However, if fewer particles are involved statistical fluctuations become increasingly significant. In the extreme case, when the mean number of particles is much less than one, there is usually no energy deposited but in those cases when $\bar{z}$ is not zero it is generally much larger than D, and its magnitude is independent of D. In this condition D merely determines the fraction of the regions that receive energy.

For regions of given dimensions the absorbed doses for which single particle action predominates depend on particle LET or, more generally, on radiation quality. Evidently single particle action obtains when D is much less than $\bar{z}_1$, the average specific energy due to one particle (or more accurately due to one event, i.e., the appearance of one particle or of several correlated particles). Taking the nucleus of the typical mammalian cell to have a diameter of 5 μm, it receives a $\bar{z}_1$ from the electrons secondary to hard gamma radiation that is about 4 mGy (0.4 rad). On the other hand $\bar{z}_1$ for the secondaries of typical fission neutrons is of the order of 400 mGy (40 rad). As will be shown the region in which energy concentration is critical is smaller than the nucleus being only about 1 μm in diameter. For such regions $\bar{z}_1$ is about 100 mGy (10 rad) for gamma rays and 10 Gy (1000 rad) for fission neutrons. It is difficult (although not impossible) to observe the effects of 100 mGy of gamma radiation on mammalian systems. On the other hand a neutron dose of 10 Gy produces such extensive and complex damage that most significant research is carried out at lower doses. Thus mammalian radiobiology generally involves multiple event action in γ or x irradiations and single event action in irradiations by neutrons having energies of the order of 1 MeV.

One reason for this is that in addition to greatly different event frequencies there is a well established difference in biological effectiveness which for somatic effects on higher organisms is invariably higher for neutrons. This in turn indicates that in general the biological effectiveness of radiation increases more than proportionately with specific energy. There can be little doubt that the dependence is at least very largely one on the square of the specific energy. This is indicated by the general dependence of RBE on absorbed dose.

As shown in Fig. 1 the relation between the logarithm of RBE and the logarithm of the neutron absorbed dose, D_N, is a line of slope -1/2 over the range from a few gray to a few milligray. Since this is clearly in the range of single particle action, ε, the fraction of cells showing any type of effect, must be proportional to the absorbed dose since the latter is proportional to the frequency with which energy of any magnitude is deposited in cells. Thus,

$$\varepsilon = K D_N \qquad (1)$$

On the other hand the RBE ($=D_x/D_N$) is according to Fig. 1 related to D_N by:

$$\log(D_x/D_N) = \log C - 1/2 \log D_N \quad (2)$$

or

$$D_x/D_N = C/\sqrt{D_N} \quad (3)$$

Combining (1) and (3):

$$\varepsilon = KC^2 D_x^2$$

where C is another constant which for the fission and 0.43 MeV neutrons in Fig. 1 is about 4.5 with absorbed doses expressed in Gy. Relation (2) applies to low LET doses that are so large that specific energies do not differ substantially from them in domains larger than a fraction of a micrometer. Although these considerations only show a dependence on z^2 for low LET radiation it seems reasonable to assume the same dependence for high LET radiation particularly since observations at intermediate LET are also consistent with a z^2 dependence.

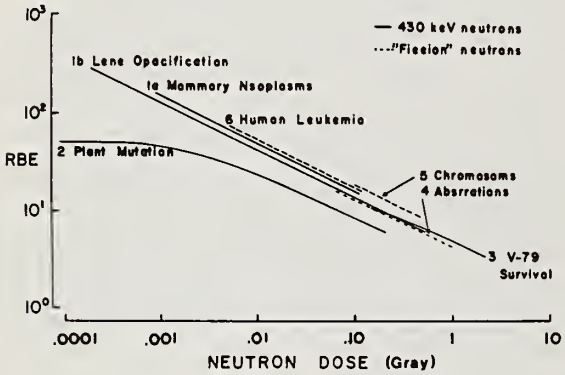

Fig. 1 - Logarithmic plot of the RBE of low energy neutrons vs. neutron dose.
1a: Shellabarger et al.[1]
1b: Bateman et al.[2]
2: Sparrow et al.[3]
3: Hall et al.[4]
4: Biola et al.[5]
5: Awa[6]
6: Rossi[7]

The quadratic dependence of biological effect on specific energy is one of the basic tenets of the theory of dual radiation action.[8] The other tenet derived from a detailed analysis of the relations shown in Fig. 1 is that the average diameter of the subnuclear volume in which the specific energy is pertinent is about 1 μm.

The theory postulates that the lesions responsible for radiation injury are due to the combinations of pairs of sublesions. In the site approximation the latter are assumed to be produced at a rate that is proportional to the specific energy in the site in which they combine at a rate that does not depend on their separation. If a correction is applied for saturation at high values of z one obtains a relation between neutron energy and RBE (Fig. 2) that is in general agreement with observations (Fig. 3).

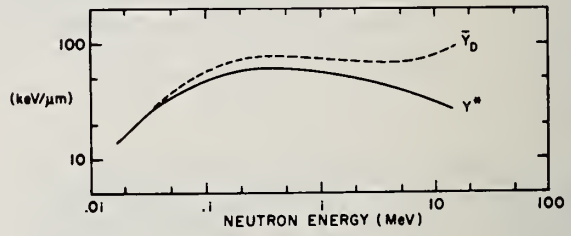

Fig. 2 - Theoretical relation between $\bar{y}_D$, the dose mean lineal energy, and neutron energy. y* is the value of $\bar{y}_D$ corrected for saturation. According to theory the RBE should be proportional to y*.[8]

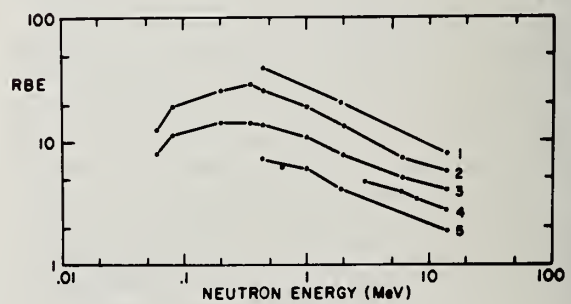

Fig. 3 - Observed dependence of RBE on neutron energy.
1: Lens opacification at x-ray dose 40 rad (Bateman et al.)[2]
2,3: 50% growth reduction of Vicia Faba (anoxic and oxygenated) (Hall et al.)[4]
4: Cellular inactivation (initial part of the survival curves) (Barendsen)[9]
5: 37% depletion of spermatogonia (Bateman)[10]

The curves in Fig. 3 refer to various kinds of effect at selected levels of effect. At the same absorbed doses there is frequently not a strong dependence of RBE on effect as indicated in Fig. 1. Thus for many effects a fair approximation to the RBE of neutrons relative to x-rays can be derived by determining from Fig. 3 the RBE for the neutron energy of interest relative to that of 0.5 MeV neutrons, dividing the absorbed dose of interest by this RBE and noting in Fig. 1 the RBE corresponding to this (equivalent) dose of 0.5 MeV neutrons.

Recent research has indicated that the site model is an approxmation of limited accuracy. In particular the molecular ion experiment[11] has shown that the distance of about 1 μm is the mean of a highly skewed distribution with about half of the interactions taking place at separations that are at least 10 times smaller and the remainder probably occurring throughout the nucleus. A recently published generalization of the theory[12] takes account of this complication but does not permit an accurate numerical determination of neutron RBE since this requires the knowledge of presently unknown parameters.

A factor that may be related to differences in the distribution of separations is the fact that the maximum RBE values at low doses vary between effects. As shown in Fig. 1 the RBE of neutrons having energies of the order of 0.5 MeV reaches a maximum of about 50 for a somatic mutation while for at least two effects it exceeds more than 100. On the other hand the maximum RBE for the killing of cells in tissue culture is unlikely to exceed 30 and there is one *in vivo* effect[13] for which it differs little from 1.

Thus, the above conclusions on the RBE of neutrons are general but may not fit specific cases. However it is clear that in the great majority of instances the neutron RBE increases with decreasing dose and that it can, at least for energies of the order of a few hundred KeV, reach values of the order of 100.

This behavior is strongly indicated by the difference in cancer mortality between Hiroshima (where roughly 10% of the organ doses were due to neutrons) and Nagasaki (where the neutron doses were much less). Fig. 4 shows mortality (1950 - 1974) from all malignant neoplasms as a fraction of the total free-in-air tissue kerma for the two cities indicating that the relatively small neutron dose at Hiroshima had a profound effect. It can be calculated that for a neutron kerma of 1 rad the cancer mortality was about 3×10^{-5}. Although the risk factor for gamma radiation is difficult to quantitate it evidently depends on the dose and is probably more than two orders of magnitude less at doses of a few rad.

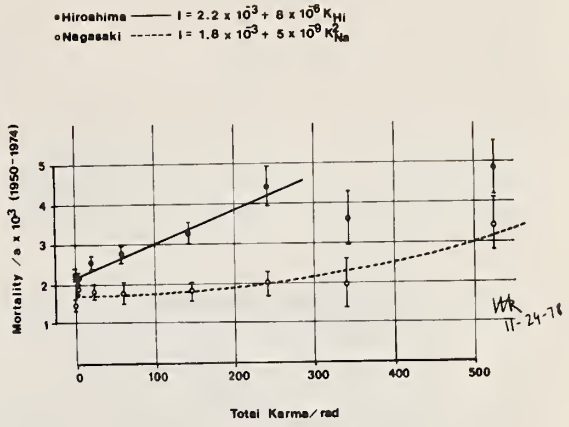

Fig. 4 - Annual mortality from all malignant neoplasms in Hiroshima and Nagasaki (1950-1974) vs. total kerma. The limits correspond to ± one standard deviation.

In applying these findings to the radiation from high energy accelerators it should be kept in mind that the neutrons usually have higher energies which reduces their RBE compared with moderated fission neutrons ($\bar{E}$ eff ≃ 0.5 MeV) as is indicated in Fig. 2. Furthermore because of the high doses in the direct beam the effect of these neutrons is probably low compared with that of the x-rays. For leakage radiations which impart much lower doses the contribution of neutrons may well be dominant. Although the attendant risk may be small - especially considering the seriousness of the condition being treated - all reasonable efforts should be made to reduce the doses due to leakage neutrons and to do this in preference to similar reductions of x-ray doses.

References

1 Shellabarger, C.J., Brown, R.C., Rao, A.R., Shanley, J.P., Bond, V.P., Kellerer, A.M., Rossi, H.H., Goodman, L.J. and R.E. Mills. Rat Mammary Carcinogenesis following Neutron or X-Irradiation. Symp. on the Effects of Neutron Irradiation upon Cell Function, Munich 1973. In Biological Effects of Neutron Irradiation, IAEA-S-179/28, 405-416, 1974.

2 Bateman, J.L., Rossi, H.H., Kellerer, A.M., Robinson, C.V. and V.P. Bond. Dose-dependence of fast Neutron RBE for Lens Opacification in Mice. Radiat. Research 61: 381-390, 1972.

3 Sparrow, A.H., Underbrink, A.G. and H.H. Rossi. Mutations Induced in Tradescantia by Millirad Doses of X-rays and Neutrons: Analysis of dose-response curves. Science 176: 916-918, 1972.

[4] Hall, E.J., Rossi, H.H., Kellerer, A.M., Goodman, L. and S. Marino. Radiobiological Studies with Monoenergetic Neutrons. Radiat. Research 54: 431-443, 1973.

[5] Biola, M.T., LeGo, R., Ducatez, G., Dacher, J. and Bourguignon, M. Formation de chromosomes dicentriques dans les lymphocytes humains soumis in vitro a un flux de rayonnement mixte (gamms, neutrons). In: Advances in Physical and Biological Radiation Detectors, pp. 633-645, IAEA, Vienna, 1971.

[6] Awa, A.A. Chromosome Aberrations in Somatic Cells. J. Radiat. Res. Suppl. 16:122-131, 1975.

[7] Rossi, H.H. The Effects of Small Doses of Ionizing Radiation: Fundamental Biophysical Characteristics. Radiat. Res. 71:1-8, 1977.

[8] Kellerer, A.M. and H.H. Rossi. The Theory of Dual Radiation Action. Current Topics in Radiat. Res. Quarterly 8: 85-158, 1972.

[9] Barendsen, G.W. Cellular Responses Determining the Effectiveness of Fast Neutrons Relative to X-rays for effect on Experimental Tumors. Europ. J. Cancer 7: 181-190, 1971.

[10] Bateman, J.L., Johnson, H.A., Bond, V.P. and H.H. Rossi. The Dependence of RBE on the Energy of Fast Neutrons for Spermatogonia Depletion in Mice. Radiat. Res. 35:86-101, 1968.

[11] Rossi,H.H., Bird, R., Colvett, R.D., Kellerer, A.M., Rohrig, N. and Y.M.P. Lam. The Molecular Ion Experiment. Proc. Sixth Int. Symp. on Microdosimetry. Euratom, Eds. J. Booz and H. Ebert, p. 937-947, Brussels, June 1978.

[12] Kellerer, A.M. and H.H. Rossi. A Generalized Formulation of Dual Radiation Action. Radiat. Res. 75: 471-488, 1978.

[13] Carsten, A.L., Bond, V.P. and K. Thompson. The RBE of Different Energy Neutrons as Measured by the Haematopoietic Spleen Colony Technique. Int. J. Radiat. Biol. 29(1):65-70, 1976.

RISK OF CANCER BASED ON PROMOTION FROM CYTOTOXICITY*

T. D. Jones
D. G. Jacobs[1]
J. A. Auxier[2]
G. D. Kerr

Health Effects and Epidemiology Group
Health and Safety Research Division
Oak Ridge National Laboratory
Oak Ridge, Tennessee 37830

Cytotoxicity is reviewed as a basis of risk assessment for environmental cancers. Linear relations of several cancers to organ-specific cell-surviving fractions have led to the practical assumption that cytotoxicity can stimulate cell proliferation which may permit altered cells to become tumors. Furthermore, an insult which retards cell proliferation or selectively blocks or destroys transformed cells may decrease tumor incidence. This simple assessment model for cancer growth seems to be unique because it requires no assumptions about the number of initiating events per cell, bases the increased demand for proliferation on cytotoxicity estimates by mathematical analyses of *in vivo* and *in vitro* irradiation of cells, and also assumes that the exact number of neoplastic cells, their death rate, and the repair rate, are of secondary importance. The significant point appears to be that a sufficient quantity of altered cells exist in order to respond to the proliferation stimulus from normal or enhanced cell turnover. The use of this model for extrapolation to spontaneous cancer incidence in a population is discussed. Many investigators suggest that cancers occur linearity with low dose; however, carcinogenic response based on linearity with cytotoxicity does not seem inconsistent with linearity at low dose, and furthermore this relation seems to hold to saturated cell-killing levels. Cytotoxicity may also provide a common basis for comparing risk from ionizing insults with risk from chemical insults; relating risk in different organisms (over a wide insult range) to an experimental determination at a single insult level; summing risk to different tissues; and estimating risk for partial body or nonuniform irradiation.

(Cell-proliferation; cell-turnover; cytotoxicity; homeostasis; promotion; RBE; risk)

Background and Objective

There is an increasing interest in the extension of radiobiological concepts in order to establish protection guidelines for cancers induced by chemical agents. Committee 17 of the Council of the Environmental Mutagen Society has reviewed the problem and has suggested a unit of chemical insult, the rem-equivalent chemical (REC) to correspond to radiation doses [1]. The REC is "that dose or product of concentration multiplied by the time which produces an amount of genetic damage equal to that produced by 1 rem of chronic irradiation". It seems unlikely, however, that a direct equivalence will be adequate for carcinogenesis, and we may have to reconsider basic concepts if we wish to make a more appropriate prediction of effects from other carcinogens or to the synergistic or antagonistic effects arising from exposure to mixtures of carcinogens.

Committee 17 goes on to state [1] "A system is urgently needed for monitoring the cells of individuals, particularly those at greater than average risk." One method, which is explored in this paper, would be to relate cancer incidence to cytotoxicity (observed *in vitro* or estimated *in vivo* by mathematical simulation) rather than to radiation or chemical exposure dose. At the present time, absorbed dose serves as the basis of cell-survival and insult-response models (for radiation) and, in this paper, will only be used as an index to relate carcinogenesis to the surviving fraction of cells. Protection concepts based on cytotoxicity to cell cultures in conjunction with other screening techniques [2,3] should quickly and inexpensively determine most safe situations and also provide direct knowledge about the degree of carcinogenicity of the insult. The objective of this paper is to develop a simple model for risk assessment and not be overly concerned about the understanding of cancer or advancement of biology — tasks for which we are not qualified.

Calculation of Radiation Cytotoxicity For Marrow Cells

A formula for the surviving fraction of a cellular population exposed to a mixed radiation field has been expressed by Katz [4]. In dose ranges of interest for risk assessments, the precision with which Katz's analogue can describe the action of ionizing radiation on cell survival is well known and essentially depends upon the determination of

*Research sponsored by the Office of Health and Environmental Research, U.S. Department of Energy under contract W-7405-eng-26 with the Union Carbide Corporation.

three radiosensitive parameters plus the ion-kill probability of the track segment, P, and the stopping power (LET_∞) of the track segment. These parameters have been determined for hamster, HeLa, kidney, leukemia, and mouse bone marrow cells for several radiation environments [4]. This "fitted" model can also "predict" survival in a different radiation environment once the parameters have been evaluated. Katz estimated the radiosensitive parameters from the survival of colony-forming units in mouse bone marrow after *in vivo* irradiation with D-T neutrons, X and gamma radiation [5,6].

The choice of Katz's survival model was based on the availability of necessary parameters and the fact that it can be "predictive" in an untested radiation environment. Linear-quadratic cell-survival "fitted" models based on only two parameters [i.e., $\ell n\ (S) = -\alpha D - \beta D^2$] are preferred by most investigators, but even though a corresponding theory is attached to all models, they essentially remain empirically "fitted" equations with an implied biological significance [7-p52]. For many applications, the initial slope of the survival curve governs the extrapolation of effects; however, none of the malignancies investigated herein will depend upon this low-dose region. Once survival has been computed for the various insult-response levels, the cell survival model is no longer needed in the extrapolation of our model for carcinogenesis to the background level of effects.

The mean value of the recoil-ion stopping power in the atomic-bomb survivors is about 56.2 keV $cm^2\ g^{-1}$ [8] which is nearly identical with Katz's value of 56.1 keV $cm^2\ g^{-1}$ for mouse marrow cells exposed to 1 MeV neutrons. Katz's parameters of P and L (LET_∞) are selected in pairs and it is essential that the relative magnitudes be correct.

The distribution of dose to the active bone marrow for the A-bomb produced radiation environments was obtained by the application of geometrical probability-distribution-functions (CHORD dose-attenuation operators) [9] to the depth-dose curves corresponding to the A-bomb radiations.

Katz's equation, separated into the high-LET (neutrons) and low-LET components (γ-rays) was evaluated as a function of dose for mouse marrow cells exposed to the A-bomb radiations and the respective curves are shown in Fig. 1. Till and McCulloch [10] estimated the survival of mouse marrow cells for *in vivo* irradiation. Over a wide dose range, they found a statistically higher factor for *in vitro* irradiation and estimated an extrapolation number of 2.5 for *in vitro* versus 1.5 for *in vivo*. We used an extrapolation number based on Broerse et al. [5] and estimated by Katz [4] at 2.5. The curve labeled as low-LET in Fig. 1 appears to be practically identical to the *in vivo* curves of Chadwick and Leenhouts [11] and McCulloch and Till [12]. The data in Fig. 1 seem to be also in good agreement with estimates by Mole [13] for the A-bomb survivors.

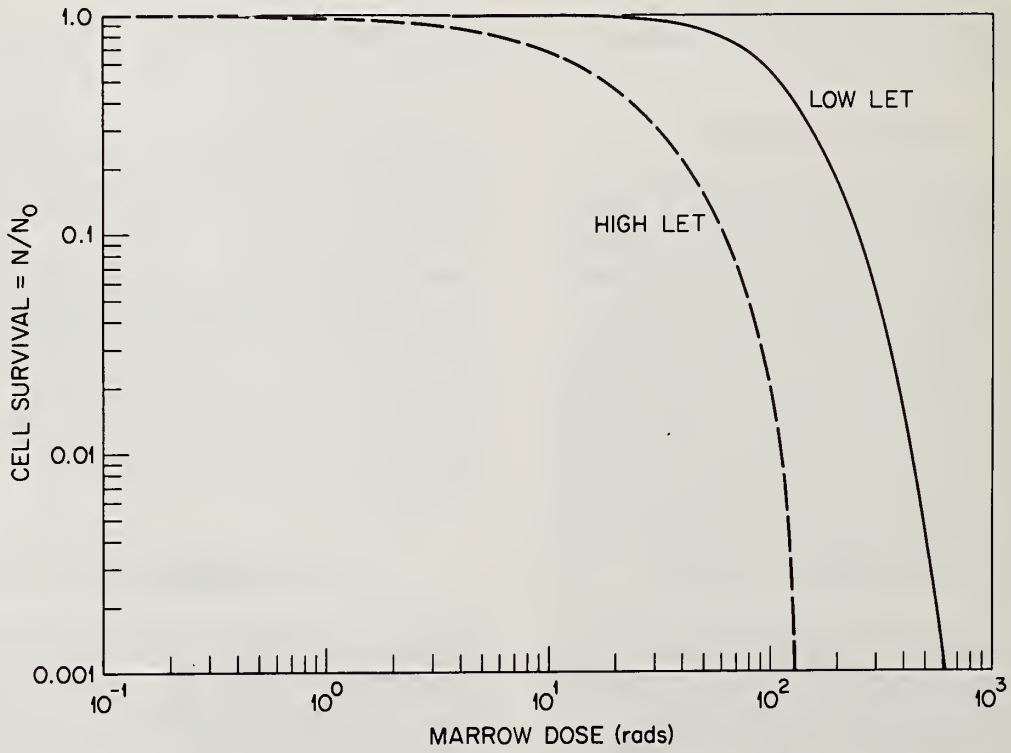

Fig. 1. Cell survival for the bone marrow exposed to fission neutron radiations.

Regression of Mouse Leukemia to Surviving Fraction of Marrow Cells

Myeloid leukemia in mice [14] plotted as a function of cell survival is shown in Fig. 2. Data above about 400 rads for low LET and 100 rads for high LET are not shown in this paper because of statistical uncertainties associated with saturated sterilization processes (cell kill → 100%) and the frequently observed "therapeutic effect" of large single doses of ionizing radiations [15, 16]. At these high insult-levels, altered cells are readily killed and it appears that cell-killing effects outweigh increased carcinogenesis [17] (personal communication from W. V. Mayenord). Ullrich (personal communication) suggested that bone marrow induced thymic lymphoma rates are higher at low insult levels than myeloid leukemia and should be investigated relative to cytotoxicity. Cells in the thymus gland do not proliferate but are produced presumably by thymus-dependent (committed) cells from the bone marrow [18]. Thymic lymphoma incidence as a function of marrow-cell survival, down to dose levels of 4.8 rads of fast neutrons [19], is shown in Fig. 3. At once it becomes apparent that myeloid leukemia and thymic lymphoma in certain inbred strains of mice are more closely related to cytotoxicity or cytological alterations than to the robust[3] concept of absorbed dose.

Regression of Human Leukemia to Surviving Fraction of Marrow Cells

We assumed that human-marrow cells exhibit the same degree of radiosensitivity for lethality as mouse-marrow cells. Similar sensitivities are expected from tabulations of Okada [20-p266] and extrapolation techniques based on gene activation for cell differentiation and total nuclear DNA content [21,22,23]. For the Japanese atomic-bomb survivors, the mean neutron dose was 0.26 K(n),[4] the mean autointegral gamma dose was 0.07 K(n), and the mean photon dose was 0.55 K(γ) [9]. The mean cell-survival values from insult profiles were compared with cell-survival values corresponding to the mean-dose values for the marrow in adult survivors. These values were very nearly equal, and the mean marrow-dose factors were applied to chronic and acute leukemia in the A-bomb survivors [24]. Leukemia, plotted as a function of cell survival, is shown in Figs. 4 and 5. The individual points are at the centers of H used for Hiroshima and N used for Nagasaki. Because of statistical uncertainties in shielding,[5] dose,[5] and cell survival, confidence intervals of the individual points should be two-dimensional and the deviation of the points about the straight lines should be measured along a normal as shown in Fig. 4. The marrow-dose estimates were based on in-air doses or kerma. The

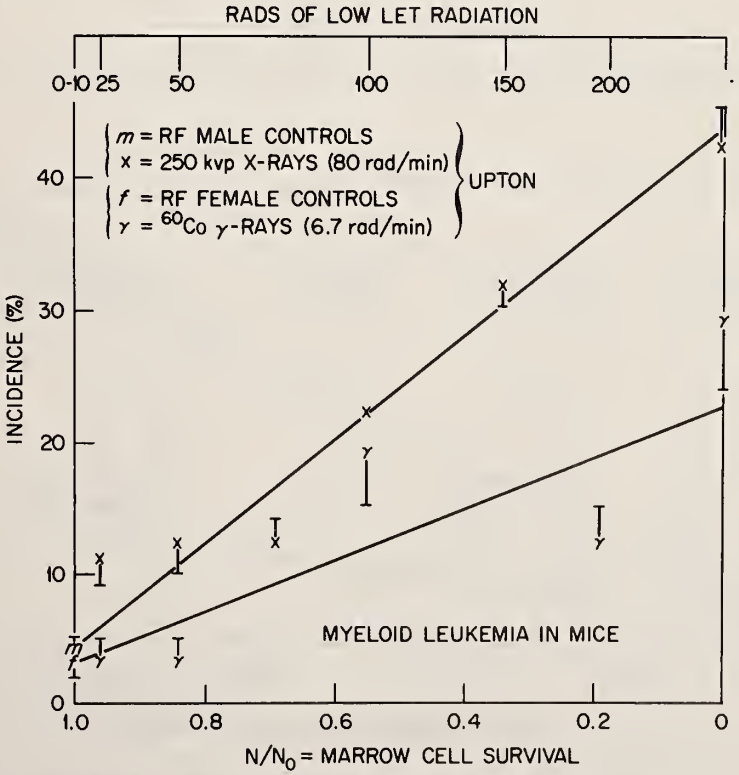

Fig. 2. Incidence of myeloid leukemia in mice vs marrow cell survival.

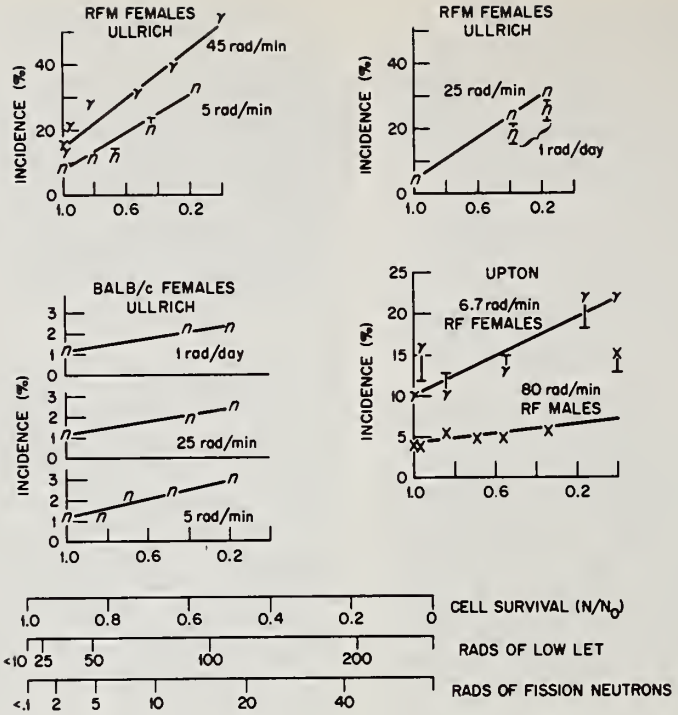

Fig. 3. Incidence of thymic lymphoma in mice vs marrow cell survival.

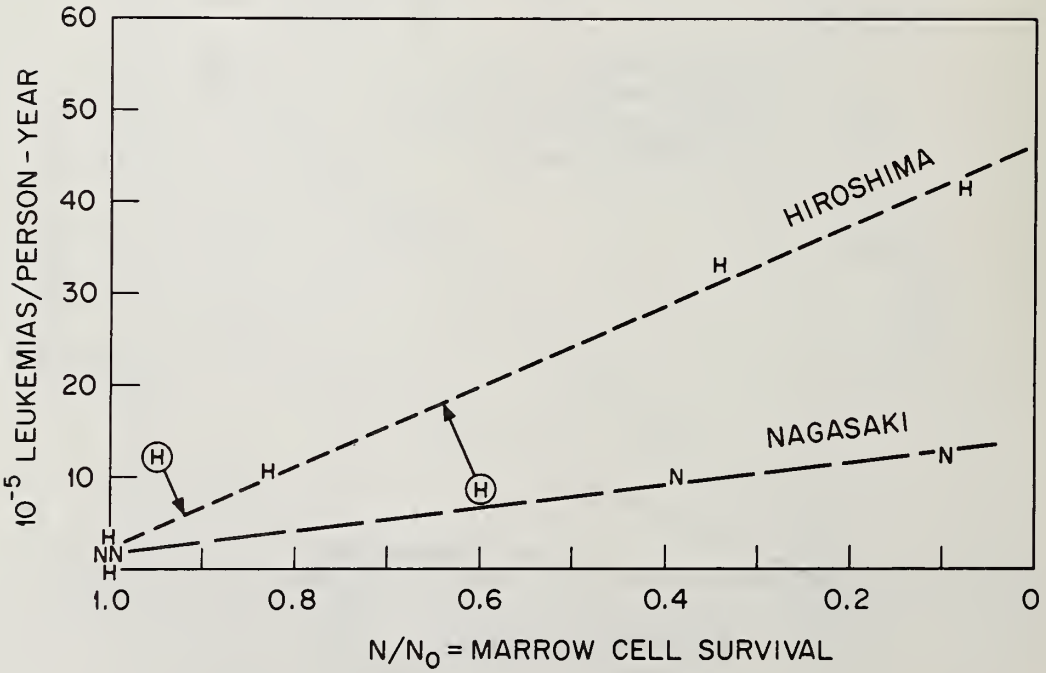

Fig. 4. Incidence of chronic leukemia vs cell survival in A-bomb survivors.

ncertainties are most prominent for acute leukemia in Hiroshima at the high dose levels; nevertheless, the data do not seem inconsistent with linearity between leukemia incidence and cytotoxicity. The incidence rates of chronic leukemia seem highly responsive to radiation quality, illustrated by the different slopes in Fig. 4, but linearity with cell killing seems apparent.

Based on Figs. 4 and 5, risk can be estimated as shown in Table I. In Table I, the absorbed dose to the active marrow is given in column 3 and the neutron or gamma kerma which yields such a dose is given in column 1 or 2, respectively. Risk estimates from Table I are in good agreement with Court-Brown and Doll's recommendation[6] that if the entire red marrow within the body were treated with radiation of the same average energy, a dose

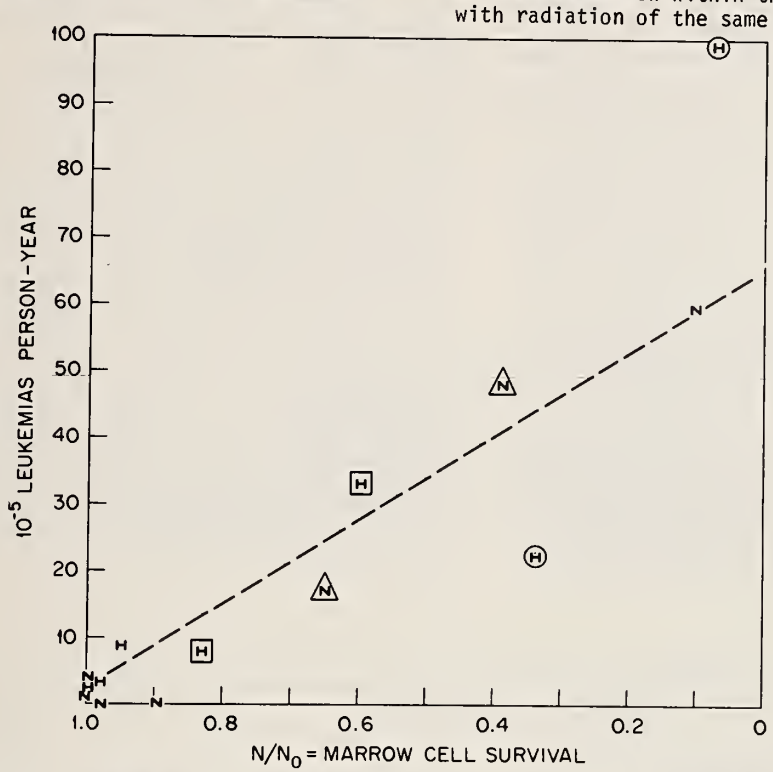

Fig. 5. Incidence of acute leukemia vs cell survival in A-bomb survivors.

TABLE I. Risk of Leukemia in the Japanese A-Bomb Survivors Based on Cell Survival

Kerma[a] (rads)		Marrow dose (rads)	Surviving fraction of marrow cells		Risk of Acute[b] 10^{-5} (person-yr)$^{-1}$		Risk of Chronic[c,d] 10^{-5} (person-yr)$^{-1}$		Relative Risk Acute		Relative Risk Chronic	
(n or γ) →		d →	(n or γ) →		(n or γ)	+	(n[e] or γ[f])	or	(n or γ)	+	(n or γ)	
0.4	0.2	0.1	>0.99	>0.99	∿0	∿0	∿0	∿0	1	1	1	1
3.9	1.8	1	0.96	>0.99	2.5	∿0	1.5	∿0	2	1	2	1
19	9	5	0.82	>0.99	12	∿0	8.5	∿0	5.6	1	5.5	1
38	18	10	0.68	>0.99	21	∿0	17	∿0	9.2	1	9.5	1
77	36	20	0.46	0.97	34	2	27	∿0	14.4	1.8	15	1
115	55	30	0.32	0.94	43	4	31	0.5	18	2.6	17	1.3
154	73	40	0.22	0.89	50	7	---	1	21	3.8	---	1.5
192	91	50	0.14	0.84	55	11	---	1.5	23	5.2	---	1.8
231	109	60	<0.01	0.78	63	14	---	2.5	26	6.8	---	2.2
---[g]	182	100	---	0.55	---	29	---	5.5	---	12	---	3.8
---	364	200	---	0.18	---	52	---	10	---	22	---	6
---	545	300	---	<0.01	---	63	---	12	---	26	---	7

[a] $K_n = D_n/0.26$, $K_\gamma = D_\gamma/0.55$.

[b] Spontaneous rate taken at 2.5×10^{-5} leukemias/(person-yaar).

[c] Spontaneous rate taken at 2.0×10^{-5} leukemias/(person-year).

[d] Estimated according to $\frac{N}{N_0}(0_n) \times \frac{N}{N_0}(D_\gamma) = \frac{N}{N_0}$ which determines an incidence $I\left(\frac{N}{N_0}\right)$ but incidence from neutrons becomes $I\left(\frac{N}{N_0}\right) - I\left\{\frac{N}{N_0}(D_\gamma)\right\}$.

[e] From Jones et al. (8), $1.5 < K_\gamma/K_n < 2.5$ for survivors at 1000 m < distances < 1500 m; hence, $K_\gamma = 2K_n$ assumed to obtain $D_\gamma = 4.2\ D_n$.

[f] Curve from Figure 9 for Nagasaki.

[g] Decreased incidence because of saturation.

of 30 to 50 R would double the expected incidence of leukemia.

Other Radiation Diseases vs Cytotoxicity

Puck et al. [26] investigated survival curves of cells from normal human tissues of skin, spleen, ovary, conjunctiva, liver, appendix, and lung. Except for lung cells, the radiosensitivities were not greatly different for the other six tissues. Todd (personal communication) also suggested that, except for hematopoietic and lymphatic tissues, most other mammalism cells display a similar response to insults of ionizing radiation [20-p266]. Mean tissue-kerma-in-air estimates[7] were modified by CHORD operators for active bone marrow [9] in order to estimate whole-body dose levels [27], and Katz's cell-survival model was evaluated for human kidney cells [28] exposed to the atomic-bomb radiation environments. Fatal malignancies[8] from 1950-1972, excluding leukemia, were then normalized to the incidence rate in the 0-9 rad exposure group and plotted vs cell survival in Fig. 6.

As shown in Fig. 7, Albert et al. [29] found linearity between the number of skin tumors in rats and atrophic follicle incidence which probably is an estimator of tissue destruction. A single-dose-radiation-cell-survival curve for Fischer-rat mammary-gland cells [30] was used in order to plot the percent of animals with mammary neoplasms as a function of cytotoxicity. The results are shown in Fig. 8 for Sprague-Dawley rats [31-34], Fischer rats [35], RFM mice [19], and the female atomic-bomb survivors in Nagasaki [36]. The survival of mammary cells *in vivo* has now been found to have a broader shoulder (Gould-personal communication) than published data [30]. These newer data are not available, but the net effect would only be a rotation, through the spontaneous tumor values, of the relationships in Fig. 8. If error bars of one standard deviation are added to data in Fig. 8, then a linear fit cannot be rejected on statistical grounds. The survivor data is normalized to risk for the 0-9 rad group and the data above 200 rads were excluded because of possible neutron contributions. Although the RFM mouse and human mammary tumors do not appear to demonstrate a significant dose-response, none of these plots seem in conflict with linearity between cancer incidence and cytotoxicity.

Radiation induced cancer is such that almost no observation seems universally true. The best methodologies for risk assessments, then, should probably be based on relationships that are commonly reliable. The only cancer (which we observed) to conflict with linear incidence as a function of cytotoxicity was ovarian tumors in mice [19] plotted against Chinese hamster ovary (CHO) cell-survival data [37]. Our coupling of

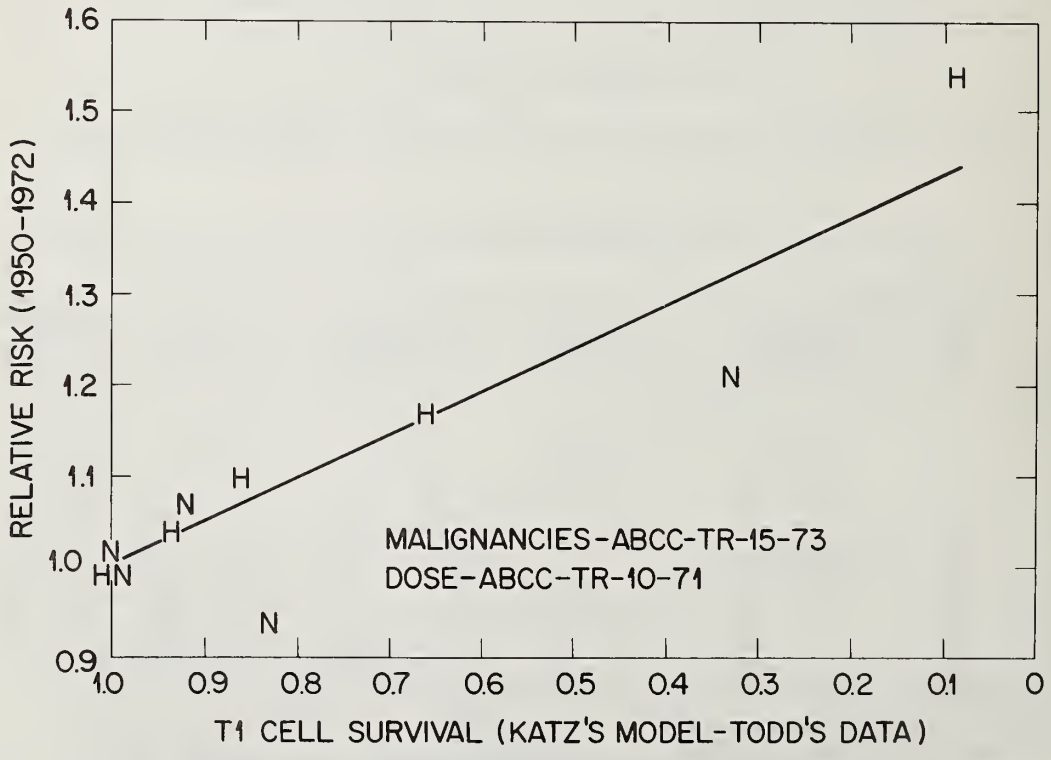

Fig. 6. Fatal malignancies, relative to 0-9 rad groups, vs cell survival in Hiroshima and Nagasaki A-bomb survivors (leukemias not included).

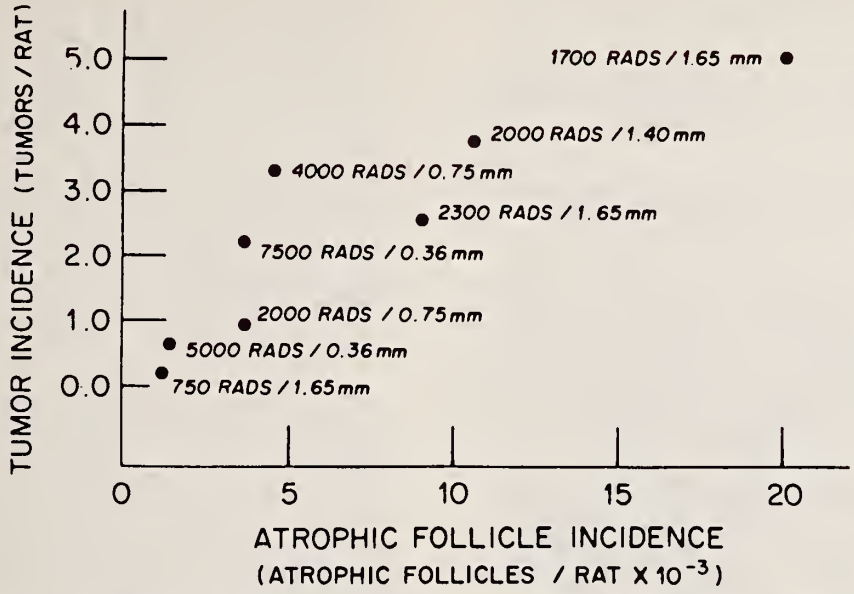

Fig. 7. Incidence of skin tumors vs atrophic follicle incidence in rats--reproduced with permission of R. E. Albert and publisher.

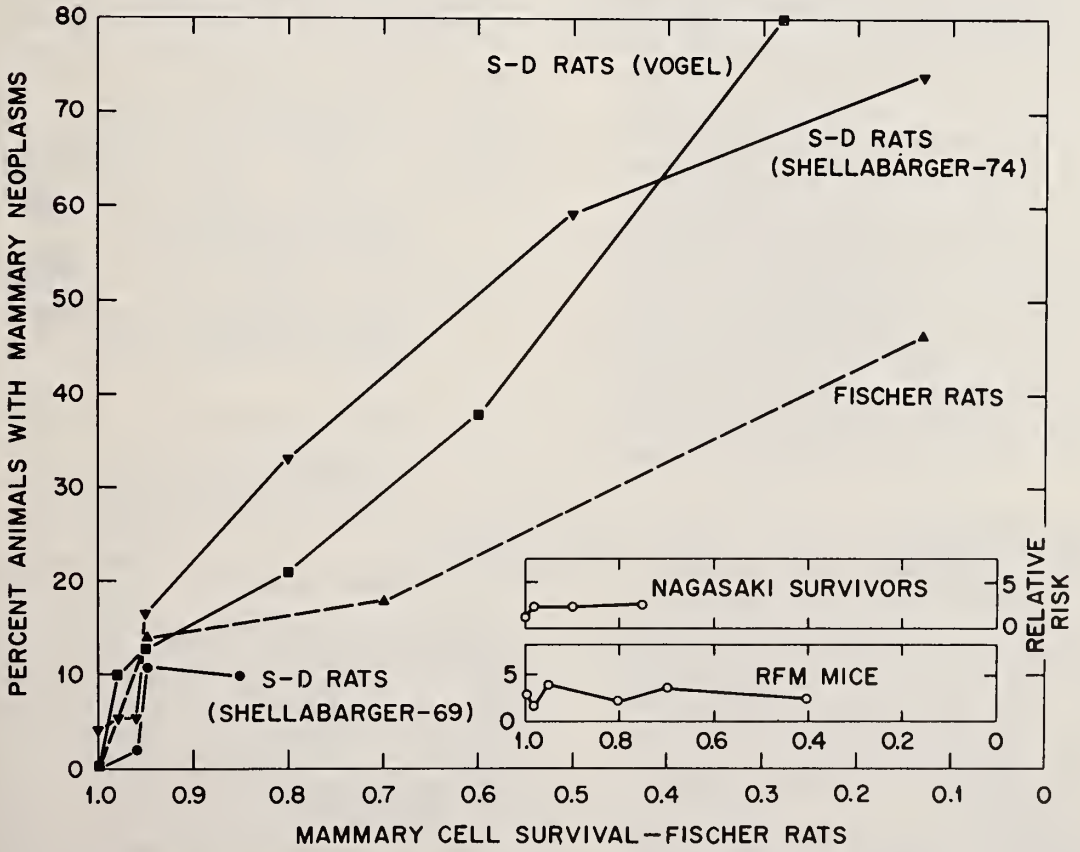

Fig. 8. Incidence of mammary neoplasms vs mammary cell survival in Fischer rats.

these two studies was also encouraged by relative DNA contents and similar gene activation. The incidence of ovarian tumors rose rapidly for low cytotoxicity and seemed to plateau at 40-50% for cell lethality greater than about 20%. Ovarian and certain other tumors may be justifiable exceptions to usual cell kinetics because the adult ovary is incapable of proper regeneration [38].

A Simple Model for Environmental Cancer

Hyperplastic agents, irritants, viruses,[9] and cytotoxic insults have been assessed varying and confusing roles in theories describing the induction of neoplastic diseases. It has been observed that many effects, e.g., injury to blood-forming and GI organs, are probably caused by the death of cells [40]. Some studies have revealed a clear parallelism between the carcinogenicity of a substance and its cytotoxic effect.

Physicians and oncologists have frequently noted that accelerated tissue renewal due to surgery, toxic or hyperplastic stimuli, growth hormones, immunological treatment, partial hepatectomy, unilateral nephrectomy, chemotherapy of non-malignant disorders, etc., often results in an increased risk of cancer [41-43] — especially if accompanied by an initiator, e.g., a small dose of ionizing radiation. The 1977 UNSCEAR report [44] provides a good review of the carcinogenic role of cell proliferation and states that, "Cellular proliferation is implicit in the notion of promoting action and is clearly necessary for the tumor progression, and the evidence reviewed is generally in accordance with these concepts. However, so far there is no unequivocal evidence that the induction of proliferation in the target cells is a key event in radiation carcinogenesis . . . . In any case, a systematic comparative analysis of events associated with the induction of tumours in target cells would be required before any postulated promotional role of cell proliferation could be fully elucidated." In addition, continued insults of estrone or testosterone can control proliferation and be used to stimulate or regress specific cancers in primary and secondary sex organs [45]. A vivid illustration is 100% mammary tumor incidence resulting from estrone injections in male mice belonging to a strain in which only the females normally experienced a high incidence rate of mammary tumors [45].

Biological techniques are entirely inadequate for quantification of the role of cell proliferation [44-p577] and the UNSCEAR Committee expresses doubt about a direct role probably because normal tissue renewal rates sometimes seem unrelated to cancer rates [44-p617] and because induced bone fractures failed to enhance bone tumor rates in mice [47]. Also, a biochemical experiment led Raick et al. [48] and the UNSCEAR to the conclusion that hyperplastic changes due to very weak insult levels and promoting action at higher levels are independent processes [44-p578].

Cancer is expected to derive from stem cells and amplification of cell populations by cells committed to differentiation obscure any conclusions based on tissue renewal where both factors are present [46]. Unenhanced bone tumor rates could be explained in terms of an equilibrium cell population and the migration of cells as no significant amount of cell killing should accompany fractures [39]. The conclusions, that hyperplastic changes due to very weak insult levels and promotion are independent processes, seem unsubstantiated because the low-level hyperplasia, of duration less than the period between the administrations of the chemical, leads to a time-integrated cell-population that is exactly equal to the steady-state or zero-dose time-integrated population. Additional insults to a hyperplastic state (or a promotion which results in necrosis) yields a greatly elevated time-integrated cell population and an increased cancer rate.

It has been observed generally that precancerous lesions occur at a rate that leads to a large overestimation of the incidence of neoplastic diseases [49]. For low LET insults, these transformations usually occur at a much greater rate than does cell inactivation. Most cancer models specialize in the production of altered cells and repair processes but it seems unlikely that the immune response or repair enzymes would reduce the populations of altered cells at a rate that is often linear with cytotoxicity yet relatively insensitive to the number of transformed cells. It has frequently been observed that a single neoplastic cell has a very low probability of ever becoming a cancer, yet cell-marker analysis has demonstrated that many tumors are of a single-cell origin [50,15]. Promoters such as croton oil, TPA, etc., are often strongly inflammatory, producing edemas and hyperplasia, but the inductions of all cancers cannot be described simply. However, it appears that a few conditions can be noted that will permit the development of general protection guidelines. These include:

1. Production of altered cell populations by damage events or mis-repair processes [51];
2. Cellular abnormalities must be "fixed" by cell division [51, 52];
3. Stimulus to proliferate;
4. Attainment of critical mass [53] or state in an individual of a certain sensitivity [54,55], and
5. Escape from normal systemic regulation processes.

We essentially reoffer the practical hypothesis of Bergonie and Tribondeau [7-p3,56-p261,57] in that normal or accelerated cell turnover may permit altered-cell populations to become tumors [58-68]. Furthermore, an insult which retards cell proliferation, e.g., malnutrition, or an insult which selectively blocks (if repair processes continue [51,72-p403] or destroys transformed cells may produce no observable excess of tumors [65-p269]. In fact, every agent, that is known to affect cancer incidence rates, has mitotic or antimitotic behavior, without any exceptions. It is apparent

that some altered cells are never repaired and can be "scored" later by insults which stimulate proliferation [59]. Our hypothesis is illustrated in Fig. 9. Generally it is quite difficult to obtain quantative information on cell-proliferation kinetics [7-p17] and this paper demonstrates, that, for protection guidelines, cytotoxicity should be considered as a substitute index.

Carcinogenesis is often modeled in terms of time-sequential events to a single cell, e.g., probability of the production of sequential initiating transformations multiplied by the probability of survival of the transformed cell. For protection purposes it appears that because individual altered cells are usually expected to be present in the human body, the important factor is the processes which permit altered cells to clone. Thus, we subscribe to Nordling [60] because "cancer is caused by mutations multiplied and accumulated usually through large-scale proliferation of cells" and "the unexpected high incidence of internal neoplasms in childhood is explained by the high frequencies of cell division in the fetal stage. Other high cancer incidence rates in particular organs may be explained on the basis of exposure of the tissues to mutagens or to agents increasing cell proliferation" [73,38]. Several cancer vs dose-response models suggest that the population of altered cells, decreased by a cell-killing factor, is related to the incidence of cancer. Indeed, the resulting dose-response curve has the correct shape, which is very gratifying. However, subcarcinogenic doses of ionizing radiation accompanied by partial hepatectomy [74], CCl_4 [59], uninephrectomy [43], etc. result in decreased populations of altered cells and increased cancer rates--a serious contradiction to the simplicity of these models.

The observation of a linear relationship between the cumulative incidence of late-onset cancers in man and the sixth power of age has led to theories involving kinetic mechanisms [70,60,65]. This approach seems consistent with time-to-diagnosis periods depending upon many doublings (>30) of tumor volume after proliferation stimuli have adjusted to maintain homeostasis.

The lower tumor incidence generally observed for fractionated and chronic exposures, relative to acute exposure, seems consistent with slower proliferation resulting from a lesser degree of cell killing. Repair enzymes should be more reliable than when a large population of altered cells must undergo DNA repair [51] during a strong growth stimulus. Furthermore, according to Brown [61], "A relationship between the number of virus particles and the number of sterilized cells is a possibility which would explain the higher incidence of thymic lymphomas following weekly fractionated exposure as opposed to single doses."

Another model [70] based on "the transforming agent imagined to be passed from "dead" to viable cells may be a virus" could possibly help explain the behavior of ovarian tumors in mice because for high levels of cell killing, viable cells would receive redundant stimuli. More generally, such a process would almost certainly produce a convex-shaped response (as was observed for ovarian

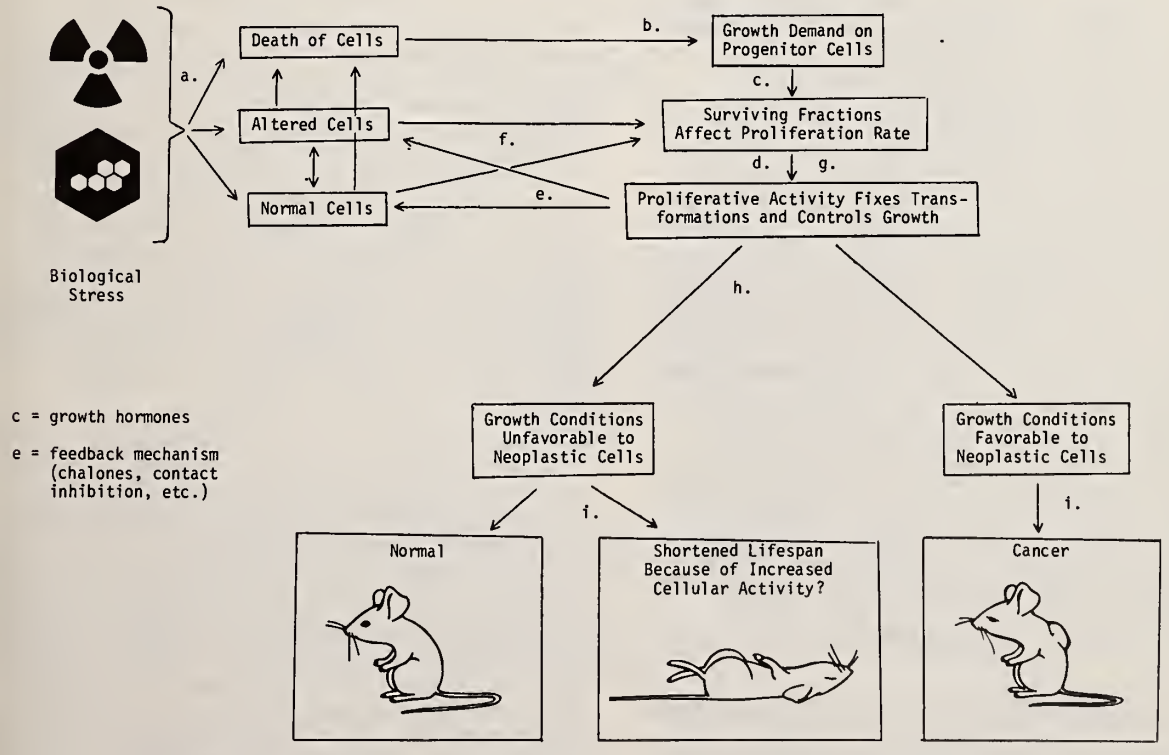

Fig. 9. A simplified model for environmental cancer as a linear function of cell survival.

tumors) which would conflict with other relationships described in this paper.

Thresholds for Risk Assessments

Curvilinear dose-response relationships present special problems, since they suggest either that the mutagenic response may become insignificant at very low levels, or even that true thresholds may exist [1]. The question of a threshold is not easily resolved and must be investigated on a "mechanistic" rather than a "dose-response" basis. On a cellular level Chadwick and Leenhouts [11] have explained the possible absence of a threshold based on the difficult process of exact repair of all nonlethal DNA double-strand breaks. Zasukhina and Sinelushikova [71] suggest that mutagenesis and carcinogenesis are connected with the formation of crosslinks between strands of DNA and alkylation of nitrogenous bases; however, other work [56-p202] indicates only DNA degradation is important in the presence of oxygen because the ends become peroxides which prevent crosslinking. These studies and many others will have to be more clearly understood before "threshold" applications will be accepted.

There appears to be many modes of cell death from a variety of insults [49,75]. In addition, there is a small but definite probability that normal cell-turnover in non-insulted or "low-dose" tissue will "fix" or "lock" a DNA lesion, which in certain individuals, may escape the immune response [54] and be diagnosed as cancer 30-40 volume doublings later.

From this paper it appears that incidence rates, in a population, are straight-line, no-threshold, relationships from spontaneous or background cancer rates to cancer rates associated with saturated cell-killing levels. Terzaghi and Little [51] have suggested that DNA errors may be inserted by repair processes and fixed by prompt cell division. If given sufficient time before the first division, the damage structure and even the misrepairs could be corrected. This behavior could be confused with a threshold effect; however, for a population, a threshold for ionizing radiation generally seems inconsistent with cancer genesis from a single cell and latency periods expressed in cell lifetimes. Radiation insults are self delivered, but chemical insults depend upon metabolic processes. Thus, it has been suggested that "very low levels of some agents will be inactivated before they reach the biochemical element of the cell (DNA) required for the production of malignancy" [76]. Such behavior could not be expected for all chemicals because some require metabolic conversion in order to reach a carcinogenic state. For all practical purposes, the excess cancer incidence may approach zero for low insult levels (as shown in Fig. 10) and threshold debates become academic.

Partial Body Irradiation and Risk to Spondylitics

The problems of partial body and nonuniform irradiation are quite easily solved for cancers which occur linearily with proliferation estimated from cytotoxicity. The risks of these malignancies need not be based on the absolute number of transformed, misrepaired, or killed cells but rather on the surviving fraction which is the integration of the probability of cell survival over the organ of interest. According to UNSCEAR [77] an average of 30-40% of the bone marrow in the ankylosing spondylitis patients treated by X-rays was irradiated. The BEIR Committee [24] estimates 42.3%. The marrow dose levels in the path of the beam were greater than 300 rads while outside the beam, the dose fell quite rapidly.[6] Thus, it appears that the surviving fraction was in the range of 0.5-0.7 of the total marrow. From Fig. 4 and 5, the risk for a first exposure[10] can be estimated, based on the atomic-bomb survivors, to be 0.7×10^{-5} leukemias/person-year for chronic leukemia and $(22\text{-}34) \times 10^{-5}$ leukemias/person-year for acute leukemia. The 52 observed cases of leukemia in the spondylitics divided by 141,796 person-years of observation yields a risk of 36×10^{-5} which seems to agree better than expected because of multiple exposures to many of the spondylitics, the fact 80-90% of the spondylitics were men — incidence in males is higher, and many other differences in the populations at risk. This agreement may indicate that patients having a "predisposition" to leukemia were sufficiently insulted by a single exposure and more resistant patients were not subjected to significantly greater risk by multiple treatments. Leukemia rates in other populations show equally good agreement and are discussed elsewhere [75].

Discussion and Conclusions

Thus from our simple model for a population, the dominant condition necessary to estimate the risk of a particular tumor [assuming non-zero altered-cell populations (initiation)] is an index of the growth stimulus (promotion). It also appears that cancer incidence need not be based on the number of initiation events per cell, the number of altered cells, or the number of cells at risk [13], but instead on a mechanism that prescribes the fractional cell-replenishment requirement. For organ-specific promotion insults not connected with initiation insults, the neoplastically transformed cell-population may be null or low and normal cancer rates may result as illustrated by hepatoma rates in rats stressed only by hepatectomy or CCl_4 [74,59].

Assessments based on cell survival seem to provide hope for summing risk to different organs, relating effects in mouse to those in man, relating risk from radiation insults to risk from chemical insults, describing multicentered and single-cell origin of cancer, understanding hot-particle behavior,[11] and explaining the synergistic effects of different insults. Risk analyses based on product-type models can explain synergism which has been noted for combinations of severe insults and also the behavior of weak insults in conjunction with a strong insult where additivity currently seems possible. A generalized cell-survival model may permit the assessment of overall cancer risk from all hazards.

Randi and Thomas [78] suggest that absorbed dose is a sterile concept for operational health physics in that it produces little or nothing. In fact, it is becoming more apparent that dose-type parameters are insufficient to assess biological response [79] because in order to put radiations of different quality on the same basis for the prediction of effects, it is necessary to establish correction factors--physical factors (Quality Factors) and biological factors (Relative Biological Effectiveness). Such processes seem unscientific and will always be subject to technical abuse and criticism.

If one prefers to follow the traditional dose-response approach then, curves are shown in Fig. 10 and the ratios of photon dose to neutron dose for specific levels of cell survival are shown in Table II. The dose-response curves are amazingly similar to acute myelogenous leukemia grown in culture, [80-if the abscissa is made linear]. The RBE values in Table II are also quite consistent with RBE's for late effects [81-83] but "Turning concepts upside down can sometimes straighten them out" [65-p92].

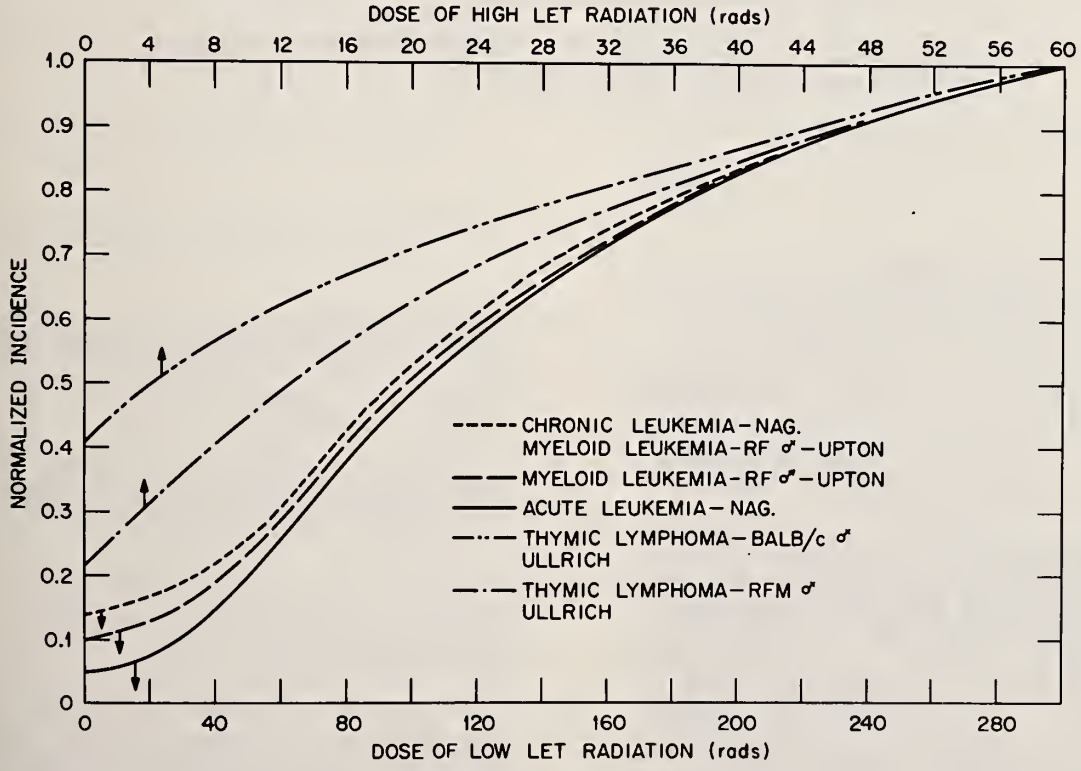

Fig. 10. Dose-response curves obtained from the assumption of linearity between cancer and cell survival.

Table II. Cytotoxicity RBE for Fission-Neutron Radiation Environments

	Marrow Cells			Kidney Cells		
% Survival	D_n (rads)	D_γ[a] (rads)	D_γ/D_n	D_n (rads)	D_γ (rads)	D_γ/D_n
>99	<0.2	<10	80[b]	>0.3	<20	100[b]
98	0.5	20	40[b]	0.5	30	60[b]
95	1	30	30[b]	1	40	40[b]
90	3	40	13	2	60	30
80	6	60	10	5	90	18
70	9	70	8	8	110	14
60	13	90	7	11	140	13
50	18	110	6	15	170	11
40	23	130	6	20	200	10
30	30	150	5	26	240	9

[a]The biological effectiveness of high LET radiation should not dimenish for fractionated or chrnoic exposure; however, the effectiveness of low LET radiations may be influenced by repair processes.

[b]Values of D_γ/D_n above 90% survival are in the region where models begin to differ and investigators commence to argue about the effect of slope at zero dose. These values are based on Katz's model.

Footnotes

1. Office of Environmental Policy Analysis, presently with Evaluation Research Corp.

2. Industrial Safety and Applied Health Physics Division

3. Robust is used in the statistical sense to denote a high degree of insensitivity to minor parametric variations.

4. Tissue-kerma-in-air or "air-dose" is considered to apply to infinitesimal amounts of biological tissue under exact analogue exposure conditions, except for the absence of the specific survivors. The kerma represents the kinetic energy released in materials and becomes equal to the absorbed dose if, and only if, all energy released when a particle interacts is assumed to be locally deposited, i.e., the pathlengths of the secondary particles are short in comparison to the dimensions of the critical biological organs. For the Atomic-Bomb Survivors, these estimates are usually called "T65D doses."

5. S. Jablon, "Atomic Bomb Radiation Dose Estimation at ABCC," Atomic Bomb Casualty Commission Technical Report ABCC-TR-23-71.

6. W. M. Court-Brown and R. Doll, "Leukemia and Aplastic Anemia in Patients Irradiated for Ankylosing Spondylitis," Medical Research Council Special Report Series No. 295, Her Majesty's Stationery Office.

7. S. Jablon and H. Kato, "Mortality Among Atomic-Bomb Survivors, 1950-1970," Atomic Bomb Casualty Commission Technical Report, ABCC-TR-10-71.

8. I. M. Moriyama and H. Kota, "Mortality Experience of Atomic-Bomb Survivors 1970-72," Atomic Bomb Casualty Commission Technical Report, ABCC-TR-15-73.

9. "Viral agents...are capable of eliciting the whole spectrum of proliferative lesions from mild hyperplasia and near-neoplastic reactions to highly malignant neoplasias of the dependent type. These agents...provoke neoplastic reactions when supplied on a continuing basis" [39-p231].

10. Risk estimates to spondylitics are often brought into line with Atomic-Bomb Survivors and other populations by averaging the absorbed dose over irradiated and non-irradiated marrow centers. Averaging helps to account for "wasted radiation", i.e., the excess above saturated cell-killing levels. Although averaging may produce reasonable estimates, it is dangerous and misleading [44-p365].

11. ORNL-TR-4241, The Problem of Hot Particles. A report written for the conference, "Medical and Biological Problems of Radiation Exposure," Research Institute, Borstel, May 30, 1975.

References

1. Committee 17 of the Environmental Mutagen Society, "Environmental mutagenic hazards," *Science* 187, 503-514 (1975).

2. B. N. Ames, "The detection of chemical mutagens with enteric bacteria," *Chemical Mutagens*, Vol. I, pp. 267-282 (1971).

3. Ed. by Alexander Hollaender, *Chemical Mutagens Principles and Methods for Their Detection*, Plenum Press, New York (1971).

4. R. Katz and S. C. Sharma, "RBE - dose relations for neutrons and pions," *Phys. Med. Biol.* 20, No. 3, 410-419 (1975).

5. J. J. Broerse, A. C. Engels, P. Lelieveld, L. M. Van Patten, W. Duncan, D. Greene, J. B. Massey, C. W. Gilbert, J. H. Hendry, and A. Howard, "The survival of colony-forming units in mouse bone-marrow after *in vivo* irradiation with D-T neutrons, x- and gamma-radiation," *Int. J. Radiat. Biol.* 19, 101-110 (1971).

6. R. Katz, B. G. Fullerton, Jr., R. A. Roth, and S. C. Sharma, "Simplified RBE-dose calculations for mixed radiation fields," *Health Phys.* 30, 148-150 (1976).

7. V. P. Bond, T. M. Fliedner, and J. O. Archambeau, *Mammalian Radiation Lethality*, Academic Press, New York (1965).

8. T. D. Jones, J. A. Auxier, J. S. Cheka, and G. D. Kerr, "*In vivo* dose estimates for Atomic-bomb survivors shielded by typical Japanese houses," *Health Phys.* 28, 367-381 (1975).

9. T. D. Jones, "CHORD operators for cell-survival models and insult assessment to the active bone marrow," *Radiat. Res.* 71, 269-283 (1977).

10. J. E. Till and E. A. McCulloch, "A direct measurement of the radiation sensitivity of normal mouse bone marrow cells," *Radiat. Res.* 14, 213-222 (1961).

11. K. H. Chadwick and H. P. Leenhouts, "A common molecular mechanism in radiobiology, its implications in radiological protection," Third International Congress of the IRPA, Washington, D.C. (1973).

12. E. A. McCulloch and J. E. Till, "The sensitivity of cells from normal mouse bone marrow to gamma radiation *in vitro* and *in vivo*," *Radiat. Res.* 16, 822-832 (1962).

13. R. H. Mole, "Ionizing radiation as a carcinogen practical questions and academic pursuits," *Brit. J. Radiol.* 48, No. 567, 137-169 (1975).

14. A. C. Upton, M. L. Randolph, and J. W. Conklin, "Late effects of fast neutrons and gamma-rays in mice as influenced by the dose rate of irradiation: Induction of neoplasia," *Radiat. Res.* 41, 467-491 (1970).

15. L. J. Cole and P. C. Nowell, "Radiation carcinogenesis: The sequence of events," *Science* 150, 1782-1786 (1965).

16. E. J. Hall, "Radiation and the single cell: The physicist's contribution to radiobiology," *Phys. Med. Biol.* 24, No. 3, 357 (1976).

17. A. E. Reif, "Radiation carcinogenesis at high dose-response levels: A hypothesis," *Nature* 190, No. 4774, 415-417 (1961).

18. O. Vos, "Repopulation of the stem-cell compartment in haemopoietic and lymphatic tissues of mice after x-irradiation," *The Effects of Radiation on Cellular Proliferation and Differentiation, IAEA*, Monoco, pp. 149-160 (1968).

19. R. L. Ullrich, M. C. Jernigan, G. E. Cosgrove, L. C. Scatterfield, N. D. Bowles, and J. B. Storer, "The influence of dose and dose rate on the incidence of neoplastic disease in rfm mice after neutron irradiation," *Radiat. Res.* 68, 115-131 (1976).

20. S. Okada, *Radiat. Biochem.*, Vol. I Cells, Academic, 153 (1970).

21. K. Bachmann, "Genome size in mammals," *Chromosome* 37, 85-93 (1972).

22. S. Abrahamson, M. A. Bender, A. D. Conger, and S. Wolff, "Uniformity of radiation-induced mutation rates among different species," *Nature* 245, 460-462 (1973).

23. J. G. Brewer, R. J. Preston, K. P. Jones, and D. G. Gosslee, "Genetic hazards of ionizing radiations: Cytogenetic extrapolations from mouse to man," *Muta. Res.* 17, 245-254 (1973).

24. "The effects on populations of exposure to low levels of ionizing radiation," *Report of the Advisory Committee on the Biological Effects of Ionizing Radiations*, (National Academy of Sciences, National Research Council, Washington, D.C.) (1972).

25. G. D. Kerr, T. D. Jones, J.M.L. Hwang, F. L. Miller, and J. A. Auxier, "An analysis of leukemia data from studies of Atomic-bomb survivors based on estimates of absorbed dose to active bone marrow," *International Radiation Protection Association Communications N335*, Paris (1977).

26. T. T. Puck, D. Morkovin, P. I. Marcus, and J. J. Cieciura, "Action of x-rays on mammalian cells," *Journal Exptl. Med.* 106, 485-503 (1957).

27. A. C. Upton "Radiobiological effects of low doses - implications for radiation protection," *Radiat. Res.* 71, 51-74 (1977).

28. P. Todd, "Heavy-ion irradiation of cultured human cells," *Radiat. Res.* Suppl. 7, 196-207 (1967).

29. R. E. Albert, F. J. Burns, R. D. Heinboch, "The association between chronic radiation damage of the hair follicles and tumor formation in the rat," *Radiat. Res.* 30, 509-599 (1967).

30. M. N. Gould and K. H. Clifton, "The survival of mammary cells following irradiation *in vivo*: A directly generated single-dose-survival curve," *Radiat. Res.* 72, 343-352 (1977).

31. H. H. Vogel, Jr. and R. Zoldivar, "Experimental mammary neoplasms: A comparison of effectiveness between neutrons, x- and gamma-radiation," *Symposium on Neutrons in Radiobiology*, CONF-691106, Clearinghouse for federal scientific and technical information (1969).

32. C. J. Shellabarger, R. D. Brown, A. R. Rao, J. P. Shanley, V. P. Bond, A. M. Keller, H. H. Rossi, L. J. Goodman, and R. E. Mills, "Rat mammary carcinogenesis following neutron or X-radiation," *Proceedings of 1973 IAEA Symposium*, Neuherberg, 391-401 (1974).

33. C. J. Shellabarger, V. P. Bond, E. P. Cronkite, and G. E. Aponte, "Relationship of dose of total-body ^{60}Co radiation to incidence of mammary neoplasia in female rats," *IAEA Symposium on Radiation Induced Cancer*, 161-172 (1969).

34. H. H. Rossi, A. M. Kellerer, "Radiation carcinogenesis at low doses," *Science* 175, 200-202 (1972).

35. K. H. Clifton, B. H. Sridharan, and M. N. Gould, "Risk of mammary oncogenesis from exposure to neutrons or gamma rays," *Proc. of IAEA Symp. on Biological and Environmental Effects of Low-Level Radiation*, Chicago, 205-211 (1975).

36. S. Jablon and H. Kato, "Studies of the mortality of Atomic-bomb survivors," *Radiat. Res.* 50, 649-698 (1972).

37. A.H.W. Nias and C. W. Gilbert, "Response of HeLa and Chinese hamster cells to low doses of photons and neutrons. Cell survival after low doses of radiation: Theoretical and clinical implications," *Proc. Sixth L. H. Gray Conf.*, 93-100 (1974).

38. L. G. Lajtha and R. Oliver, "Cell population kinetics following different regimes of irradiation," *British J. of Radiology* 35, 131-140 (1962).

39. W. R. Bryan, "A reconsideration of the nature of the neoplastic reaction in the light of recent advances in cancer research," *J. Natl. Cancer Inst.* 24, 221-251 (1960).

40. A. C. Upton and R. F. Kimball, "Radiation biology," *Principles of Radiation Protection*, John Wiley and Sons, Inc., New York (1967).

41. S. M. Sieber and R. H. Adamson, "Toxicity of antineoplastic agents in man," *Adv. Cancer Res.* 22, 104-138 (1975).

42. P.O.P. Ts'o, W. J. Caspary, B. I. Cohen, J. C. Leavitt, S. A. Lesko, Jr., R. J. Lorentzen, and L. M. Schechtman, "Basic mechanisms in polycyclic hydrocarbon carcinogenesis," *Chemical Carcinogenesis*, p. 138 (1974).

43. J. L. Van Lancker, "Carcinogenesis and DNA repair," *Chemical Carcinogenesis*, p. 432 (1974).

44. United Nations Scientific Committee on the Effects of Atomic Radiation 1977 Report to the General Assembly, "Sources and effects of ionizing radiation," No. E.77.IX.1.

45. J. C. Arcos, "French research on chemical carcinogenesis in the last quarter century with special reference to the contributions of A. Lacassagne and N. O. Buu-hoi," *Chemical Carcinogenesis*, Part A, Marcel Dekker, Inc. (1974).

46. B. I. Lord, C. S. Potten, and R. J. Cole, (Eds.), *Stem Cells and Tissue Homeostasis*, Cambridge University Press (1978).

47. W. Gössner, B. Hindringer, O. Hug et al., "Early and late effects of incorporated ^{224}Ra in mice," *Proceedings of the First International Congress of the French Society for Radioprotection*, Commissariat a l'Energie Atomique, Grenoble, 528-548 (1971).

48. A. N. Raick, K. Thumm, and B. R. Chivers, "Early effects of 12-O-tetradecanoyl-phorbol-13-acetate on the incorporation of tritiated precursor into DNA and the thickness of the interfollicular epidermis, and their relation to tumor promotion in mouse skin," *Cancer Res.* 32, 1562-1568 (1972).

49. J. A. Miller and E. C. Miller, "Some current thresholds of research in chemical carcinogenesis, *Chemical Carcinogenesis*, p. 76 (1974).

50. P. Emmelot and E. Scherer, "Multi-hit kinetics of tumor formation, with special reference to experimental liver and human lung carcinogenesis and some general conclusions," *Cancer Res.* 37, 1702-1708 (1977).

51. M. Terzaghi and J. B. Little, "Repair of potentially lethal radiation damage in mammalian cells is associated with enhancement of malignant transformation," *Nature* 253, 548-549 (1975).

52. L. J. Cole and P. C. Nowell, "Accelerated induction of hepatomas in fast neutron-irradiated mice injected with carbon tetrachloride," Annals New York Academy of Science, 114, 259-267 (1963).

53. J. C. Fisher and J. H. Hollomon, "A hypothesis for the origin of cancer foci," *Cancer* 4, 916-918 (1951).

54. J. L. Marx, "DNA repair: New clues to carcinogenesis," *Science* 200, 518-521 (1978).

55. R. D. Evans, "Radium in man," *Health Phys.* 27, 497-510 (1974).

56. Z. M. Bacq and P. Alexander, *Fundamentals of Radiobiology*, Pergamon, New York (1961).

57. S. I. Rubinow, "Human Leukemia: Kinetic aspects and speculations concerning its cellular origin," *Proceedings of a Conf. on Envir. Health*, Alta, Utah, July 5-9 (1976).

58. National Council on Radiation Protection and Measurements, "Review of the current state of radiation protection philosophy," *NCRP Report No. 43* (1975).

59. H. J. Curtis, C. Czernik, and J. Tilley, "Tumor induction as a measure of genetic damage and repair in somatic cells of mice," *Radiat. Res.* 34, 315-319 (1968).

60. C. O. Nordling, "A new theory on the cancer-inducing mechanism," *Brit. J. Cancer* 7, 68-72 (1953).

61. J. M. Brown, "Linearity vs non-linearity of dose response for radiation carcinogenesis," *Health Phys.* 31, 230-247 (1976).

62. H. M. Patt, "Radiobiology of cell renewal systems," _____. IAEA, Monoco, 3-19 (1968).

63. S. Lesher and J. Bauman, "Recovery of reproductive activity and the maintenance of structural integrity in the intestinal epithelium of the mouse after single-dose whole-body ^{60}Co gamma-ray exposures," _____, IAEA, Monoco, 507-513 (1968).

64. R. Suss, V. Iknzel, J. D. Scribner, *Cancer Experiments and Concepts*, Springer-Verlag, New York, 51, 200 (1973).

65. P.R.J. Burch, *The Biology of Cancer — A New Approach*, University Park Press, Baltimore (1976).

66. F. Devik, "Studies on the duration of DNA-synthesis and mitosis in irradiated and regenerating epidermia cells in mice, by means of tritium-labelled thymine," *Int. J. Radiat. Biol.* 5, 59-66 (1962).

67. A. E. Needham, *The Growth Process in Animals*, Van Nostrand Press, Princeton, 95 (1964).

68. J. E. Till, "Prospects in the study of stem-cell kinetics," _____, IAEA, Monoco, 117-122 (1968).

69. J. M. Brown, "The effect of acute x-irradiation on the cell proliferation kinetics of induced carcinomas and their normal counter-part," *Radiat. Res.* 43, 627-653 (1970).

70. W. V. Mayneord and R. H. Clarke, "Carcinogenesis and radiation risk: A biomathematical reconnaissance," *Br. J. Radiol.*, Suppl. 12, 1-112 (1975).

71. G. D. Zasukhina and T. A. Sinelushikova, "Toward an understanding of the action of certain mutagens of DNA in human cells," *ORNL-TR-4325* translated from *Dokl. Akad. Nauk SSSR* 230, No. 3 (1976).

72. J. J. Roberts, J. E. Sturrock, and K. N. Ward, "DNA repair and alkylation — induced toxic mutagenic, and cytological effects in mammalian cells," *Chemical Carcinogenesis* (1974).

73. A. J. Becker, E. A. McCulloch, L. Siminovitch and J. E. Till, "The effect of differing demands for blood cell production on DNA synthesis by hemopoietic colony-forming cells of mice," *Blood* 26, 307 (1965).

74. A. L. Wiley, Jr., H. H. Vogel, Jr., and K. H. Clifton, "The effect of variations in LET and cell cycle on radiation hepatocarcinogenesis," *Radiat. Res.* 54, 284-293 (1973).

75. T. D. Jones, "Radiation protection based on risk: Optional RBE for cancer," in review.

76. N. Nelson, "Comments on extrapolation of cancer response from high dose to low dose," *Envir. Health Perspectives* 22, pp. 93-95 (1978).

77. A report of the United Nations Scientific Committee on the Effects of Atomic Radiation to the General Assembly, "Ionizing radiation levels and effects," E.72.IX.18 (1972).

78. A. Rindi and R. H. Thomas, "Povera e nuda vai, dosimetria," *Health Phys.* 23, 715-727 (1972).

79. W. V. Mayneord, "The time factor in carcinogenesis," Sievert Lecture, Fourth International Congress of IRPA, Paris, April 1977, 1, 430, *Health Phys.* 34, 297-309 (1978).

80. H. P. Koeffler and D. W. Golde, "Acute myelogenous leukemia: A human cell line responsive to colony-stimulating activity," *Science* 200, 1154 (1978).

81. H. H. Vogel, Jr., "Neutron-induced mammary neoplasms," *Proceedings of a Symposium in Neuherberg (October 22-26, 1973)*, International Atomic Energy Agency, Vienna (1974).

82. National Council on Radiation Protection and Measurements, "Basic Radiation Protection Criteria," NCRP Report No. 39, January 15, 1971.

83. H. H. Rossi and C. W. Mays, "Leukemia risk from neutrons," *Health Phys.* 34, 353-360 (1978).

NBS SP 554 (1979)

CLINICAL TRADEOFF: THE MAXIMUM PROBABILITY OF UNCOMPLICATED CURE

Lionel Cohen
Michael Reese Medical Center
Chicago, Illinois 60616

Any new procedure intended to yield more effective tumor control in clinical radiation therapy carries the concomitant risk of more severe acute and remote side effects. The effective gain or trade-off can then be evaluated in two ways. One is an instantaneous optimization function (cure-rate minus complication-rate) determining the probability of uncomplicated cure, which can presumably be maximized by judicious choice of technique. Consideration of long-term effects however suggests that a different optimization algorithm, integrating the total expectation of disease-free person-years is more realistic. It can be shown that even if higher energy radiation leads to a small increase in the rate of local control, or in the time to recurrence in uncontrolled cases, these gains would effectively offset the risk of induced neoplasia or similar remote complications.

Introduction

There are many precedents in the history of radiation therapy where the transition to a new modality of treatment has raised questions in regard to the merit and safety of the supposedly more effective procedure. Any change in technique or departure from well-established procedures in a therapeutic regime could result in a more or less significant change in the probability of controlling the disease as well as in the risk of serious side effects. To some extent both the advantages and hazards can be assessed in advance, and some estimate made of the probable gain to be expected. Since the new modality has necessarily not been studied exhaustively, the information required to estimate the expected gain is seldom complete. More often the new procedure must be explored in the belief that the inevitable errors, difficulties and complications that will be encountered can be minimized with experience, and that any improved results which can be achieved will be maximized by the necessary attention to technical detail. The sequence of exploration, information feedback, error correction and optimization provides the conditions under which the clinical gain can be made to offset the additional risks.

As an example of the foregoing reasoning, one recalls the occasion when radiation oncologists were required to justify the acquisition of cobalt units at a time when the best available modality was 250 Kv x-ray therapy machines. The main motivation for acquiring the new equipment was better depth dose and skin sparing. These were attractive advantages in view of the severe skin reactions which invariably accompanied radical orthovoltage radiation therapy. On the other hand, the advantages of the high-energy beam could be discounted by many new problems. Not the least of these was the absence of a visible skin reaction. Previously the skin reaction had been used as a biological dosimeter, prescribed treatments being supplemented if reactions were mild or curtailed if they were excessively severe. In practice the radiation therapist had implicitly corrected calibration or dosimetric errors by standardizing normal tissue reactions. Without this safeguard the new modality required a new order of dosimetric precision if severe complications from excessive dosage in deeper tissues were to be avoided.

Whether improved cure-rates with cobalt therapy would be large enough to justify the additional risks, the major physics effort needed for calibration and planning, and the extensive rethinking in regard to dosage and tolerance limits required on the part of the prescribing radiotherapist was seriously questioned. Many years of accumulated experience by both radiation oncologists and medical physicists were required before the superiority of the new technique could be proved by hard statistics.

There were to be similar difficulties in the transition from cobalt therapy to megavoltage linear accelerators, with further complications as the radiotherapeutic art evolved to include high-energy electron beams. A further escalation in complexity both in the physics and biological understanding of the beam was entailed when use of heavier particles (nuclei, neutrons or pions) was implemented. In each case the theoretical rationale for exploring the new modality needed to be strong enough to justify the professional effort and financial cost involved in developing the new modality, and the many years of research and experience were necessary before clear-cur statistics on the efficacy of the new modality could be presented.

Instantaneous Optimization Functions

The possible existence of an optimal dose, or even an optimal fractionation scheme, was recognized early in the history of radiation oncology. Holthusen first noted that the steep sigmoid dose and normal tissue damage leads to the conclusion that the probability of uncomplicated cure after a course of radiation therapy depends critically upon the dosage delivered (Ho36). If the probability of tumor control (P_t) and the probability of normal tissue injury (P_n) are stochastically independent, then the conditional probability of uncomplicated cure (P_c) is given by: $P_c = P_t)1-P_n)$. The shape of this function (Fig. 1) is clearly related to the relative positions of the curves for tumor control and for normal tissue complications on the dose axis. The greater the separation of these two curves the higher the probability of uncomplicated control at the defined optimal dose.

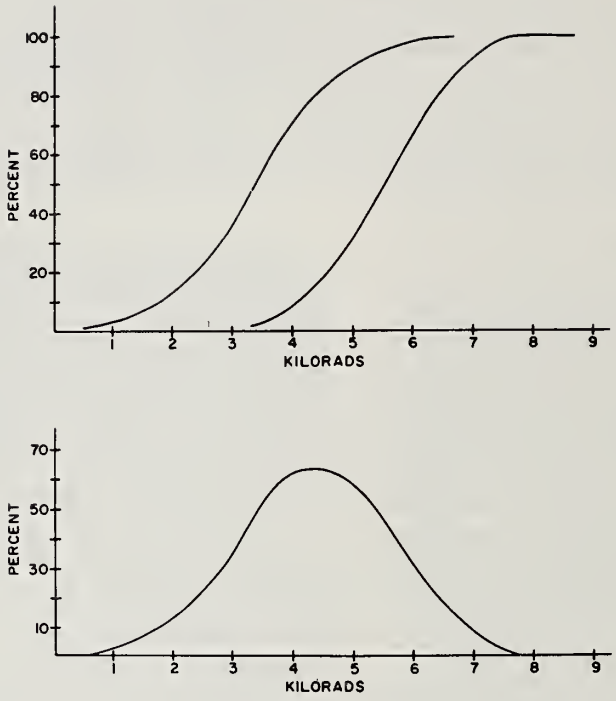

Figure 1 Dose-effect relationships. Sigmoid response curves for control of mammary carcinoma (left) and damage to normal tissues (right-hand curve) treated on 10 fractions over 3 weeks. The probability of uncomplicated control (lower curve) has a clearly defined maximum at 45 Gy.

Strandqvist (ST44) demonstrated the dependence upon treatment time of the median doses required to produce a standard reaction in radiation therapy. Later DuSault (Du56) showed that different tissues and tumors have different dose-time relationships and that the separation between the sigmoid curves of Figure 1 could vary widely depending upon the fractionation scheme used. Treatment could be optimized in regard to both the dosage delivered and the particular fractionation scheme chosen, and the optimal procedure could be computed for various combinations of tumor and normal tissues irradiated. A model for optimizing the treatment scheme was proposed by Moore and Mendelsohn (No72) from which the most acceptable procedure could in principle be determined, given appropriate weighting coefficients for the probability of tumor cure and the risk of complications.

A consequence of this analysis is that cautious radiotherapy (never exceeding safe dosage limits) is not the best policy if cure-rates are to be maximized. Aggressive radiotherapy, in which the incidence of significant complications is at least as high as the incidence of local recurrent, is more likely to be associated

with the highest probability of uncomplicated cure (Co73). Since tumor recurrence or failure to cure is in reality the most serious outcome of a course of treatment, the total incidence of complications (which in this instance includes recurrence) is minimized by the more aggressive approach. This trend is becoming increasingly recognized in modern radiation oncology. Current practice encourages delivery of higher doses to wider fields in order to approach the theoretical optimum.

There is, however, an inherent limitation to this approach which should be recognized. In this discussion cure, complications and probabilities were considered as if they described instantaneous events, in which the application of a particular treatment leads to a specified immediate outcome. Under these circumstances the probability of uncomplicated cure is a meaningful figure of merit to be maximized. In practice, the outcome is not instantaneous but a protracted, time-dependent process spread over many years. The practicing radiation oncologist recognizes that a tumor may regress initially and appear to be cured, and yet recur or metastasize in later years. If the remission period were sufficiently prolonged, such a late recurrence might not be considered a failure. Similarly, the most significant side effects may be acute reactions following immediately after the course of radiation, but more commonly we are concerned with late effects appearing characteristically between 1 and 3 years after treatment. At this juncture we are considering an even later side effect, namely that of induced neoplasia which may occur between 5 and 25 years after exposure. Under these circumstances the instantaneous optimization function based on the response observed at a specific follow-up date is clearly inappropriate, and a new figure of merit is required for optimization. This should take into account not only the probability of uncomplicated control, but a time-integrated response, possibly the number of disease-free person-years, generated by the particular treatment policy under scrutiny.

INTEGRAL OPTIMIZATION FUNCTIONS

An optimization algorithm based on the total proportion of disease-free person-years, that is the integrated sum of uncomplicated tumor control over survival time, is a complex function of dosage and treatment technique which can probably only be evaluated in qualitative terms at the present time. The variables that will need to be considered include the probability that the tumor is completely sterilized, the time to recurrence if the tumor does recur, the expected incidence of acute reactions of unacceptable severity, the anticipated incidence of late radiation damage, the anticipated incidence of "very late" effects such as neoplasia, and the actuarial expectation of life for a normal population corresponding in age and other social factors to the patient population at risk. Some of these rates can undoubtedly be estimated on the basis of current therapeutic experience, but others will need to be evaluated with future experience, paying particular regard to dose-effect relationships. Although increasing dosage may well increase the risk of all side effects, including late neoplasia, higher tumor doses may well lead to improved local control in two respects. Firstly, since ionizing radiation provides a measure of tumor control by killing or sterilizing tumor cells following a deterministic survival function, the probability that the tumor is completely ablated (surviving cell population reaches zero or some critically small number incapable of maintaining continued growth) is a function of dosage. Secondly, if a small residual viable cell population persists, the time to recurrence will depend on the number of surviving cells, and hence the remission-time is likely to be directly proportional to tumor dose. Consequently, both the cure-rate and the number of disease-free person-years (or any equivalent time-integrated figure of merit) will increase with increasing dosage or increasing treatment efficiency, independently of the increasing risk of complications.

The conditional probability of uncomplicated time-integrated survival is illustrated, albeit in a qualitative manner, in Figure 2. In this representation line A indicates the actuarial expectation of life of the corresponding normal population. It is assumed that a certain proportion of tumors are cured (line B 60%) and the remainder will eventually recur (line C, 40%), with a specified median time to recurrence (R = 2 years). Line S = (B + C) is the total survival curve for the treated population. In this diagram complications are assumed to comprise 5% severe acute reactions, 5% severe late effects arising between 1 and 3 years after treatment and 5% late neoplasia arising between 8 and 12 years after treatment. These complications are super-imposed upon the surviving population and will consequently resemble the complex functions illustrated by D1, D2 and D3 in the diagram. The total prevalence of radiation induced complications in the population at any one time is then given by the summation shown by line D. The curve for disease-free or uncomplicated survival can then be described by the stepped function shown by line E in the diagram.

It will be noted that the total effect attributable to late neoplasia with an incidence of 5% represents a very small fraction of the number of disease-free person years as illustrated by the shaded area (F) in Figure 2. Clearly a very small increase, on the order of 2%, (raising the origin of line B from 60% to 62%) or a prelongation of the average time to recurrence (R in Figure 2) from 2 to 3 years would be sufficient to counterbalance the 5% incidence of neoplasia occurring at a median survival time of 10 years. Naturally, should the real incidence of induced neoplasia be different from the assumed 5%, the necessary improvement in cure rate or remission time would have to be adjusted proportionally. The general rule, however, remains that a relatively hish incidence of late neoplasia appearing many years after treatment is readily offset by quite a modest improvement in local control.

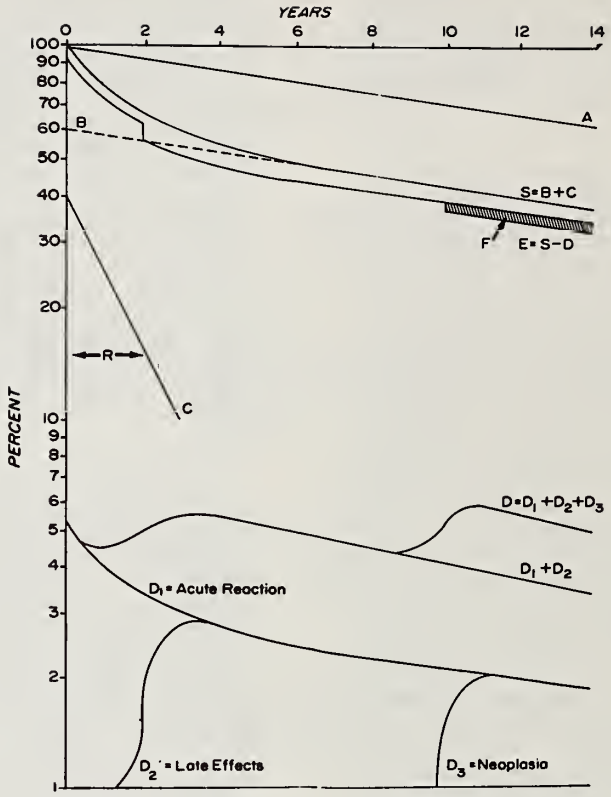

Figure 2 Integrated probability of long-term control. A = actuarial survival rate; B = survival in "cured' group; C = survival of "failed" group; D = incidence among survivors of early and late side effects; E = resultant symptom-free survivals; F (shaded area) = net loss in person-years attributed to induced late neoplasia.

CONCLUSIONS

Since the state-of-the-art in radiation oncology at the present timeis such that local cure rates (excluding the problem of metastases) seldom approach 100%, methods for improving local control by optimizing the treatment plan and fractionation scheme will be pursued vigorously. All such technical innovations carry risks of side effects, either increased frequency or severity of expected complication compared to the risk with more conventional procedures; or new reactions not normally observed. In the few clinical situations where local control rates do approach 100% (early Hodgkins' Disease, seminoma, and small epidermoid carcinoma) the use of a new modality carrying a significant risk of additional late effects, obviously cannot be justified. In all situations where local control rates fall

short of this ideal, and where a modest improvement in local control can be expected by virtue of higher or more effective local dosage being achieved with a new modality, or better definition of the target volume with the exclusion of dose-limiting vital organs in the irradiated field, the expected gains are likely to offset the additional risks. The risk of late neoplasia, which is the major concern of neutron contamination in high-energy electron accelerators, would therefore appear to be a trivial one relative to possible benefits, provided those cases in whom 100% local control can be achieved with low energies are excluded from treatment by this modality.

REFERENCES

Co60 Cohen L., 1960, "The Statistical Prognosis in Radiation Therapy, Radiology, 84, 741.

Co73 Cohen L., 1973, "Cell Population Kinetics in Radiation Therapy: Optimization of Tumor Dosage", kCancer, 32, 236.

Du56 DuSault L., 1956, "Time-dose Relationships", Amer. J. Roentgenol, 75, 597.

Fl73 Fletcher G.H., 1973, "Clinical Dose-response Curves of Human Malignant Epithelial Tumors:, Brit. J. Radiol., 46, 1.

Ho36 Holthusen H., 1936, "Erfahrungen uber die Vertraglichkeitsgrenze fur Rontgenstrahlen und deren Nutzanwendung zur Verhutung von Schaden", Strahlentherapie, 57, 254.

Mo72 Moore D.H. and Mendelsohn, M.L., 1972, "Optimal Treatment Levels in Cancer Therapy", Cancer, 30, 97.

St44 Strandqvist M., 1944, "Studien uber die kumulatiewe Wirkung der Rontgenstrahlen bei Fraktionierung", Acta Radio., Suppl. 55.

DEPENDENCE OF RADIATION-INDUCED NEOPLASTIC TRANSFORMATION IN VITRO UPON RADIATION QUALITY AND REPAIR

A. Han and M. M. Elkind
Division of Biological and Medical Research
Argonne National Laboratory
Argonne, IL 60439

C3H/10T1/2 mouse embryo cells grown in culture were irradiated with single or fractionated doses of fission-spectrum neutrons from the JANUS reactor or with 50-kV X-rays; survival and frequencies of neoplastic transformation were measured and the relative biological effectiveness (RBE) for each end point was estimated. As expected, for both survival and transformation, RBE's depend upon level of effect, being higher for small than for large doses. Changes in transformation frequencies following X-ray dose fractionation indicate appreciable repair of both sublethal and subtransformation damage. Results of fractionation of the fission-spectrum neutron dose suggest repair of the first-dose subtransformation damage and no repair of sublethal damage. The observed results for the induction of neoplastic transformation in C3H/10T1/2 cells are qualitatively similar to data for tumor induction in animals.

(Carcinogenesis; neutron; repair; survival; transformation; X-ray)

Introduction

Radiobiological effects of fast neutrons are currently receiving considerable attention mainly because of the potential usefulness of fast neutrons in tumor radiotherapy. Interest in fast neutrons also stems from the fact that they are a by-product of nuclear power and there is a need to evaluate the hazards to man. For these reasons, fast neutrons are of a major importance in considering the influence of radiation quality in various radiobiological endpoints relevant to determination of their relative biological effectiveness (RBE).

Studies with experimental animals provide ample evidence that ionizing radiations induce tumors. This is true for both low and high LET radiations. In view of the complexity of the whole organism and studies of carcinogenesis in the whole animal, it is useful to employ simpler systems such as cultured mammalian cells. Such systems can provide basic information of dose-effect relationships, proliferation kinetics of normal and transformed cells, and can help in our understanding of tumor induction in vivo. Mammalian cells in culture are widely used to study mechanisms of radiation action as they provide reproducible data free of interactions that exist in whole organism.

Aside from cell survival, one of the most important responses studied is the potential of surviving cells to produce cancer. In the past decade a number of mammalian cell systems in culture became available for evaluating the neoplastic transformation of cells in vitro. It has been generally established that exposure of normal cells in culture to ionizing radiations[1,2,3,4,5] results in neoplastic transformation, i.e., the conversion of normal cells that exhibit a high degree of growth control through contact inhibition and oriented growth patterns into cells that lose the growth control, begin to pile up, and grow at random.[1,2,3] In contrast to normal cells, transformed cells induce neoplasms in appropriately treated hosts.[2,3,5]

To date, two systems have been used for studies of radiation-induced neoplastic transformation in vitro, primary cultures of Syrian hamster embryo cells[1,2,4] and mouse embryo derived C3H/10T1/2, Clone 8, cells.[3,5] In both systems, cells isolated from transformed foci produced tumors upon inoculation into appropriately treated hosts. Despite certain differences in the results obtained with the two systems, very useful information concerning the cellular aspects of neoplastic transformation has been provided thus far. Dose-response curves for neoplastic transformation following X-rays[2,3,5] and neutrons,[4,5] have been determined including the estimates of RBE of fast neutrons relative to X-rays for cell killing and neoplastic transformation,[4,5] changes in the frequency of neoplastic transformation following dose fractionation of X-rays[5,6,7,8] and neutrons[5] have been studied.

We review here comparative observations of the capacity of fission-spectrum neutrons and X-rays to induce neoplastic transformation in C3H/10T1/2 cells following single and fractionated exposures. The effect of dose fractionation on neoplastic transformation is examined in greater detail to determine if repair processes are involved in repair of sublethal damage and neoplastic transformation.

Dose Responses for Survival and Neoplastic Transformation

The survival curves of 10T1/2 cells after fission-spectrum neutrons and X-rays (Fig. 1) have shoulders indicating that these cells have appreciable capacity to accumulate sublethal damage caused by both radiations. The neutron survival curve has a relatively large shoulder, as may be estimated from the specific shoulder width of 1.5 (see legend of Fig. 1). Smaller shoulders, that is almost exponential survival, are generally observed

for high LET radiations like fission-spectrum neutrons.[10] The RBE for survival in these cells exhibits relatively small dependence on dose. The estimates of RBE gives a nominal value of 2.9 for small exposures producing about 0.8 surviving fraction, with progressive decrease with dose to a nominal value of about 2.2 at 0.001 survival.

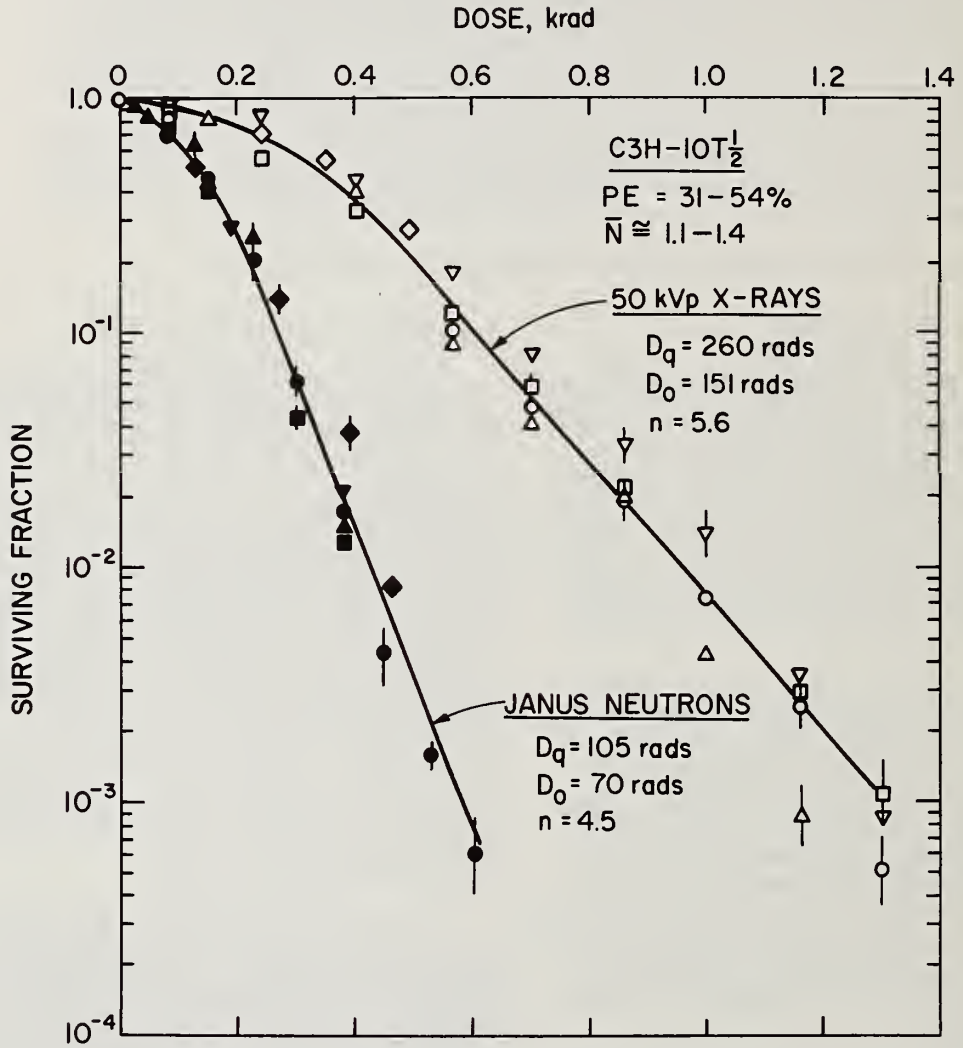

Fig. 1. Survival (colony formation) of C3H/10T1/2 cells after exposure to different doses of 50 kVp X-rays (open symbols) or fission-spectrum neutrons (closed symbols). Various symbols represent different experiments. Error bars, standard errors of individual data points, are shown where they are larger than the points. The survival curve parameters shown have the following meanings: D_0 is the dose required to reduce survival by 1/e along the terminal straight line portion of the curve; D_q, is the quasi-threshold dose;[9] n, is the extrapolation number [exp (D_q/D_0)]; the specific shoulder width is given by $\rightarrow$ D_q/D_0, and $\bar{N}$, is the average number of cells in microcolonies at the time of irradiation, i.e., the average cellular multiplicity. Cells were incubated at 37°C for 10-14 days following irradiation and colonies were then counted. (From Han and Elkind, Cancer Res. 39, 123-130, 1979)

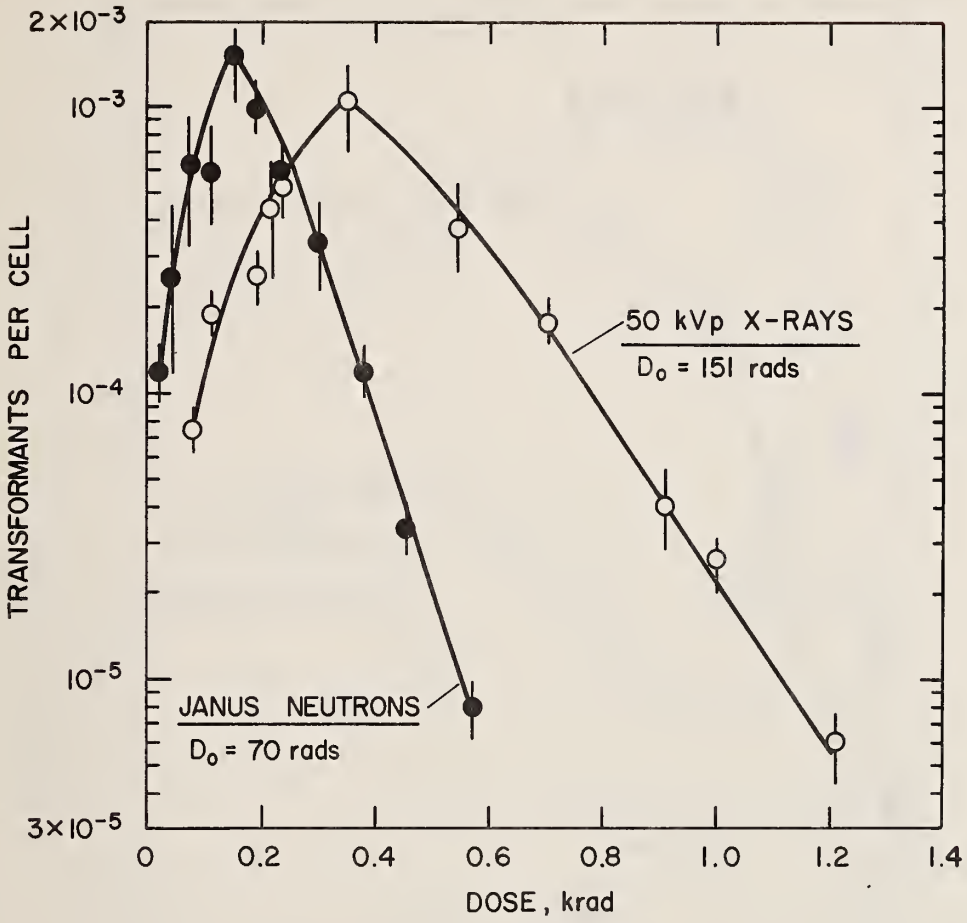

Fig. 2. Induction of transformed cells by 50 kVp X-rays (O) and fission spectrum neutrons (●) in C3H/10T1/2 cells. Transformation is expressed on a per irradiated cell basis (i.e., independent of cell killing). Error bars represent the standard errors of data pooled from different experiments. The cultures were incubated 6 weeks after irradiation and refed weekly with fresh medium (Basal Eagle Medium + 10% fetal calf serum). Incubations were carried out at 37°C in humidified mixture of air (98%) and CO_2 (2%). (From Han and Elkind, Cancer Res. 39, 123-130, 1979)

The incidence of neoplastic transformation following a range of single exposures of neutrons and X-rays is shown in Fig. 2. The data shown are expressed on a per cell basis, that is, the transformation frequency is expressed as a number of transformed cells as a fraction of the total number of cells at risk and no correction is made for cell killing. Presentation of the data in this way is relevant in comparing the radiosensitivity of potentially transformed and nontransformed cells, as well as relating the dose response curves to the observations on tumor induction in vivo. The two curves, although similar in shape, exhibit significant quantitative differences. The shapes of these curves, as first noted by Gray,[11] reflect the combined effects of transformation induction (ascending part) and the killing of target cells (descending part). The D_0's of the final slopes of the induction curves on Fig. 2 are equal to those of the survival curves (see Fig. 1), indicating that in the region of large doses, at least, potentially transformed cells are killed at the same rate as untransformed mouse cells. This observation is in contrast to data obtained with the Syrian hamster embryo cells[2] which indicate that at doses above 300 rad potentially transformed cells are preferentially killed by X-rays.[12]

As noted, the induction curves in Fig. 2 are calculated on the basis of the total number of cells at risk, that is, they do not account for cell survival. When this correction is applied to induction curves from Fig. 2, the transformation frequency per surviving cell is obtained. The dose-response relationship for the induction of neoplastic transformation per surviving cell

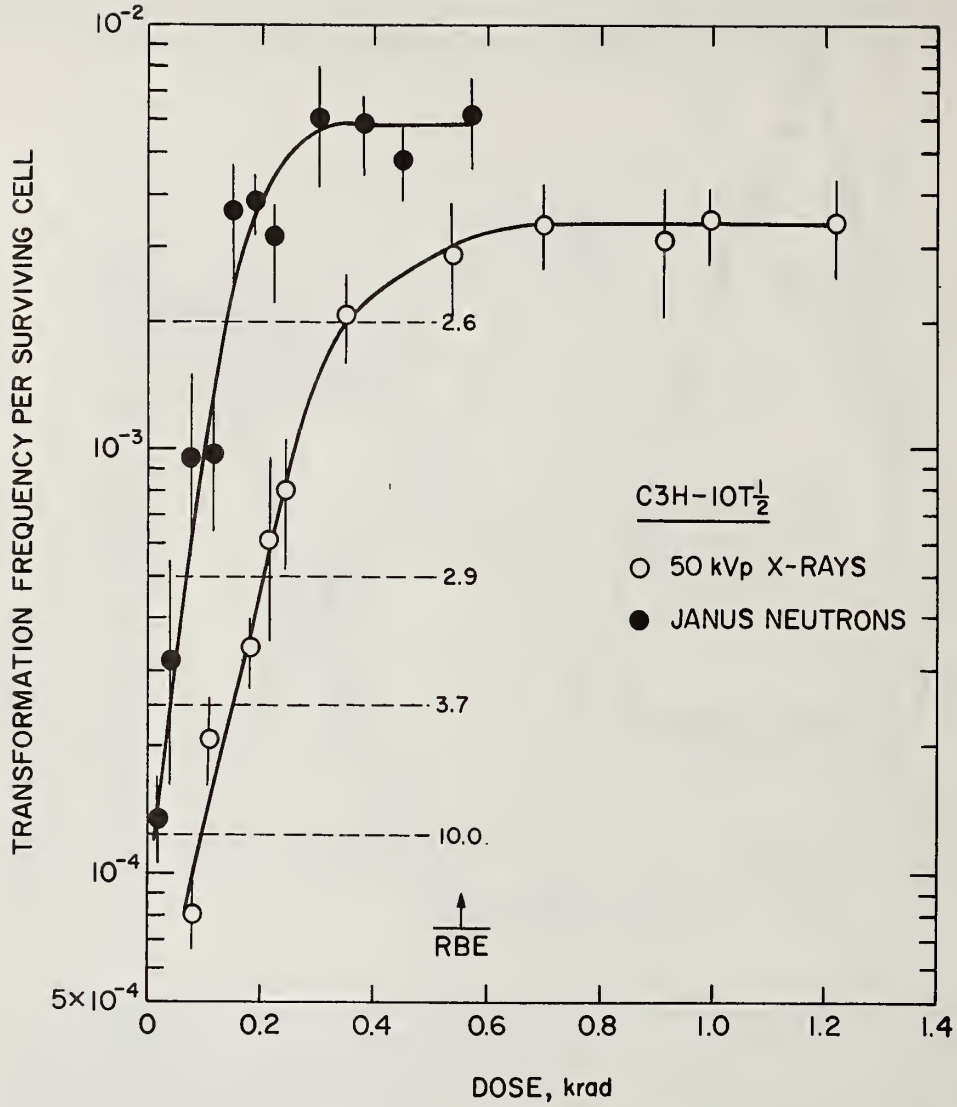

Fig. 3. Transformation frequency of C3H/10T1/2 cells induced by 50 kVp X-rays (O) and fission-spectrum neutrons (●). RBE stands for relative biological effectiveness and at the frequency levels shown, was determined from the ratio of the X-ray to neutron doses. Error bars represent the standard errors of data pooled from different experiments (2-5 per point). The experimental conditions were as described in Fig. 2. (From Han and Elkind, Cancer Res. 39, 123-130, 1979)

is obtained. The dose-response relationship for the induction of neoplastic transformation per surviving cell by fission-spectrum neutrons and X-rays is shown in Fig. 3. As can be seen, both curves appear to be initially exponential, with the neutron induction curve having a steeper slope. The maximum frequency induced by neutrons of about 6×10^{-3} transformants per survivor is reached at a dose of about 300 rads. The X-ray induction curve rises up to about 600 rads where a plateau at a frequency of about 3.5×10^{-3} transformants per survivor is reached. The neutron induction curve shows the transformation frequencies for single doses ranging from 21-568 rads, and X-ray curve for a range of doses from 80-1238 rads. As indicated on Fig. 3, the RBE for neoplastic transformation is about 10 in the region of small doses and decreases to about 2.6 as the dose increases. It would seem, therefore, that the RBE of neutrons relative to X-rays, for induction of neoplastic transformation, is somewhat different from that for cell survival. In the region of the plateaus, RBE cannot be estimated because the requirement of "equal level of effect" is not satisfied.[13]

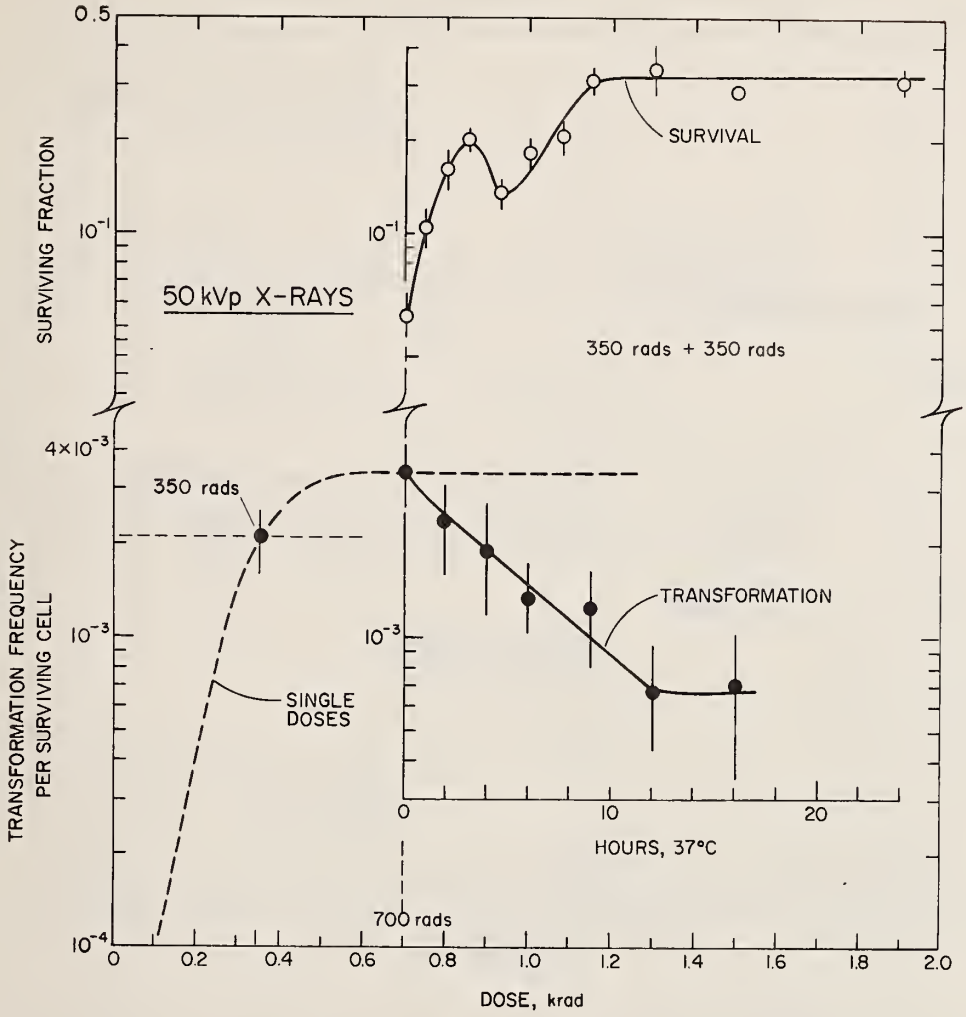

Fig. 4. Changes in survival and transformation frequency per survivor in C3H/10T1/2 cells exposed to fractionated doses of 50 kVp X-rays. Cell survival (O); transformation (●). Error bars represent standard errors of the pooled data from different experiments. The single-dose induction curve (dashed line) comes from Fig. 3. Inset abscissa, time at 37°C between the two exposures; the 0 fractionation time is plotted from the total dose of 700 rads. (From Han and Elkind, Cancer Res. 39, 123-130, 1979)

Effect of Dose Fractionation on Survival and Neoplastic Transformation

Thus far we have shown a greater ability of neutrons to induce neoplastic transformation and variation in incidence of neoplastic transformation as a function of a single dose of neutron or X-rays. However, in view of the possible modes of neutron applications, the likelihood of exposure to a relatively large single dose of radiation is rather small. As far as the radiation hazard is concerned, it is likely that therapeutic exposure will almost certainly be in several fractions rather than in one single exposure. It is also likely that our environmental exposure will be essentially a fractionation or protraction experience. In this context, damage registration cannot be dissociated from the possible effect of repair on damage expression. During the fractionation interval, various repair processes may act upon the induced damage and as the ultimate result we observe increased survival. Thus, it is important to establish what, if any, is the effect of repair of sublethal damage or repair of sub-transformation damage during the dose fractionation upon the incidence of neoplastic transformation.

To facilitate comparison of our observations with results from animal experiments, we again analyze our data expressed both as the transformation frequency on the per cell at risk basis, and the number of transformants per surviving cell. The effect of dose fractionation on survival and

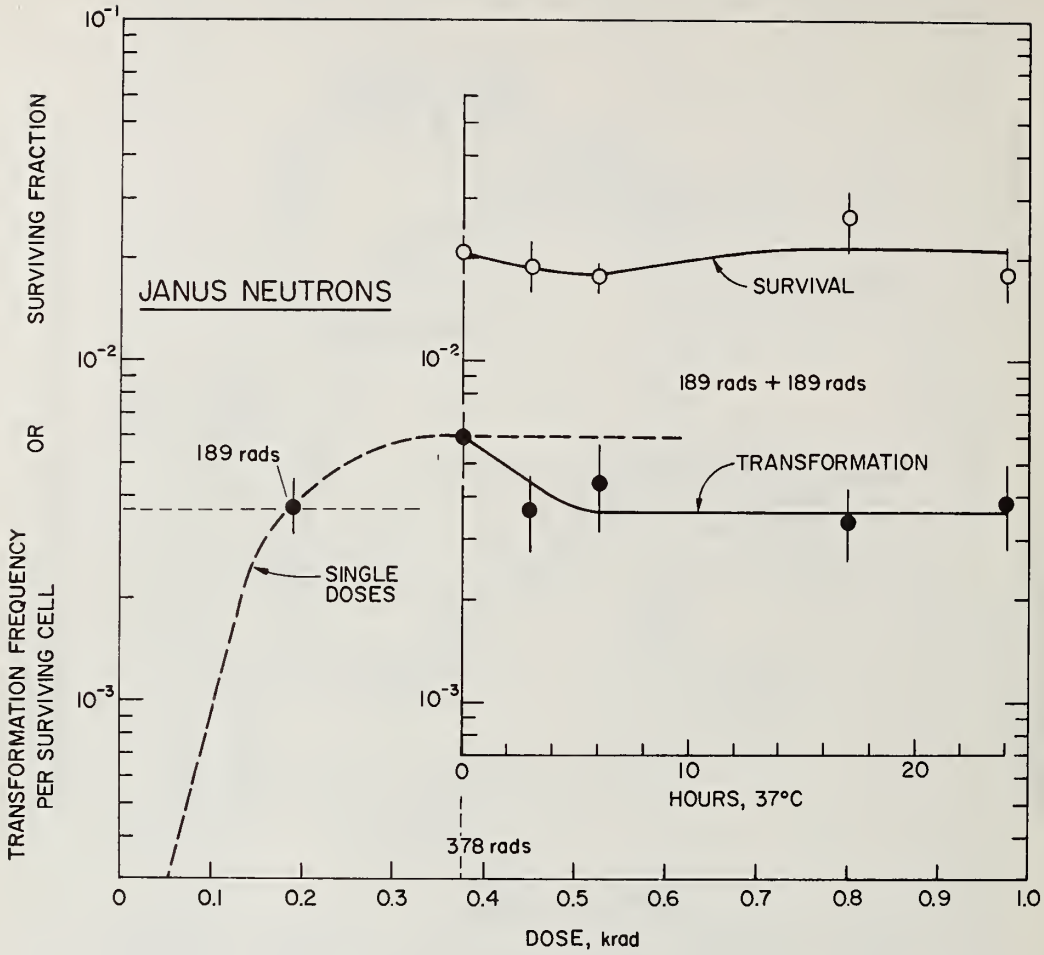

Fig. 5. Changes in survival and transformation frequency per survivor in C3H/10T1/2 cells exposed to fractionated doses of fission-spectrum neutrons. Cell survival (○); transformation (●). Error bars represent standard errors of pooled data from different experiments. The single-dose curve (dashed line) comes from Fig. 3. Inset abscissa, time at 37°C between the two exposures; the 0 fractionation time is plotted from the total dose of 700 rads. (From Han and Elkind, Cancer Res. 39, 123-130, 1979)

transformation frequency following X-rays and neutrons is shown in Figs. 4 and 5, respectively. We first note that the effects of dose fractionation on survival shown in these two figures are qualitatively similar to data obtained with other cell lines in vitro[10,14] and clonogenic cells in vivo.[15] As expected, fractionation of the X-ray dose results in prompt increase in cell survival due to repair of sublethal damage, whereas for neutrons there is no increase in survival with fractionation.[16] It is of interest to note that in C3H/10T1/2 cells large capacity of these cells to accumulate sublethal neutron damage (note the specific shoulder width on neutron survival curve--Fig. 1) is not accompanied by the repair of sublethal damage. The number of transformants per surviving cell decreases significantly with time between X-ray exposures (Fig. 4), but only slightly with time between the two neutron exposures (Fig. 5). The number of transformants per survivor after X-irradiation declines steadily with increase in time between fractions up to about 12 hr giving about 5-fold reduction in transformation frequency. In comparison, fractionation of neutron dose results in about 1.7-fold reduction in transformation per survivor, at most. Since the fractionation of X-ray dose results in substantial increase in net survival, and that of neutron dose in essentially no change in net survival, it is probable that differences in cell survival are an important contributing factor, but not necessarily the only factor, in evaluating the effect of X-ray and neutron dose fractionation on the incidence of neoplastic transformation. Support for this view also comes from data in Fig. 6 where the transformation results after fractionated neutron and X-ray irradiation are expressed

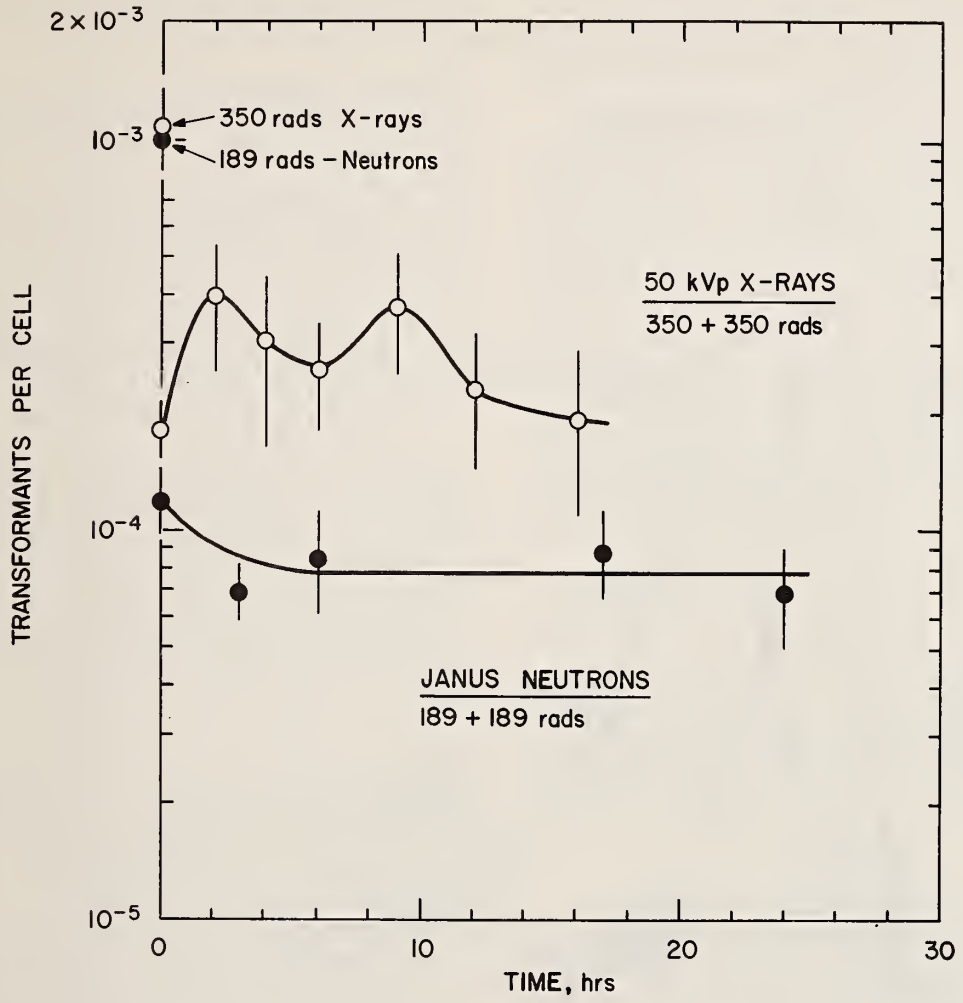

Fig. 6. Changes in transformation frequencies for C3H/10T1/2 cells exposed to fractionated doses of X-rays (O) or fission-spectrum neutrons (●) when expressed on a per irradiated cell basis. Error bars represent standard errors for data pooled from different experiments. Cells were incubated at 37°C between exposures. (From Han and Elkind, Cancer Res. 39, 123-130, 1979)

as transformants per exposed cell, and the shape of the fractionation curve is not influenced by the repair of sublethal damage in surviving cells. This plot suggests a 1.5 to 2-fold increase in transformation frequency of X-irradiated cells during the first 9 hr and comparable decrease of neutron irradiated cells up to 24 hr. The shape of neutron curve is essentially the same as in Fig. 5, while the shape of X-ray curve differs appreciably from the transformation curve in Fig. 4. From the data in Fig. 6, one might infer that for small doses of X-rays that produce little or no cell killing, dose fractionation with an interval up to about 9 hr between the two fractions might result in a higher incidence of neoplastic transformation than the same total dose in a single fraction. Such inference would be in agreement with observations in Syrian hamster embryo[6] and 10T1/2 cells[7,8] that fractionation of X-ray doses with little or essentially no killing, when compared to a single dose, resulted in about 2-fold increase in transformation frequency with 2 equal dose fractions separated by a 5 hr interval. However, our X-ray data suggest that by 16 hr no enhancement is observed.

Relevance of in Vitro Observations to Animal Experiments

The results with cultured C3H/10T1/2 cells on radiation-induced neoplastic transformation are relevant to tumor induction in the whole organism. The incidence of induced tumors depends primarily upon the number of cells at risk. Since the fraction of cells that survives a particular treatment is generally not known, our data may be applied, as already pointed out, to tumor induction by considering transformation frequencies per cells at risk rather than per surviving cell. Therefore,

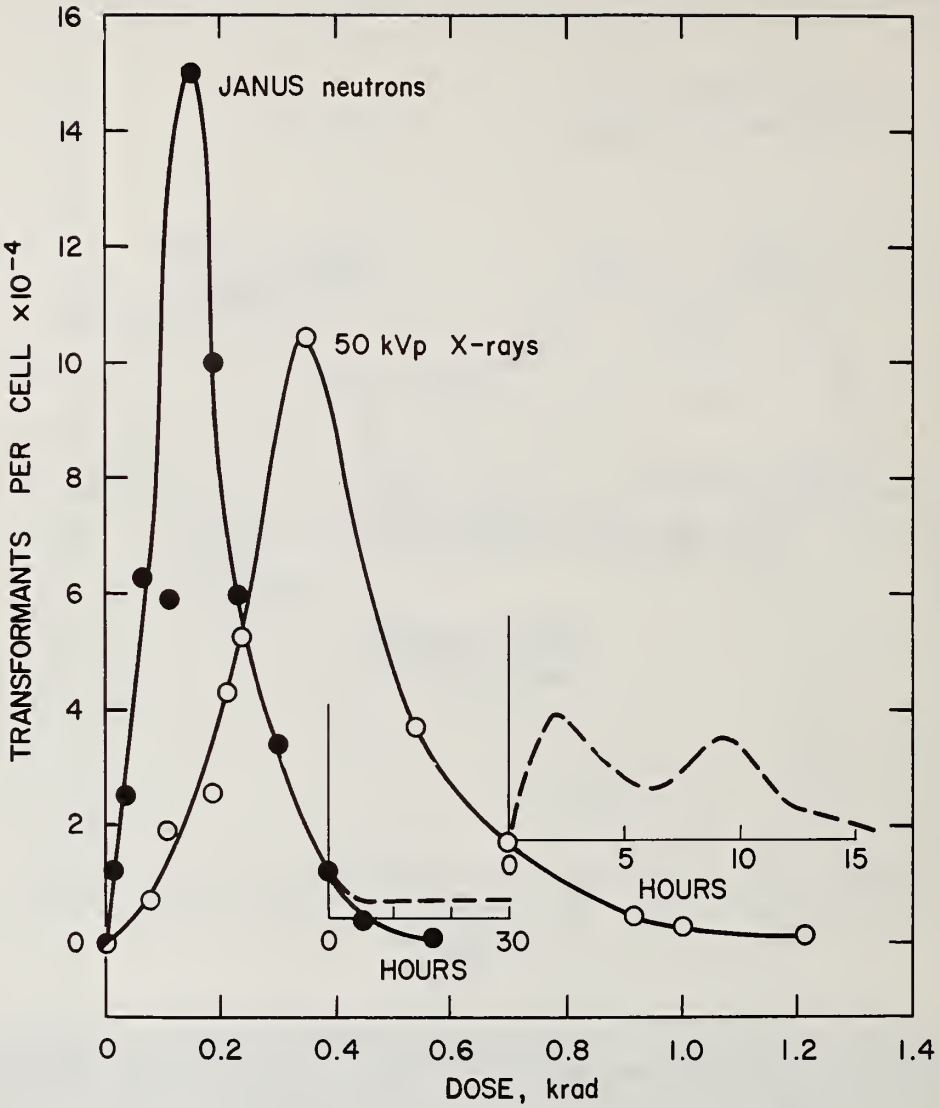

Fig. 7. Changes in transformation frequency of C3H/10T1/2 cells exposed to single (———) or fractionated (-----) doses of X-rays (○) or fission-spectrum neutrons (●). Data from Figs. 2 and 6 are replotted on linear coordinates to simulate the way in which tumor induction data from animal experiments are usually plotted. Inset abscissas, time at 37°C between fractions. From Han and Elkind, Cancer Res. 39, 123-130, 1979)

the results from Figs. 2 and 6 are replotted on linear coordinates and shown in Fig. 7 for comparison with the data for tumor induction in animals. Thus plotted induction curves are similar in shape to the curves for tumor induction.[cf 17,18] As noted earlier in this paper, the shape of the tumor induction curve reflects the combined effects of the induction and killing process in target cells.[11] It is clear that because of the displacement of the curve for induction of neoplastic transformation by neutrons toward the smaller doses, compared to the X-ray curve (see Fig. 7), the RBE of neutrons is consistently greater than 1. Furthermore, the differences in the shapes of the initial portions of the two induction curves imply that RBE in the region of small doses decreases with increasing dose. This feature is generally observed in animal studies.[19]

Experimental data with animals indicate that tumor incidences following neutron radiation with relatively low doses are not affected by dose fractionation and decreased dose rate.[17,20] Since survival following neutron dose fractionatio is not modified to any significant extent, the minor reduction in the frequency of neoplastic

transformation following fractionation of neutron dose is consistent with only minor contributions from repair processes on neoplastic transformation.

In contrast to the neutron data, animal experiments generally indicate reduced tumor incidence following X-ray dose fractionation[17,18,21,22] or irradiation at reduced dose rates.[23] Mammalian cells in culture and clonogenic cells exhibit increased survival following X-ray dose fractionation or irradiation at decreased dose rates.[24,25] This being the case, the questions arise, what does the increase in transformation in Fig. 7 represent, and is the increase consistent with the notion of the repair of transformation damage? In arriving at an adequate explanation, three possibilities have to be considered.

First we consider the possibility that sublethal damage is fully repaired, and subtransformation damage is not repaired at all. If the sublethal damage in transformed and nontransformed cells is the same, the number of transformants per cell should rise with time by the same factor as does survival. We would expect, therefore, the transformation frequency to increase to essentially the level at the maximum on the single dose X-ray curve (i.e., from 1.7 to 10.2 x 10^{-4}/cell). Such a rise obviously did not occur.

The second possibility is that no repair of sublethal damage takes place, but subtransformation damage is fully repaired. This consideration first of all requires that the transformation due to the first dose of 350 rad is progressively lost with time. Consequently, when the transforming influence of the first dose completely disappears, the X-ray induction curve from Fig. 2 would be displaced to the right by 350 rads and downward for the survivals (Fig. 1) corresponding to 350 rads plus the second dose. When the repair is completed and at a total dose of 700 rads, the net transformation frequency should be about 10-fold below that for a single 350 rad dose because of the additional cell killing at 700 rad as compared to 350 rad (i.e., 1.1 x 10^{-4}/cell). Since transformation frequency per cell after fractionated exposure is greater in the interval up to about 12 hr, not less, than that due to the total dose, it is unlikely that there is no sublethal damage repair with complete repair of subtransformation damage.

Finally, the third possibility assumes repair of both sublethal and subtransformation damage. In order to predict the level of transformation for full repair of the first dose subtransformation damage concomitant with the repair of sublethal damage according to the data in Fig. 4, the survival for 700 rads in the preceding paragraph should be increased by the survival due to fractionation. As a consequence, the expected transformation frequency would increase sixfold if repair of subtransformation damage is completed by the time fractionation survival reaches maximum (expected frequency 6 x 1.1 x 10^{-4}/cell). Since the fractionation results in Fig. 7 lie between the predicted extremes, and are reasonably close to the expected level considered in this third possibility, we conclude that at least some repair of subtransformation damage occurs together with repair of sublethal damage. The repair of sublethal and subtransformation damage does not have to be mediated by the same repair process and could have, therefore, different time dependencies.

In preceding considerations we ignored the cell cycle dependent changes in survival and in transformation frequency. It is well established that response of mammalian cells to radiation, as determined by various end points, depends upon their position in their growth cycle at the time of radiation.[26,27] The cell cycle dependent changes in the frequency of neoplastic transformation by chemicals have been reported.[28,29,30] It is reasonable to assume, therefore, that there is a growth cycle specific dependence for radiation-induced neoplastic transformation. The net effect of repair of transformation damage and cell cycle dependent variations in transformation, different from those for survival, could result in a somewhat lower level of response following dose fractionation than is predicted above.

The X-ray induction curve in Fig. 7 is qualitatively similar to data for rat skin tumor induction,[18] and for induction of leukemia and hepatic tumors in mice.[17,22] Furthermore, our interpretation that both repair of sublethal damage and the repair of transformation damage are responsible for observed changes after low LET dose fractionation is in agreement with the interpretation of data for rat skin tumor induction.[18]

Conclusions

The main points that can be extracted from presented data on radiation-induced neoplastic transformation can be summarized as follows. (1) Fission-spectrum neutrons are more effective than low LET radiation in inducing neoplastic transformation. In the region of small doses (about 20 rads) RBE for transformation is about 10. (2) Fractionation of the fission-spectrum neutron dose results in a small decrease in transformation frequency, suggesting a repair of first dose subtransformation damage and no repair of sublethal damage. The change is rather small and further data are needed to support this interpretation with confidence. (3) The X-ray data suggest that subtransformation damage due to the first dose is repaired to a great extent. This conclusion rests, in part, on the assumption that survival properties of transformed and nontransformed cells following exposure to single and fractionated doses are similar. There is no indication, thus far, that they are different. Finally, (4) the fact that transformation frequency per cell due to the fractionation of the X-ray dose lies below the expected level predicted by the full sublethal and subtransformation damage repair implies the involvement of other factors, perhaps cell cycle dependent variations in the frequency of neoplastic transformation.

The results discussed here, as well as those of others, clearly show that in vitro study of neoplastic transformation is a valuable approach in studies of basic mechanisms and concepts of

carcinogenesis and that in vitro system is amenable to experiments and approaches that are almost impossible to explore effectively in vivo.

Acknowledgments

This work was supported by the United States Department of Energy.

References

[1] Borek, C., and L. Sachs. In vitro cell transformation by X-irradiation. Nature 210, 276-278, 1966.

[2] Borek, C., and E. Hall. Transformation of mammalian cells in vitro by low doses of X-rays. Nature 243, 450-453, 1973.

[3] Terzaghi, M., and J. B. Little. X-radiation-induced transformation in C3H mouse embryo-derived cell line. Cancer Res. 36, 1367-1374, 1976.

[4] Borek, C., E. J. Hall, and H. H. Rossi. Malignant transformation in cultured hamster embryo cells produced by X-rays, 430-keV monoenergetic neutrons and heavy ions. Cancer Res. 38, 2997-3005, 1978.

[5] Han, A., and M. M. Elkind. Transformation of mouse C3H/10T1/2 cells by single and fractionated doses of X-rays and fission-spectrum neutrons. Cancer Res. 39, 123-130, 1979.

[6] Borek, C., and E. Hall. Effect of split doses of X-rays on neoplastic transformation of single cells. Nature 252, 499-501, 1974.

[7] Terzaghi, M., and J. B. Little. Oncogenic transformation after split-dose X-irradiation. Int. J. Radiat. Biol. 29, 583-587, 1976.

[8] Miller, R., and E. J. Hall. Effect of X-ray dose fractionation on the induction of oncogenic transformation in vitro in C3H/10T1/2 mouse embryo cells. Nature 72, 58-60, 1978.

[9] Alper, T., J. F. Fowler, R. L. Morgan, D. D. Vonberg, F. Ellis, and R. Oliver. The characterization of type "C" survival curve. Brit. J. Radiol. 35, 722, 1962.

[10] Elkind, M. M. Damage and repair processes relative to neutron (and charged particle) irradiation. Curr. Topics in Rad. Res., Vol. 7, (M. Ebert and A. Howard, eds.), pp. 1-44, N-44, North Holland Publ. Co., Amsterdam, 1970.

[11] Gray, L. H. Radiation Biology and Cancer. In Cellular Radiation Biology, A Collection of the Papers Presented at the 18th Annual Symposium on Fundamental Cancer Research at the University of Texas M. D. Anderson Hospital and Tumor Institute, pp. 7-20, The Williams & Wilkins Co., Baltimore, MD, 1965.

[12] Borek, C. In vitro cell transformation by low doses of X-irradiation and neutrons. In Biology of Radiation Carcinogenesis (J. M. Yuhas, R. W. Tennant, and J. D. Regan, eds.), Raven Press, New York, 1976.

[13] ICRU, Report of the RBE Committee, Health Phys. 9, 357-386, 1963

[14] Elkind, M. M., and H. A. Sutton. Radiation responses of mammalian cells grown in culture. I. Repair of X-ray damage in surviving Chinese hamster cells. Radiat. Res. 13, 556-593, 1960.

[15] Withers, H. R., and M. M. Elkind. Radiosensitivity and fractionation response of crypt cells of mouse jejunum. Radiat. Res. 38, 598-613, 1969.

[16] Ngo, F. Q. H., H. Utsumi, A. Han, and M. M. Elkind. Sublethal damage repair: Is it independent of radiation quality? Int. J. Radiat. Biol., 1979, in press.

[17] Upton, A. C., M. L. Randolph, and J. W. Conklin. Late effects of fast neutrons and gamma-rays in mice as influenced by the dose rate of irradiation: Induction of neoplasia. Radiat. Res. 41, 467-491, 1970.

[18] Burns, F. J., and M. Vanderlaan. Split-dose recovery for radiation induced tumors in rat skin. Int. J. Radiat. Biol. 32, 135-145, 1977.

[19] Rossi, H. H., and A. M. Kellerer. Radiation carcinogenesis at low doses. Science 175, 200-202, 1972.

[20] Ullrich, R. L., M. C. Jernigan, G. E. Cosgrove, L. C. Satterfield, N. D. Bowles, and J. B. Storer. The influence of dose and dose-rate on the incidence of the neoplastic disease in RFM mice after neutron irradiation. Radiat. Res. 68, 115-131, 1976.

[21] Burns, F. J., R. E. Albert, P. I. Sinclair, and M. Vanderlaan. The effect of a 24-hour fractionation interval on the induction of rat skin tumors by electron radiation. Radiat. Res. 62, 478-487, 1975.

[22] Metalli, P., G. Silini, S. Castillo, and V. Covelli. Induction of tumors and leukemia by split doses of X-rays. In Radiation Induced Cancer, IAEA-SM-118/14 (Internationational Atomic Energy Agency), p. 227, 1969.

[23] Shellabarger, C. J., V. P. Bond, G. E. Aponte, and E. P. Cronkite. Results of fractionation and protraction of total-body radiation on rat mammary neoplasia. Cancer Res. 26, 509-513, 1966.

[24] Fox, M., and A. H. W. Nias. The influence of recovery from sublethal damage in the response of cells to protracted irradiation at low dose-rate. Curr. Topics in Radiat. Res. (M. Ebert and A. Howard, eds.) Vol. 7, pp. 71-103, North Holland Publ. Co., Amsterdam, 1970.

[25] Withers, H. R., G. D. Oliver, and D. W. Glenn. Response of mouse jejunal crypt cells to low dose rate irradiation with Californium neutrons or radium gamma rays. Radiology 103, 741, 1972.

[26] Sinclair, W. K. Cyclic X-ray responses in mammalian cells in vitro. Radiat. Res. 33, 620-643, 1968.

[27] Sinclair, W. K. Dependence of radiosensitivity upon cell age. In Time and Dose Relationship in Radiation Biology as Applied to Radiotherapy, pp. 97-116, BNL-50203 (C57), 1970.

[28] Bertram, J. S., and C. Heidelberger. Cell cycle dependency of oncogenic transformation induced by N-methyl-N'-nitrosoguanidine in culture. Cancer Res. 34, 526-537, 1974.

[29] Marquardt, H. Cell cycle dependence of chemically induced malignant transformation in vitro. Cancer Res. 34, 1612-1615, 1974.

[30] Jones, P. A., M. S. Baker, J. S. Bertram, and W. F. Benedict. Cell cycle-specific oncogenic transformation of C3H/10T1/2 Clone 8 mouse embryo cells by 1-β-D-arabinofuranosylcytosine. Cancer Res. 37, 2214-2217, 1977.

NEUTRON SOURCES AND THEIR CHARACTERISTICS*

R. C. McCall and W. P. Swanson
Stanford Linear Accelerator Center
Stanford University, Stanford, California 94305

The significant sources of photoneutrons within a linear-accelerator treatment head are identified and absolute estimates of neutron production per treatment dose are given for typical components. It is found that the high-Z materials within the treatment head do not significantly alter the neutron fluence but do substantially reduce the average energy of the transmitted spectrum. Reflection of neutrons from the concrete treatment room contribute to the neutron fluence, but not substantially to the patient integral dose, because of a further reduction in average energy. The ratio of maximum fluence to the treatment dose at the same distance is given as a function of electron energy. This ratio rises with energy to an almost constant value of 2.1×10^5 neutrons cm^{-2} rad^{-1} at electron energies above about 25 MeV. Measured data obtained at a variety of accelerator installations are presented and compared with these calculations. Reasons for apparent deviations are suggested. Absolute depth-dose and depth-dose-equivalent distributions for realistic neutron spectra that occur at therapy installations are calculated, and a rapid falloff with depth is found. The ratio of neutron integral absorbed dose to leakage photon absorbed dose is estimated to be 0.04 and 0.2 for 14 and 25 MeV incident electron energy, respectively. Possible reasons are given for lesser neutron production from betatrons than from linear accelerators. Possible ways in which neutron production can be reduced are discussed.

Introduction

The radiation field around a medical therapy electron accelerator is a complicated mixture of photons leaking from the head, scattered photons from the patient, beam stopper and room walls, and photons from electrons stopped elsewhere than the target. If the accelerator energy is high enough to produce neutrons, i.e., greater than about 10 MeV, there is also a neutron component. This paper is primarily concerned with the generation and propagation of this neutron field.

Neutron Production

The primary production of neutrons is through (γ,n) reactions with smaller quantities produced by (γ,pn) and $(\gamma,2n)$ if the energy is high enough. The direct production of neutrons by electrons, (e,n), is smaller by about two orders of magnitude -- the fine structure constant modified by several other factors -- and can be neglected. Medical electron accelerators at present are limited to energies less than 45 MeV and our discussion will be limited to that energy range. In this energy domain, neutron production is due to the "giant photonuclear resonance", more commonly called the "giant resonance". The cross section for the giant resonance is characterized by a threshold energy, a rapid rise to a prominent peak and a more gradual decrease at higher energies. For the medium and heavy nuclei ($A > 40$) which are of interest to us, the peak occurs at 13-18 MeV. Threshold energies for some materials of interest are listed in Table I. A recent compilation of threshold energies has been published by Howerton.[4] A recent and comprehensive set of photoneutron cross sections is by Berman.[2]

Table I. Thresholds of Photoneutron Reactions.

Element	Atomic Number	Abundance (Percent)	(γ,n) Threshold Energy (MeV)
Pb	206	25.1	8.08
	207	21.7	6.74
	208	52.3	7.37
Fe	54	5.8	13.4
	56	91.7	11.2
W	182	26.4	8.05
	183	14.4	6.19
	184	30.6	7.41
	186	28.4	5.75

The yield of photoneutrons is proportional to the convolution of the (γ,n) cross section and the bremsstrahlung spectrum, which decreases rapidly with photon energy. The result is a yield curve which increases rapidly with primary electron energies for constant electron current up to approximately 25 MeV and more slowly thereafter. For constant electron beam power, the neutron yield is almost constant with primary electron energy above 35 MeV. Swanson[16] has recently published electron yield calculations applicable to this energy range.

Neutron spectra in the giant resonance contain two components -- the evaporation spectrum and the direct emission spectrum. The evaporation spectrum is the larger component and can usually be described adequately by a Maxwellian distribution

$$\frac{dN}{dE_n} = \frac{E_n}{T^2} \exp\left(\frac{-E_n}{T}\right)$$

* Work supported by the Department of Energy under contract number EY-76-C-03-0515.

where T is the nuclear "temperature" in MeV for the particular nucleus and is also a function of the excitation energy. One should note that the spectrum peaks at $\hat{E}_n = T$ (most probable energy) and has an average energy of $\bar{E}_n = 2T$. The evaporation neutrons are emitted almost isotropically.

The direct emission neutrons tend to be higher energy than the evaporation neutrons and may be emitted nonisotropically. Mutchler[8] found that for medium to high atomic number materials and energies near the resonance peak, direct emission amounted to about 14% of the total neutrons. Figure 1[9] shows typical photoneutron spectra with the direct emission neutrons responsible for the "bump" on the high-energy side of the spectrum. For comparison a fission neutron spectrum is also shown in Fig. 1.

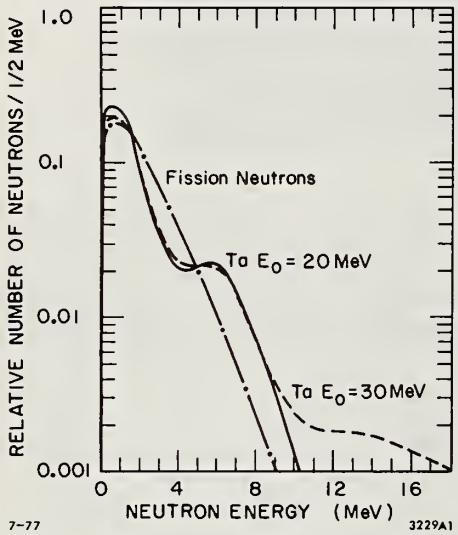

Fig. 1. Photoneutron spectra for Ta with peak bremsstrahlung energies of 20 and 30 MeV, compared to a fission spectrum. From NBS-97.[9]

It will be shown later that the spectrum of photoneutrons can be degraded rapidly in heavy metals so published spectra must be considered as representative of a particular target thickness.

Transport of Neutrons in the Treatment Head

The typical medical accelerator has massive shielding around the target to provide photon shielding and produce a collimated beam of x-rays. Neutrons which are produced inside the head are produced approximately isotropically and penetrate the head shielding in all directions. The photon shielding is usually of some heavy metal such as tungsten or lead, and there is also a certain amount of iron and copper from bending magnets in the head. These materials provide some photon shielding action since these are all heavy elements. The only significant neutron energy loss mechanisms in these heavy elements are inelastic scattering or (n,2n) reactions. Both of these processes are effective in the MeV energy region but the (n,2n) reaction is most effective at the higher energies. Inelastic scattering can occur only at energies above the lowest excited state of the shielding material. These lowest excited states are in the neighborhood of 0.6 to 0.8 MeV for lead and iron but about 0.1 MeV for tungsten; therefore tungsten is more effective in reducing the energy of neutrons by inelastic scattering. The energy loss in any inelastic collision cannot be exactly determined or predicted, but there is a minimum energy loss equal to the energy of the lowest excited state. Often there is large energy loss in a single collision resulting in excitation of higher energy states followed by a cascade of gammas. In the (n,2n) reaction the minimum energy loss is equal to the binding energy of a neutron, and since the energies of two emerging neutrons tend to be similar, they produce large numbers of quite low energy neutrons. The total of the inelastic plus (n,2n) cross sections is of the order of 1 or 2 barns for these materials. This means that the typical neutron penetrating the photon shielding undergoes several collisions. In addition, a large amount of elastic scattering takes place in these materials at these energies. The elastic scattering results in negligible energy loss but does, however, have the effect of lengthening the path length for the neutrons in the shielding material and offering greater opportunity for the inelastic and (n,2n) reactions to occur. The attenuation of neutron fluence is small, however, since the capture cross sections of these materials are small down to thermal energies. With a spectrum containing high-energy neutrons, such as a fission or PuBe spectrum, there can, in fact, be a slight buildup of neutron fluence due to the (n,2n) reactions.

In a previous paper[6] hereafter referred to as MJS, the Monte Carlo computer program MORSE[14] was used to explore the effects of the head shielding on several photoneutron spectra. It was shown that while there is very little attenuation of neutrons by lead and iron, there is some attenuation by tungsten amounting to about 15% in the typical therapy machine shielding. It was also shown that the dose equivalent is attenuated by the shielding because of the reduced energy of the spectrum. In the course of the calculations in MJS, it was found that the average energy of a neutron spectrum is a very useful parameter for studies around radiotherapy machines. Figure 2, taken from MJS, shows the fluence-to-dose-equivalent conversion factor for a neutron spectrum with average energy $\bar{E}$, plotted against $\bar{E}$. It is seen that these data can be fit with a straight line which is almost parallel to the curve (labeled ICRP-21 in Fig. 2) drawn through the points listed in ICRP-21[5] for the conversion of monoenergetic neutron fluences to dose equivalent. It should be kept in mind that these conversion factors from ICRP-21 are calculated at the depths where the dose equivalent is maximum. For a spectrum, each energy component has it's maximum does-equivalent at a different depth, so a simple addition of dose-equivalent components will result in an overestimate. The estimates of Fig. 2 are slight overestimates for this reason. However, it will be shown that the average neutron energies around medical accelerators are so low that this is probably not significant. In Figs. 3 and 4 are shown the average energy of several

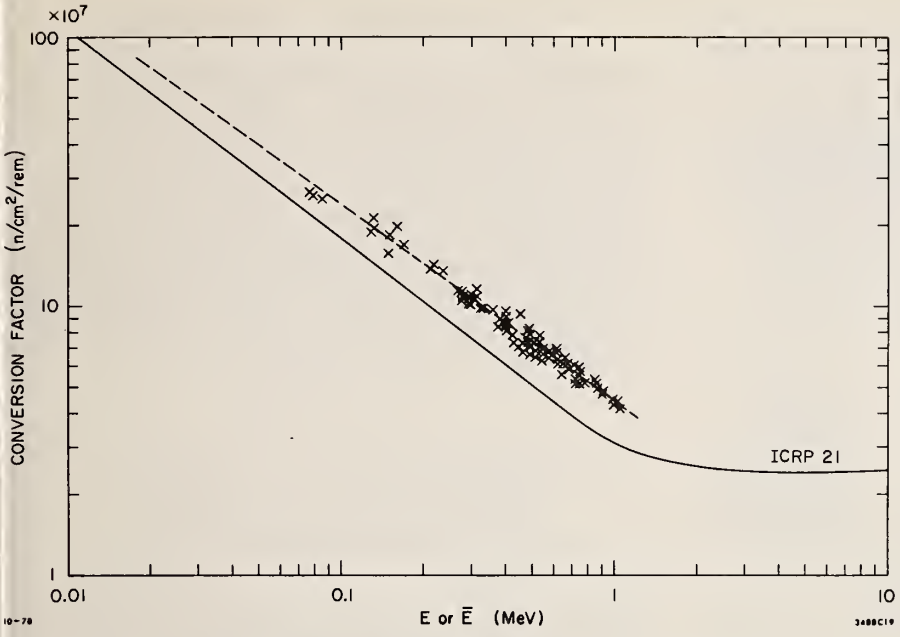

Fig. 2. Factor for converting dose-equivalent to neutron fluence. The curve is based on recommendations of ICRP-21[5] and is a function of monoenergetic neutron energy. The x's are the result of averaging the ICRP-21 conversion factor over spectra from a large variety of sources, and are presented as a function of average neutron energy. The dashed line is a least squares fit which is nearly parallel to the ICRP monoenergetic values.

spectra calculated after passing through various thicknesses of tungsten and lead.[6] It can be seen that tungsten reduces the average energy faster than lead, and also that this reduction continues out to greater depths. After a certain thickness, of any material, virtually all of the neutrons will have their energy reduced below the lowest excited state, and inelastic scattering can no longer occur. This is well below the (n,2n) threshold. Thereafter, the neutrons penetrate for very large distances through these heavy metals with no further attenuation or decrease in dose equivalent.

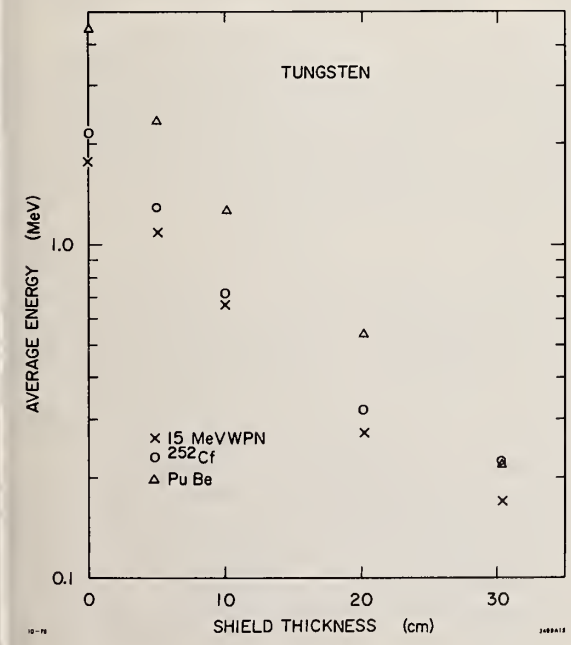

Fig. 3. Calculated average neutron energy as a function of W thickness for 15 MeV (incident electron energy) photoneutrons, and ^{252}Cf and PuBe neutron spectra. Over the range of W thickness typically used, there is a substantial decrease in average neutron energy in penetrating the head shielding. Data are from the Monte-Carlo program MORSE.

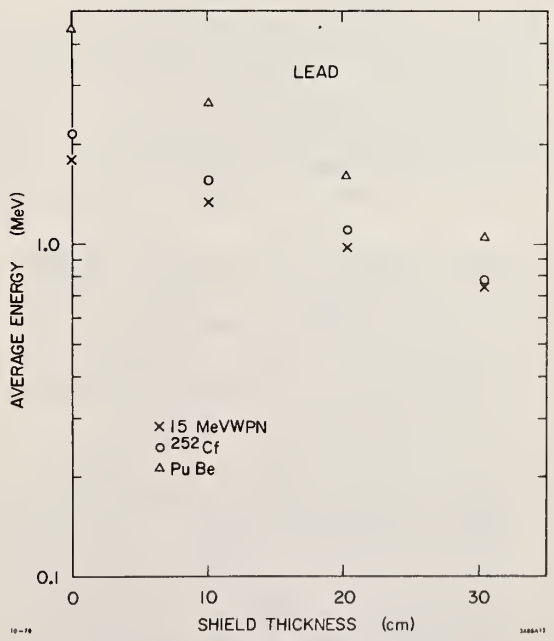

Fig. 4. As for Fig. 3 but for Pb. The reduction in average neutron energy is somewhat less for Pb than for W, even when the two materials are compared on an areal-density basis.

It is frequently stated that a fission spectrum is very similar to the photoneutron spectrum found in machines in this energy range. This is true for the primary spectra, but not for the spectra after they have penetrated the head shielding. In Fig. 5, we show the integral photoneutron spectra for 15 MeV electrons on tungsten and for ^{252}Cf fission neutrons; these are indeed seen to be quite similar.

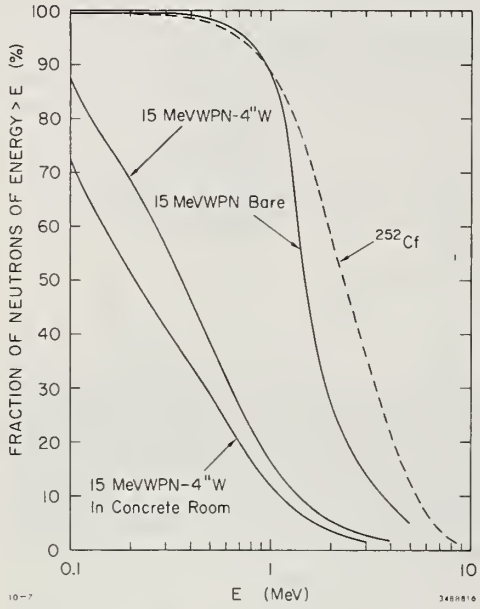

Fig. 5. Comparison of various neutron integral spectra to illustrate spectral modification by W shielding and a concrete room. The median energy can be reduced from 1.5 to about 0.2 MeV by the combined effects of the W and concrete. The bare ^{252}Cf spectrum is shown for comparison. Data are from the Monte-Carlo program MORSE.

On the same figure, we show the spectrum from 15 MeV electrons on tungsten after the neutrons have penetrated 10 cm of tungsten. It is clear that there is a large difference between these spectra. In particular, one can see that if one measures the neutrons from a 15 MeV medical accelerator, using a threshold detector calibrated with a bare ^{252}Cf source, the results will be considerably off. Also shown on this figure is the further degradation due to the concrete room in which medical accelerators are commonly placed. This will be discussed in a later section. In MJS a method was described of measuring accelerator leakage by measuring neutron fluence at various points in the room and using MORSE to simulate the room and the accelerator and to provide factors for converting the fluence measurements to dose equivalent or absorbed dose. Since this method requires the use of a computer and the availability of the MORSE program, MJS also developed a "cookbook" method using graphs and tables to provide the same conversion factors for fluence measurements.

Neutron Transport in a Concrete Room

Nearly every medical accelerator is placed in a concrete treatment room. In such a room, neutrons from the accelerator scatter in the concrete and may be absorbed or scattered back into the room. These neutrons add to the neutron field coming directly from the accelerator head. MJS investigated this scattered neutron field in order to evaluate their fluence measurements. Some time ago, Patterson and Wallace[10] discovered that if a fast neutron source is placed in a concrete room, a thermal fluence is produced which is approximately uniform over the entire room and is related to the fast neutron source strength by

$$\phi = k(Q/S)$$

where

ϕ = Thermal neutron fluence, Q is the fast neutron source strength, S is the inside surface area of the room, and k is a dimensionless constant.

Since the thermal neutrons represent a single point of the wall-scattered neutron spectrum, it was suspected that a similar relationship might hold for the entire wall-scattered spectrum. By a series of simulations using MORSE, this was found to be true; exactly the same relationship was found as for thermals but with a different constant coefficient. Measurements in MJS indicated that the scattered neutrons were indeed constant throughout the room. These wall-scattered neutrons are of quite low energy; this can be inferred from the lowest curve on the preceding figure which shows the effect of the walls of a typical therapy-sized room on the neutron spectrum. MJS found that the average energy of the scattered neutron spectrum was proportional to the average energy of the direct spectrum as shown in Fig. 6.[6] The fluence of the scattered spectrum is given in the following equation:

$$\phi = k_1(Q/S)$$

From MORSE we found that k_1 is equal to 4.6 for the tungsten-shielded machines and 5.4 for lead-shielded accelerators. The values of k_1 are different since there is no attenuation of the fluence in practical thicknesses of lead, and a transmission of about 0.85 in typical thicknesses of tungsten. This relationship enables one to correct calculated or measured values of the direct fluence for a particular room. The wall-scattered component often makes a significant contribution (20-30%) to the measured neutron fluence. However its contribution to the patient's integral dose is a much smaller fraction of the total, because of the softening of the scattered spectrum discussed above (Fig. 6).

It should be noted that the original paper by Patterson and Wallace enables one to calculate the fast neutron source strength in a room of normal concrete simply by measuring the thermal neutron fluence at any point in that room. This method works quite well. The variation in the thermal neutron capture in normal concretes

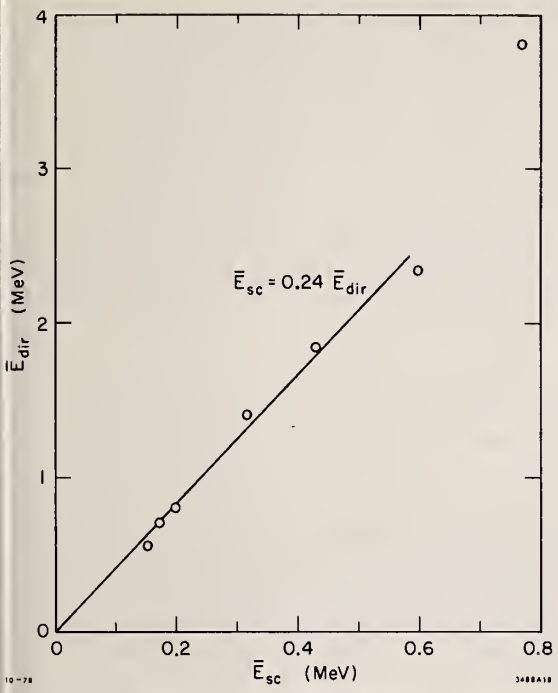

Fig. 6. Comparison of the average energy of source spectra and neutrons scattered from a concrete room within which the source is placed. The straight line illustrates the close proportionality of these average energies.

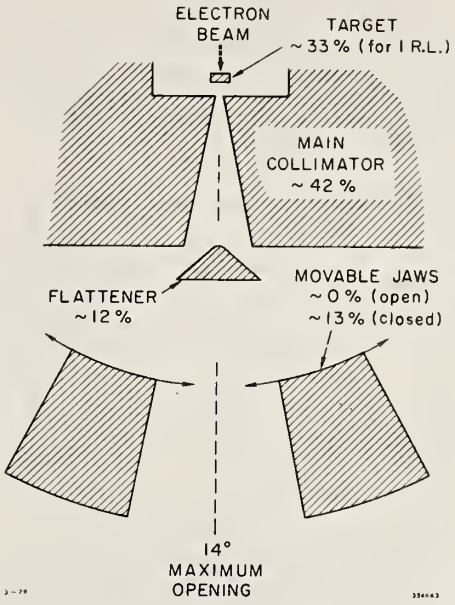

Fig. 7. Arrangement of neutron-producing parts within a radiation treatment unit (not to scale). All of these components are practically indispensible and are found on all standard models. Numbers indicate the approximate percentages of neutrons produced at 25 MeV relative to the maximum number possible, assuming all parts are of high-Z materials (W or Pb).

does not vary enough to cause a large error. It should be noted however, that if the room is built of heavy concrete such as ilmenite or barite concrete, the thermal neutron capture cross sections are considerably larger than in normal concrete, and the method will then underestimate the source strength. In such cases, there is enough variation in the various heavy concretes that one would have to make a calibration of each room by putting, for example, a PuBe source in the room and measuring the thermal fluence and redetermining the constant in the equation, then using this constant in evaluating the thermal neutron measurements with the accelerator operating.

Neutron Production in a Medical Accelerator

From Swanson's[15,16] calculations, one can calculate the neutron yield from a single target material of finite or infinite thickness ($\gtrsim 10$ R.L.). It is of interest to compare the neutron yield from an accelerator with these models.

We will consider a typical therapy machine with the geometry of Fig. 7.

Case 1. Target, Flattener, Jaws and Shielding All of the Same Material

This would always be Pb or W and, to a reasonable approximation, the n yield of these can be considered the same. The only photons effective in producing neutrons are those above about 8 MeV. These are mostly forward directed and will either be absorbed in the main collimator or pass through its opening and through the flattener. Those which penetrate the flattener may or may not strike the jaws, depending on their opening. Those passing through the jaws' opening may be absorbed in the patient, the beam stopper if there is one, or the room concrete. The neutron yield from concrete can be considered negligible, especially since self-shielding would be large. We then have the following possibilities:

Case 1a - Jaws closed - Yield will be that of an infinite target;

Case 1b - Beam stop in place - Yield will be that of an infinite target;

Case 1c - No beam stop in place - Yield will depend on position of jaws.

Cases 1a and 1b provide upper limits to the amount of neutron production. Case 1c is more complicated and we will consider it in more detail. Most medical linacs provide fields up to about 35×35 cm^2 at 100 cm from the target. The main collimator covers all forward directions beyond the extremes of these fields. The half-angle of the main collimator is then about 14 degrees. In order to see what fraction of the high-energy (> 8 MeV) photons are within this angle we have used the Monte Carlo program EGS[3] for various target thicknesses and electron energies. We have used what we believe to be practical linear accelerator target thicknesses. At these thicknesses,

about 2% of the incident electron energy is transmitted by electrons in the cone within 14°. Since the average energy of these transmitted electrons has been reduced sharply, the radiation yield will be low and there should be no penumbra problems from bremsstrahlung produced in the flattener or elsewhere. The target thicknesses we have considered are listed in Table II.

Table II. Target Thicknesses Considered

Electron Energy (MeV)	Target Thickness (R.L.)	
	Copper	Tungsten
14	0.3	0.7
20	0.4	0.85
25	0.74	1.00
30		1.1
35	0.92	
45	1.05	

From our Monte-Carlo calculation we can construct curves such as are shown in Fig. 8.

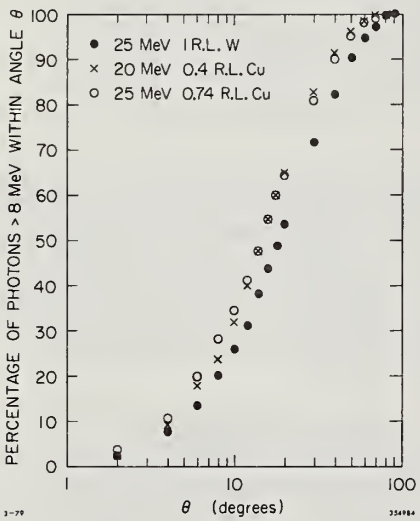

Fig. 8. Percentage of high energy photons (> 8 MeV) emitted within the angle θ from an accelerator target, as a function of θ. Three target material and thickness combinations are shown. Data are based on Monte-Carlo calculations using the program EGS.

As a calculational example consider a 25 MeV accelerator with a 1.0 R.L. W target, W head shielding and a W flattener. From Fig. 10 of Swanson,[15] we find that the neutron yield from this target is about 33% of that from an infinite target. From Fig. 8 we see that the remaining high-energy photons are 38% inside the main collimator angle and 62% outside, and these strike the main collimator which is practically an infinite absorber. The 38% inside the main collimator strike only the flattener. A tungsten flattener for this target would be about 2.3 cm (6.6 R.L.) thick in the center and approximately conical. If we weight this conical shape with the high-energy photon distribution, we effectively have 2.9 R.L. over this angular range. Using Fig. 10 of Swanson again we find that these photons produce 47% of the infinite target yield (difference between 1 R.L. and 1 + 2.9 = 3.9 R.L.). Our total neutron yield relative to the infinite target then is as follows:

Target	-	= 33%
Main Collimator	- 0.61 × 67%	= 41.5%
Flattener	- 0.47 × 0.38 × 0.67	= 12%
Total	-	= 86.5%

From Fig. 8 of Swanson,[16] the yield for an infinite target of W at 25 MeV would be 1.5×10^{12} n/sec per kW. In Fig. 9 we have plotted the Monte-Carlo unflattened and flattened photon dose rates at a typical 1 meter target distance per mA of electron current for the target thicknesses of Table II.

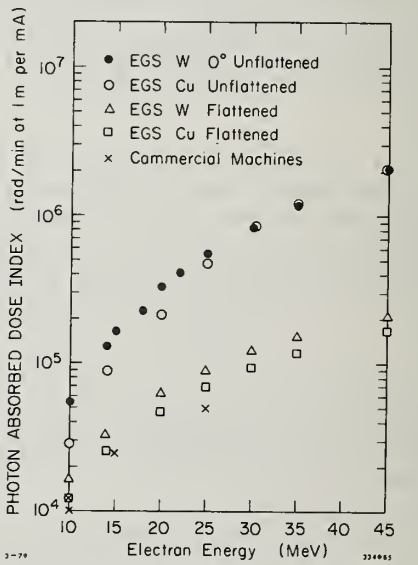

Fig. 9. Photon absorbed dose index as a function of incident electron energy, as obtained from the Monte-Carlo program EGS. Upper data are from W and Cu targets without flattener. Lower points show same data but after flattening. Measured values obtained on existing commercial accelerators are shown for comparison.

From this figure we have 8.95×10^4 rads/min per mA or 60 rads/sec per kW for our example. Then the yield of neutrons relative to the photon output would be 1.5×10^{12} n/sec-kW × 0.865 ÷ 60 rads/sec-kW = 2.16×10^{10} neutrons/rad. This would be

the yield with the jaws fully open. Fully closed the yield would be $2.16/0.865 \times 10^{10} = 2.5 \times 10^{10}$ n/rad. With intermediate jaw openings the yield can be calculated by converting the jaw opening to angle and using Fig. 8 to calculate the yield.

Case 2. Target, Flattener, Jaws and Shielding of Different Materials

In all cases, the jaws and shielding will be of Pb or W, (the only other possible shielding material, depleted uranium, becomes activated due to photofission at energies too low to have significant photoneutron production). There are actually relatively few choices for the other elements. The required physical properties of the target limit the possibilities to copper, tungsten, gold, tantalum, platinum and silver. Tungsten, gold, tantalum and platinium are nearly identical in neutron production. The authors know of no example of silver being used. Therefore, we can limit the discussion of target material to copper and tungsten. Flatteners have been made of lead, tungsten and iron. Aluminum flatteners have been used in betatrons and proposed for linacs,[11,12] but are too long for rotational therapy machines and produce undesirable changes in beam hardness across the field.[7] In calculating neutron production then, it is sufficient to consider only iron and tungsten for the field flattener. We must finally consider the following cases.

Case 2a - W target and shielding with an Fe flattener;

Case 2b - Cu target and W shielding and flattener;

Case 2c - Cu target, W shielding and Fe flattener.

Case 2a is not too different from our previous example. The neutron components from the target and the main collimator are the same. An iron flattener for 25 MeV would be about 9.4 cm = 5.3 R.L. long. If we assume that the spectral difference between the bremsstrahlung produced in a Cu and a tungsten target is insignificant we can proceed as before. The effective thickness of the flattener is 2.4 R.L. The photons striking the flattener produce 42% of the infinite target yield (difference between 1 R.L. and 1.0 + 2.4 R.L. from Fig. 10 of Ref. [15]). The flattener neutron yield is given by $0.42 \times 0.38 \times 0.67 \times$ Fe yield/W yield = 1.6% of the infinite W yield. The total yield for this machine would be 75.9% of the infinite tungsten target or 1.6×10^{10} n/rad with the jaws open.

Case 2b. It is easier to consider this case as relative to an infinite copper target. In the same manner as before we find the following:

0.74 R.L. Cu Target Yield - 25% of infinite (Fig. 10 of Ref. [15])

Fraction of High-Energy Photons Passing through Main Collimator - 47.5% (from Fig. 8)

Effective Flattener Thickness = 3.3 R.L.

Infinite Target Cu Yield = 0.36×10^{12} n/sec-kW

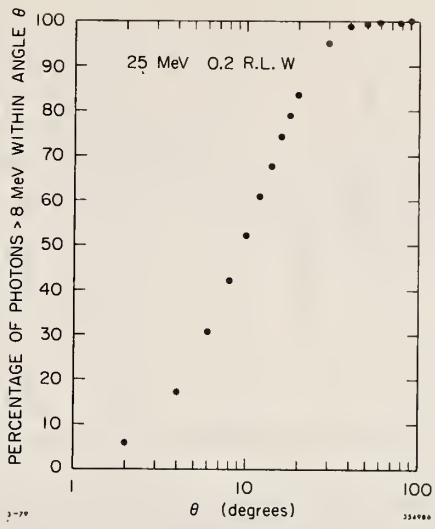

Fig. 10. Percentage of high-energy photons (> 8 MeV) emitted within the angle θ, as a function of θ, when 25 MeV electrons are incident on an 0.2 R.L. W target. Data are from the Monte-Carlo program EGS.

Infinite Target W yield = 1.5×10^{12} n/sec-kW

Target Yield = 25% of Infinite Cu Target Yield

Flattener Yield = $0.55 \times 0.75 \times 0.475 \times 1.5$ × W Yield/Cu Yield
= 82% of Infinite Cu Target Yield

Main Collimator Yield = $0.525 \times 0.75 \times 1.5$ × W Yield/Cu Yield
= 164% of Infinite Cu Target Yield

Total: = 271% of Infinite Cu Target Yield
= 9.76×10^{11} n/sec-kW

The flattened dose rate from the machine would be 6.95×10^{4} rads/min at 1 meter for 1 mA. Then the relative neutron yield would be = 2.11×10^{10} n/rad.

Case 2c. This case is the same except that the neutron yield from the flattener has an effective thickness of 3.0 R.L. The infinite target yield for Fe is 0.23×10^{12} n/sec-kW.

Flattener Yield = $0.50 \times 0.475 \times 0.75$ × Fe Yield/Cu Yield
= 11.4% of Infinite Cu Yield

Total Yield = 200% of Infinite Cu Yield
= 7.2×10^{11} n/sec-kW

Since the flattened dose rate would be the same, the relative neutron yield would be 1.56×10^{10} n/rad.

The results of these calculations are summarized in Table III below.

Table III. Summary of Neutron Source Calculations (25 MeV electrons)

Target	Flattener	Main Collimator	n/rad	Fraction of Infinite W Yield (Percent)	Percentage From		
					Target	Flattener	Main Collimator
W	W	W	2.2×10^{10}	86.5	38	14	48
W	Fe	W	1.6×10^{10}	64	43	2	55
Cu	W	W	2.1×10^{10}	84	9.2	30	60.5
Cu	Fe	W	1.6×10^{10}	64	12.5	5.7	82

Note that while the total neutron yield does not change very much the fraction of the neutrons originating in different areas changes. This is useful information for an accelerator designer trying to minimize neutron production.

It is of some interest to compare the above results with those calculated for a 25 MeV betatron. The effective target thickness for a betatron is difficult to obtain since it is never known exactly where the electrons strike the target. However, we can get some indication from the angular distribution of the unflattened beam. ATC Betatron Corp. gives a graph of this in their literature.[11] The target is platinum which is very similar to tungsten. An EGS calculation for angular distribution of bremsstrahlung from a 0.2 R.L. W target matches the ATC graph quite well. Information kindly supplied by ATC indicates the electrons strike a nearly triangular target with a minimum thickness of 0.08 R.L. and a maximum thickness of 0.27 R.L. so assuming an effective target thickness of 0.2 R.L. seems quite reasonable. In this betatron the flattener is aluminum and the maximum field size is 14×14 cm^2 at 1 meter. The corner of this field would be at an angle of 5.7 degrees. The main shielding and jaws are lead. From Swanson[15] and interpolated results of Seltzer and Berger,[13] the neutron yield from the target would be about 3% of an infinite target. The angular distribution of the photons above 8 MeV is shown in Fig. 3. We can see that 29% of these photons are within 5.7 degrees. These photons strike only the aluminum flattener. The Al to W yield ratio is about 3.1% so the yield from the Al flattener is negligible. The 71% of the high-energy photons striking the main collimator give $0.71 \times 0.97 = 69\%$ of the infinite target yield; the total yield will be 72% of the infinite target yield or 1.08×10^{12} sec^{-1} kW^{-1}. The photon dose rate flattened to 5.7 degrees, 1 m from this target would be about 2.4×10^5 rads/min-mA and the relative neutron yield would therefore be 6.8×10^9 n/rad.

One might ask what happens to the electrons transmitted through this target. From the EGS calculation one can find that essentially all of the electrons are transmitted and carry an average energy of 19.6 MeV. Presumably, a few of these lose so little energy that they make another revolution and strike the target a second time. Most of the electrons, however, must spiral in and strike the donut. They would produce bremsstrahlung which would make neutrons but would not add to the useful photon yield. The neutron production from these electrons is difficult to estimate but because (1) the photon production is in low Z material, (2) the energy is lower, and (3) the neutron production would be partly in iron and copper rather than lead, it seems that these neutrons would add not more than 10% to the total.

We have made calculations similar to the above for several accelerators for which we have sufficient data on the geometry and materials. In each case, we made measurements of the total fast-neutron source strength (determined by the method described previously of measuring thermal neutrons in the room) and we have compared our results with these.* The results of these calculations are shown in the Table IV. In general, the comparison is fairly good. One should remember that we are comparing only the neutrons produced by electrons which produce the usable photon dose. In most machines, there are other electrons which are accelerated and lost, and these can contribute to the neutron leakage dose but not to the useful photon dose. It is believed that this is the largest part of the discrepancy for both models of the Clinac 35. This machine has two bends with energy analyzing slits before the beam strikes the target, and the authors suspect that there is a large beam loss at one or both of those bends. Both the Clinac 18 and the Mevatron XX would be expected to have a much smaller beam loss. These results indicate that, in accelerators where the beam losses are reasonably well-known and if target thicknesses and geometries are known, one can probably calculate the neutron yield per photon rad to within ±20%. With these calculations and the "cookbook" methods described in MJS, one could also calculate the head leakage for medical accelerators. The total accuracy one would expect should be no worse than about ±50%.

* The authors wish to express their thanks to Siemens Medical Laboratories, Inc., and to Varian Associates for making available measurements and information about their accelerators for these calculations and comparisons.

Accelerator	Energy (MeV)	Relative Neutron Yield (n/rad)	
		(Calculated)	(Measured)
ATC 25 MeV Betatron	25	6.8×10^{9}	6.9×10^{9}
Siemens 42 MeV Betatron	42	3.8×10^{9}	3.7×10^{9}
Varian Clinac 35 (Old)	25	4.3×10^{10}	8.1×10^{10}
Varian Clinac 35 (New)	25	2.2×10^{10}	6.2×10^{10}
Varian Clinac 18	10	3.9×10^{8}	4.2×10^{8}
Siemens Mevatron XX	15	5.8×10^{9}	7.6×10^{9}

Table IV. Calculated and Measured Neutron Yield per Photon Rad

Leakage Neutron Depth-Dose Curves

There has not been very much attention paid to the depth-dose distribution of the leakage neutrons in a patient. It has been shown that these neutrons are of very low energy, and one would expect them to be attenuated quite rapidly in tissue. We have made an attempt to calculate this depth-dose distribution using the computer code MORSE. In the calculation, we have assumed a point source 1 m from the center of the phantom. The source spectrum used was that of either a 14 MeV (incident electron energy) photoneutron spectrum surrounded by 4 inches of tungsten, or a 25 MeV photoneutron spectrum surrounded by 4 inches of tungsten. The phantom was a water cylinder one meter long and thirty centimeters in diameter, centered at 1 m from the target perpendicularly to the beam axis. In Fig. 11, we show the results of these calculations of absorbed dose for the two spectra. In Fig. 12, we show the dose-equivalent calculations for the same two spectra, using the ICRP-21 conversion factors (see Fig. 2). There are several things of interest in these two figures. First, it can be seen that there is a quality factor of about 10 throughout the depth of the phantom for both spectra. Second, it can be seen that the attenuation is quite sharp, so that there would be very little dose to the patient beyond 10 centimeters. Because of the large difference in penetration between these low-energy neutrons and the high-energy photon leakage, the integral dose-equivalent to the patient would be much less from the neutrons than from the photons, for the same dose-equivalent. In the calculations just presented, the radiation source and phantom were both in vacuum rather than in a concrete room. If the same calculation were done for a concrete room, a portion of the leakage dose to which the patient would be subjected would be the scattered component from the walls which would be much softer than the direct leakage spectrum. Therefore the attenuation of the scattered component would be much faster.

Figure 13 shows the calculated neutron fluence rate at 1 m per mA of incident electron current, plotted as a function of electron energy (from Fig. 5 of Ref. [16]). The conditions for which these curves hold correspond to the case in which all neutron-producing parts (Fig. 7) are of W or

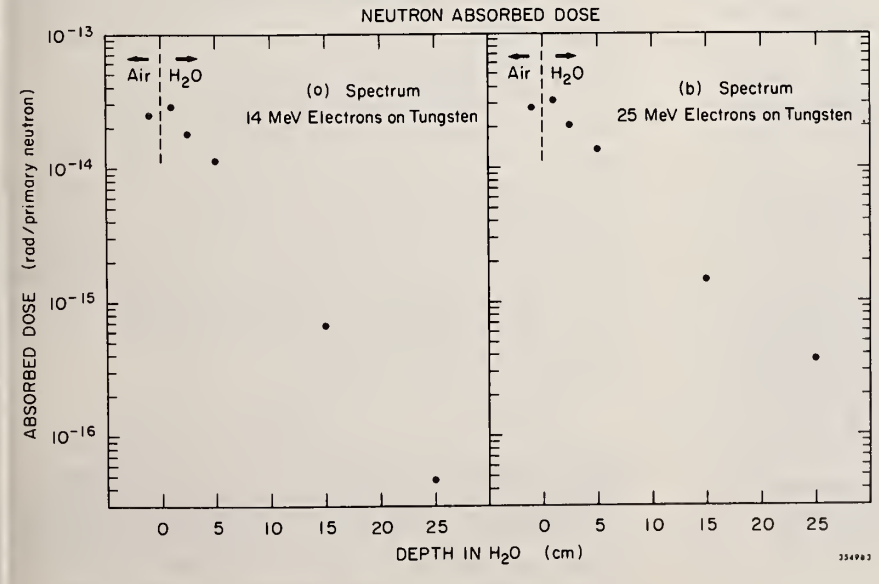

Fig. 11. Absolute depth-dose distributions in H_2O for neutron spectra from therapy targets, modified by 10 cm of W. The water phantom is a 30 cm-diameter cylinder, 2 m long, oriented perpendicularly to the beam axis and centered at 1 m from target. Units are rads per primary (photo-) neutron. The air-water interface is indicated at 0 cm (the leftmost point represents the air dose). Data are from the Monte-Carlo program MORSE.
(a) 14 MeV incident electrons;
(b) 25 MeV incident electrons.

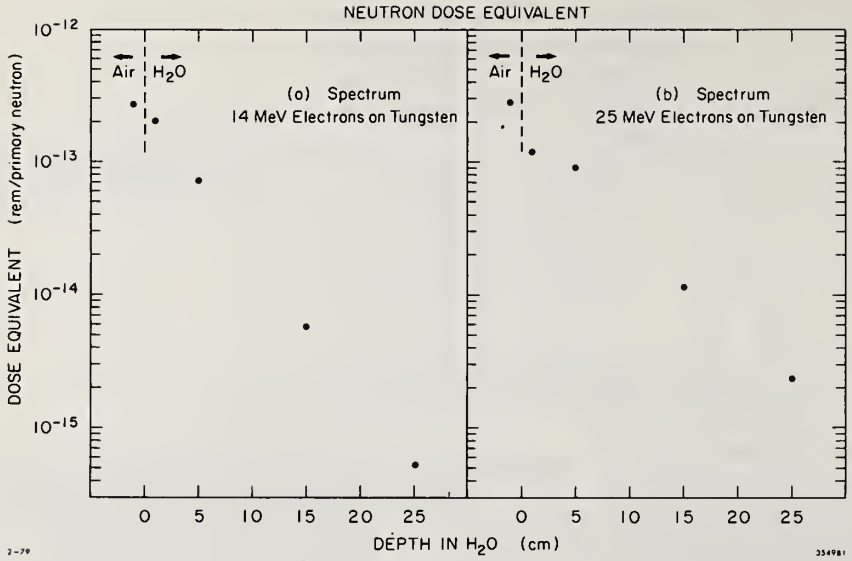

Fig. 12. Absolute depth-dose-equivalent distributions in H_2O for neutron spectra from therapy targets modified by 10 cm of W. Conditions are the same as for Fig. 11, except units are rem per primary neutron.
(a) 14 MeV incident electrons;
(b) 25 MeV incident electrons.

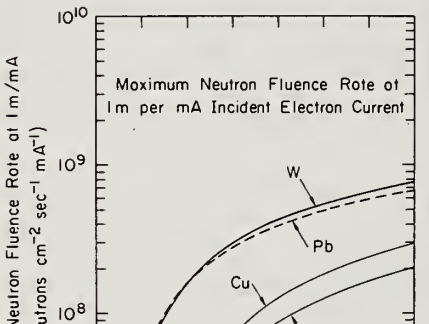

Fig. 13. Calculated maximum neutron fluence rate at 1 m per mA of incident electron current, plotted as a function of electron energy. The conditions for which these curves hold correspond to the case in which all neutron-producing parts (Fig. 7) are of W or Pb and the movable jaws are fully closed. Isotropic neutron production and no attenuation of neutrons in shielding materials are implicitly assumed. Lower two curves correspond to cases in which all neutron-producing parts are made of Fe or Cu and are shown for comparison. Data are derived from Fig. 5 of Ref. [16].

Pb and the movable jaws are fully closed or almost so. Note that the contribution of the movable jaws would amount to about 13% of the total (at 25 MeV; see examples above). Isotropic production of photoneutrons is implicitly assumed. For this graph we also neglect the attenuation of neutron fluence in high-Z shielding as well as the room-scattered component discussed above. The high-Z materials would change the fluence by a factor in the range 0.85 (for W) to 1.0 (Pb). The room-scattered component would boost the fluence by about 20% but increase the patient's integral dose by a relatively smaller amount. As these effects are not large and tend to cancel, we believe that the curves of Fig. 13 reliably represent the maximum neutron fluence of significance to the patient, assuming that the electron beam only strikes the intended target.

The result of dividing the data of Fig. 13 by those of Fig. 9 gives us the ratio of the maximum neutron fluence ϕ_{max} to the useful photon dose at the same distance. This is an absolute prediction to which comparison with measurement is invited. This ratio becomes nearly constant above about 25 MeV incident electron energy where its value is about 2.1×10^5 neutrons cm^{-2} rad^{-1}. As discussed by examples above, measured data that fall significantly below the curve are likely due to cases in which energy-absorbing accelerator components are not all of high-Z materials, or measurements were made with the movable jaws open. Points that fall significantly above probably represent cases in which there is substantial loss of beam on "targets" within the transport system before it reaches the intended target.

Using the above information, we are in a position to compare numerically the integral dose from neutrons to the integral dose from leakage photons. For the numerator of our comparison we integrate the curves of Fig. 11 over the range 0-30 cm and multiply by the strength of the neutron source per photon treatment dose (from Fig. 14). For the denominator we integrate an exponential

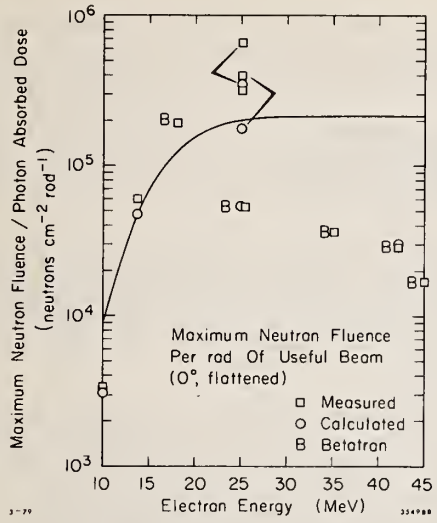

Fig. 14. Maximum neutron fluence per rad of useful beam 0°, flattened). Data are from the W curve of Fig. 13, divided by the photon absorbed dose index for W (flattened) as calculated by the Monte-Carlo program EGS (the triangles of Fig. 9). The conditions for which this curve holds are the same as for Fig. 13. Calculated points (circles) and measured points (squares) are mostly from Table IV.

over the same interval 0-30 cm, using -0.041 and -0.037 cm^{-1} as values of the attenuation coefficient for 14 and 25 MeV, respectively. The attenuation of the photon distributions includes the inverse-square reduction with distance, as is the case for the neutron distributions (Fig. 11). The denominator is multiplied by 0.001, corresponding to the ratio of leakage radiation to useful beam found in most standard accelerator models. This is meant only to be a rough comparison and details of the phantom geometry are neglected. The results are:

$$\frac{\text{neutron integral absorbed dose}}{\text{leakage photon integral absorbed dose}}$$

$$= 0.04 \quad \text{(at 14 MeV), and}$$

$$= 0.20 \quad \text{(at 25 MeV).}$$

Using the quality factor estimated by comparison of Figs. 11 and 12, we would multiply by $\bar{Q} = 10$ to obtain

$$\frac{\text{neutron integral dose-equivalent}}{\text{leakage photon dose-equivalent}}$$

$$= 0.4 \quad \text{(at 14 MeV), and}$$

$$= 2.0 \quad \text{(at 25 MeV).}$$

We note that most of the difference between these two energies is directly traceable to the increase in neutron yield per useful photon dose seen in Fig. 14.

Conclusions

Based on what we consider quite reasonable models, we can make the following statements regarding neutron sources and their characteristics:

(a) We have identified the significant sources of neutrons within the treatment head, and given absolute estimates of the amount of neutron fluence per treatment dose for various choices of target.

(b) MORSE calculations show that the neutron fluence is nearly unaffected by transport in the high-Z shielding contained in standard treatment units.

(c) On the other hand, the same calculations show that the neutron spectrum is softened significantly by transport by the high-Z material.

(d) We have considered the component of neutrons scattered by the concrete room and found its average energy to be about 0.24 of the primary source average energy. The scattered component can make a significant contribution to fluence measurements (about 20%), but considerably less to the patient's integral dose.

(e) We have submitted an absolute prediction of the ratio of neutron fluence (at 1 m) to the useful photon dose at the same distance. This ratio rises to an approximately constant value of 2.1×10^5 neutrons cm^{-2} rad^{-1} at incident electron energies above 25 MeV.

(f) Measurements at a variety of linear accelerator installations fall within a factor of three of this curve. We suggest that significant deviations of correct measurements can be explained by (1) use of materials other than high-Z within the treatment head (if the data fall below), or, (2) partial loss of the electron beam before it strikes the target (if above).

(g) The neutron fluence from betatrons is substantially below that from linear accelerators. The reasons are twofold: (1) Because most of the energy of the electron beam is expended in the low-Z material of the donut, there is smaller neutron production per incident electron beam current. (2) Because the smaller treatment fields permit a thinner flattener there is higher photon output per incident electron beam current.

(h) By means of MORSE, we have calculated absolute depth-dose and depth-dose-equivalent distributions for realistic neutron spectra in H_2O phantoms and found a rapid falloff with depth.

(i) Using the neutron depth dose curves presented in this work, together with the estimate of neutron fluence, we are able to calculate the ratio of neutron integral absorbed dose to leakage photon absorbed dose. These values are 0.04 and 0.2 for 14 and 25 MeV incident electron energy, respectively. If a quality factor $\bar{Q} = 10$ is applied, these correspond to 0.4 and 2.0 neutron integral dose-equivalent per leakage photon integral dose-equivalent.

(j) As for reducing the neutron fluence per useful photon dose, the following remarks may be made: (1) As the effective use of these machines for photon therapy depends on the use of high-Z materials to produce intense, wide fields with sharp edges, the possible reduction in neutron production is not very great. Thinner targets would be of some help, and certainly most of the neutron production by electrons striking parts of the transport system can be eliminated by improved design or lower-Z materials at critical points. Other than these steps, the only alternative is to treat patients at lower energies where possible. There is a factor of two reduction from the maximum in neutron production per treatment dose at about 17 MeV and a steep drop as the energy is reduced further.

Acknowledgement

The authors wish to express their appreciation to R. A. Shore for his help in doing computer calculations.

References

[1] ATC Betatron Corporation, Twenty-Five Million Volt Betatron for Radiation Therapy, P. O. Box Drawer 14248T, West Allis, WI 53214 (1974).

[2] B. L. Berman, "Atlas of Photoneutron Cross Sections Obtained with Monoenergetic Photons," Bicentennial Edition, Lawrence Livermore Lab, Report No. UCRL-78482 (1976). Also see "Atlas of Photoneutron Cross Sections Obtained with Monoenergetic Photons," Atom. Data Nucl. Data Tables 15, 319 (1975).

[3] R. L. Ford and W. R. Nelson, "The EGS Code System: Computer Programs for the Monte-Carlo Simulation of Electromagnetic Cascade Showers (Version 3)," Stanford Linear Accelerator Center, Stanford, CA, Report No. SLAC-210 (1978).

[4] R. J. Howerton, "An Integrated System for Production of Neutronics and Photonics Calculational Constants," Lawrence Livermore Lab, Report No. UCRL-50400, Vol. 9 (1970).

[5] International Commission on Radiological Protection, "Data for Protection Against Ionizing Radiation from External Sources:" Supplement to ICRP Publication 15, ICRP Publication No. 21, Table 9, p. 19 (1973). (Oxford: Pergamon Press.)

[6] R. C. McCall, T. M. Jenkins and R. A. Shore, "Transport of Accelerator Produced Neutrons in a Concrete Room," (IEEE Transactions on Nuclear Science NS-26 P. 1593 (1979), Stanford Linear Accelerator Center, Stanford, CA, Report No. SLAC-PUB-2214 (1978).

[7] R. C. McCall, R. D. McIntyre and W. G. Turnbull, "Improvement of Linear Accelerator Depth-Dose Curves," Med. Phys. 5, 518 (1978).

[8] G. S. Mutchler, "The Angular Distributions and Energy Spectra of Photoneutrons from Heavy Elements," Ph.D. Thesis, MIT, Report No. MIT-2098-224 (1966).

[9] National Bureau of Standards, National Council on Radiation Protection and Measurements, "Shielding for High-Energy Electron Accelerator Installations," NBS Handbook No. 97 and NCRP Report No. 31, Washington, D.C., Fig. 15, p. 25 (1964).

[10] H. W. Patterson and R. Wallace, "A Method of Calibrating Slow Neutron Detectors," Lawrence Berkeley Lab, Berkeley, CA, Report No. UCRL-8359 (1958).

[11] E. B. Podgorsak, J. A. Rawlinson, M. I. Glavinovic and H. E. Johns, "Design of X-Ray Targets for High Energy Linear Accelerators in Radiotherapy," Am. J. Roentgenol. Rad. Therapy Nucl. Med. 121, 873 (1974).

[12] E. B. Podgorsak, J. A. Rawlinson and H. E. Johns, "X-Ray Depth-Doses from Linear Accelerators in the Energy Range from 10 to 32 MeV," Am. J. Roentgenol. Rad. Therapy Nucl. Med. 123, 182 (1975).

[13] S. M. Seltzer and M. J. Berger, "Photoneutron Production in Thick Targets," Phys. Rev. C7, 858 (1973).

[14] E. A. Straker, P. N. Stevens, C. C. Irving and V. R. Cain, "The MORSE Code - A Multigroup Neutron and Gamma-Ray Monte-Carlo Transport Code," Oak Ridge National Lab, Oak Ridge, TN, Report No. ORNL-4585 (1970). Also see Radiation Shielding Information Center, RSIC Computer Code Collection, "MORSE-CG, General Purpose Monte-Carlo Multigroup Neutron and Gamma-Ray Transport Code with Combinatorial Geometry," Radiation Shielding Information Center, Oak Ridge, TN, Report No. CCC-203 (1976).

[15] W. P. Swanson, "Calculation of Neutron Yields Released by Electrons Incident on Selected Materials," Stanford Linear Accelerator Center, Stanford, CA, Report No. SLAC-PUB-2042; and Health Phys. 35, 353 (1978).

[16] W. P. Swanson, "Calculation of Neutron Yields Released by Electrons near the Photoneutron Threshold," Stanford Linear Accelerator Center, Stanford, CA, Report No. SLAC-PUB-2211 (Rev. 1979); and Health Phys., to be published (1979).

MIXED PHOTON-NEUTRON FIELD MEASUREMENTS

Ravinder Nath
Yale University School of Medicine
Department of Therapeutic Radiology
333 Cedar Street
New Haven, Connecticut 06510

and

K. W. Price and G. R. Holeman
Yale University
Health Physics Division
260 Whitney Avenue
New Haven, Connecticut 06520

High energy x-ray radiotherapy machines produce neutrons by photonuclear reactions which present a potential radiation hazard to the personnel and patient. A series of measurements of the neutron flux and spectrum from a 25 MV x-ray linear accelerator, inside and outside the treatment room, have been performed using a multisphere spectrometer, Nemo dosimeter, and activation detectors. These results are compared with other mixed photon-neutron field measurements for the same machine using an argon/propane ionization chamber, moderated gold foil, silicon diode, track-etching detectors, and Monte Carlo calculations illustrating some of the experimental difficulties which are encountered in an accurate measurement of the neutron contamination of a high energy photon beam.

(High energy x-ray radiotherapy machine; Mixed photon-neutron field dosimetry; Neutron leakage)

Introduction

High-energy x-ray radiotherapy machines in the super-megavoltage region also generate neutrons by photonuclear reactions in the target, field-flattening filter, and beam-defining collimators, resulting in a mixed radiation field in the beam and peripheral areas. The photonuclear cross sections for most materials commonly used for targets, filters, and collimators have photon energy thresholds of about 7-8 MeV and peak cross sections at about 12-14 MeV (1). Therefore, significant numbers of neutrons may be produced in accelerators with photon energies above 10 MeV. These neutrons present additional shielding problems for radiation protection and may lead to significant neutron dose to patients. Several recent biological and epidemiological studies (2,3,4) indicate that the relative biological effectiveness of fast neutrons may be higher than the currently accepted values. Some of the investigators have suggested quality factors in the range of 30-50 for low level neutron irradiation. These high values of the neutron quality factors necessitate accurate measurements of small amounts of fast neutron dose (hundredth of a mrad/hour) to personnel in a mixed photon-neutron field (mrads/hour). In addition, the hazard to the radiotherapy patient from the small amount of neutron contamination must be determined.

Accurate neutron dose measurements have generally been more difficult than x-ray measurements for several reasons. Many of the neutron detectors, such as activation foils measure particle fluence which is converted to absorbed dose using appropriate flux-to-dose conversion factors. These factors depend strongly on neutron energy and hence, the neutron energy spectrum must be known or approximated. Even for detectors which measure absorbed dose directly, such as the tissue equivalent ionization chamber, it is necessary to determine the neutron energy spectrum in order to evaluate the dose equivalent, because the neutron quality factors vary from about 2 to 11 as the neutron energy changes from thermal energies to 1 MeV (5,6). In many of the measurements reported, the neutron detector is calibrated against a Pu-Be, Am-Be or Cf neutron source. Since Pu-Be and Am-Be sources have a much higher effective neutron energy, their use can lead to systematic uncertainties. It is well known that the spectrum of fission neutrons from Cf-252 approximates a typical photoneutron spectrum, and that the shape of a photoneutron spectrum is rather independent of the incident electron energy (7). However, when heavy metal shielding is placed around a photoneutron source, as is the case in the treatment head of a radiotherapy machine, the photoneutron spectrum may deviate considerably from a fission spectrum. McCall, Jenkins, and Shore (8), and McCall (9) have obtained quantitative information about this effect and have shown that assuming a fission spectrum may lead to significant errors in evaluating experimental results, especially outside of the primary photon treatment beam.

Considerable attention has been devoted to the problems of mixed-field dosimetry for neutron radiotherapy (10). All neutron radiotherapy machines have a small, but finite photon component which must be determined. Although this problem is the opposite of the case of small neutron contamination of photon beams of high energy x-ray machines, it is still instructive to review the methods employed. In order to separate absorbed dose due to the photon and neutron components, two dosimeters with different sensitivities to neutrons and photons are employed. One instrument is usually constructed to have equal response to both neutrons and photons, and the other, a small response to neutrons. Since photons contribute a small fraction of the total dose, this combination results in one dosimeter responding predominantly to neutrons and the other to photons. It has been shown (10) that with this combination even a very large uncertainty in determining the neutron sensitivity of the photon-sensitive dosimeter contributes only a small uncertainty to the overall uncertainty in the neutron dose. Using the same argument for the present problem, if the neutron detector has a low sensitivity to photons, even a large uncertainty in the evaluation of its photon sensitivity would contribute a small amount to the overall uncertainty.

Another problem which arises with mixed field measurements is that the high energy photon beam results in photoneutron production in the detector. As these neutrons produced in the detector are indistinguishable from the external neutrons, this leads to a serious problem in measuring the dose from neutrons in the beam. Kushelevsky and Shani (11) have reported order of magnitude calculations of the photoneutron yield per gram for Si, O, Al and carbon irradiated by bremsstrahlung beams with energy of up to 24 MeV and have used these to calculate the photoneutron yield of two neutron detectors, NE213 scintillation detector and 8" polyethylene spherical rem-meter. Their calculation shows that the total number of neutrons produced in an 8" spherical rem-detector by the primary beam of 20-24 MV can be quite comparable to the flux of neutrons in the primary beam and gross errors in the estimation of neutron flux will result. McCall, Jenkins and Tochlin (12) have reported similar calculations for a moderated neutron detector, an In foil in a polyethylene cylinder. Also, McCall, Jenkins and Oliver (13) have calculated the photoneutron production in silicon diodes. Since the number of neutrons entering the detector depends on the area of the detector while the photoneutron production depends on the mass, detectors with large surface-to-mass ratio, i.e., small detectors, would have lesser interference from internal photoneutron production. Also, detectors made from hydrocarbon material have lesser photoneutron production within them because the threshold photon energy for photoneutron production in carbon is 18.7 MeV.

Neutron production resulting from high-energy x-ray beams in radiotherapy has been investigated at various centers for many years. Neutron dose levels outside the treatment room for radiation protection, neutron dose in the photon beam to the patient, and whole-body neutron dose to the patient have been extensively reported in the literature. Moderated neutron detectors have been used by Laughlin (15), Pohlit (40), Axton and Bardell (16), McGinley et al (17), Stranden (18), Holeman, Price, Friedman and Nath (19); fast neutron activation detectors by Ernst and Ovadia (22), Frost and Michel (41), Adams and Paluch (23), Brenner (24), Fox and McAllister (21), Stranden (18), Deye and Young (20), Price, Nath and Holeman (25), Gur, Rosen, Bukovitz and Gill (47); track detectors by Lofgren and Spring (26), Kehler and Robinson (27), Sohrabi, Morgan and McGinley (28), Wilenzick et al (29); silicon diodes by Wilenzick, Almond, Oliver and DeAlmeida (29), Marbach (14); scintillation detectors by Devanney (30), Daniels and Silberberg (37), Silberberg, Walchie and Daniels (32); and an ionization chamber by Schulz (33). It is difficult to compare these methods quantitatively because of differing experimental conditions and radiation sources. However, a series of measurements of the neutron dose equivalent at various locations in the vicinity of a 25 MV Sagittaire x-ray radiotherapy accelerator have been performed by Schulz (33), Holeman, Price, Friedman and Nath (19), Price, Nath and Holeman (25), McCall (9), Marbach (14), and Wilenzick et al (29). In the sections to follow, these measurements will be described and compared to illustrate the problems associated with these mixed field measurements.

Methods

A schematic drawing of the treatment room of the Sagittaire accelerator is shown in figure 1. All of the radiation protection measurements described below were made with the accelerator producing 25 MV x-rays at a dose rate of 400 rad/min. The entire installation is made from ordinary concrete, with steel plate in those parts of the wall struck by the primary beam. The sliding door, B, contains 2 inches of lead and 2 inches of polyethylene. A second swinging door, A, containing 10 inches of polyethylene was added to reduce the neutron dose to acceptable radiation levels.

Multisphere Spectrometer

The multisphere spectrometer consisted of a bare detector, a 0.03 inch thick cadmium cap, and six polyethylene moderating spheres (2-, 3-, 5-, 8-, 10-, and 12-inch diameter). The detector within the spheres used in this study (19) consisted of a set of four lithium fluoride thermoluminescent dosimeter chips, two Harshaw TLD-600 (^{6}LiF, ~ 95.6% ^{6}Li) and two Harshaw TLD-700 (^{7}LiF, ~ 99.99% ^{7}Li). The TLD-700 and TLD-600 are both sensitive to photons, while the TLD-600 is many times more sensitive to thermal neutrons than is the TLD-700. Thus, the photon contribution to the TLD-600 may be subtracted,

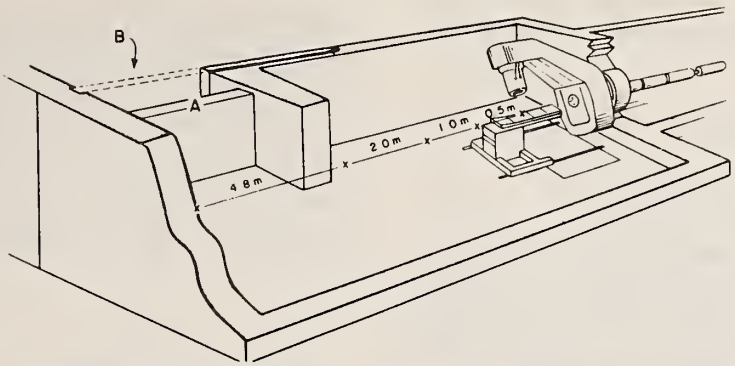

Figure 1. Schematic drawing of the treatment room of the Sagittaire linear accelerator.

leaving only a thermal-neutron response. A set of four TLD chips is placed at the center of each sphere and measures thermal neutrons produced as a result of moderation of the incident neutron spectrum.

The photon and thermal-neutron responses of individual TLD chips within a batch were found to vary significantly. Therefore, each chip was calibrated for photon response using a ^{137}Cs source and for thermal-neutron response using a calibrated plutonium-beryllium source (PuBe) in a moderating water tank. Each detector assembly was exposed to the PuBe source and a calibration of the system was made. This calibration was performed by forcing the spectrometer to yield a total number of neutrons equal to the known source output. The resultant neutron energy spectrum peaked at 5.5 MeV, very near the average of 4.1 to 4.5 MeV, as reported in the literature (34). The response matrix, which relates the incident neutron energy in a given detector-sphere geometry to thermal neutrons at the sphere center, was based on machine calculations (35). In order to compute absorbed dose and dose equivalent from a neutron spectrum measurement, dose and dose-equivalent conversion factors were applied (35). The present calculations represent 27 neutron energy groups ranging from 0.2 eV up to 35.2 MeV neutron energy.

Nemo Dosimeter

The Nemo dosimeter, based on the design of Bramblett, Ewing and Bonner (43), and Hankins (44), (model 9140, NEMO spherical Neutron Dosimeter System, Texas Nuclear, Chicago) was also employed for neutron measurements outside the treatment room. It consists of a 10" diameter polyethylene sphere with a ^{6}LiI scintillation detector at the center of the sphere. This instrument is designed to have an energy response closely proportional to the thick tissue RBE dose curve.

Phosphorus Activation Method

The reactions $^{31}P(n,p)^{31}Si$ and $^{31}P(n,\gamma)^{32}P$ were employed (25) to determine fast and thermal neutron fluxes in and just outside of the primary treatment beam. The $^{31}P(n,p)^{31}Si$ reaction is sensitive to fast neutrons above ~ 0.7 MeV, as shown in figure 2. The neutron-capture

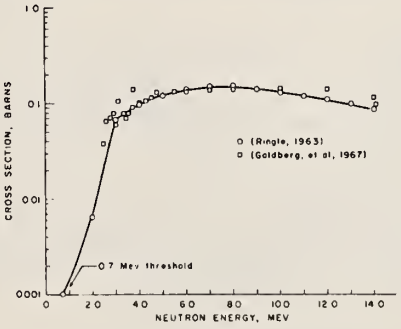

Figure 2. The $^{31}P(n,p)^{31}Si$ activation cross section.

reaction $^{31}P(n,\gamma)^{32}P$ is significant only for thermal neutrons. The activation products ^{31}Si and ^{32}P are essentially pure beta emitters and are counted using a liquid scintillation spectrometer. Details of the activation analysis using the liquid scintillation spectrometer have been presented in a previous publication (36). The phosphorus is used in the form of P_2O_5 powder placed into a small vial. The vial (1.2 cm in diameter by 3.5 cm high) usually contains on the average of 2.5 g P_2O_5. The irradiated powder is later dissolved in water, then mixed with a scintillation cocktail and counted in a liquid scintillation spectrometer. This technique leads to counting efficiencies of 95% and 97% for ^{31}Si and ^{32}P respectively. When P_2O_5 is exposed to a mixed neutron-photon flux, many reactions are possible. It has been shown that all activation products have either short half lives or are stable except for ^{31}Si and ^{32}P, which are produced by fast and thermal neutrons, respectively (36). The fast neutron flux $\phi_F(n/cm^2\text{-}s)$ is obtained from the measured ^{31}Si saturation activity, and the thermal neutron flux from the ^{32}P saturation activity. In order to utilize the ^{31}Si activation data for fast flux determination, the $^{31}P(n,p)^{31}Si$ activation cross section must be known as well as the normalized differential

neutron energy spectrum (45). The thermal flux is assumed to be constant in evaluating the ^{32}P activation data (46).

Results

Neutron Spectrum Measurements

Neutron spectrum measurements were only possible outside of the photon beam, and the multisphere spectrometer was the only instrument used which could provide neutron energy spectrum information. As an evaluation of the multisphere technique, a neutron spectrum measurement was made at the Yale Electron Accelerator Laboratory. The neutron spectrum from 32 MeV electrons impinging on a thick lead target was measured at 90° to the beam line by the multisphere spectrometer and a neutron time-of-flight technique (37). Figure 3 compares the unfolded

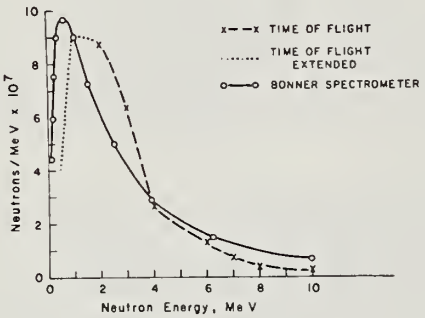

Figure 3. Comparison of neutron spectra determined by time of flight and Bonner spectrometer, normalized to 1 MeV neutron energy.

neutron spectrum versus the time-of-flight spectrum above 0.5 MeV neutron energy. The neutron source term calculated from the time-of-flight spectrum was 2.53×10^{11} n/sec, while the multispheres indicated a source term of 3.62×10^{11} n/sec, comparing favorably with the time-of-flight source term. Considering the low resolution of the multisphere technique and possible interference due to the large photon flux, the agreement in the determination of the neutron source term and spectrum is surprisingly good. It should be noted that the neutron spectrum derived from multisphere data represents a general trend in the neutron energy distribution, and any fine structure generated should not be taken seriously. The main advantages of the system are determination of total neutron flux and resultant dose equivalent.

The multispheres were placed at various locations within and outside the treatment room of the Sagittaire accelerator (outside the treatment beam, in all cases). It was found that the measured spectra were the same with or without a phantom in the beam, which agrees with the findings of others (33). All measurements were performed without the phantom. The data for the neutron spectrum just inside the shielding door (location A) were accumulated for 2997 photon rad with the beam directed into the floor. The data for the neutron spectrum outside the door (location B) were based on integrated patient photon doses of 85,479 and 26,770 rad. Some of these measured spectra are shown in figure 4. Although the neutron spectrum measurements suffer from poor energy resolution, it is

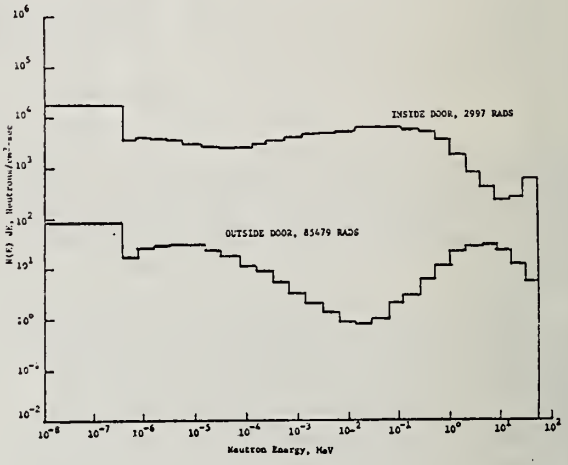

Figure 4. Measured neutron spectra at the inside and outside shielding door of the treatment room.

apparent that neutron intensities and doses are reduced in passing through the door, and the neutron spectrum hardens in passing through the door (see Table I).

Table I

Measured Neutron Dose Equivalent Rates and Inferred Quality Factors

Perpendicular Distance (m)	Neutron Dose Rate (rem/min)	QF
0.5	1.0×10^{0}	7.6
1.0	8.3×10^{-1}	7.5
2.0	4.2×10^{-1}	6.9
4.8	2.0×10^{-1}	6.7
Inside Shielding Door	2.6×10^{-2}	5.3
Outside Shielding Door	3.3×10^{-6}	6.5
	5.9×10^{-6}	7.0
PuBe	2.6×10^{-4}	7.7

Measurements inside the treatment room were taken at perpendicular distances of 0.5, 1.0, 2.0 and 4.8 m from the beam axis with a field size of 10 x 10 cm^2. Some of the resulting neutron spectra are shown in figure 5. The integrated

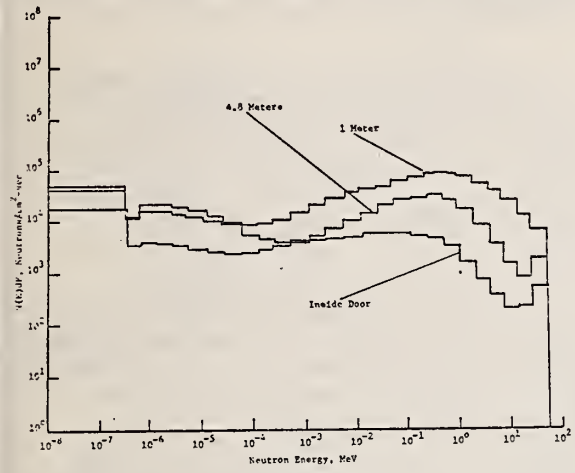

Figure 5. Measured neutron spectra inside the treatment room at a perpendicular distance of 1m and 4.8m, and at the inside door.

fast-neutron flux (> 0.1 keV) varies with the inverse-square law when the distance from the target is used rather than the distance from the beam axis. This would indicate that the major source of photoneutrons is the target and collimator assembly. Slow-neutron fluxes of less than 0.1 keV do not vary significantly with the distance from the beam axis and contribute only a small fraction to the total neutron dose equivalent throughout the treatment room.

Figure 6 illustrates a comparison between the differential neutron energy spectra determined by the multisphere spectrometer, neutron transport calculations of McCall (9), and an unfiltered photoneutron spectrum from Ta and Pb (7,39). All of these spectra are normalized at 1 MeV neutron energy. The calculated spectrum agrees reasonably well up to about 5 MeV and is in general, more degraded in energy compared with the spectrometer results. Considering the low resolution of the spectrometer, the overall agreement with the neutron transport calculation is fair. It may be noted here that assuming the neutron energy spectrum to be the same as a fission spectrum or unfiltered photoneutron spectrum, is reasonable only in the beam. As one moves away from the beam axis, the neutron spectrum is markedly degraded compared to the fission spectrum (8,9). This is due to neutron interactions in the treatment head shielding and general scatter throughout the room.

Measurements in the beam with the multisphere were attempted but failed due to a variety of interferences, including: (γ,n)

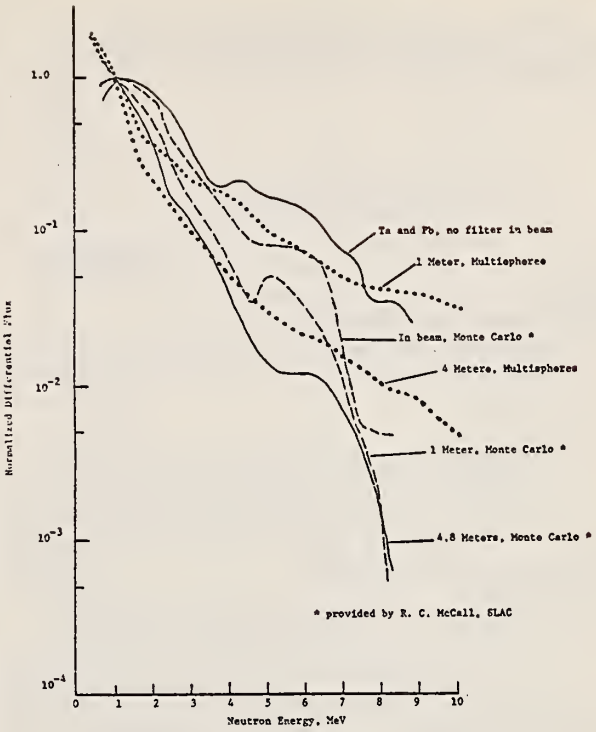

Figure 6. Comparison of various determinations of the neutron spectrum inside the treatment room.

reactions in the cadmium, unequal photonuclear cross sections of ^6Li and ^7Li, and (γ,n) reactions in the polyethylene spheres. As long as the spheres were located outside the beam there was no indication of these interferences.

Neutron Dose Equivalent Measurements Far From Treatment Beam

Each neutron spectrum measured using the multisphere spectrometer was converted to absorbed-dose rate and dose-equivalent rate by utilizing maximum values of flux-to-dose conversion factors (6) and the appropriate quality factor at each energy interval of the spectrum. The resultant total dose equivalent rates and quality factors at various locations within and outside the treatment room are given in Table I. As a calibration of the multisphere system, the neutron dose-equivalent rate, and quality factor from a PuBe neutron source are also shown in Table I. Previous studies indicate a calculated quality factor of 7.1 to 7.5 for PuBe neutrons (34). For PuBe neutrons a quality factor of 7.3 was inferred from measurements at a source-to-detector distance of 50 cm. This good agreement between theoretical and measured PuBe-neutron quality factors provided confidence in determination of average quality factors for fast neutrons.

Table II shows a comparison of neutron dose equivalents measured by various methods. For measurements outside the room, with the doors closed, neutron dose measurements using an argon/propane ionization chamber, Nemo survey meter, and Bonner spectrometer, are in good agreement with the Nemo dosimeter indicating the largest dose equivalent. The Nemo dosimeter was calibrated using PuBe and Cf-252 sources, in order to evaluate its capability to perform under different energy spectra. It was found that the Nemo results did not differ by more than 25% depending on the source used for calibration. Also, it may be pointed out that the Nemo dosimeter is known to overestimate neutron dose equivalent especially in the intermediate neutron energy range (44). In the usage of the multisphere spectrometer, maximum values of flux-to-dose equivalent conversion factors were employed. The ionization chamber underestimates the dose by about 15% because of a lack of proton equilibrium (33). Considering these factors, the overall agreement between various methods outside the room is fairly good. Neutron dose rate with the door open and in the maze was measured by McCall (9) using a moderated gold foil and a neutron transport calculation using MORSE code for subsequent determination of dose equivalent. His results compare very well with the results from the multisphere spectrometer and differ by a factor of about 2.5 from the ionization chamber results.

Table II

Comparison of Various Methods for Neutron Measurements Far From the Treatment Beam

Method	QF	Dose Equivalent (mrem/hr)
Outside treatment room with doors closed		
Multisphere Spectrometer	7.0	0.33
NEMO (PuBe Calibration)	—	0.51
(Cf Calibration)	—	0.62
Ionization Chamber*	7.1**	0.35†
Outside treatment room with doors open		
Moderated Au Foil**	—	150.
Ionization Chamber*	7.1**	62.
In the Maze		
Multisphere Spectrometer	5.4	1560.
Moderated Au Foil**	—	1488.

* Schulz (33)

** McCall (9)

† Corrected for by a factor of 2.64 for difference in location of detectors.

The Nemo dosimeter was not used in the treatment room because of the pulse pile-up problem in a high photon flux.

Neutron Dose Equivalent Measurements In and Near Treatment Beam

Because of the large flux of high energy photons in and near the treatment beam, fast neutron measurements in this area were performed using the $^{31}P(n,p)^{31}Si$ activation method. Thermal neutron measurements were performed using the reaction $^{31}P(n,\gamma)^{32}P$. There are no direct photonuclear interactions which will produce ^{31}Si or ^{32}P. The only photon contamination is due to a two-step process: [γ, (n, pn, or 2n)] in P_2O_5 followed by ^{31}P[n, (p or γ)] reaction. In order to determine this photon sensitivity of the detector, several experiments were performed at the Yale University Electron Accelerator Laboratory. Capsules of P_2O_5 were placed in the intense 32 MeV bremsstrahlung beam which also had a neutron component. In addition, capsules were placed just outside of the photon beam where neutrons were dominant. Activities induced by the mixed n-γ fields with different amounts of photon component were measured. From these data, the photon sensitivity of the neutron detector was determined (36). The neutron source term was measured using a neutron time-of-flight spectrometer, and the high-energy photon fluxes (> 7.5 MeV) were determined using gold activation foils $^{197}Au(\gamma,n)^{196}Au$ and a GeLi-γ spectroscopy system for determination of ^{196}Au saturation activity. The photon differential flux ϕ_γ (γ/cm^2-s-MeV) was then calculated from the ^{196}Au saturation activity. By taking the difference between the "in" and "out" of beam ^{31}Si induced activities and correcting for the known neutron source term, the ^{31}Si saturation activity due to the photons was determined. It was found that a good estimate for the photon sensitivity of the P_2O_5 capsule is 1.12×10^{-29} (^{31}Si dps/target nucleus)/(γ/cm^2-s-MeV). Photon fluxes at the 25 MV Sagittaire were measured with gold foils and the photon sensitivity for the Sagittaire beam with various field sizes was found to be less than 4%, as shown in Table III.

Capsules of P_2O_5 were placed at various distances from the Sagittaire photon central axis in a plane 105 cm from the target, with no scattering material near the detectors. The capsules were given 4000 photon rad per field size measured. Field sizes utilized in the present work were 5 x 5, 10 x 10, 20 x 20 and 30 x 30 cm^2. In a separate experimental run, a gold foil was placed on the photon beam axis for a photon-flux determination for each field size. Shown in figure 7 are plots of the fast-neutron fluxes and dose equivalent rates obtained from the measurements. The edges of the field are rounded in all cases, and the neutron flux increases as the field size increases. The activation data were

Table III

Estimated Photon Sensitivities of Neutron Detector in Sagittaire Beams

Field Size (cm)	Estimated* Photon Sensitivity (%)
5 x 5	3.8
10 x 10	2.7
20 x 20	1.9
30 x 30	1.7

*Using 1.12×10^{-29} (^{31}Si dps/target nucleus)/(γ/cm^{2}s MeV).

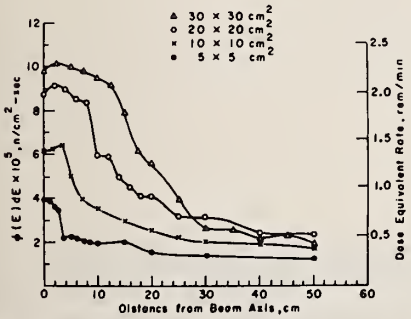

Figure 7. Measured fast-neutron flux and dose-equivalent rates vs. distance from photon central axis.

converted to neutron flux by assuming a neutron spectrum shape equivalent to a Ta-Pb photoneutron spectrum (discussed later in this section). For every energy group in the assumed neutron energy spectrum (0.5 to 11.0 MeV), maximum dose equivalent conversion factors were obtained from ICRP 21 (6). From these conversion factors, dose-equivalent rates were computed from the activation data. The maximum values of dose equivalent at each neutron energy represent the dose equivalent at the depth of maximum dose equivalent. This procedure overestimates the dose because d_{max} for the various neutron energies occurs at different depths. The largest neutron flux measured was 1.0×10^6 n/cm^2-s for the 30 x 30 cm field, representing a dose-equivalent rate of ~ 2.25 rem/min (using the Ta-Pb spectrum).

Measurements were also made of the thermal neutron flux for all of the photon beam sizes given above. Plots for a 5 x 5 and 20 x 20 cm beam are given in figure 8. Thermal-flux profiles were essentially constant for all beam sizes. Thermal neutron fluxes were low and near the threshold of detection for ^{32}P. Thermal fluxes varied between 1.5×10^5 and 3.0×10^5 n/cm^2-s,

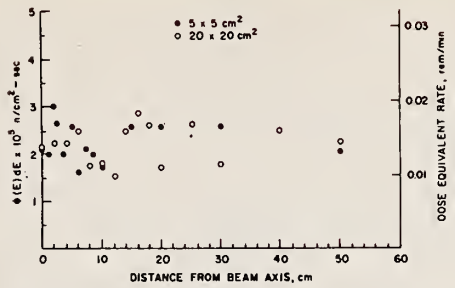

Figure 8. Measured thermal-neutron fluxes and dose-equivalent rates vs. distance from photon central axis.

or, using maximum dose-equivalent conversion factors, 0.01 and 0.02 rem/min. Thermal-neutron dose equivalent was about 0.7% of the maximum fast-neutron dose-equivalent measured.

In addition to the measurement of photon sensitivity (described earlier), two further confirmations of the lack of photon sensitivity of this activation technique were observed. Plotted in figure 9 are the photon and fast-neutron normalized fluxes for a 5 x 5 cm field size. It may be seen that the photon flux falls

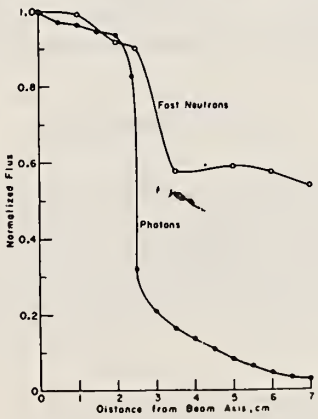

Figure 9. Comparison of fast-neutron and photon profile for 5 x 5 cm field.

off much more rapidly than does the neutron flux. In addition, the neutron profile has a rounded shoulder as opposed to the photon profile. Since the measured neutron profile does not follow the same shape as the photon profile, this provides an indirect check on the insensitivity of the neutron detector to photonuclear interferences. Shown in figure 10 is the variation of the on-axis neutron and photon fluxes as a function of field size, normalized to the 10 x 10 cm field. As the field size increases, the neutron fluxes increase much more rapidly than do the photon fluxes. This again provides an indirect check on the photon insensitivity of the system.

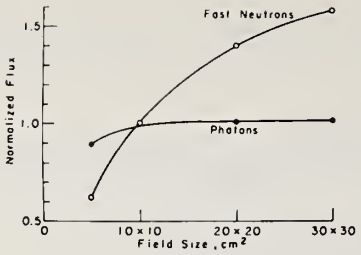

Figure 10. Photon and fast-neutron central-axis flux vs. field size.

One important assumption in the determination of the fast flux from the ^{31}Si activity is the shape of the differential neutron spectrum. In order to evaluate the uncertainty in the determination of fast neutron flux resulting from a lack of knowledge of the exact neutron spectrum, the factor for converting the ^{31}Si saturation activity to fast flux was evaluated for neutrons produced by 32 MeV electrons on a thick Pb target, 23-30 MeV electrons in Ta and Pb targets (7,38, 39), neutrons from a ^{252}Cf source (42), and McCall's in-beam Monte Carlo generated neutron spectra (see figure 6). The values of this conversion factor are presented in Table IV. It

Table IV

Conversion Factors from Saturation Activity to Flux

Source	Conversion Factors
32 MeV electrons on Pb target	2.325×10^{25}
23-30 MeV electrons Pb and Ta targets	2.451×10^{25}
^{252}Cf source	2.897×10^{25}
Monte Carlo * calculation	3.205×10^{25}

*McCall (9)

may be noted that maximum deviation for these different spectra is from 2.3×10^{25} to 3.2×10^{25}. The overall uncertainty in the fast neutron flux in the photon beam arising from a lack of knowledge of the exact neutron spectrum is significant, but is not as large as one might expect. However, one would expect the uncertainty to increase as the distance from the beam axis increases (see figure 6).

Figure 11 and Table V illustrates the comparison of neutron dose measurements in and around the treatment beam using the P_2O_5 activation method, silicon diodes (14,29), track etching detectors (29) and multisphere spectrometer. Neutron dose equivalent measurements

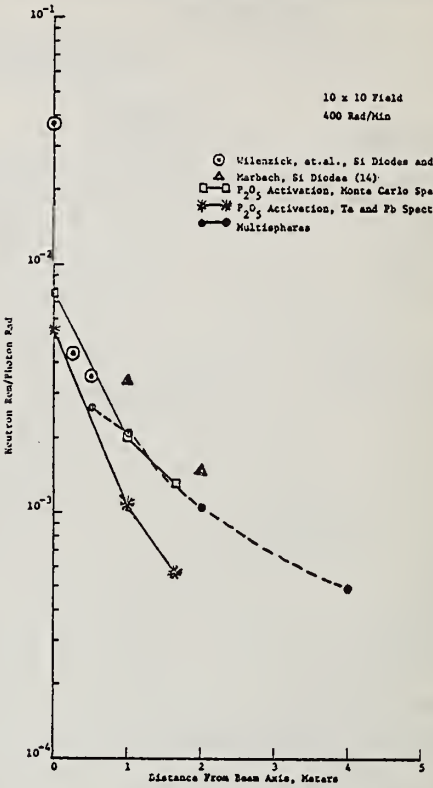

Figure 11. Comparison of neutron dose profiles measured using P_2O_5 activation method, silicon diodes, multispheres, and track-etching detectors.

plotted here are for a 10 x 10 cm^2 field at a photon dose rate of 400 rad/min. Two plots are shown for the fast neutron dose equivalent as determined from the P_2O_5 activation measurements. The upper curve represents a varying spectrum shape with distance from the beam axis as computed by McCall using Monte Carlo calculations. The lower curve represents a constant spectrum assumption from a combined tantalum and lead target (7,39). As mentioned earlier, the choice of spectrum makes a significant difference in the measured neutron dose, especially at points outside the x-ray beam. Since the Monte Carlo calculated spectrum includes the details of filteration, collimation and room scatter, it represents a better choice than the assumed unfiltered photoneutron spectrum, as one moves out of the treatment beam. A quality factor of 7 has been used in converting the data of Wilenzick et al from neutron rad/photon rad to neutron rem/photon rad. The quality factor used by Marbach was 10. Wilenzick et al observed that outside the x-ray beam, the silicon diode and track detector agreed very well with each other. However, in the x-ray beam, their track detector was sensitive to photo-

Table V

Comparison of Various Methods for Neutron Measurements In and Near the Treatment Beam

	Neutron Dose Equivalent Rate (rem/min)		
	At Isocenter	At 50 cm to the side	At 1m
P_2O_5 Method	3.04	1.52	.80
Multisphere	—	1.04	.82
Monte Carlo*	2.25	1.07	—
Silicon Diode**	14.8	1.40	—
Silicon Diode†	—	—	1.36
Track Etching**	—	1.40	—

* McCall (9)

**Wilenzick et al (29)

† Marbach (14)

fission and was not used. Their measurements with Si diode in the beam are an order of magnitude higher than activation detector results, and this has been attributed to the photon sensitivity of the silicon diode by McCall, Jenkins and Oliver (13). Marbach's diode data outside the x-ray beam are slightly larger than the activation results, but this difference can be attributed almost entirely to his choice of a quality factor of 10 which is most likely too large. Also plotted in figure 11 are the multisphere data. It should be pointed out that the multisphere results represent the total neutron dose equivalent from thermal to fast neutrons. At distances greater than 50 cm the multisphere data agree quite well with the P_2O_5 activation detector results. It appears that the P_2O_5 data, when the Monte Carlo spectra are applied in interpreting the results, yield a good estimate of the total neutron dose equivalent. This would indicate that the contribution from neutrons less than 0.5 MeV are not significant in the dose equivalent determination.

Discussion

Most of the results from the measurements of neutrons far from the treatment beam using the multisphere spectrometer, Nemo survey meter, ionization chamber of Schulz, moderated gold foil method of McCall, and P_2O_5 activation method, agreed with each other within a factor of 2. In and near the treatment beam, measurements using the P_2O_5 activation method, silicon diodes, track etching detectors, and multisphere spectrometer were found to agree well only outside the x-ray beam. In the x-ray beam, the activation detector was the only detector with sufficiently low photon interference. One of the requirements for the use of most dosimeters including the P_2O_5 activation detectors is that the neutron energy spectrum must be known. Although the neutron spectra in the beam has not been measured, reliable Monte Carlo calculations for specific geometries have been made and employed. Thus, a combination of the P_2O_5 activation detector with the calculated neutron energy spectra for specific installations offer the best available method among the techniques used here for determination of neutron contamination in the x-ray beam.

In this series of measurements to determine the neutron dose from a 25 MV x-ray machine, it was found that overall agreement between different methods is in the range of a factor of 2. Chief sources of uncertainty are the photon sensitivity and photoneutron production in the neutron detector, and the determination of the energy spectrum of neutrons. If the relative biological effectiveness of low-level neutron irradiation is significantly higher than currently accepted values, more accurate methods for the measurement of neutron contamination, with special attention to the problems addressed in this paper, would need to be developed.

Acknowledgement

The authors gratefully acknowledge the assistance of Drs. R. J. Schulz and R. C. McCall in providing their data and helpful discussion. We would also like to thank Ms. Ann Marie DePetto for her assistance in preparing this manuscript. The work was partially supported by NCI grant CA-06519.

References

1. B. L. Berman, University of California Lawrence Radiation Laboratory, Rep. UCRL-78482 (1976)

2. Symposium on the Radiobiological Response Relationships at Low Doses; Radiat. Res. 71, 1 (1977)

3. J. W. Baum, Proceedings of the IV International Congress of the IRPA, Paris, April, 1977. Paper No. 467

4. G. D. Kerr, T. D. Jones, J. M. L. Hwang, F. L. Miller and J. A. Auxier, Proceedings of the IV International Congress of the IRPA, Paris, April, 1977. Paper No. 335

5. "Protection Against Neutron Radiation", NCRP Report 38, 1971

6. "Data for Protection Against Radiation from External Sources", ICRP Report No. 21, Pergamon Press (1971)

7. "Shielding of High Energy Accelerator Installations", NCRP Report No. 31, NBS (1964)

8. R. C. McCall, T. J. Jenkins and R. A. Shore, Med. Phys. 4, 339 (1977)

9. R. C. McCall, (private communication)

10. "Neutron Dosimetry for Biology and Medicine", ICRU Report 26 (1977)

11. A. P. Kushelevsky and G. Shani, Nucl. Instr. Meth. 137, 71 (1976)

12. R. C. McCall, T. M. Jenkins and E. Tochlin, SLAC Report SLAC-PUB-1768, June (1976)

13. R. C. McCall, T. M. Jenkins and G. D. Oliver, Jr., Stanford Linear Accelerator Publication, SLAC-PUB-1782 (1976); Med. Phys. 5, 37 (1978)

14. J. R. Marbach (private communication)

15. J. S. Laughlin, Nucleonics 8, 5 (1951)

16. E. J. Axton and A. G. Bardell, Phys. Med. Biol. 17, 293 (1972)

17. P. H. McGinley, M. Wood, M. Mills and R. Rodrigues, Med. Phys. 3, 397 (1976)

18. E. Stranden, Phys. Med. Biol. 22, 1011 (1977)

19. G. R. Holeman, K. W. Price, L. F. Friedman and R. Nath, Med. Phys. 6, 508 (1977)

20. J. A. Deye and F. D. Young, Phys. Med. Biol. 22, 90 (1977)

21. J. G. Fox and J. D. McAllister, Med. Phys. 4, 387 (1977)

22. W. Ernst and J. Ovadia, Radiology 66, 105 (1956)

23. G. D. Adams and I. R. Paluch, Phys. Med. Biol. 10, 355 (1965)

24. M. Brenner, Commentat. Phys. Math. Soc. Sci. Fenn. 31,3,1 (1965)

25. K. W. Price, R. Nath and G. R. Holeman, Med. Phys. 5, 285 (1978)

26. K. Lofgren and E. Spring, Acta Radiol. 9, 274 (1970)

27. M. L. Kehrer and J. E. Robinson, Int. J. Appl. Radiat. Isot. 23, 141 (1972)

28. M. Sohrabi, K. Z. Morgan, P. H. McGinley, HPS Atlanta Meeting, Neutron Dosimetry in High Energy X-Ray Beams Produced in Medical Accelerators (1977)

29. R. M. Wilenzick, P. M. Almond, G. D. Oliver, Jr. and C. E. DeAlmeida, Phys. Med. Biol. 18, 398 (1973)

30. J. A. Devanney, Fourth Conference on Application of Small Accelerators, North Texas State University (1976)

31. C. J. Daniels and J. L. Silberberg, Proceedings of IEEE, Southeastern, Williamsburg, Virginia (1977)

32. J. L. Silberberg, R. L. Walchie and C. J. Daniels, IEEE Transactions in Nuclear Science, Vol. NS-25, No. 1 (1978)

33. R. J. Schulz, Med. Phys. 5, 525 (1978)

34. D. Nachtigall, IAEA Tech. Report No. 133, Handbook on Calibration of Radiation Protection Monitoring Instruments. IAEA, Vienna, p. 28 (1971)

35. R. S. Sanna,"Modification of an Iterative Code for Unfolding Neutron Spectra from Multisphere Data", HASL Report No. 311 (1976) and HASL Report No. TM-76-10 (1976)

36. K. W. Price, G. R. Holeman and R. Nath, Health Phys. (1978)

37. R. Nath, F. W. K. Firk and H. L. Schultz, Nucl. Instr. Meth. 108, 199 (1973) and F. W. K. Firk, Nucl. Instr. Meth. 43, 312 (1966)

38. G. Cortini, C. Milone, T. Papa and R. Rinzvillo, Nuovo Cimento 14, 54 (1959)

39. M. E. Toms and W. E. Stephens, Phys. Rev. 108, 77 (1957)

40. W. Pohlit, Strahlentherapie 113, 469 (1960)

41. D. Frost and L. Michel, Strahlentherapie 124, 321 (1964)

42. A. B. Smith, P. R. Fields and J. H. Roberts, Phys. Rev. 108, 411 (1957)

43. R. L. Bramblett, R. I. Ewing and T. W. Bonner, Nucl. Instr. Meth. 9,1 (1960)

44. D. E. Hankins, "A Comparison of the Neutron Dose Rates Obtained with the Single-Sphere Instrument, Multisphere Method and Hurst Proportional Counter", LAMS-2977 (1964)

45. J. C. Ringle, University of California, Lawrence Radiation Lab, UCRL-10732 (1932); M. D. Goldberg et al, Brookhaven National Lab, BNL-325 (1967)

46. D. I. Garber and R. P. Kinsey, Brookhaven National Report, BNL-325 (1976)

47. D. Gur, J. C. Rosen, A. G. Bukovitz and A. W. Gill, Med. Phys. 5, 221 (1978); D. Gur, A. G. Bukovitz, J. C. Rosen and B. G. Holmes, Phys. Med. Biol. 23, 1183 (1978)

NEUTRON CONTAMINATION IN THE PRIMARY BEAM

P. H. McGinley
Emory University Clinic
1365 Clifton Road
Atlanta, GA 30322

and

M. Sohrabi
School of Nuclear Engineering
Georgia Institute of Technology
Atlanta, GA 30322

In this work the absorbed dose due to neutrons was measured at points inside and outside of a 10 x 10 cm photon beam for several medical treatment units (Varian Clinac - 18, Allis-Chalmers 25 MeV betatron, and Brown Boveri 45 MeV betatron). The neutron dose was evaluated using a moderated activation detector, solid state track detectors, and by the fast neutron activation of phosphorous. For the linac it was found that the maximum neutron dose at the beam center was 0.004% the photon dose and maximum values of 0.054% and 0.08% were observed for the Allis-Chalmers betatron and the Brown Boveri betatron.

(Activation; detectors; dose; fast; neutrons; track)

Introduction

High energy photons are generated for use in radiation therapy by the decelleration of electrons in metal targets. The radiation beams produced by medical electron accelerators are usually contaminated with neutrons resulting from photon interactions in target, shield, collimator, and flattening filter. The dose delivered by these neutrons in patients undergoing radiation treatment and personnel operating the accelerator is of concern to the therapist and medical health physicist. It was for this reason that a study was initiated to evaluate the neutron dose in and near the primary photon beam using a number of neutron dosimeters.

In Figure 1 is shown the major components of the accelerator which may act as sources of fast neutrons. All components located above the dotted line are found in the linac and the parts shown below this line are common to both the linac and betatron.

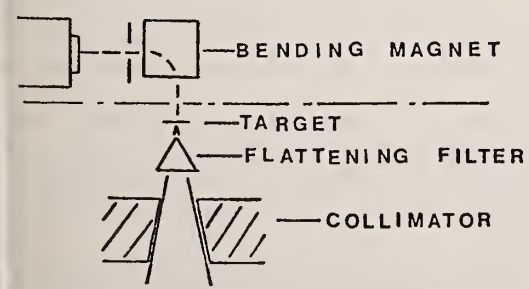

Figure 1. Simplified diagram of electron accelerator.

The materials which act as neutron sources are summarized in Table 1 for the accelerators used in this work.

Table I. Accelerator materials

Accelerator	Energy (MeV)	Collimator Material	Beam Fil. Mat.	Target Mat.	Target Thick. (mm)
Clinac - 18	10	W	W	Cu	6.3
AC-Betatron	25	Pb	Al	Pt	1.6
BBC Betatron	45	W & Pb	Pb	Pt	2.0

Figure 2 shows a typical cross section curve for the production of neutrons by photodisintegration of nuclei by photons.

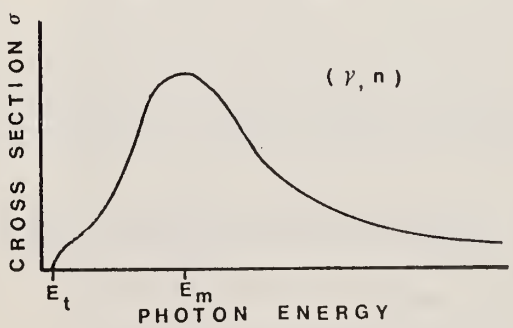

Figure 2. Photoneutron cross-section curve.

High Z materials such as Pb and W have photoneutron cross section thresholds near 7 MeV; copper has a threshold of approximately 10 MeV. Three to six MeV beyond the threshold the photoneutron cross section rises to a maximum and then falls off to exhibit a resonance peak. The majority of neutrons generated by photon interactions in high Z materials are produced by compound nucleus formation. The nucleus may be pictured as heated by the photon with the result that a neutron is "boiled out" of the nucleus. The resulting energy distribution is Maxwellian in form and resembles a fission spectrum.[1,2] This process predominates for nuclei with atomic mass number greater than 40 and the angular distribution of emitted neutrons is approximately isotropic.[3,4] To a lesser degree fast neutrons may be produced in high Z materials by a "direct" or "photoionization" process, whereby the neutron acquires all of the photon's energy minus the binding energy of the neutron to the nucleus. Direct neutrons thus form a high energy tail on the energy distribution. For direct ejection of neutron the angular distribution is expected to be slightly peaked at 90° to the direction of the incident photon.

MATERIAL AND METHODS

Moderated Activation Technique

The measurement of neutron dose levels in and near photon beams used in radiation therapy requires a dosimeter with the following properties. First, the dosimeter must be insensitive to pulsed photon fields. Secondly, the dosimetry system must have adequate sensitivity to neutrons. Any detector used in the integrating mode should be able to detect fast-neutron fluence levels of 1×10^8 n/cm^2 or less in order to keep the irradiation time to a reasonable value. Third, it would be desirable to have a simple and rugged system.

Based on the above requirements a moderated thermal activation detector was investigated in this research. The fast neutron component of each accelerator was measured by suspending a bare indium foil (1.69 g in mass) in a cubical water-filled container in a 10-cm X 10-cm photon beam. The base of the container was 15-cm X 15-cm square and it was filled with water to a height of 15 cm. Fast neutrons that enter the water moderator are slowed by elastic collisions and some are captured by the indium foil. The activation of ^{115}In by neutron capture to form ^{116m}In was employed to detect photoneutrons. In this reaction ^{115}In has a neutron-capture cross section of the order of 155 b for thermal neutrons and the ^{116}In product has a metastable state with a half-line of 54.2 min. The reaction causing the formation of ^{116}In in its ground state is not observed due to the short half-life of 13 sec. A single-channel analyzer was used to detect the photon activity induced in the indium foil by an irradiation. The equipment consisted on an Ortec counter, an Ortec model 452 amplifier and preamplifier, an Ortec single-channel analyzer model 406, and Ortec model 456 high voltage power supply, a timer, and a 2-in. X 2-in. NaI (Tl) scintillation crystal. The pulse height analyzer was calibrated with a ^{22}Na source, which has a γ ray of 1.275-MeV energy. Indium-116m decays with the emission of five photons and three γ rays of which one of the γ photons (1.293 MeV) was used for neutron detection. After the irradiation of a foil, a delay of 5 min was taken before counting so that short metastable states of indium would not interfere with the count. Counting time (real) for all measurements was 5 min. The net count rate was corrected back to its value at the end of the exposure and also adjusted to its saturation value as shown in Eq. (1)

$$(c/m)_{sat} = \frac{\lambda(\text{total counts})}{1 - e^{-\lambda t_c}} \frac{e^{\lambda t_d}}{1 - e^{-\lambda t_1}}, \quad (1)$$

where

$(c/m)_{sat}$ = saturation count rate at end of exposure (counts/min),

t_d = decay time (5 min),

t_c = counting time (5 min).

t_1 = irradiation time (min),

λ = 0.693/54.2 (min^{-1}).

A 5- μg ^{252}Cf source, whose neutron emission rate had been determined by the U.S. Atomic Energy Commission to an accuracy of ± 3%, was used to calibrate the dosimetry system. Indium foils were irradiated in the water moderator for a period of 4 h at a distance of 100 cm from the ^{252}Cf source. After the exposure a 5-min delay period was observed before counting of the foil was begun. The foil was counted for a period of 5 min employing a single-channel analyzer and the net count observed was used in Eq. (1) to obtain the saturation count rate at the end of the irradiation period. Equation (2) was then used to evaluate the flux density of fission neutrons at the position of the detector for the calibration exposure.

$$\phi = \frac{(\text{source strength } \mu g)(2.4 \times 10^6 \text{n/sec } \mu g)}{4 \pi r^2} \quad (2)$$

where ϕ is the neutron flux density at the detector position (n/cm^2 sec) and r is the distance from ^{252}Cf source to detector (cm). The factor of 2.4 X 10^6 n/sec µg shown in Eq. (2) was obtained from a study performed by Stoddard and Hootman[5] of the ^{252}Cf neutron spectrum. The neutron flux density established for the ^{252}Cf calibration and the observed saturation count rate were used in Eq. (3) to evaluate the flux density of photoneutrons associated with the various photon beams.

$$\phi' = \frac{\phi}{(c/m)_{sat}} (c/m')_{sat}, \quad (3)$$

where ϕ' is the fast-neutron flux-density component of photon beam $(n/cm^2)'_{sat}$ is the saturation count rate for foil exposed in photon beam.

Thermal-neutron flux-density levels were also determined by employing a technique similar to the one outlined above for fast neutrons. In this case a bare and a cadmium-covered foil were used without the water moderator to detect thermal neutrons in the photon beams. The bare and cadmium-covered foils were calibrated by placing them in a known thermal neutron field produced by a 5-Ci ^{239}Pu-Be neutron source housed in a paraffin moderator of 10-cm radius. The difference in induced activity between the bare and shielded foils was used to obtain the thermal-neutron component of the photon beams.

The fast- and thermal-neutron flux density were measured in the center of a 10-cm X 10-cm photon beam at the target to skin distance commonly employed for each accelerator (100-cm Allis-Chalmers betatron and Clinac-18 and 110 cm for the BBC 45-MeV betatron). Neutron flux densities were also established for a point 5 cm outside each photon beam. Activation of the foils was produced by delivering photon dose levels of the order of 1000 rad at the point of maximum dose buildup. Irradiation times of 15-25 min were required for the two betatrons and approximately 10 min for the Varian Clinac-18. A conversion factor of 3.97 X 10^{-9} cm^2 rad/n suggested by Stoddard and Hootman[5] for the ^{252}Cf neutron spectrum was used to convert the fast-neutron fluence levels to the absorbed dose in a small mass of muscle located in the photon beam and 5 cm outside the beam edge. A similar procedure was employed to establish the absorbed dose due to thermal neutrons based on the difference between the activation of a bare and cadmium-shielded indium foil. A thermal neutron fluence to dose conversion factor of 4.57 X 10^{-10} cm^2 rad/n[6] was used to obtain absorbed dose values.

Dose values due to neutrons in the primary beam and in the area occupied by the patient were also established using a second In moderated system. The system consisted of a 2.54-cm diameter indium foil placed at the center of a 6-in. diameter paraffin sphere encased in a cadmium shield. It has been shown by a number of workers that for this moderator the activation of indium foil per unit flux density of fast neutrons is fairly insensitive to neutron energy in the range 20 keV-20 MeV[7]. A gas-flow proportional counter was employed to measure the activity of each foil after irradiation. Calibrations were carried out with the same ^{252}Cf source described earlier in this article. Equation (3) was used to evaluate the fast-neutron flux density at the position of the detector. A decay time of 5 min was observed before counting of the foil was begun. All foils were counted for 10 min and Eq. (1) was used to calculate the saturation count rate for a given irradiation.

Fast Neutron Activation of Phosphorous

Price and co-workers have developed methods for measuring fast and thermal neutron flux density based on the activation of phosphorous.[8] This technique has low sensitivity to high energy photons and should be suitable for use in intense photon beams. Of the many reactions produced by neutrons and photons in phosphorous only the following result in radioactive products with half lives greater than 2.5 minutes.

$$^{31}P\ (n, p)\ ^{31}Si \qquad T_{1/2} = 2.62\ h \qquad (4)$$

$$^{31}P\ (n, \gamma)\ ^{32}P \qquad T_{1/2} = 14.28d \qquad (5)$$

The first reaction has a threshold value of 0.7 MeV neutron energy and can be used to establish the fast neutron fluence for a given irradiation. On the other hand, the second reaction is caused by thermal neutrons and the ^{32}P activity can be determined by counting the sample a few days after activation.

The phosphorus was irradiated in the form of phosphorus pentoxide (P_2O_5). All radioactive products of photon and neutron interactions in the oxygen portion of the sample have half lives less than 123 sec. The sample is then prepared for liquid scintillation counting using the method described by Price, et al.[8] The neutron flux density is related to the saturation activity, A_s (dis/sec/target nucleus), of the sample by

$$A_s = \int_{E_{th}}^{E_{max}} \phi(E)\ \sigma(E)\ dE \qquad (6)$$

where $\phi(E)$ is the differential neutron flux (n/cm^2 sec MeV) and $\sigma(E)$ is the activation cross section in (cm^2/atom). The activity obtained when the sample is counted, A_t, is related to A_s by Eq. (7)

$$A_s = \frac{A_t\ (\lambda t_c)\ e^{\lambda t_d}}{N_p\ (1 - e^{-\lambda t_I})\ (1 - e^{-\lambda t_c})} \qquad (7)$$

where λ is the decay constant for the activation product (4.408×10^{-3} min^{-1} for Si), t_d is the delay time from the end of the irradiation to the beginning of the count, t_c is the counting time, t_I is the irradiation time and N_p is the number of phosphorous atoms. The activity, A_t, was evaluated from the count rate C_t (counts/sec) observed in a portion of the irradiated sample and the counting efficiency of the scintilliation detector (93%).

Based on the value of A_s obtained from Eq. (7) the fast neutron flux density was calculated by

$$\phi_F = A_s \frac{\int_{E_{th}}^{E_{max}} \phi_n(E)\, dE}{\int_{E_{th}}^{E_{max}} \phi_n(E)\ \sigma_{n,p}(E)\, dE} \qquad (8)$$

where ϕ_F is the total integrated flux in n/cm^2 sec and $\phi_n(E)$ is the normalized neutron spectrum. A value of 2.451×10^{25} for the second term in Eq. (8) reported by Price et al. [8] for 20-30 MeV bremsstrahlung radiation on Ta and Pb targets was used in this work to evaluate ϕ_F.

The P_2O_5 powder was exposed in small glass vials at a number of points inside and outside of photon beams (10 X 10 cm) produced by the various accelerators. After several hours time delay each sample was beta counted in a liquid scintillation counter for a period of 5 minutes and ϕ_F was calculated from the measured count rate (C_t).

Polycarbonate Foil Detector

The registration of tracks induced directly inside polymers by particles was used as a third method of detecting photoneutrons. The tracks observed in polycarbonate such as Lexan $(C_{16}H_{14}O_3)_n$ are due to recoil carbon, oxygen, nitrogen, alpha, and hydrogen atoms.[9] Only recoil particles causing a damage density above a threshold value can be registered. For example, the polycarbonate foils used in this research have a threshold value such that neutrons with less than about 0.5 MeV do not induce tracks.

Polycarbonate foils of 250 μ m thickness were exposed in a 10 X 10 cm beam at each of the medical accelerators to photon dose values ranging from 20 to 2000 rads. The foils were etched by use of the electrochemical technique[9, 10] for a period of 4 hours at 25° C in a 28% KOH solution applying 800 V at 2 kHz. The track densities were then obtained and converted to absorbed dose and dose equivalent values by use of conversions factors established in the following manner. Foils were irradiated at the various facilities shown in Table II to neutron dose levels from 1 to 1000 rads.

Table II. Fast Neutron Sources Used in This Study.

Source	Facility	Neutron Energy at Maximum Yield (MeV)
Fission Source	HPRR ORNL	1
5 Ci Pu-Be	GA Tech	4.1
16 MeV d^+ on Be	Texas A & M Cyclotron	7
50 MeV d^+ on Be	Texas A & M Cyclotron	20
16 MeV d^+ on Be	Univ. of Washington	7
35 MeV d^+ on Be	Naval Research Laboratory	15

The absorbed dose and the quality factor associated with the peak energy of each neutron beam were used to evaluate the dose equivalent produced by the irradiation. Based on this procedure it was found that the neutron sensitivity (tracks/neutron) as a function of neutron energy follows approximately the shape of the ICRU rem curve (rem/neutron/cm^2). Therefore, the polycarbonate foil may be used to establish the dose equivalent of a fast neutron field without knowledge of the neutron energy distribution. At the indicated

etching conditions, a track density-to-rem conversion factor of 105 $\pm$ 7 tracks/cm^2 rem was obtained from 1-20 MeV neutron energy. The dose equivalent values associated with the neutron component of the photon beams was evaluated using this factor. On the other hand, the absorbed dose associated with the neutron component of the photon beams was determined using the conversion value obtained for the fission spectrum at ORNL.

The photon sensitivity of the polycarbonate foil should be very low since the authors of this paper could find only one photon induced reaction that could lead to track production. Some tracks might be produced by the betatron beams as a result of the $^{16}O(\gamma, np)^{14}N$ reaction which has a threshold at about 22 MeV photon energy and a cross section of less than 0.5 mb.[11] Work is now underway to establish the photon sensitivity of the polycarbonate foil to high energy photons.

RESULTS AND DISCUSSION

Central Axis Dose and Fluence

Table III summarizes the results obtained for the fast neutron fluence at the center of a 10 x 10 cm beam for the three medical accelerators. All values in Table III have been normalized to unit dose of photons at the point of maximum dose build up in a water phantom. As can be seen the fluence values vary by as much as a factor of 1.8 for the Allis-Chalmers betatron and by a factor of about 2 for the other accelerators depending on the measurement technique.

Table III. Fast neutron fluence per unit absorbed dose due to x-rays at center of a 10 x 10 cm beam

Accelerator	TSD (cm)	(n/cm^2/rad photon) In + H_2O Mod	In + Paraffin Mod	P_2O_5 Activ.
Varian C-18	100	1.06 x 10^4	0.55 x 10^4	---
AC Betatron	100	1.36 x 10^5	1.22 x 10^5	0.76 x 10^5
BBC Betatron	110	1.44 x 10^5	1.05 x 10^5	1.98 x 10^5

A number of factors may contribute to the variability shown in Table III. For example, the In plus water moderator system was calibrated by use of a ^{252}Cf neutron source. If the fission neutron spectrum is not a good approximation of the photoneutron energy spectrum then corrections may be required. Another source of error is the fact that no thermal neutron shielding material was used to encase the water moderator and the system may over respond in the presence of a thermal neutron field. The production of photo neutrons in the moderator material may also lead to an over estimation of the neutron fluence. The paraffin plus indium system should have a very low response to thermal neutrons due to the cadmium shield. However, the cadmium as well as the moderator will act as a source of photoneutrons when exposed in the x-ray beam. It has been estimated[12] that an over response of approximately 22% will occur for 25 MeV photons. The phosphorous activation method is sensitive to fast neutrons with energy greater than 0.7 MeV. It expected that the mean energy of the photoneutron spectrum produced by the Varian Clinac-18 will be low and little phosphorous activation will occur. No detectable neutron activation was observed when 20,000 rads was delivered by the Varian Clinac-18 x-ray beam. Therefore, one should not use the phosphorous activation method for accelerators with energy of 10 MeV or less. It should also be pointed out that the neutron energy spectrum employed in Eq. (8) is based on Ta or Pb targets bombarded with 20 to 30 MV x-ray beams. As can be seen from Table I none of the accelerators utilized a Ta target and two of the accelerators operated outside of the voltage range indicated above.

In general the major uncertainty in the neutron fluence values obtained with the moderated indium foil detectors is caused by the photon sensitivity of the systems. On the other hand, the phosphorous activations results are uncertain due to the lack of adequate neutron spectral information. Table IV list the major features of each detector employed to measure the neutron fluence at the center of the beams. The minimum detectable flux levels shown in Table IV are based on a photon dose rate of 100 rad/min., 5 minute count time, 30 minute irradiation and a 10 minute decay time for the indium detectors and 1 hour decay time for the phosphorous activation.

Table IV. General features of flux detectors used in this work

Instrument	Photon Sensitive	Neutron Energy Depent.	Min. detec flux (n/cm^2/sec)	Thermal neutron sensitive
H_2O + In	yes	yes	57	yes
Paraffin + In	yes	no	20	no
P_2O_5 Activation	low	yes	5 x 10^4	no

All of the values shown in Table III were converted to the absorbed dose due to neutrons per rad of x-ray by use of the conversion factor for

the ^{252}Cf fission spectrum (3.97×10^{-9} cm^2 rad/n). [5] As can be seen from Table V a minimum value of 0.22×10^{-4} rad neutrons per rad x-ray and a maximum value of 7.8×10^{-4} rad neutrons per rad photons were obtained.

Table V. Absorbed dose due to neutrons per rad x-ray at center of 10 x 10 cm beam

	(rad n/rad x)		
Accelerator	In + H_2O Mod.	In + Paraffin Moder.	P_2O_5 Activa.
Varian C-18	0.42×10^{-4}	0.22×10^{-4}	---
AC Betatron	5.40×10^{-4}	4.84×10^{-4}	3.0×10^{-4}
BBC Betatron	5.72×10^{-4}	4.17×10^{-4}	7.8×10^{-4}

The measurements carried out with polycarbonate foils yielded a ratio of neutron dose equivalent to that of photons of 0.006 and 0.013 at the beam center for the 25 to 45 MeV betatrons respectively. Unfortunately this dosimeter was insensitive to the neutron field produced by the Varian Clinac-18. This was expected since the mean neutron energy of this beam may be lower than the threshold of the dosimeter. No correction of the dosimeter response due to photons was made. However, work is now under way to evaluate the photon sensitivity of the polycarbonate foil which is expected to be very low.

The slow neutron fluence and absorbed dose per rad of x-ray based on the activation of indium are shown in Table VI. As can be seen the dose and fluence values are a factor of about 100 times smaller than the fast neutron values.

Table VI. Slow neutron fluence and dose at center of 10 x 10 cm x-ray beam

Accelerator	Slow Neutron fluence per rad x-ray ($n/cm^2/rad$)	Slow Neutron dose per rad of x-ray (rad n/rad x)
Varian Clinac-18	6.8×10^2	3.1×10^{-7}
AC Betatron	9.5×10^3	4.3×10^{-6}
BBC Betatron	6.3×10^3	2.9×10^{-6}

Transverse Fluence Distributions

In Figures 3 and 4 are shown the neutron fluence profiles for each betatron based on the activation of phosphorous by fast neutrons. The neutron fluence for each experimental run was calculated using Eq. (8) and then expressed as a percentage of the maximum fluence.

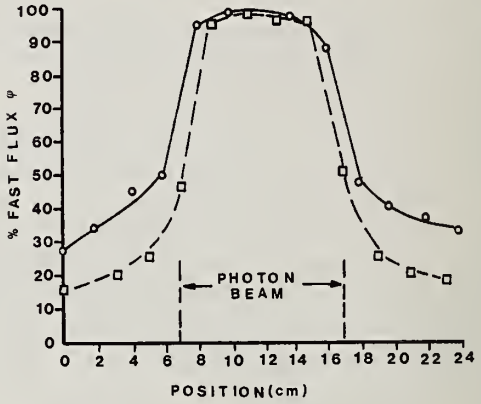

Figure 3. Percent fast neutron flux verses position for 10 x 10 cm 45 MV X-ray beam based on phosphorus activation (O = in plane of electron orbit, □ = perpendicular to electron orbit).

No corrections were made to account for changes in the neutron energy spectrum for points not in the photon beam. As a result of this procedure the neutron fluence is underestimated for points outside of the photon beam where the energy of the neutrons have been lowered by interactions in the shielding of the accelerator.

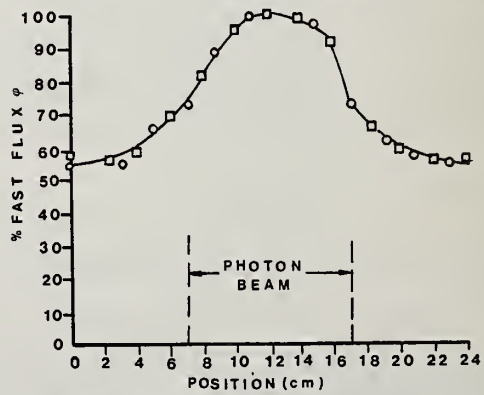

Figure 4. Percent fast neutron flux verses position for 10 x 10 cm 25 MV X-ray beam based on phosphorus activation (O = in plane of electron orbit, □ = perpendicular to electron orbit).

To illustrate this point the effect of filteration by 5 cm of Ta on the neutron energy spectrum produced by 20 to 30 MV x-ray beams impinging on a Ta target is shown in Figure 5. The neutron energy distribution shown in Figure 5 were calculated by Ford [13] using the evaporation model and considering only inelastic scattering of neutrons in the 5 cm Ta layer. As would be expected, the average energy of the neutron spectrum is decreased. The largest increase in number of neutrons per energy channel occurs in the range 0.5 to 1.0 MeV. However, there is only a small increase in the lowest energy channel (0.0 - 0.5 MeV).

If one uses Eq. (8) and the data shown in Figure 5 to determine the factor by which the saturation activity A_s must be multiplied to obtain the neutron flux density for the neutron energy spectrum before and after it enters the slab it is found that the value increases by a factor of 1.57 after the beam has been filtered by the 5 cm Ta layer. In this case if one did not allow for changes in the neutron energy spectrum the neutron flux after penetrating the Ta would be underestimated by 36%. It should also be noted that due to the relative number of neutrons and the value of the cross-section for the P(n,γ) reaction the neutron energy interval which is most effective in causing activation of phosphorous is 3-3.5 MeV.

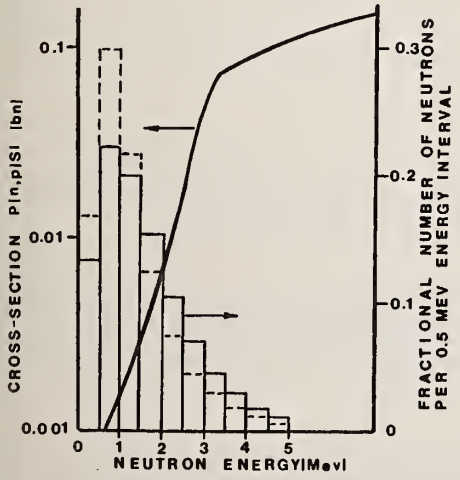

Figure 5. Cross section for fast neutron activation verses neutron energy and photoneutron energy spectrum before and after passing through 5 cm of Ta. (– – – = after 5 cm of Ta, ——— = before passing through 5 cm Ta).

A well defined neutron beam whose size is approximately the same as the collimator setting (10 x 10 cm) was found for the 45 MeV betatron. The neutron fluence is reduced by a factor of 4 or 5 for points greater than 5 cm from the edge of the photon beam. It should also be pointed out that the neutron beam profile in the plane of the electron orbit has a lower neutron fluence outside of the beam than the profile observed perpendicular to the orbit. A less well defined neutron fluence profile was found for the Allis-Chalmers 25 MeV betatron. The neutron fluence level outside of the beam was on the order of a factor of 2 less than that found at the beam center.

In order to access the whole body neutron fluence experienced by the patient measurements were made with the paraffin moderator plus indium foil detector. The neutron fluence was established in the plane of the treatment table with the moderator positioned at various distances from the central axis. Table VII presents the neutron fluence in the plane of the electron orbit (N-S) and perpendicular to the orbital plane (E-W) for a 10 x 10 cm x-ray beam produced by the Allis-Chalmers betatron.

Table VII. Fast neutron fluence per rad x-ray in plane of treatment table for 10 x 10 cm 25 MV x-ray beam. Electron orbit is in N-S direction.

Distance from central axis (cm)	N ⟶ S (n/cm^2/rad-x)	W ⟶ E (n/cm^2/rad-x)
100	2.1×10^4	2.4×10^4
70	3.4	3.5
50	4.6	4.4
30	5.7	6.9
0	12.2	12.2
30	6.4	6.2
50	3.7	4.0
70	2.3	3.0
100	1.3	1.9

Similar measurements (Table VIII) were made for the Varian Clinac-18 in a direction transverse (N-S) and radial (W-E) to the electron path in the bending magnet. The neutron fluence per unit absorbed dose of x-ray falls by a factor of about two as one goes from the central axis to a point 30 cm away. However, the absorbed dose due to neutrons will decrease by a larger factor due to the reduction of the neutron energy outside the primary x-ray beam.

Table VIII. Fast neutron fluence per rad x-ray in plane of treatment table for 10 x 10 cm 10 MV x-ray beam

Distance from Central axis (cm)	N S ($n/cm^2/rad-x$)	W E ($n/cm^2/rad-x$)
100	2.1×10^3	---
85	---	2.5×10^3
70	2.6	3.1
50	3.3	3.3
30	4.1	4.1
0	5.5	5.5
30	3.4	3.4
50	3.0	3.0
70	2.7	2.7
100	2.1	2.1

The maximum fast neutron dose received by a 20 cm thick patient treated to 5000 rads tumor dose through parallel opposed 10 x 10 cm ports (1:1) has been estimated using the paraffin plus In foil fluence values shown in Table VII and VIII. The percent depth dose due to x-ray for each accelerator was utilized to calculate the given dose for the ports. A fission spectrum was assumed for the neutron beam and the neutron depth dose data in reference [14] was used to evaluate the maximum neutron dose. Table IX presents the maximum dose at the central axis as well as the neutron dose 30 cm transverse to the central axis.

Table IX. Neutron dose for a typical treatment of 5000 rads tumor dose

Accelerator	Maximum fast neutron dose at central axis (rad)	Maximum fast neutron dose 30 cm from central axis (rad)
Varian Clinac-18	0.081	0.062
AC-Betatron	1.60	0.90
BBC-Betatron	1.30	0.52

The dose 30 cm from the central axis should be viewed as an upper limit due to the assumption of a fission spectrum. Inelastic scattering of neutrons in the shielding material will lower the average energy of the neutron beam and a larger fluence to dose conversion factor will be required. For example, it has been reported [15] that 15 cm of lead shielding will reduce the average energy of the ^{252}Cf fission spectrum from 1.8 to 1.0 MeV.

Acknowledgement - We wish to thank Mr. Russell Marian who assisted with the experimental measurements and the staff of Atlanta West Hospital for the use of the BBC 45 MeV betatron.

References

[1] Dose Levels Due to Neutrons in the Vicinity of High-Energy Medical Accelerators, P. H. McGinley, M. Wood, M. Mills, and R. Rodriguez, Medical Physics 3, 397 (1976).

[2] Measurement of Fast Neutrons Produced by High-Energy X-ray Beams of Medical Electron Accelerators, R. M. Wilenzick, P. R. Almond, G. D. Oliver, and C. E. DeAlemida, Phys. Med. Biol. 18, 396 (1973).

[3] Energy and Angular Distributions of Photoneutrons Produced by 70-MeV X-rays, W. R. Dixon, Canadian Journal of Physics 33, 785 (1955).

[4] Photoneutrons from Lead, M. E. Toms and W. E. Stephens, Physical Review 108, 77 (1957).

[5] ^{252}Cf Shielding Guide, D. H. Stoddard and H. E. Hootman, U. S. AEC Rep. DP-1246 (1971).

[6] Protection Against Neutron Radiation, NCRP Rep. No. 38 (1971).

[7] Fast Neutron Surveys Using Indium Foils Activation, L. D. Stephens and A. R. Smith, U. S. AEC Rep. UCRL-8418 (1958).

[8] A Technique for Determining Fast and Thermal Neutron Flux Densities in Intense High-Energy (8-30 MeV) Photon Fields, K. W. Price, G. R. Holeman, and R. Nath, Health Physics 35, 341 (1978).

[9] Electrochemical Etching Amplification of Low LET Recoil Particle Tracks in Polymers for Fast Neutron Dosimetry, M. Sohrabi, Ph.D. Thesis, Georgia Institute of Technology (1975).

[10] The Amplification of Recoil Particle Tracks in Polymers and its Application in Fast Neutron Personnel Dosimetry, M. Sohrabi, Health Physics 27, 598, (1974).

[11]
Atlas of Photoneutron Cross Sections Obtained with Monoenergetic Photons, B. L. Berman, Preprint UCRL-78482 (1976)

[12]
High Energy Photon Response of Moderated Neutron Detectors, R. C. McCall and T. M. Jenkins, SLAC-PUB-1768 (1976).

[13]
Private Communication, J. Ford, Atlanta, GA (1977).

[14]
Neutron Dose. Dose Equivalent, and Linear Energy Transfer From ^{252}Cf Sources, T. D. Jones and J. A. Auxier, Health Physics 20, 253 (1971).

[15]
Accelerator Health Physics, H. W. Patterson and R. H. Thomas, Academic Press, New York, p. 310 (1973).

NEUTRON PRODUCTION FROM ELECTRON ACCELERATORS USED FOR MEDICAL PURPOSES

E J Axton and A G Bardell
National Physical Laboratory
Teddington, Middlesex

Measurements have been made of the photoneutron production in and out of the photon and electron beams produced by the SL75-20 linear accelerator installed at Addenbrookes Hospital, Cambridge. The in-beam neutron dose-equivalent to the patient per treatment rad in water is estimated at 4.38 mrem in the photon mode and 0.249 mrem in the electron mode. The present results confirm less accurate measurements published earlier by the same authors, based on a prototype accelerator of this type. Similar measurements on a 33 MV Brown Boveri betatron published at the same time should be reduced by 25 - 30% to obtain the neutron dose-equivalent to the patient from externally generated neutrons, although the published values were probably a truer representation of the total patient dose-equivalent.

(Dose-equivalent: Electrons; Kerma; Multisphere; Photon; Photoneutrons; Radiotherapy; Spectrometry).

Introduction

Several years ago some preliminary measurements[1] were made on the Brown Boveri 35 MV betatron at St Luke's Hospital, Guildford, to determine whether a significant whole body neutron dose-equivalent would be received by a patient undergoing radiotherapy with either X-rays or electrons. Further measurements were made on a prototype M.E.L. Equipment Co.Ltd linear accelerator operated at 16 MV. The method of multi-sphere spectrometry was used for the measurements, which were then at an early stage of development at NPL.

Published curves[2] giving the shapes of the response for each sphere size as a function of neutron energy were adopted and these were normalised by calibrating two spheres (8 inch (a) and 12 inch diameter) with monoenergic neutrons of 0.511 MeV and 1.22 MeV energy from the NPL Van de Graaff accelerator using the $^{7}Li(p,n)$ reaction. The same two spheres were then irradiated both in and out of the collimated X-ray or electron beam, and a crude estimate of the mean neutron energy was taken as that which predicted the measured ratio of response for the two sphere sizes. In-beam dose-equivalent rates of about 0.5 per cent of the central axis X-ray dose rate were obtained with both accelerators, the results for the betatron in the electron mode being a factor of about 30 lower.

With more detailed knowledge of the sphere responses as a function of neutron energy, and the use of more sphere sizes, it was thought to be worthwhile to repeat these measurements in order to obtain an estimate of the neutron energy spectrum from which a more realistic estimate of the neutron dose-equivalent could be obtained. Unfortunately the Guildford betatron is no longer operated in the X-ray mode. It turned out that the only machine which was available for measurements in time for this conference was the 16 MV M.E.L. Equipment Co.Ltd SL 75/20 linear accelerator installed at the Addenbrookes Hospital, Cambridge, England, the higher energy machines being available only in the electron mode. The results obtained with the Cambridge accelerator which are described below, tend to confirm the earlier measurements.

The Detection System

The detectors consist of a set of six polyethylene spheres of density 922 $kg.m^{-3}$ each containing a thermal neutron detector in the form of a gold foil 1 cm^2 in area and 100 $mg.cm^{-2}$ in thickness. Gold foils were chosen rather than a dynamic counting device as they are completely stable and reproducible, independent of electronic drifts, and suitable for use in pulsed beams. Furthermore the response to photons is zero below the threshold for photoneutron production at 8 MeV. Above this threshold photoneutron production leads predominantly to ^{196}Au which is easily separated from the ^{198}Au produced by (n,γ) reactions by its half life. The major drawback of these detectors for some applications is their low sensitivity, and poor spatial resolution.

The sphere efficiency is defined as the saturation disintegration rate per mg of gold (equal to the neutron capture rate per mg) for unit neutron fluence rate at the centre of the sphere in the absence of the sphere. Six sphere sizes were used with diameters 5.1, 7.62, 12.70, 20.32, 25.4 and 30.48 cm (2, 3, 5, 8, 10 and 12 inches), *

* As the spheres were constructed to exact inch diameters, reference to these spheres in this paper will be given in inches.

Sphere efficiencies have been calculated by a Monte Carlo technique in which the energy scale is divided into logarithmic bins eight to a decade, and using the hydrogen and carbon neutron cross section data obtained from the European data centre in 1972. The efficiencies were computed for energies at logarithmic intervals five to a decade. The programme also records, for each energy, the thermal neutron fluence and the Westcott[3] epithermal flux parameter r which enable the relevant efficiencies to be obtained when other thermal neutron detectors are placed at the centres of the spheres, provided that they are not 'black'. The Monte Carlo calculations did not extend above 5 MeV because the computing power available was insufficient to cater for the inelastic scattering reactions in the carbon. There are now several sets of sphere response computations published in the literature which show general agreement in the shape above 5 MeV, although there are wide differences at lower energies. The shapes of reference[2] were therefore used to extend the efficiency calculations by a further two bins (mid points 6.3 MeV and 10 MeV). Thus there are 41 bins covering the energy range from 0.08 eV to 12.6 MeV, with an additional bin for thermal neutrons at 0.0322 eV, the mean energy of a Maxwellian distribution characterised by a temperature of 20 °C. In order to test the calculations the five smaller spheres were calibrated in the NPL thermal column, and the four smaller spheres were also calibrated with a standard Sb-Be neutron source (mean energy 22.8 KeV). These calibrations were in agreement within a few percent with the Monte Carlo calculation. However, the calibrations referred to in the introduction indicated that the calculated results might be about 14% too high at 0.511 MeV and 20% too high at 1.22 MeV. Further calibrations of the 8 inch sphere at 0.116 and 0.565 MeV confirmed the apparent energy-dependent trend. It is very important that the detector efficiencies should not be over-estimated since this would eventually lead to an under-estimation of the neutron radiation levels. Accordingly efficiencies above 25 keV were adjusted downwards by an energy-dependent correction amounting to 25% at 10 MeV. The correction is given by the expression, $(i > 28)$.

$$\varepsilon'_{i,j} = \varepsilon_{i,j} \exp((i - 28) \times 0.02214) \qquad (1)$$

where $\varepsilon_{i,j}$ is the efficiency for j^{th} sphere in the i^{th} energy bin.

As an example of the effect of this correction, the estimated central axis dose-equivalent rate per rad * of in-beam dose was increased by 18% in the X-ray mode and by 20% in the electron mode by the use of the modified efficiency matrix. This difference may be regarded as an overall limit of estimated systematic error in the measurements of dose-equivalent. The modified efficiency matrix is shown in appendix 1, together with the modified thermal neutron fluence and the Westcott epithermal flux parameter r.

* The SI unit of absorbed dose is the gray, equal to 100 rads. However the latter special unit, the rad, has been retained in this paper for ease of comparison with previous references. Similarly the rem has been retained in place of the SI unit of dose-equivalent, the sievert, equal to 100 rems.

The Measurements

Before planning the measurements it is convenient to consider the type of neutron spectrum likely to be encountered. From theoretical considerations the primary emitted spectrum is likely to approximate to a Maxwellian distribution characterized by a certain 'temperature' T(MeV) shown as a dotted histogram in figure 1. The primary spectrum will be degraded by scatter in the target, collimator assembly, beam-flattening filter etc., and the degraded beam will then interact with the detectors. The degraded beam will also go on to interact with the walls, floor and contents of the room to produce a well moderated '1/E' shaped spectrum culminating in an approximation to a thermal Maxwellian characterised by another 'temperature' T_m. The room scattered background will then interact with the detectors so that the overall spectrum interacting with the detectors will look something like the solid line in figure 1.

Although most of the contribution to dose-equivalent and tissue kerma will come from neutrons above, say 100 keV energy, a significant proportion of the fluence will be in the lower energy region and will contribute to the detector activation, particularly in the case of the smaller spheres. In order to interpret the measurements it is convenient to divide the spectrum into two parts at the energy of the cadmium 'cut off' just below 1 eV. In other environments this is easily achieved by enclosing the detectors in a cadmium box. In the present situation this would not be wise because photoneutron production in the cadmium would interfere with the field. However, the problem can be overcome by irradiating metallic foils, bare and under cadmium, to measure the thermal neutron fluence at the point of interest. Furthermore, the cadmium ratios give a measure of the epithermal fluence per unit lethargy interval at the energy of the principal capture resonance of the foil.

It is then possible to calculate the responses of the spheres to neutrons below the cadmium cut-off energy and subtract it from the measured response before carrying out the fast neutron analysis. The correction is small except for the 2 and 3 inch spheres (20% and 8% respectively).

The procedure for these thermal calculations is an extension of the method of Westcott[3] and is described in appendix 2. The treatment is strictly applicable only in well moderated environments since activation integrals are evaluated in 1/E shaped spectrum, and the presence of a preponderance of higher energy neutrons will give undue weight to higher energy resonances in the foil. On the other hand, the resulting errors in the low energy fluence will have little effect on the ultimate derived dose-

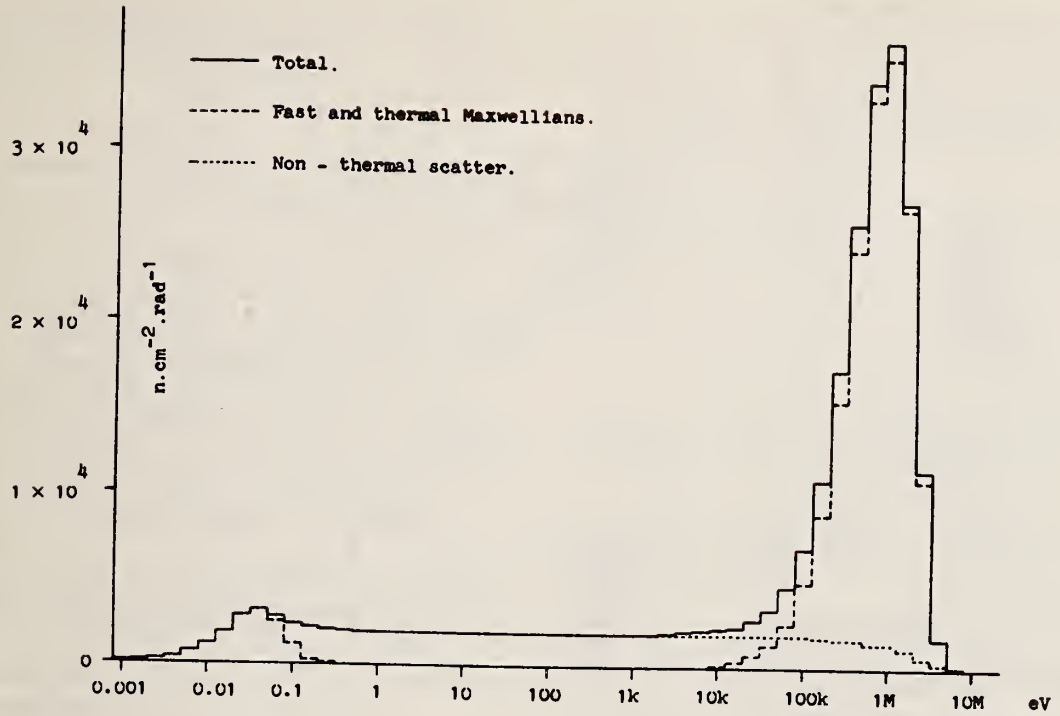

Figure 1. Maxwellian Spectrum Model.

equivalent or tissue-kerma rates.

For the X-ray measurements each sphere was irradiated in turn on the central axis (C) of the beam at a distance of 103 cm from the target. The accelerator was operated at a peak energy of 16 MeV and irradiations were of 10 to 20 minute duration at dose rates of 600 to 400 rad.min^{-1}. The rad in this context is a rad in water, measured at a depth of 5 cm in a water phantom the front surface of which was at 100 cm from the target, normalised to the maximum of the depth-dose curve at 3 cm. Simultaneously, two other spheres were irradiated at distances of 40 cm from the central sphere on either side (L and R) of it, on a horizontal line perpendicular to the beam axis, the left (L) spheres being towards the accelerator gantry, as shown in figure 2. The field size was 30 × 30 cm so that the edge of the largest (12 inch) out-of-beam sphere was about 10 cm clear of the beam, and a few millimetres at the edge of the in-beam 12 inch sphere were not irradiated.

The electron irradiations were performed with the centre of the in-beam spheres 11.5 cm from the face of the largest applicator available (20 × 20 cm) giving a window-to-sphere-centre distance of 107 cm. The accelerator was operated at 20 MV, and irradiations were of 30 to 20 minutes duration at dose rates of 300 and 400 rad.min^{-1}. The rad in this case is a rad in water at 1.5 cm depth in a water phantom with the face of the phantom placed against the exit aperture of the applicator, i.e. 10 cm nearer the electron window than the centre of the spheres. A measurement of the dose rate at 1.5 cm depth with the face of the phantom 10 cm from the applicator (i.e. at sphere centre position) indicated a reduction of 0.836 in the dose rate. No correction has been applied for this difference in distance. Again two other spheres were irradiated at the same time and in the same relative positions as in the X-ray case. The applicator size of 20 × 20 cm results in parts of the edges of the 10 and 12 inch spheres not being irradiated, however, since these regions only contribute a small percentage to the gold foil activities produced, no corrections were made for this effect. The X-ray and electron irradiations were performed with the central beam axis parallel to the floor and at a height of 123 cm. The left (L) spheres were irradiated in 1 mm thick cadmium boxes. All spheres were supported on expanded polystyrene foam above the treatment table which was not exposed to the direct beam in either case. A comparison of the L and R results thus gives a measure of the effectiveness of the thermal subtraction.

The simultaneous irradiation of three spheres, which was necessary in order to accomplish the measurement programme in the time available, introduces some small partially self-compensating aberrations. When there is a large sphere nearby it can shield another sphere from part of the scattered radiation, but at the same time it can act as an additional source of scattered neutrons. The latter effect would be most important when an out-of-beam small sphere is close to an in-beam large sphere.

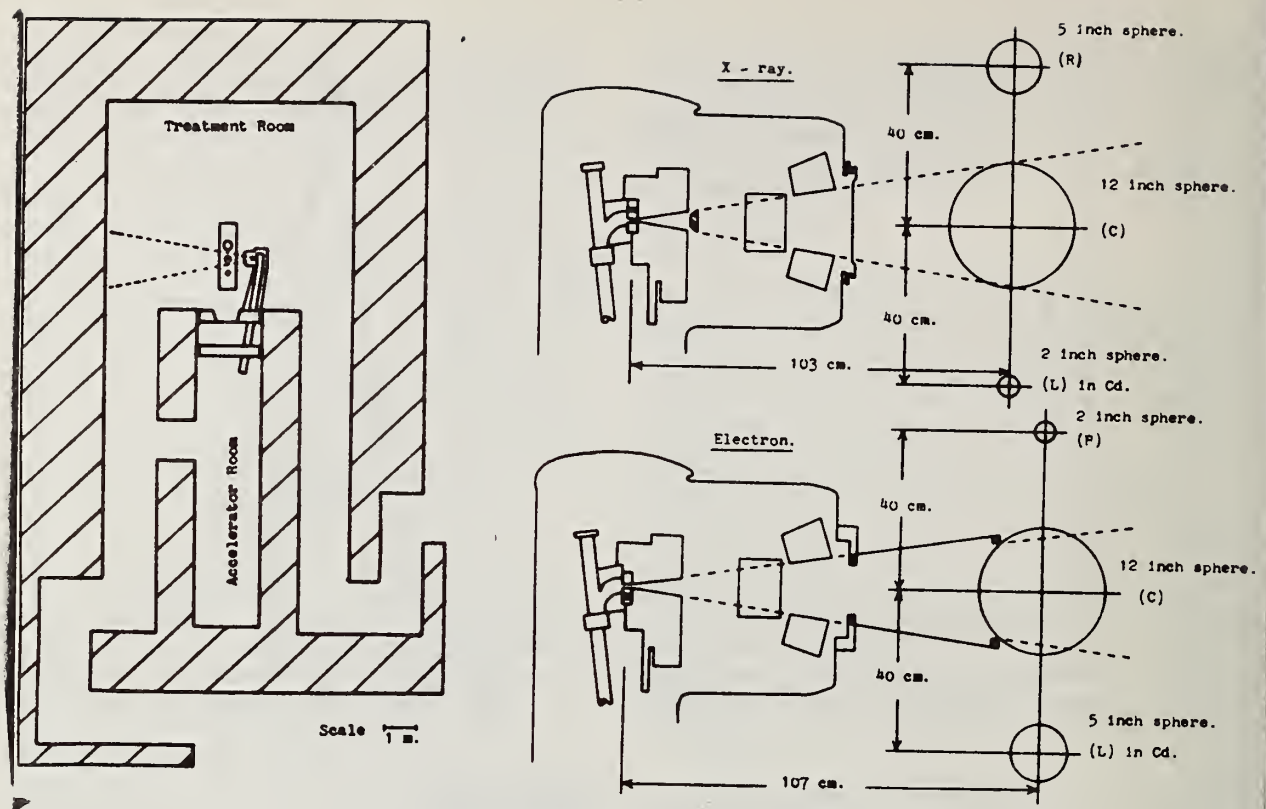

Figure 2. Radiation Geometry.

The ^{198}Au activities of the gold foils were counted in the NPL anticoincidence low background counter which has a background of about 0.04 s^{-1}. Foil β-counting rates varied from 2 to 40 s^{-1} in the X-ray mode from 0.1 to 2 s^{-1} in the electron mode. Interference from ^{196}Au was easily separated out by half life. Other aspects of photoneutron production in the detectors will be discussed in a later section.

Derivation of the Neutron Spectra

After subtraction of the thermal response to neutrons below the cadmium cut-off energy each irradiation of the set of six spheres yields a set of 6 disintegration rates B_j. 36 energy bins cover the energy range from $\exp(-(\ln 10)/10)$, (0.8 eV) to $10^6 \exp((\ln 10)/10)$, (12.6 MeV). The problem is to determine a set of energy bin fluences ψ_i which satisfy the Fredholm equations

$$\sum_i \psi_i \varepsilon_{ij} = B_j \pm \Delta B_j \qquad (2)$$

where ε_{ij} is the sphere efficiency as previously defined for the j^{th} sphere at the mean energy of the i^{th} bin and B_j is the saturation count rate of the gold foil in the j^{th} sphere.

With six measurements and 36 unknown bin fluences the equations are underdetermined and therefore have an infinite number of solutions. The task is to introduce constraints which lead to particular unique plausible solutions. There are several methods by which this may be accomplished, some but not all of which require some pre-knowledge of the spectrum. Having thus determined a set of ψ_i the expected disintegration rate C_j $(= \sum_i \psi_i \varepsilon_{ij})$ can be calculated and the quantity s, given by $\left[\sum_j (1 - C_j/B_j)^2/(n-1)\right]^{1/2}$ (where n is the number of spheres, in this case 6) is then a measure of the goodness of fit, and it determines the random uncertainty attributed to the quantities evaluated from the ψ_i.

Four methods will be mentioned as examples.

1. Choose a mathematical representation of the spectrum which is determined by a few unknown parameters which can be determined in a least squares analysis.

2. Minimise $\sum_i (\psi_i - F_i)^2$ where F_i is an initial guess.

The above methods require pre-knowledge of the shape. However, for the following two methods it is only necessary to make the assumption that the spectrum is smooth:

3. Minimise $\sum_i (\psi_{i+1} - 2\psi_i + \psi_{i-1})^2$. This minimises the deviation from a straight line of every set of three consecutive points.

4. Minimise $\sum_i (\psi_{i+2} - 3\psi_{i+1} + 3\psi_i - \psi_{i-1})^2$. This minimises the deviation from a quadratic through every set of four consecutive points. It generally turns out that different methods produce different spectrum shapes, but all shapes which fit the data yield the same total dose-equivalent rate, and the same dose-equivalent rates integrated over a few broad energy bands[4]. This implies that the system is primarily measuring dose or dose equivalent, rather than fluence.

In the present application it was found that good agreement with the measurements could readily be obtained by method 1. The first step is to establish a set of energy bin fluences ψm_i from a Maxwellian distribution characterised by an arbitrary temperature T, namely

$n(E) \propto E^{\frac{1}{2}} \exp(-E/T)$, where n(E) is the probability per unit energy interval of the emission of a neutron of energy E MeV. The ψm_i, which are shown by the dotted line in figure 1, are then used to calculate a set of sphere responses Bm_j.

$$Bm_j = \sum_i \psi m_i \, \epsilon_{i,j} \qquad (3)$$

The ψm_i are also used to calculate a set of scattered bin fluences ψs, by sharing each ψm_i equally between all the bins of lower energy.

The ψs_i are then used to compute a set of sphere responses Bs_j

$$Bs_j = \sum_i \psi s_i \, \epsilon_{i,j} \qquad (4)$$

It is assumed that the true bin fluences ψ_i are a weighted sum of ψm_i and ψs_i

$$\psi_i = C_1 \psi m_i + C_2 \psi s_i \qquad (5)$$

where C_1 and C_2 are unknown constants to be determined by a least squares fitting procedure from observational equations such as

$$B_j = C_1 Bm_j + C_2 Bs_j \qquad (6)$$

In other words, by minimising

$\sum_j W_j (B_j - C_1 Bm_j - C_2 Bs_j)^2$

It is assumed that the B_j have equal fractional uncertainties, so the weights W_j are taken as proportional to $1/B_j^2$. The fit gives the best values of C_1 and C_2 together with their uncertainties and covariances, determined from the root mean square residual s given by

$$s = \left[\sum_j W_j (B_j - C_1 Bm_j - C_2 Bs_j)^2 / (6-2) \right]^{\frac{1}{2}} \qquad (7)$$

The ψ_i so derived can be converted to dose equivalent by means of dose fluence curves[5] and to kerma by kerma fluence curves[6].

The temperature T is then varied to obtain minimum s. Figure 3 shows s as a function of T for the three X-ray cases and the three electron cases, for which the B_j's are shown in table 1. The dotted curves were obtained with the modified Monte Carlo matrix. Unambiguous minima are obtained with the three X-ray cases, and the resulting value of T is the same for the modified and un-modified Monte Carlo matrix and for L and R positions. Also included in figure 3 is the dose-equivalent rate calculated for the in-beam X-ray case. The dose-equivalent is a slowly varying function of T. Values of 0.6 and 0.25 are obtained for the in-beam and out-of-beam X-ray temperatures, and the random uncertainties are of the order of 1.5 - 3.5% of the dose-equivalent rate.

The electron cases present a slightly different picture. The uncertainties are higher, partly because the fluence rates are lower by a factor of 25, but there are probably other factors contributing to the poorness of the fit.

Table 2 shows the fluence, dose equivalent and kerma for the six sets of measurements and the totals are broken down into five broad energy bands.

In all cases the results are in reasonable agreement with the values published earlier in reference (1) although these were for different machines.

In the X-ray case, 30% of the neutron fluence below 100 keV contributes less than 3% to the dose equivalent. This demonstrates that fluence is not a good quantity to use for comparisons between different authors. In the electron case the accelerator was operated at the higher energy of 20 MeV, (21.5 in vacuo). The neutron energies are higher, and the contribution of neutrons below 100 keV is even lower. There is some evidence that the L dose rates are higher than the R dose rates, more so in the case of the electrons. The L position is nearer to the main part of the accelerator, and it could be that the latter forms additional sources. A study of the electron energy spectrum of this accelerator shows the presence of a secondary low energy peak in the energy distribution of electrons entering the 96° bending

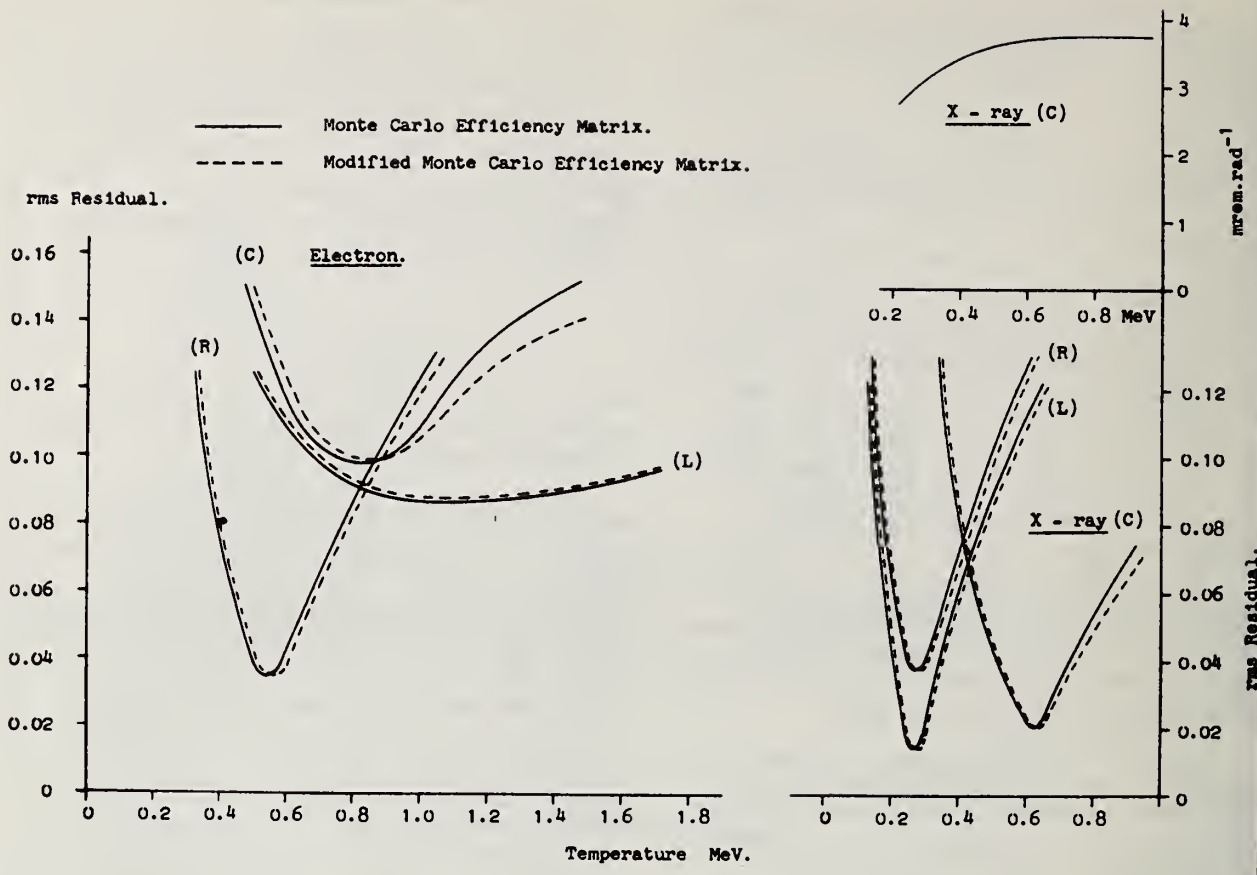

Figure 3. rms Residuals as a Function of Energy.

TABLE 1

Measured response (B_j) bq. mg^{-1} normalised to a dose rate of 1 rad in water per minute

	2"	3"	5"	8"	10"	12"
X-ray C	0.3930	0.7759	1.3630	1.0999	0.6405	0.3720
X-ray L	0.3164	0.6164	0.9003	0.5345	0.2811	0.1287
X-ray R	0.2602	0.5829	0.7721	0.5213	0.2714	0.1222
Electron C	0.00825	0.02389	0.06028	0.04410	0.03704	0.02293
Electron L	0.01252	0.02509	0.02359	0.01754	0.01200	0.00610
Electron R	0.00584	0.01276	0.02555	0.02139	0.01286	0.00675

magnet. This low energy component will be deflected in the magnet so as to strike the bending chamber walls and produce a secondary source to the left (using the same convention for the sphere positions). Neutrons produced in this region would be scattered predominantly towards the accelerator waveguide where there is less shielding. Secondary sources could also be produced where the electron beam impinges on any beam defining aperatures in this region. Beam wander would cause this source to be unstable. These sources would be relatively more important in the electron mode. Furthermore, such sources would worsen the aberrations caused by mutual shielding amongst simultaneously irradiated spheres. These effects would all worsen the goodness of the fit. Alternatively, perhaps, the neutron spectrum in the electron mode has a different shape and could be fitted better by a different spectrum. Temperatures of 0.9 MeV and 0.6 MeV for the C and R positions were obtained.

The L position fit did not give an unambiguous minimum possibly due to the secondary sources mentioned above. The spectra were also determined using methods 3 and 4 described above which require no pre-knowledge of the spectrum other than that it is smooth. As an example the derived spectra are shown in figure 4 for the X-ray in-beam case. Methods 3 and 4 show a broader peak, and a different, possibly less plausible low energy shape, but the dose-equivalents obtained by these, cruder, fits are within 20% of those obtained by Method 1, as shown in Table 2.

Photoneutron Production in the Detectors

The reactions to be considered are photoneutron production in deuterium, gold, and carbon. Photoneutron reaction rates can be calculated readily from the information available in the IAEA Handbook on Nuclear Activation Cross Sections[7]. This reference contains a comp-

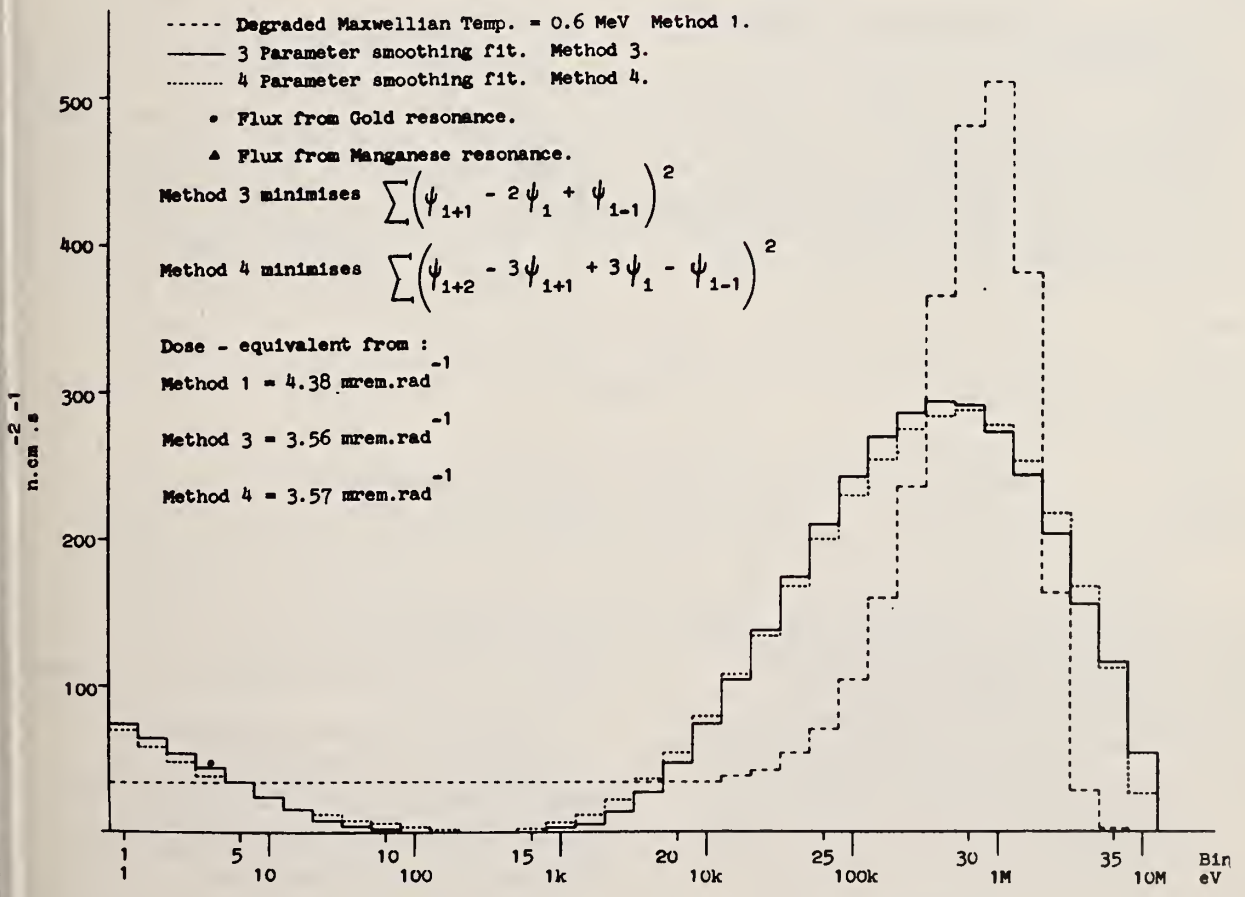

Figure 4. Spectra Produced by Different Fitting Methods.

TABLE 2

Neutrons per rad of dose in the Treatment Beam

(a) X-rays

Energy eV	Thermal %	Cd - 10K %	10K - 100K %	100K - 1M %	> 1M %	Total	Uncertainty %	Units
IN BEAM								
Fluence	5.80	16.77	7.25	45.67	24.51	2.41×10^{5}	1.20	$cm^{-2}.rad^{-1}$
Dose-Equiv.	0.36	1.05	1.10	47.79	49.70	4.38×10^{-3}	1.74	$rem.rad^{-1}$
Kerma	0.08	0.14	1.87	50.18	47.73	3.53×10^{-4}	1.75	$rad.rad^{-1}$
OUT OF BEAM - RIGHT								
Fluence	10.41	16.55	13.79	55.71	3.66	$1.44\ 10^{5}$	2.10	$cm^{-2}.rad^{-1}$
Dose-Equiv.	1.12	1.79	4.03	80.99	12.06	1.497×10^{-3}	3.25	$rem.rad^{-1}$
Kerma	0.23	0.24	6.22	83.00	10.31	1.32×10^{-4}	3.34	$rad.rad^{-1}$
OUT OF BEAM - LEFT								
Fluence	8.96	20.47	14.13	52.97	3.46	1.55×10^{5}	0.97	$cm^{-2}.rad^{-1}$
Dose-Equiv.	1.03	2.34	4.23	80.48	11.92	1.54×10^{-3}	1.57	$rem.\ rad^{-1}$
Kerma	0.20	0.30	6.56	82.73	10.21	1.35×10^{-4}	1.62	$rad.rad^{-1}$

(b) Electrons

IN BEAM								
Fluence	5.78	5.47	3.96	43.77	41.03	9539	5.26	$cm^{-2}\ rad^{-1}$
Dose-Equiv.	0.42	0.25	0.49	35.91	62.92	2.49×10^{-4}	6.46	$rem.rad^{-1}$
Kerma	0.10	0.04	0.82	37.02	62.02	2.01×10^{-5}	6.47	$rad.rad^{-1}$
OUT OF BEAM - RIGHT								
Fluence	18.54	10.62	5.59	42.20	23.05	5084	1.97	$cm^{-2}.rad^{-1}$
Dose-Equiv.	0.70	0.71	0.95	47.59	50.05	8.64×10^{-5}	2.70	$rem.rad^{-1}$
Kerma	0.18	0.10	1.61	49.97	48.14	6.94×10^{-6}	2.71	$rad.rad^{-1}$
OUT OF BEAM - LEFT								
Fluence	12.63	36.03	9.33	19.90	22.10	4596	4.36	$cm^{-2}.rad^{-1}$
Dose-Equiv.	1.09	3.16	1.65	28.61	65.49	6.81×10^{-5}	7.50	$rem.rad^{-1}$
Kerma	0.25	0.41	2.84	29.73	66.77	5.56×10^{-6}	7.64	$rad.rad^{-1}$

ilation of photoneutron cross sections as well as photon spectra as a function of accelerator energy. The photon spectra $\Phi(k_i,k_o)$ are proportional to the energy fluence ($MeV.cm^{-2}$) in unit energy intervals at energy k_i(MeV) from an accelerator with a maximum photon energy of k_o.

The reaction rate per g of material exposed to this fluence is:

$$\frac{N}{A} \sum_i \Phi(k_i,k_o)\ \sigma_i\ (\gamma,\ n + np + 2n + ...)/k_i$$

where N is the Avogradro constant and A is the atomic weight of the material.

The absorbed dose delivered by this energy fluence is given by:

$$1.602 \times 10^{-8} \sum_i \Phi(k_i,k_o)(\mu_{en}/\rho)_{water} \text{ rads in water.}$$

Where μ_{en}/ρ is the mass energy transfer coefficient ($cm^2.g^{-1}$) for water[8], and the initial constant is the conversion factor from $MeV.g^{-1}$ to rads. The ratio of these two summations gives the reaction rate normalised to an absorbed dose of 1 rad in water.

The total neutron production is obtained by multiplying each partial cross section by the number of neutrons produced per reaction and the production rate for any given product nucleus is obtained by considering just the particular partial cross section.

The neutron production in $g^{-1}.\ rad^{-1}$ has been calculated using this recipe for a number of elements and accelerator energies. For the higher energies it was necessary to extend the cross section curves on the basis of the Lorenz shape[7] and apply appropriate neutron multiplicity factors. The results which are shown in table 3 therefore only give a general guide to the manner in which the neutron production varies with accelerator energy.

Measurements with a 16 MeV accelerator

The carbon effect in this case is zero. The total $^{2}H(\gamma,n)$ neutrons produced in each sphere is (from table 3) 4×10^{5} × mass of the sphere, which is proportional to R^{3}. This may be compared with the number of neutrons entering the sphere from the accelerator surroundings which is given by πR^{2} × fluence (table 2). The number of neutrons produced in the sphere as a function of the number of neutrons striking the sphere is thus proportional to R. In the worst case (12 inch) the ratio is less than 0.01%.

The gold problem is treated differently. It has already been stated that the ^{196}Au activity has been separated from the ^{198}Au activity by half-life. The ^{196}Au saturation counting rate in the β-counter was nearly the same for all sphere sizes, amounting to about 0.04 and 0.0036 $s^{-1}.mg^{-1}$ for the X-ray and electron cases respectively, normalised to a dose rate of 1 $rad.min^{-1}$. From table 3 the ^{196}Au saturation disintegration rate mg^{-1} (equal to the reaction rate) normalised to 1 $rad.min^{-1}$ is $6.8 \times 10^{4}/60\ 000$ or 1.1 $s^{-1}.mg^{-1}$. The observed β-count rate of 0.04 $s^{-1}.mg^{-1}$ implies an efficiency for the detection of ^{196}Au decay of 0.036, in good agreement with estimates. On this basis the ^{196}Au saturation disintegration rate in the electron mode would be 0.1 $s^{-1}.mg^{-1}$.

The Monte Carlo Method has been used to calculate the conventional thermal neutron fluence rate nv_{o} created at the centre of the spheres by a source of 1 MeV neutrons of strength Q s^{-1} situated at the centre. nv_{o}/Q varies from 0.004 for the 2 inch sphere to 0.022 for the 12 inch sphere. The ^{198}Au reaction rate due to such a thermal neutron fluence, expressed as a fraction of the ^{198}Au reaction rate, β_{j}, shown in table 1 for both the in-beam X-ray and electron cases, is less than 0.01%. It can be concluded that the measurements with the 16 MV accelerators are free of any distortions due to photoneutron production in the detectors.

Measurements with a 33 MV accelerator operated in the X-ray mode

Although the neutron production rate for gold, (see table 3), is about 50% higher than for 16 MV the resulting enhancement of the ^{198}Au activity would still be negligible. In the Guildford experiment[1] the ^{196}Au activity was not separated out by half-life, although it is still possible to do this. However the amount of ^{196}Au produced would be significantly lower, as at the higher accelerator energy the situation would be dominated by the $^{197}Au(\gamma, pn)$ reaction leading to

TABLE 3

Neutron production $g^{-1}.rad^{-1}$ as a function of accelerator energy

MeV	16	22	27	32	36	25
^{2}H	4.0×10^{5}	3.5×10^{5}	3.2×10^{5}	2.9×10^{5}	2.7×10^{5}	3.4×10^{5}
C	0	7.0×10^{2}	5.8×10^{3}	7.8×10^{3}	8.3×10^{3}	3.9×10^{3}
W	7.6×10^{4}	1.2×10^{5}	1.2×10^{5}	1.1×10^{5}	1.1×10^{5}	1.2×10^{5}
Fe	6.3×10^{3}	2.9×10^{4}	3.7×10^{4}	3.8×10^{4}	3.8×10^{4}	3.4×10^{4}
Au	6.8×10^{4}	1.0×10^{5}	1.0×10^{5}	1.0×10^{5}	9.5×10^{4}	1.0×10^{5}
Cd	3.4×10^{4}	7.3×10^{4}	7.8×10^{4}	7.6×10^{4}	7.2×10^{4}	7.5×10^{4}

stable ^{195}Pt, and the ^{197}Au (γ, 2n) reaction leading to 185 d ^{195}Au. The presence of a small amount of ^{196}Au in the foils would lead to an over estimation of the neutron dose-rates but such an over estimation is thought to be fairly small.

Table 1 indicates also that photoneutron production from deuterium would be negligible in the Guildford experiment.

However the same cannot be said of carbon.

Kushelevsky and Shani[9] calculated the neutron production rate in the carbon in an 8 inch polyethylene sphere of unit density as being a factor of approximately 2.5 higher than the number of neutrons impinging on the sphere from a 24 MV accelerator. Their calculation was based on the photon spectra of Johns, Katz, Douglas and Hasham[10] which are not inconsistent with those of reference (7). However, their calculations contained two important errors. The first of these was a factor of 60 due to a misinterpretation of the statement of fluence (2960 $cm^{-2}.\ s^{-1}$ for 1 $rad.min^{-1}$) as being the integrated fluence $cm^{-2}.rad^{-1}$. The second of the errors, in the calculation of the total number of neutrons striking the sphere, was the multiplication of the fluence by the surface area of the sphere ($4\pi R^2$) instead of by the cross section area (πR^2). Thus the fractional neutron production in the sphere becomes 2.5/15 = 17%. The first of these errors has been corrected in a letter[11] where the fraction was re-estimated as 4.3%. The second error was not detected at that time so the revised figure of 4.3% has now to be increased by a factor of 4 to 17%.

But there is more. The calculation[9] was for a 24 MV accelerator. The carbon photoneutron production for a 33 MV accelerator would be a factor of 2 higher, and with the cross section data used in table 3 the fraction could possibly be as high as 48%. The conclusion is that it would not be unreasonable to reduce the in-beam neutron dose-equivalent rates of reference (1) by 25 - 30% (to 0.45% of the X-ray dose and to 0.015% of the electron dose) in order to obtain the dose-equivalent to the patient delivered by neutrons generated in the Guildford accelerator.

Field size dependance

The measurements which have been described were carried out with a field size of 30 × 30 cm. In one case the measurements were repeated with the field size reduced to 20 × 20 cm and 10 × 10 cm. The results shown in figure 5 show a linear decrease with field area for the 3 inch in-beam sphere, amounting to 11%. The out-of-beam (R) 2 inch sphere response remained approximately constant, whilst the out-of-beam (L) 8 inch sphere showed a linear increase amounting to about 14%.

Conclusions

The multisphere spectrometry system has been used to measure neutron dose-equivalent and tissue-kerma rates in in-beam and out-of-beam positions associated with the 16 MV linear accelerator at Cambridge. The systematic uncertainty is estimated at ± 20% at the 99% confidence level and is attributed to uncertainties in the response matrix. Random uncertainties at the 68% confidence level are shown in table 2 as derived from the

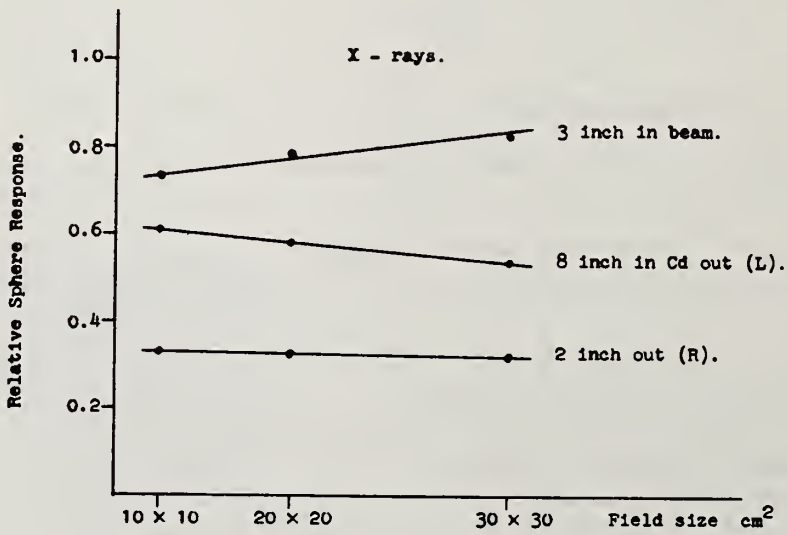

Figure 5. Effect of Field Size on Detector Response.

fitting procedures. The results indicate that the earlier published results obtained with a prototype linear accelerator at 16 MV were not seriously in error.

At higher energies, the photoneutron production in the carbon of the spheres is not insignificant. It is now realised that the earlier published results for the 33 MV Brown Boveri betatron should be reduced by perhaps 25 - 30% in order to obtain the true tissue equivalent kerma rates and dose-equivalents for the neutrons produced in the accelerator. On the other hand the carbon and oxygen (γ,n) cross sections are not dissimilar. The carbon in the spheres could therefore be regarded as simulating the oxygen in tissue, and the published results would then be a truer representation of the total dose-equivalent to the patient.

References

1. Neutron Production from Electron Accelerators used for Medical Purposes. E. J. AXTON and A. G. BARDELL, Phys Med Biol, 17, 293 - 298 (1972).

2. Use of the Multispheres neutron detector for Dosimetry of Mixed Radiation Fields. M. AWSCHALOM. Proceedings of Symposium on Neutron Monitoring. IAEA Vienna (1967).

3. Effective Cross Sections and Cadmium Ratios for the Neutron spectra of Thermal Reactors. C. H. WESTCOTT, W. H. WALKER and T. K. ALEXANDER. Proc. Second Intern.Conf. Peaceful Uses At.Energy, Geneva, A/Conf. 15/P/202 (1958).

4. Neutron Fields available at the National Physical Laboratory and the Need for Low Energy Neutron Standards. E. J. AXTON and A. G. BARDELL. Proceedings of Advisory Group Meeting on Reactor Neutron Dosimetry IAEA Vienna (Nov. 1978).

5. Conversion Factors and Effective Quality Factors for Neutrons. Recommendations of the International Commission on Radiation Protection. ICRP Publication 21. Pergamon Press (1971).

6. Kerma Factors. ICRU Report 26. Appendix A. (1977).

7. Handbook on Nuclear Activation Cross-Sections. Technical Report Series No 156. IAEA Vienna (1974).

8. Photon Mass Attenuation and Mass Energy Absorption Coefficients. J. H. Hubbell, Radiation Research, 70, 58 - 81 (1977).

9. Photoneutron Production in detectors in high Energy X-ray beams. A.P. Kushelevsky and G. Shani. Nuclear Instruments and Methods 137 71 - 73, (1976).

10. Gamma-Neutron Cross-Sections. H. E. Johns, L. Katz. R. A. Douglas, and R. N. H. Haslam. Physical Review 80, 1062 - 1068 (1950).

11. Photoneutron Production in Neutron Detectors in High Energy X-ray beams. E. J. AXTON A. G. BARDELL. Nuclear Instrument and Methods 155 563 (1978).

12. Absolute Measurement of the Thermal Neutron Flux in the AERE Reactor GLEEP E. J. AXTON. Journal of Nuclear Energy 17, 125 - 135, (1963)

APPENDIX 1

Monte Carlo Calculations

The efficiency ε, (table 1), the conventional thermal fluence (table 2) and the epithermal flux parameter $r(T_m/T_o)^{\frac{1}{2}}$ are related by the equation:-

$$\varepsilon = 0.001(N/A)\ nv_o\ (Fg + r(T_m/T_o)^{\frac{1}{2}}\ Gs_o)$$

where the symbols are as defined in appendix 2.

The energy of bin zero is 0.0322 eV. The energy of bin i is given by exp((i - 6).ln (10)/5)

Table 1

$\varepsilon_{i,j} \times 10^7$

	Sphere diameter in inches.					
1	2	3	5	8	10	12
00	1988	1572	897	304	136	59
01	2674	2067	1131	366	159	67
02	3369	2635	1399	439	184	76
03	3709	3230	1703	490	207	84
04	4224	3419	1821	563	237	94
05	4377	3894	2071	614	261	103
06	4044	4196	2271	671	277	112
07	4380	4332	2425	723	296	119
08	4359	4389	2743	763	311	130
09	4250	4577	2664	806	336	135
10	5197	4977	2640	864	359	137
11	5046	5129	2859	900	363	146
12	4343	5125	3024	912	385	152
13	4374	5126	3173	986	390	161
14	4125	5113	3374	1008	408	156
15	3932	5162	3320	1069	422	174
16	3783	4880	3549	1090	447	177
17	3435	4735	3686	1097	459	181
18	3156	4696	3706	1168	479	188
19	3035	4673	3761	1207	517	194
20	2751	4489	3763	1314	551	204
21	2609	4394	3780	1352	547	212
22	2306	4180	3899	1316	538	221
23	2140	4224	3983	1390	570	229
24	1974	3914	4124	1396	606	231
25	1809	3899	3837	1466	624	247
26	1606	3615	4139	1534	668	250
27	1591	3636	4045	1633	695	269
28	1486	3377	4214	1669	708	282
29	1256	3285	4036	1756	777	307
30	1094	3021	3972	1837	856	321
31	919	2685	4054	1971	875	374
32	761	2464	4080	2361	1030	429
33	649	2100	4275	2398	1218	489
34	516	1771	4028	3142	1526	707
35	367	1557	3816	3303	1938	942
36	240	1046	3480	3639	2473	1401
37	141	781	2928	4427	3179	2111
38	90	514	2197	3740	3133	2485
39	55	282	1509	3007	3139	2510
40	30	215	916	2606	2951	2487
41	23	120	736	1850	2071	2124

Table 2.

$nv_o \times 10^3$

	Sphere diameter in inches.					
1	2	3	5	8	10	12
00	697	552	314	107	48	21
01	937	725	396	123	56	24
02	1182	924	490	154	65	26
03	1300	1073	571	172	73	29
04	1481	1198	638	197	83	33
05	1535	1365	726	215	92	36
06	1418	1471	796	235	97	39
07	1535	1519	850	254	104	42
08	1528	1539	964	267	109	45
09	1429	1605	931	283	118	48
10	1398	1566	928	303	124	48
11	1355	1597	985	318	127	51
12	1238	1588	1033	321	135	53
13	1155	1570	1090	342	137	57
14	1086	1558	1158	353	143	55
15	1032	1569	1134	375	148	60
16	994	1475	1204	379	157	62
17	953	1426	1260	383	161	64
18	818	1398	1234	407	168	66
19	789	1398	1243	418	181	68
20	711	1342	1251	458	188	71
21	680	1298	1252	457	191	74
22	614	1233	1294	460	189	77
23	565	1242	1317	483	200	80
24	516	1153	1344	480	211	81
25	467	1142	1250	507	219	87
26	436	1063	1343	533	232	88
27	411	1064	1305	553	243	94
28	385	983	1376	570	249	99
29	384	946	1308	599	269	108
30	283	874	1286	631	305	113
31	233	777	1221	672	307	130
32	201	713	1348	807	359	151
33	165	601	1329	817	418	170
34	127	512	1254	1053	523	261
35	97	451	1215	1091	656	319
36	63	299	1130	1200	829	488
37	36	224	917	1408	1056	711
38	25	149	687	1221	1030	821
39	15	80	462	1002	1050	826
40	8	61	282	849	964	806
41	6	34	225	603	663	686

Table 3

$r(T_m/T_o)^{\frac{1}{2}} \times 10^5$

	Sphere diameter in inches.					
i	2	3	5	8	10	12
00	0	0	0	0	0	0
01	80	5	0	0	0	0
02	236	7	0	0	0	0
03	312	44	0	0	0	0
04	395	63	0	0	0	0
05	463	145	0	0	0	0
06	563	150	0	0	0	0
07	549	164	14	0	0	0
08	530	198	19	0	0	0
09	598	243	17	0	0	0
10	636	240	22	0	0	0
11	642	247	35	0	0	0
12	661	277	53	0	0	0
13	689	304	57	0	0	0
14	697	315	67	0	0	0
15	706	323	56	0	0	0
16	705	336	103	5	0	0
17	713	345	86	7	0	0
18	742	373	111	14	0	0
19	716	361	127	26	0	0
20	749	367	113	14	53	0
21	724	393	122	37	22	0
22	757	405	119	13	0	0
23	743	404	127	19	0	0
24	748	399	157	48	18	0
25	753	413	158	33	1	0
26	761	403	169	17	15	0
27	763	415	182	21	6	0
28	763	428	148	63	0	0
29	771	458	172	51	3	0
30	748	447	174	38	0	0
31	794	446	186	71	0	0
32	872	445	188	55	31	0
33	791	472	255	60	44	19
34	768	453	232	100	45	88
35	747	441	213	120	75	72
36	724	447	229	130	96	79
37	833	468	250	153	115	87
38	831	471	254	154	140	167
39	783	497	270	132	157	144
40	750	500	290	160	180	170
41	750	500	310	160	200	180

Appendix 2

The Low Energy Component of the Fluence. Interpretation of Cadmium Ratio Measurements.

This procedure is an extension of the Westcott[3] treatment for the expression of effective neutron reaction cross sections and reaction rates in well-moderated environments. The treatment pre-supposes a Maxwellian distribution of the neutron energies characterised by a temperature T_m, supplemented by a '1/E' shaped slowing down spectrum starting at a lower energy $\mu E_o T_m/T_o$ and terminating at a source energy E_s, where μ is a moderator-dependent constant or cut-off function, $T_o = 293.6^oK$, and $E_o = 0.0253$ eV.

Following the Westcott formalism[12], expressions can be derived for the 'conventional thermal neutron fluence', $n_{th}v_o$ and the cadmium ratio R_{Cd}. n_{th} is defined as the neutron density in the energy range below the cadmium cut-off energy, E_{Cd} and $v_o = 2200$ m.s.$^{-1}$, the velocity of neutrons of energy E_o. Note that the true fluence would be $n_{th}\bar{v}$, where $\bar{v}$ is the average velocity of the neutron density n_{th}. The conventional fluence is simply the foil reaction rate divided by the product of the number of nuclei and the effective 2200 m.s.$^{-1}$ neutron capture cross-section

$$n_{th}v_o = \frac{(Do - Do_{Cd} F_{Cd}) A}{0.001 F N_o g \sigma_o} \qquad (1)$$

Where Do is the reaction rate (equal to the saturation disintegration rate) in the bare foil per milligram of foil, Do_{Cd} is the reaction rate per milligram of the cadmium covered foil, A is the atomic weight of the foil, N_o is the Avogadro constant, σ_o is the thermal neutron capture cross section of energy E_o, F is a correction for thermal neutron self shielding in the foil, and g is the Westcott correction factor for cross section resonances in the thermal Maxwellian energy region.

The cadmium ratio is given by

$$R_{Cd} = Do/Do_{Cd} = \frac{(F/r(T_m/T_o)^{\frac{1}{2}} + Gs_o/g)}{f_\delta G(s_o/g - W) + 1/K_\delta} \qquad (2)$$

Where r is the Westcott epithermal flux parameter which is related to the fraction f of the total neutron density n which comprises the Maxwellian part of the spectrum:

$$r = f(\pi\mu)^{\frac{1}{2}}/4. \qquad (3)$$

If T_m is unknown the quantity derived from the cadium ratio measurement is $r(T_m/T_o)^{\frac{1}{2}}$. s_o is the normalised reduced resonance activation integral I' (integrated in a 1/E shaped flux, 1/v component subtracted),

$$s_o = (4/\pi)^{\frac{1}{2}} I'/\sigma_o. \qquad (4)$$

G is the correction for resonance self shielding, f_δ represents the attenuation of the resonance neutrons in cadmium of thickness δ, W is a correction which is necessary when part of the first resonance extends below E_{Cd}. K_δ is related to E_{Cd} by the equation

$$K_\delta = (\pi E_{Cd}/E_o)^{\frac{1}{2}}/4 \qquad (5)$$

K_δ is tabulated in reference (3).

The essential information derived from the foil measurements is thus $n_{th} v_o$ and $r\left[T_m/T_o\right]^{\frac{1}{2}}$, from which the total conventional fluence nv_o may be derived.

$$nv_o = n_{th} v_o R/(R-1) \qquad (6)$$

Where R is the cadmium ratio of a pure '1/v' absorber, given by $K/r(T_m/T_o)^{\frac{1}{2}}$. The two components of conventional fluence are then given by

$$n_m v_o = nv_o (1 - 4r/(\pi\mu)^{\frac{1}{2}}) \qquad (7)$$

$$n_e v_o = nv_o \, 4r(\pi\mu)^{\frac{1}{2}} \qquad (8)$$

where n_m and n_e are the Maxwellian and epithermal neutron densities.

These conventional fluences have to be converted to true fluences by multiplying by the appropriate $\bar{v}/v_o$.

For the Maxwellian part, $\bar{v}/v_o$ is given by $(4T_m/\pi T_o)^{\frac{1}{2}}$

For the epithermal part

$$n_e\bar{v} = c\int_{\mu E_o T_m/T_o}^{E_s} dE/E \text{ and}$$

$$n_e v_o = c\int_{\mu E_o T_m/T_o}^{E_s} (E_o/E)^{\frac{1}{2}} \, dE/E \qquad (9)$$

where c is the normalisation constant. From which

$$\bar{v}/v_o = \frac{\ln(E_s) - \ln(\mu E_o T_m/T_o)}{2E_o((\mu E_o T_m/T_o)^{-\frac{1}{2}} - E_s^{-\frac{1}{2}})} \qquad (10)$$

Neglecting $E_s^{-\frac{1}{2}}$ and dividing by the lethargy:-

$$n_e\bar{v} \text{ (per unit lethargy)} = nv_o(4/\pi)^{\frac{1}{2}} r(T_m/T_o)^{\frac{1}{2}} \quad (11)$$

Hence the total true fluence is given by

$$n\bar{v} = nv_o (4T_m/\pi T_o)^{\frac{1}{2}}\left[(1 - 4r(\pi\mu)^{-\frac{1}{2}}) + r\sum_i u_i\right] \quad (12)$$

where the u_i are appropriate lethargy intervals from $\mu E_o\, T_m/T_o$ to E_{Cd}.

The response of the j^{th} sphere in this fluence is given by

$$nv_o(4T_m/\pi T_o)^{\frac{1}{2}}\left[(1 - 4r(\pi\mu)^{-\frac{1}{2}}\varepsilon_{\text{thermal, j}} + r\sum_i u_i\, \varepsilon_{ij}\right] \quad (13)$$

Similarly the dose-equivalent or tissue kerma are given by

$$nv_o(4T_m/\pi T_o)^{\frac{1}{2}}\left[(1 - 4r(\pi\mu)^{-\frac{1}{2}}\, DF_{\text{thermal}} + r\sum_i u_i\, DF_i\right] \quad (14)$$

where DF_i are the appropriate fluence-dose conversion factors.

β-Particle Counting

Because of the low foil activities achieved, the foils were counted in a low background anticoincidence counter rather than in a $4\pi\beta\gamma$ coincidence counter. It is therefore necessary to ensure that the correct β counting efficiency is used to convert observed counting rates to absolute disentegration rates. Each of the foils used was activated in a standard thermal neutron flux and then counted by $4\pi\beta\gamma$ coincidence to determine the appropriate β-counting efficiencies ε_β.

A cadmium covered foil is activated by resonance neutrons which are rapidly attenuated in the foil so that the activity is confined to a thin surface layer. The counting efficiency $\varepsilon_{\beta,Cd}$, for a foil activated under cadmium is thus higher than the counting efficiency $\varepsilon_{\beta,\text{thermal}}$, appropriate to thermal neutron activation whereby the activity is produced more uniformly throughout the foil thickness. The efficiency $\varepsilon_{\beta,\text{ bare}}$ for a foil irradiated bare is thus a cadmium ratio-dependent weighted combination of $\varepsilon_{\beta,\text{thermal}}$ and $\varepsilon_{\beta,Cd}$.

If $\varepsilon_{\beta,bare,s}$ and $\varepsilon_{\beta,Cd,s}$ are the efficiencies determined from coincidence measurements following the irradiation of bare and cadmium covered foils in a standard flux which produces a cadmium ratio R_s, then the bare foil efficiency $\varepsilon_{\beta,bare,u}$ appropriate to an unknown field which produces a cadmium ratio R_u is given by

$$\varepsilon_{\beta,bare,u} = \varepsilon_{\beta,bare,s}(1-\alpha_s(1-R_s/R_u)/(R_s-1)) \quad (15)$$

where $1 + \alpha_s = \varepsilon_{\beta,Cd,s}/\varepsilon_{\beta,bare,s}$.

In the interpretation of the measurements of the foils in polyethylene spheres the appropriate R_u's were determined from the $r(T_m/T_o)^{\frac{1}{2}}$ data of appendix 1 and equation (2).

NBS SP 554 (1979)

SURVEY OF EUROPEAN MEASUREMENTS ON PHOTONEUTRON PRODUCTION FROM ELECTRON ACCELERATORS USED FOR MEDICAL PURPOSES

E J Axton and A G Bardell

National Physical Laboratory
Teddington, Middlesex

Brief details are presented of European work on problems associated with neutron production from electron accelerators used for medical purposes. For completeness, the earlier references which have already received citation in the literature have been included.

(Dose-equivalent, Electrons, Kerma, Multispheres, Photons, Photoneutrons, Radiotherapy, Spectrometry)

Compared with current activities in the United States the European effort in this field is rather limited. The material described below is the result of a search which may not have been completely exhaustive. Earlier references which have already received citation in the literature have been included for completeness.

In what follows, quoted neutron dose or dose-equivalent rates have been normalised to a central axis X-ray dose of one rad unless otherwise stated.

Frost and Michel[1] considered the total incremental dose-equivalent due to photoneutron production in the accelerator as well as all photonuclear reactions produced in the patient including the production of photoprotons. A total contribution of 0.1 rem was obtained for a 34MV bremstrahlung spectrum.

Pohlit[2] used Indium probes in a paraffin moderator to obtain the incremental dose-equivalent to the patient from neutrons generated externally. For a 35 MV betatron he derived a central axis dose-equivalent of 2.5 mrem, which fell to 1.0 mrem at a distance of 50 cm from the axis.

Kretschko, Liesen, Pohlit, Rase and Sewkor[3] carried out a comprehensive survey of the X-ray and neutron radiation levels associated with eight accelerators ranging in energy from 15 MeV to 100 MeV. The distribution of stray X-radiation was found to be dependent on the accelerator construction. Neutron levels were surveyed with a boron trifluoride counter surrounded by a double moderator. The distribution of fast neutrons is determined by the shape and dimensions of the the therapy room. The measurements provide a useful guide to the optimum design of the therapy room.

Lofgren and Spring[4] used a system of fission track etching in glass, having calibrated it with an AmBe neutron source, to determine the in-beam neutron dose-equivalent for a 32 MV betatron. The very low neutron rates observed are usually discounted in the literature (eg [5]).

The work of Kushelevsky and Shani[6] has already been mentioned in an accompanying paper[7]. They used the photon spectral data of Johns et al[8], with cross section data from the IAEA compilation[9], to calculate the neutron production per gram for a number of elements as a function of accelerator energy. The results are confirmed by those of reference[7]. They went on to calculate the total number of neutrons produced in two neutron detectors:- a NE 213 liquid scintillator detector and an 8 inch diameter spherical rem-meter. In each case they estimated that about 10^8 neutrons would be produced in a nominal exposure of 100 rontgens at 24 MV. Subsequent comparisons with the number of neutrons striking the instruments from the outside are in error[7].

Stranden[10] used indium probes surrounded by a 7.5 cm wax moderator as a fast neutron detector in order to estimate in-beam and out-of-beam neutron dose rates from a 45 MV betatron operated in the X-ray mode. He obtained 4.2 mrem in the beam and 2.0 mrem out of the beam. As an example of the consequences of these results, he estimated that a patient receiving a dose to the thorax of 200 rad would experience a gonad dose of between 0.05 and 0.1 rad from scattered photons, and a dose-equivalent of 0.4 rem from neutrons. In an earlier paper[11] he considered the whole body dose to the patient as a result of the activation of O,N,P,K and Cl in the patient. These activities are produced partly by reactions involving photoneutrons and partly by direct photonuclear reactions with the elements concerned. The dose due to reaction products, for example photoprotons, was not included. Stranden concluded that a patient would receive a whole body dose of 16 μrad as a result of the radioactivity produced by a 45 MV X-ray accelerator.

Asard[12] used an Anderson Braun (Studsvick) rem meter, consisting of a boron trifluoride counter in a hydrogeonous moderator, to measure

neutron dose rates in the control room of a Siemens 17 MV betatron. The dose-equivalent rate was found to be acceptably low, the highest level recorded being 0.2 mrem.h^{-1} for an in-beam dose rate of 27 rad.min.$^{-1}$. In a later paper from the same laboratory, (the Karolinska Institutet, Stockholm) Brahme[13] considers the therapeutic merits of mixed photon and neutron beams from a 50 MV Microtron. Photoneutron converters of uranium or lead are placed near the X-ray target to produce a combined X-ray and neutron beam for patient treatment. Depth dose curves are presented for photoneutrons from U and from Pb as well as for the photon beam.

Eipper and Manegold[14] measured neutron dose rates from the 42 MV betatron at the Koln-Merheim Radiation Clinic. They used two neutron detectors, a boron trifluoride counter in a double moderator, and an AEC neutron monitor ELM 714 LMS. Measurements were made in out-of-beam positions in the treatment room, and through the entrance maze to the control room door. A dose-equivalent rate of 0.6 mrem.h^{-1} was observed at the control room entrance to the maze for an X-ray exposure of 100 rontgen.min.$^{-1}$. It was concluded that no additional shielding would be required, such as a paraffin inlay to the door, to reduce the neutron levels in the control room.

Ulso and Christensen[15] criticised the 'often claimed' statement that a sufficient shielding for the X-rays from a medium energy electron accelerator should also be sufficient to reduce the potential neutron contamination in the control room to an acceptable level. In an experimental study, a neutron dose rate meter 2202D (Studsvick Atomenergy AB Sweden), consisting of a boron trifluoride counter inside a moderator, was used to monitor neutron dose rates at the entrance to the maze leading to a SL75/20 linear accelerator. The monitor was gated to exclude the PRF pulses from the accelerator. Additional measurements were made with nuclear track emulsions which have a sensitivity threshold of 0.7 MeV for neutrons. Initially the neutron dose-equivalent rate was 800 mrem.h^{-1} for a primary X-ray dose rate of 240Gy.h^{-1} (24000 rad.h^{-1}). The neutron rate was reduced to less than 2.5 mrem.h^{-1} by reducing by a factor of 2.4 the area of the entrance door, by adding an additional 10 cm thick borated paraffin door, and by lining parts of the walls and ceiling of the treatment room with 5 cm of borated paraffin.

Vialettes, Cariou, Duffar, Mesples, Quechon, and Rousson[16] surveyed the neutron and photon radiation levels in out of beam positions in the treatment room of the 25 MeV Saggitaire linear accelerator installed at the Henri Mondor Hospital at Creteil, France. Enriched ^{7}LiF thermoluminescent samples were used for the photon measurements. Neutron levels were surveyed with indium activation foils in a paraffin moderator. The ^{32}S(n,p) reaction was also used for neutrons above the 2 MeV threshold for this reaction. The results are presented in the form of isodose curves which show that the neutron and photon contributions to the total leakage dose-equivalent are approximately equal. The contribution of thermal neutrons is very small.

Drouet, Moreau, Quechon, and Tabot[17] of the Radiation Protection Service at Saclay performed similar measurements on an 18 MeV Saturne accelerator and reached similar conclusions.

Gunther[18] reported the isodose distribution of neutron radiation from the 17 MV betatron at the Radiation Clinic of the University of Dusseldorf. At the time of writing it has not been possible to obtain copies of the last reference for comment.

Conclusions. Only one in beam neutron measurement is reported in this survey, and it is in general agreement with our own measurements. Conclusions drawn from out-of-beam surveys are sometimes contradictory, see for example references 14 and 15. It is not clear without further study whether this is due to differences in measurement techniques or to physical differences in the installations surveyed.

References

1 Incremental Dose Value Due to Neutrons in Therapy with Fast Electrons and with Ultra-hard X-rays. D. Frost and L. Michel Strahlentherapie 124, 321-350 (1964).

2 The Measurement of Neutron Radiation from a 35 MV betatron. W. Pohlit, Strahlentherapie, 113, 469-473 (1960).

3 Radiation Protection Measurements on Different European Betatron Installations. J.Kretschko, H. Liesen, W. Pohlit, S. Rase and A. Sewkor. Fortschritte auf dem Gebiete der Rontgen-strahlen und der Nuklearmedizin, 95, 565-572 (1961).

4 Neutron Radiation Produced by the 32 MV Rontgen Beam of a Medical Betatron. K.E. Lofgren and E.Spring. Acta.Radiol. 9, 247-256 (1970).

5 Fast Neutrons from a 25 MV Betatron. J.G. Fox and J.D. McAllister. Medical Physics, 4, 387-396 (1977).

6 Photoneutron Production in Detectors in High Energy X-ray Beams. A.P. Kushelevsky and G.Shani. Nuclear Instruments and Methods 137, 71-73 (1976).

7 Neutron Production from Electron Accelerators used for Medical Purposes. E.J. Axton and A.G. Bardell. This Conference. (1979).

8 Gamma-Neutron Cross Sections. H.E. Johns, L. Katz, R.A. Douglas and R.N.A. Haslam, Phys. Rev. 80, 1062-1068 (1950).

9 Handbook on Nuclear Activation Cross Sections. Tech. Report Series No.156. IAEA Vienna (1974).

10 Neutron Doses to Patients by High Energy X-ray Therapy. E. Stranden. Phys.Med.Biol. 22, 1011-1013 (1977).

11 Activity Induced in Patients by High Energy X-ray Therapy. E. Stranden, Phys.Med.Biol. 22, 348-352 (1977).

12 Radiation Protection Measurements for a 17 MV Betatron. P.E. Asard, Acta. Radiol. 7, 59-70 (1968).

13 Photoneutron Beams for Radiotherapy Produced by a 50 MV Microtron. A. Brahme, Private Communication (1979), to be presented at the Radiation Research Congress in Tokyo (1979).

14 Neutron Radiation from a Betatron. H.H. Eipper and K. Manegold. Strahlentherapie, 140, 286-290 (1970).

15 Neutron Contamination at a 20 MV Linear Accelerator. N. Ulso and J.M. Christensen. Arhus Kommunehospital, 8000 Arhus. C. Denmark. Private Communication (1979).

16 Measurements Performed on the Sagittaire Accelerator at the Centre Henri Mondor. H. Vialettes, J. M. Cariou, M. Duffar, D. Mesples, H. Quechon and J. Rousson. Report SPR/S/72-853 GRA/121 HV/nw. 20 June 1972.

17 Measurements Performed on the Therac 20 Saturne Accelerator. J. Drouet, J. C. Moreau, H. Quechon, and L. Tabot. Report D.CEN-S/SPR/SRI/77-507 GRA-092 JD/sg. (1977).

18 Neutron Dosimetry with a 17 MV Betatron. D. Gunther. Strahlentherapie, 151, 333-337 (1976).

NEUTRON LEAKAGE FROM CURRENT MACHINES

Peter R. Almond
The University of Texas System Cancer Center
M. D. Anderson Hospital and Tumor Institute
Houston, Texas 77030

A survey has been made of published, and unpublished reports during the last ten years, of neutron leakage measurements around medical linear accelerators. The review involved seventeen different studies involving fourteen different types of machines, six betatrons and eight linear accelerators with measurements reported on twenty-eight different machines. It was found that as the energy increases, the neutron leakage increases and is a maximum at around 25 MV and then remains constant. The target appears to be the main source of neutrons. In a treatment room, the neutrons can be identified as fast primary neutrons, fast scattered neutrons from the walls and a constant background of thermal neutrons. The neutron dose in the photon beam is approximately four times higher than 50cm from the beam edge. At greater distances, the neutron dose becomes constant. Due to the large number of variables in the different reports, it is possible to draw definite conclusions. It is recommended that standards be established for neutron leakage measurements.

(Betatrons; detectors; dosimetry; leakage; linear accelerators; neutrons)

Introduction

This paper will be an attempt to survey both published and unpublished measurements of neutron leakage for radiotherapy machines operating in the photon, mode that are currently in use, and to see if any pattern can be found with regard to machine energy, target material, measuring techniques, etc. Such a review would be impossible without the cooperation of many people and I am indebted to the various companies and individuals who sent me material to review. Table I lists the sources of information and, in general, the data has been restricted to measurements reported after 1970.

Variables

In order to compare the data from the different sources, some attempt has to be made to summarize all the variables involved and to reduce the data to a common form. The basic variables in this problem can be listed as follows:

i. The treatment machines including energy, target material, flattening filter and collimator material.

ii. Measuring devices, calibration, and calculation techniques.

iii. Experimental set up and measuring conditions.

iv. Presentation of the data.

v. Treatment room information.

Table II lists the various machines that were considered in this report. Included is target and flattening material and collimator material. It should be pointed out, however, that in many of the published papers, this information was not included.

Table III lists the measuring devices used and their means of calibration and conversion factors. McCall [1] has pointed out the problems that are often encountered with the use of the various detectors. These are:

i. Reported neutron doses are too high because of unsuspected and unaccounted for high energy photon response of detectors.

ii. For fluence detectors errors in the efficiences of the dectors can arise because of incorrect assumptions regarding the neutron spectrum.

iii. For dose-equivalent detectors errors in the efficiences of the dectors can arise because of incorrect assumptions regarding the neutron spectrum.

iv. Spectral errors will also cause incorrect results when fluence is converted to dose-equivalent.

Often the experimental set-up is not adequately described, but when it is described, it is apparent that no standard experimental conditions have been followed. Table IV lists the experimental conditions that have been reported.

Table V gives the various ways in which the data is presented, again no standard form has been used.

And, finally, very few of the reports give information about the treatment room and the relationship between accelerators, detectors, and wall. When this information has been included, it is indicated in Table IV.

Table I

1. Deye and Young: "Neutron Production from a 10 MV Medical Linac", Phys. Med. Biol., 1977, Vol. 22, p. 90. [2]

2. 17. 19. McGinley, Wood, Mills, and Rodriguez: "Dose levels due to neutrons in the vicinity of high-energy medical accelerators", Medical Physics, 1976, Vol. 3, p. 397. [3]

3. McCall Associates: Neutron Measurements on 3 Mevatron XX Linear Accelerators, 1977 & 1978, Supplied by Volker Stieber Manager, Development, Siemens.

4. Gur, Bukovitz, and Gill: "Fast and Slow neutrons in an 18-MV photon beam from a Philips SL/75-20 linear accelerator", Medical Physics, 1978, Vol. 5, p. 221. [4]

5. 6. 7. Gur, Bukovitz, Rosen and Holmes: "Relative Measurements of fast neutron contamination in 18 MV Photon Beams from two linear accelerators and a betatron", Abstract Medical Physics, 1978, Vol. 5, p. 350, [5] Text supplied by Bukovitz.

8. 12. Fox and McAllister: "Fast neutrons from a 25 MeV betatron", Medical Physics, 1977, Vol. 4, p. 387. [6]

9. Drouet, Moreau, Quechon and Tabot: "Summary of Measurements Taken around a CGR/MeV Saturne Accelerator at Buc", C.E.A. C.E.N. Saclay, Department of Radiation Protection Section of Installations. Accelerator Group, May 1977, obtained from AECL and CGR-MeV.

10. Grant: "Neutron Leakage for Therac 20" Memorandum to Radiation Safety Officer, M. D. Anderson Hospital, July, 1978.

11. 13. Wilenzick, Almond, Oliver, de Almeida: "Measurement of Fast Neutrons Produced by High-Energy X-Ray Beams of Medical Electron Accelerators", Phys. Med. Biol., 1973, Vol. 18, p. 396. [7]

14. Holman, Price, Friedman, and Nath: "Neutron spectral measurements in an intense photon field associated with a high-energy x-ray radiotherapy machine, Medical Physics, 1977, Vol. 4, p. 508. [8]

15. Marbach: "Neutron Leakage from the Sagitaire Linear Accelerator at the University of Indiana at Indianapolis", June, 1975, AECL Report obtained from J. Marbach.

16. Price, Nath and Holeman: "Fast and thermal neutron profits for a 25-MV x-ray beam", Medical Physics, 1978, Vol. 5, p. 285. [9]

18. Axton and Bardell: "Neutron Production from Electron Accelerators used for Medical Purposes", Phys. Med. Biol., 1972, Vol. 17, p. 293. [10]

20. Lofgren and Spring: "Neutron Radiation by the 32 MeV Roentgen Beam of a Medical Betatron", Acta Radiologica, 1970, Vol. 9, p. 247.

21. Stranden: "Neutron Doses to Patients in High Energy X-Ray Therapy", Phys. Med. Biol., 1977, Vol. 22, 1011.

22. Oliver: "Fast neutron contamination in x-ray beams of medical accelerators from 19 to 45 MV," Abstract Phys. Med. Biol., Vol. 19, 1974. Revised 1976 data supplied by Oliver [20]

23. LaRiviere: "Summary neutron leakage numbers for the Varian machines." Data supplied by Philip D. LaRiviere of Varian.

Note on the numbers: The initial numbers in the table above can be used as a key to correlate all the Tables I through V, e.g. the number 15 refers to the report by Marbach in all tables, and the figures.

Table II

Machines

	Machine	Energy MeV	Target mm	Filter	Collimator	Photon dose rate
1.	Varian Clinac 18	10	Cu	W		200 rad min^{-1}
2.	Varian Clinac 18	10	Cu 6.3	W	W	100 rad min^{-1}
[1]3.	Siemens Mevatron XX	14	--	--	--	300 rad min^{-1}
4.	Philips SL/75-20*	18	W	W alloy	W alloy	280 rad min^{-1}
5.	Siemens Mevatron XX	18	Pt	Fe	W alloy	300 rad min^{-1}
6.	Schimadzu Betatron+	18	Pt	Pb	W alloy	50 rad min^{-1}
7.	Philips SL/75-70*	18	W	W alloy	W alloy	300 rad min^{-1}
8.	Schimadzu Betatron+	18	Pt	Pb		
9.	CGR-MeV Saturne	18	W4			400 rad min^{-1}
10.	AECL Therac 20	18	W	Pb	W alloy	400 rad min^{-1}
[2]11.	Siemens Betatron	19	--	--	--	75 rad min^{-1}
12.	Schimadzu Betatron+	23	Pt 2	Pb	W alloy	
[3]13.	Sagittaire Linear Acc.	25				400 rad min^{-1}
14.	Sagittaire Linear Acc.	25				400 rad min^{-1}
15.	Sagittaire Linear Acc.	25				400 rad min^{-1}
16.	Sagittaire Linear Acc.	25	W	Pb		450 rad min^{-1}
17.	Allis Chalmers Betatron	25	Pt 1.6	Al	Pb	100 rad min^{-1}
18.	Brown Boveri Betatron	33	--	--	--	35 rad min^{-1}
19.	BBC Betatron	45	Pt 2.0	Pb	Pb and W	100 rad min^{-1}
20.	Asklepitron	32	--	--	--	--
21.	Betatron (make unknown)	Not stated	Pt	--	--	--
22.	Data for these machines included in Table VI.					
23.	Varian Clinac 18 at 10 MV and Clinac 20 at 15 MV and 10 MV.					

*

\+ Same Machines

[1]) Target, Filter and Collimator data same as (5).

[2]) Target is Pt. Filter and Collimator are Pb.

[3]) Target is W Filter and Collimator Pb same for (14) (15) and (16).

Table III

List of Detectors

1. 5.1cm diam Rh-activation counter - calibration (ncm^{-2} $counts^{-1}$) by standard ^{252}Cf neutron sources at Naval Research Laboratory. Conversion from neutron fluence to dose by $3.0 \pm .1 \times 10^{-9}$ rad $n^{-1}cm^{-2}$ Q.F. = 10.
2. 17. 19. Fast neutrons, bare indium foil in H_2O moderator - calibration with ^{252}Cf source. Fluence converted to absorbed dose in muscle by 3.97×10^{-9} cm^2 rad/n. Thermal neutrons, bare indium foils and cadmium covered indium foils with H_2O moderator. Calibrated with a moderated Pu-Be source. Fluence converted to absorbed dose in muscle by $4.57 \times 10^{-10} cm^2$ rad/n.
3. Bare and moderated gold foils. Neutron fluence measured and results interpreted as dose equivalent based on results from Monte Carlo [13] calculation for each particular room, i.e. factor for converting fluence to dose equivalent individually calculated but averaged about 7.9×10^7 n/cm^2 per rem.
4. Aluminum and indium foils and cadmium covered indium foils to check 'so called "slow neutrons"' Same technique as 8 and 12. Fast neutron fluence converted to Fast-neutron dose by 3.1×10^{-9} rad cm^2/n and slow neutron fluence by 4.5×10^{-10} rad cm^2/n.
5. 6. 7. Aluminum foils same as 4.
8. Aluminum foils Photon sensitivity taken into account. Conversion factor of 3.1×10^{-9} rad/per unit fluence for target neutrons and 3.2×10^{-9} rad/per unit fluence for lead neutrons.
9. Indium foils in 5 cm paraffin moderator covered with cadmium. Combination of this activation foils Cu, Au, Mg, and S in box covered with cadmium and Cu. Equivalent energy is derived and equivalent dose per neutron fluence is found for this energy. 7.7×10^{-9} rem n^{-1} cm^2 at 1 meter and 5.2×10^{-9} rem n^{-1} cm^2 at 2 meter.
10. Silicon diodes calibrated with Cf-252 same as 11 and 13.
11. 13. Silicon diodes and fission fragment track detectors - Lexan using depleted U foil. Diodes calibrated by ORNL Health Physics Research Reactor and ^{252}Cf. Track detectors calibrated by ^{252}Cf. Conversion from fluence to dose by $3.0 \pm 0.1 \times 10^{-9}$ rad n^{-1} cm^2. Photo fission correction applied to track detector. No correction for diode data*. Q.F. = 10.
14. Bonner multisphere spectrometer using ^6LiF and ^7LiF thermoluminescent dosimeter. Also bare and cadmium covered chips. Maximum dose and dose-equivalent conversion factors from ERDA Health and Safety Lab [15] - applied to each energy group and summed yielding total neutron dose equivalent. Q.F. varied from 8.2 to 6.6.
15. Silicon diodes same as 11 and 13. Q.F. = 10.
16. Activation Detectors using P_2O_5 31P (np) Si for fast neutron and 31P ($n\gamma$) 32p for slow neutrons. Neutron spectrum was constructed from data in literature and for every energy group in the assumed spectrum, max dose equivalent conversion factors from ICRP 21 were used. [16] Photon sensitivity range was 1.7% to 3.8%.
18. Gold foils in two polythene sphere 20cm and 25cm diam sphere calibrated at 2 neutron energies using the Li(p.n.) at NPL. Energy of neutrons were estimated. Conversion to rem by 20 n $cm^{-2}s^{-1}$ for 2.5 m rem h^{-1} from NCRP 38. [17]
20. Solid-state track detector - glass with uranium oxide incorporated into it. Calibrated again An-Be source. Conversions factor of 7.66×10^{-9} rem(n/cm^2) Q.F. = 7.4.
21. Indium foils and Indium foils surrounded by paraffin and cadmium used to measure total flux of fast neutrons ^{12}C and ^{64}Zn and ^{56}Fe to study energy distribution. Dose equivalent obtained from spectral information and NCRP 38 data. [17]
22. Silicon Diode.
23. Moderated Indium foil calibrated against PuBe Source.

*In a subsequent report by McCall [14], et al, silicon diodes were shown to be unsuitable for use in the photon beam.

Table IV

Experimental Conditions

1. Room layout. 25cm cube polystyrene phantom 100TSD, 25cm x 25cm field, detector 100cm from edge of phantom away from gantry in patient plan. Photon dose rate 200 rad min^{-1} Data behind phantom.
2. 17. 19. Room layout. 10cm x 10cm field. Measurement in beam at standard TSD's (100cm for Clinac 18 and Allis Chalmers Betatron, 110cm for BBC betatron and 5cm from edge of beam (direction unknown). Photon dose rate approximately 100 rad/min.
3. Room layout. 20cm x 20cm field. Measurements in patient plane at isocenter and 50cm and 100cm from isocenter left and right and toward and away from gantry. Some data taken with jaws closed. Measurements in target plane at 100cm. Beam stopper retracted. Photon dose rate 300 rad/min.
4. No room layout. 5cm x 5cm, 10cm x 10cm and 20cm x 20cm field sizes. Detectors inside and outside of (5cm from edge) beam at target to foil distance of 100cm. Photon dose rate of 280 rad/min.
5. 6. 7. No room layout. 10cm x 10cm field. In center of beam only, at 100cm. Dose rate 300 rad/min for linear accelerators and 50 rad/min for betatron.
8. 2. No room layout. Different field sizes 10x10, 20x20, mainly no phantom data some phantom data. With and without flattening filter, in beam and outside beam at 5cm and 20cm, TSD 100cm.
9. No room layout. 15cm x 15cm field made in patient plane 100cm from target around circles with radii of 1 and 2 meter and on a sphere of radius 1 meter centered on target. No in beam data. Photon dose rate of 400 rad/min^{-1}.

10. No room layout. 10cm x 10cm field with phantom. Measurements made in patient plane at 100cm on circles of radii .5m 1m 1.5m and 2m. No in beam data.

11. 13. No room layout. For sagittaire 10cm x 10cm and 30cm x 30cm. In beam and out of beam data out to 60cm, toward and away from gantry. In patient plane at 1m. Photon dose rate 400 rad min^{-1}. For Siemens 7.6cm x 11.4cm field. In beam and out of beam data out to 50cm, toward and away from gantry. In patient plane at 60cm. Photon dose rate 75 rad min^{-1}.

14. Room layout. 10cm x 10cm field. No in beam data, measurements in plane of patient (105cm) at 0.5, 1.0, 2.0 and 4.8cm from beam axis. Photon dose rate 400 rad min^{-1}. No phantom.

15. No room layout. 10cm x 10cm field. Diodes in plane of patient (100cm) out of beam on circle of radii 1m and 2m. Photon dose rate 400 rad min^{-1}.

16. No room layout. 5cm x 5cm, 10cm x 10cm, 20cm x 20cm, and 30cm x 30cm. Detectors in patient plane at 105cm. In beam and out of beam data out to 50cm. No phantom. Photon dose rate varied approximately 400 to 480 rad min^{-1}.

18. No room layout. Little experiment information. Photon dose rate was 35 rad min^{-1}. In beam and out of beam data.

20. Room layout. 10cm x 10cm field at TSD 80cm. Measurements in beam and out of beam-up to 7cm.

21. No room layout. Experimental conditions not known. In primary beam and 50cm and 100cm outside the beam.

22. See Table VI.

23. Clinac 18 measurements at 3 locations 1 meter from target, collimator closed. Clinac 20 measurement in patient plane at periphery of the beam and at 1 meter from target. Collimators closed.

Table V

Data Presentation

1. Flux density (n cm^{-2} s^{-1}) and Fluence per rad (n cm^{-2} rad^{-1}). Tabular

2. 17. 19. Fast-neutron fluence per rad photons (n/cm^2 rad). Fast-neutron dose per rad photons. Slow-neutron fluence per rad photons (n/cm^2 rad). Slow-neutron dose per rad photons accuracy of ±20%. Tabular

3. Fast-neutron mrem/photon rad at isocenter. Various components given such as "Direct". "From Walls" all corrected to 1 meter from isocenter. Leakage at 1m (mrem/photon rad). "Direct" "Fast-Scattered" "Thermal" and "Total". Uncertainties given 14%. Average energy (MeV) Including thermals and excluding thermals. Tabular

4. Fast neutrons/cm^2/rad of x-ray. Fast-neutron dose in rad/rad of x-ray Slow neutrons/cm^2/rad of x-ray and Slow-neutron dose in rad/rad of x-ray. Tabular

5. 6. 7. Relative neutron contamination inside primary beam only. Overall accuracies, ±40% listed. Numerical

8. 12. Neutron fluence per rad of x-rays (neutrons cm^{-2} rad^{-1}). Graphical and Tabular

9. Dose equivalent due to neutrons in mrem/1000 rads. Diagramatic

10. Neutron rad and percentages of total photon dose. Diagramatic

11. 13. Neutron dose as percentage of central axis dose and as Neutron fluence (n cm^{-2} rad^{-1}) graphical and tabular. Experimental uncertainties shown for dose percentage data.

14. Neutron dose rates rad/min for slow, fast total and in rem/min for slow fast and total with derived Q.F. at each point. Tabular and graphical

15. Neutron dose in rad and rem dose as % of photon dose. Tabular

16. Fast neutron flux n/cm^2-sec. Thermal-neutron fluxes n/cm^2-sec and Dose Equivalent Rate rem/min for both Fast and Slow. Graphical

18. Neutron flux for 1 rad min^{-1} of photon. Neutron dose-equivalent (in mrem min^{-1} and Neutron dose-equivalent divided by x-ray dose. Uncertainties ± 30%. Tabular

20. Neutron fluence (n/cm^2)/R and mrem/R. Diagramatic, numerical.

21. Total fluence ncm^{-2} per rad of x-ray dose and dose equivalent (DE) mrem per rad of x-ray dose. Tabular

22. See Table VI.

23. Data presented as n/cm^2 rad and as rem/rad %.

Table VI

Intercomparison of Beam Characteristics and Associated Leakage Neutron Dose of High Energy Betatrons and Linacs

All fields are 10x10 cm except the Siemens 42 which is a 9x9 cm cone and the Siemens 200A which is a 7.6x11.4 cm cone. The neutron dose is measured beyond 10cm outside the edge of the open field, past the beam penumbra.

Model	Manufacturer	Photon Energy	Neutron Dose	SSD	Target Material Dimensions		Flattening Filter Material Dimensions		Collimator Material	d_{max}	$d_{50\%}$
		MVp	% of Photon Dose	cm		mm		mm		cm	cm
Clinac 35	Varian Assoc.	8	0.00001	100	Tungsten Copper	0.51 5.1	Type Metal*	Cone 19. high +0.8 base x 76. dia. base	Tungsten	2.0	17.0
Clinac 18	Varian Assoc.	10	0.0063±49%	100	Copper	6.6	Tungsten	16.1 high +3.2 base x63. dia base	Tungsten	2.1	17.6
LMR-15	Toshiba Intl. Corp.	14	0.0098±26%	100	Tungsten Brass		Lead		Tungsten Heavy Alloy	19.5	27.
Mevatron XX	Applied Rad. Co. (Siemens Corp)	15	0.012±30%	100	Stainless St. Water Platinum Copper	0.03 0.17 0.36 8.9	Copper	Cone 33. high x25. diam. base	Lead	3.0	17.
Clinac 35 S.N1-3	Varian Assoc.	25	0.059±12%	100	Tungsten Copper	5.08 3.81	90% Tungsten 6% Copper 4% Nickel	Cone 19 high + 0.8 base x76. dia. base	Tungsten	3.5	22.
A.C.25 RTM	Allis Chalmers (A.T.C.Inc.)	25	0.22±57%	100	Platinum	1.6	Aluminum Δ	Double Cone total dim. 29.5 high x68.2 dia. base	Lead	4.5	24.
Asklepitron 35	Brown Boveri	32	< 0.0001	100	Platinum	1.5	Lead Gamma 3		Lead	4.5	24.
Siemens 400A	Siemens-Reiniger Werke AG	42	0.035±20%	100	Platinum	0.3	Lead Filter No. 2		Tungsten	4.2	24.
Asklepitron 45	Brown Boveri	45	0.21±100%	110	Platinum	2.0	Lead	Cone	Lead Ring + Lead with inner face of tungsten	6.0	28.

* Alloy comprised of 85% lead, 10% antimony, 5% tin

Δ Commercially pure aluminum, AASTM B211

Review of the Studies

From Table I it can be seen that 17 different studies were considered. Of these, twelve had been reported in the literature, ten as papers and two as abstracts. Four of the studies were done for the manufacturers and one report was of a survey done for state health department requirements. Twelve of the reports have appeared in the last three years so that most of the data represents the latest work done in this area.

Machines

Data has been collected for 14 different types of machines (8 linear accelerators and 6 betatrons) with measurements reported on 28 individual machines. All of the betatrons had platinum (Pt) targets and lead (Pb) flattening filters except the Allis Chalmers which uses an aluminum (Al) flattening filter. All of the linear accelerators used tungsten (W) targets except the Mevatron XX which uses Pt and the Clinac 18 which uses copper (Cu). The flattening filters were W except for the Therac 20 - Saturne and Sagittaire which use Pb. In almost all cases W was used as a collimator material except for the Allis Chalmers which used Pb. Photon dose rates for the linear accelerators were high 300-400 rad min^{-1} and low, upto 100 rad min^{-1}, for the betatrons.

Detectors

Of the 17 studies, 11 used activation techniques with indium foils being the most common, followed by gold and aluminum. The latest technique is to use phosphorus pentoxide to measure both the fast and slow neutron component and it has a low photon sensitivity. There were four studies using silicon diodes which, because of their response to high energy photons, cannot be used directly in the photon beam.

Two studies used solid-state track detectors. One set of results gave such low results that it must be questioned.[11] The other set of data agreed well with the silicon diodes when photo fission effects were accounted for. One group used thermoluminescent dosimeters. It is quite apparent that the best results can be obtained if a measurement or accurate estimate of the neutron spectrum can be made and the appropriate conversion factors to dose or dose equivalence factor is calculated for each spectrum.

Data Presentation

The information presented in Table V is as it is presented in the papers. The data is presented in many ways using different units, these include, flux, flux density, fluence per photon rad, neutron dose rates in rad/min, neutron dose in rad per photon rad, neutron dose as percent of photon dose, equivalent ratio, dose equivalent per photon rad and dose equivalent as a percent of photon dose. Some of the units are used correctly according to ICRU 19 [18] whereas some are not.

Discussion

Review of all the data in a comprehensive way is difficult because different detectors were used with different experiment arrangements, the data was presented differently and conversions factors varied. Some factors were obtained by detailed calculations while others were taken from the literature.

However, certain conclusions can be drawn that are important to this subject.

1) That the target is the main source of the neutrons. By target is meant the x-ray target and surrounding non-moveable collimators.

2) Throughout the treatment room there will be a constant background of thermal neutrons representing about 3% of the fast neutron dose.

3) McCall[1] has shown that the fast neutrons can be divided into a direct component and a component scattered from the walls. The scattered component accounts for approximately 25% of the total dose.

4) The neutron dose becomes fairly constant at 30 to 50 cm from the beam edge. The "in-beam" data is 4 to 5 times higher than this value. At 5cm which is often reported, the neutron dose ratio "in-beam" to "out-beam" is 2 to 3.

In Figure 1 an attempt has been made to summarize the data for measurements made out of the beam. Where possible the data at distances greater than 30cm from the beam edge is plotted since this tends to represent a uniform dose levels. However, some data are only available for 5cm from the beam edge. The data plotted is the neutron rad dose as a percentage of the photon dose in the main beam. In all cases this number was obtained from the various papers using data and conversion factor contained in the papers, except for two points where Q.F.'s were used that were consistent with Q.F. used by other authors for the same energy range. Also plotted on this figure are the data from Swanson [19] for the yield of neutrons as a function of incident electron energy for Au & W targets. The curves were normalized to the neutron yield measured for the 10 MV x-rays.

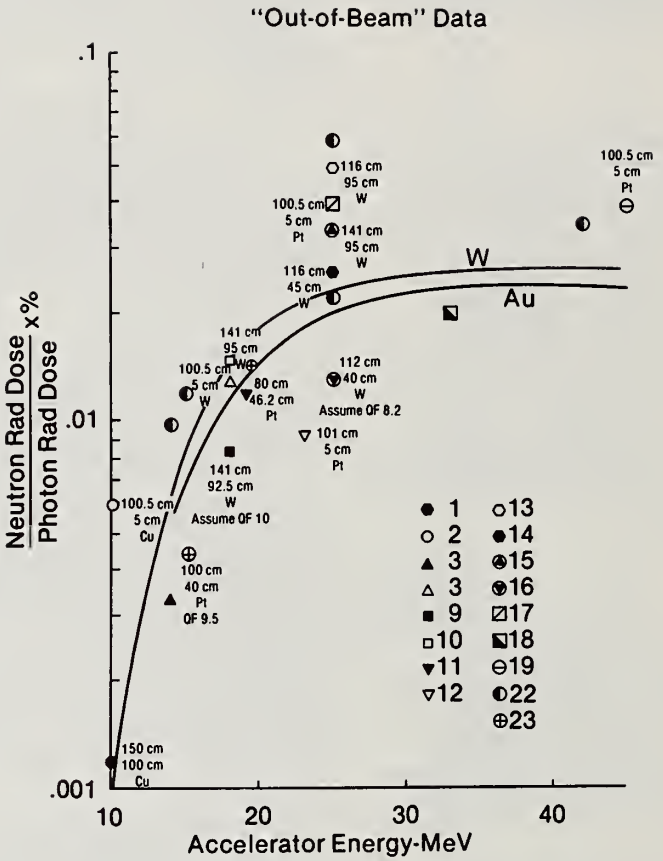

Figure 1 "Out-of-Beam" Data. The data points are keyed to the numbers in Tables 1 through V. By each data point the target detector distance is given, the distance of the detector from beam edge, target material and, if necessary, assumed or derived Q.F. Also plotted is the data from Swanson [9] on neutron yields from Au & W.

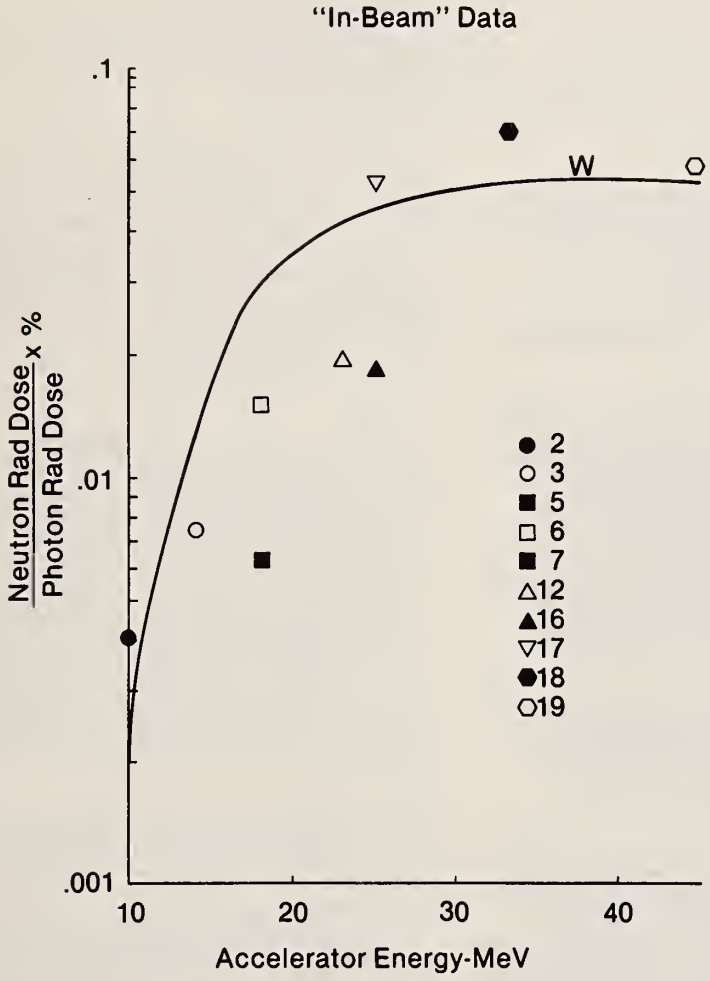

Figure 2 "In-beam" data, only the W curve is shown.

Although there is quite a wide spread in the data some definite trends can be seen.

1) Below 20 MeV the neutron yields drops off rapidly with decreasing photon energy. This agrees with the measurements that McCall made on the Siemens Mevatron XX where he noted a drop in neutron dose by 4 in going from 18 MeV to 14 MeV and supplied by LaRiviere from the Clinac 20 operated at 15 MV and 19 MV.

2) There appears to be no difference between betatrons and linear accelerators.

3) The percentages neutron dose reaches maximum at around 25 MV x-rays and then remains relatively constant with energy.

This last fact has great significance since 25 MV x-rays have been used clinically for 30 years so that there should be a large amount of clinical data available to determine if the neutrons have had an adverse effect on the patients, and if there is a time delay before late effects show up it should also be apparent in the clinical data.

In 1974 Oliver [20] measured the fast neutron contamination in x-ray beams of medical electron accelerators from 19 to 45 MV. This was updated in 1976 and the data is shown in Table VI, excluding the points for the Sagittaire linear accelerator and Siemens betatron reported above. The data was obtained with diode detectors and is plotted on Figure 1 for comparison. This data is consistent with the previous data and shows the slightly higher values usually obtained with the diodes.

Figure 2 is the data for in beam measurements. As expected, it shows exactly the same trend as the out of beam data except the neutron dose levels are several factors higher.

Conclusions

It is very apparent from doing this study that some form of standardization is required for neutron leakage measurements. Just as dose calibration procedures have been standardized in terms of equipment, technique, experimental set up and dose calculations, so the same approach must be applied to this problem.

These standards should include as a minimum:

1) Type of detector.
2) Calibration procedures and conversion factor.
3) Experimental set-up.
4) Data presentation

and some form for handling the data. The 'cookbook' approach suggested by McCall [1] might well be a good starting point for this. Recently recommendations were made to the NCRP [21] that this subject should receive their consideration and it is hopeful that in the not too distant future guidelines and protocols will be available.

References

1. McCall, R.C., T.M. Jenkins and R.A. Shore: "Transport of Accelerator Produced Neutrons in a Concrete Room", SLAC-PUB-2214, Oct., 1978.
2. McGinley, Wood, Mills, and Rodriguez: "Dose levels due to neutrons in the vicinity of high-energy medical accelerators", Medical Physics 1976, Vol. 3, p. 397.
3. McCall Associates: Neutron Measurements on 3 Mevatron XX Linear Accelerators, 1977 & 1978, Supplied by Volker Stieber Manager, Development, Siemens.
4. Gur, Bukovitz, and Gill: "Fast and Slow neutrons in an 18-MV photon beam from a Philips SL/75-20 linear accelerator", Medical Physics, 1978, Vol. 5, p. 221.
5. 6. 7. Gur, Bukovitz, Rosen and Holmes: "Relative Measurements of fast neutron contamination in 18 MV Photon Beams from two linear accelerators and a betatron", Abstract Medical Physics, 1978, Vol. 5, p. 350, Text supplied by Bukovitz.
8. 12. Fox and McAllister: "Fast neutrons from a 25 MeV betatron", Medical Physics, 1977, Vol. 4, p. 387.
9. Drout, Moreau, Quechon and Tabot: "Summary of Measurements Taken around a CGR/MeV Saturne Accelerator at Buc", C.E.A. C.E.N. Saclay, Department of Radiation Protection Section of Installations. Accelerator Group, May 1977, obtained from AECL and CGR-MeV.
11. Wilenzick, Almond, Oliver, de Almeida: "Measurement of Fast Neutrons Produced by High-Energy X-Ray Beams of Medical Electron Accelerators", Phys. Med. Biol., 1973, Vol. 18, p. 396.
13. Straker, E.A., P.N. Stevens, D.C. Irving, and V.R. Cain: "The MORSE Code - A Multigroup Neutron and Gamma Ray Monte Carlo Transport Code", Oak Ridge National Laboratory, ORNL-CFN-70-2-31, 1970.
14. McCall, R.C., T.M. Jenkins, and G.D. Oliver, Jr.: "Photon Response of Silicon Diode Neutron Detectors", Stanford Linear Accelerator Publ., Stanford, SLAC-PUB-1783.
15. Weinstein, M.S., K. O'Brien, and F. Hajnal, "Procedures for Estimating the Errors in Neutron Spectra from Bonner Multisphere Measurements", HASL, Rep. No. TM-69-4, 1969.
16. Int. Comm. Radiol. Protect. (ICRP) Publ. 21, 1971.
17. National Council on Radiation Protection and Measurements (NCRP), Rep. No. 31, 1964.
18. International Commission on Radiation Units and Measurements (ICRU) Report No. 19, July, 1971.
19. Swanson, W.P.: "Calculation of Neutron Yields Released by Electrons Incident on Selected Materials", Health Physics, Vol. 35, 1978, p. 353-367.
20. Oliver, G.D., Jr.: "Fast neutron contamination in X-ray beams of medical electron accelerators from 19 to 45 MV, Phys. Med. Biol., Vol. 19, 1974.
21. Almond, P.R., J.R. Cameron, M. Ehrlich, A.C. Lucas, R.H. Thomas, J.E. Turner, B.A. Glass: Report to the National Council on Radiation Protection and Measurements, Sept. 12, 1978.

DESIGN CRITERIA FOR PHOTON BEAM EXITS ON HIGH ENERGY MEDICAL ACCELERATORS TO MINIMIZE NEUTRON PRODUCTION

Leonhard Taumann
Siemens Medical Laboratories, Inc.
2404 N. Main Street
Walnut Creek, CA 94596

The major components of the photon beam exit of a medical linear accelerator are discussed from the viewpoint of beam quality and neutron production. It is pointed out that the optimization of the beam quality also leads to a minimum in the neutron production.

(Photon beam exit, beam quality, neutron production)

Introduction

From the viewpoint of reliability and beam quality the design of the X-ray exit for medical linear accelerators should fulfill several main requirements.

1. The major components affecting the design should be uncomplicated and easy to manufacture. Long assembly times caused by complicated alignment procedures should be avoided. Parts which have to be removed for beam testing should be easily ajustable from outside the head.

2. The required RF-power for the specified beam energy and dose rate should be as low as possible.

3. From the users viewpoint the most important aspect is the beam quality which can essentially be determined by two considerations.

   a. The energy distribution over the whole possible radiation volume should be as uniform as possible and the variation insignificant for different field sizes.

   b. The ratio between the tumor dose and the total delivered dose should be as high as possible. This also demands a low level of that kind of secondary radiation which can contribute to the total dose as whole body dose.

For linear accelerators with photon energies higher than 10 MV the neutron production has become of major concern as secondary radiation.

The magnitude of the RBE-factor which has to be applied for this kind of low level radiation is still in discussion. Recommended numbers are changing within a factor of hundred.

It is the intention to demonstrate that the optimization of the beam quality also leads to a minimum in the neutron production.

Performance of the major components of the beam-exit.

Fig. 1 shows the principal arrangement of the major components of the photon beam exit. These are the target, the beam stopper, the flattening filter, and the fixed and movable beam collimators.

Fig. 1

MEVATRON 20, Upper Defining Head, X-Ray Exit

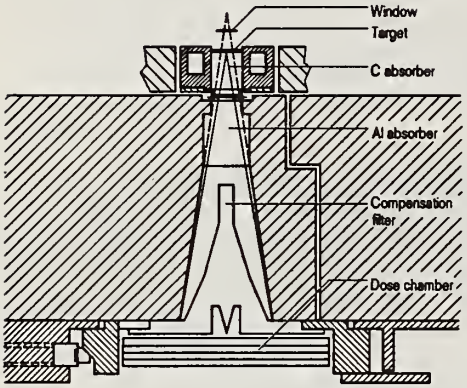

1. The Target.

Since there was no conclusive answer in the literature for the right target material for a 15 MV photon beam, central axis depth dose curves were measured for the different target materials and target thicknesses. These curves allow sufficient relative comparison of the energy spectrum produced in the target.

No significant difference in the central axis depth dose curves could be found between targets with high and low atomic charge number. No change in the beam quality could also be found for targets with ticknesses between .015 radiation length and .4 radiation length.

Fig. 2 shows the depth dose curve for a rather thin aluminium-target and a thicker tungsten target. Fig. 3 shows three depth dose curves - one written over the other - for three tungsten targets with thicknesses of .071 RL, .143 RL, and .214 RL.

As can be seen in Fig. 4 the half value angle of the photon distribution in the forward direction changes only slightly with the target thickness, approaching assymptoticly a maximum angle.

The half value angle for aluminum is considerably smaller and also the total output about 20% lower. Comparing the same flattened field size the aluminum target would require about 50% more beam current than the tungsten target.

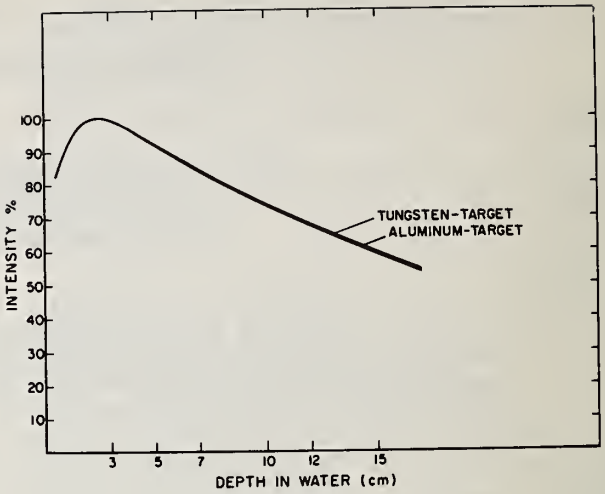

FIGURE 2

Central Axis Depth Dose Curves for 15 MV X-Rays and Different Target Materials

SSD: 100 cm, Field Size: 10 x 10 cm^2
Iron Absorber behind the targets
Target: Tungsten .214 RL
Aluminum .05 RL

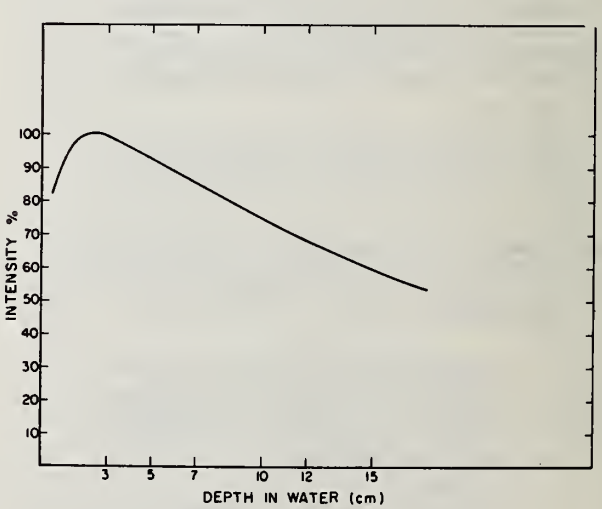

FIGURE 3

Central Axis Depth Dose Curves for 15 MV X-Rays and Different Target Thicknesses

SSD: 100 cm, Field Size: 10 x 10 cm^2
Iron Absorber behind the target
Target: Tungsten; thickness .071 RL
.143 RL
.214 RL

Thus a thin tungsten target of a thickness of about .2 radiation length appears to be the best choice. It can be shown later that the neutron production in such a thin target is almost negligible compared with other major neutron sources in the defining head.

2. The beam absorber.

The accelerated electrons lose about one fifth of their energy in the target by collision. In order to absorb them completely a beam absorber has to be situated behind the target. This absorber has four different tasks:

a. Absorb the electrons
b. Harden the beam
c. Produce a minimum of x-rays
d. Produce a minimum of neutrons

It is obvious that low z-material is the best choice. The space which is left in the target slide behind the target is therefore filled with a solid graphite plug. Since the electrons are not absorbed completely in the carbon, the beam absorber area is extended into the primary collimator. For mechanical stability an aluminum plug has been chosen instead of carbon. This aluminum plug also absorbs low energy radiation which is produced in the wall of the primary collimator by Compton Scattering.

Due to its low atomic number, the neutron production in the electron beam absorber is minimal.

3. The flattening filter.

For low neutron production and sufficient beam hardening material with a low atomic number has to be considered.

Fig. 5 shows three central axis depth dose curves:

a. One has been measured for a .214 RL thick tungsten target with a piece of iron-acting as beam absorber - behind the target.

b. The other curve has been measured for the same target absorber arrangement. In addition a piece of lead with the thickness of one inch has been placed behind the iron in order to simulate the beam hardening effect of a lead flattening filter.

c. The third curve shows a central axis depth dose curve for the same target absorber arrangement but the lead has been replaced by a piece of carbon of the same thickness.

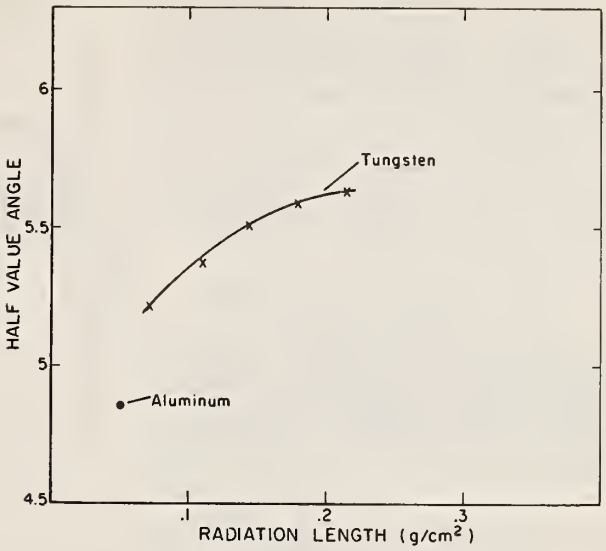

FIGURE 4

Half Value Angle of a 15 MV X-Ray Beam as Function of the Target Thickness
Target: Tungsten; thickness .0714 RL
.107 RL
.143 RL
.178 RL
.214 RL

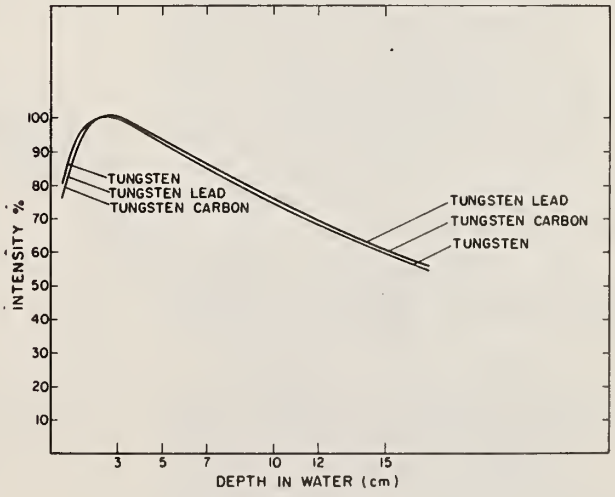

FIGURE 5

Central Axis Depth Curves for 15 MV X-Rays and Different Beam Hardener

SSD: 100 cm, Field Size: 10 x 10 cm²
Target: Tungsten, .214 RL thick
For beam hardening: lead block 1 inch thick
carbon block 1 inch thick

It can be seen that the lead filter is still hardening the beam spectrum but the hardening effect of a low z-material of the same effective thickness is considerably higher.

The length of an aluminum flattening filter which has to flatten a field size of 35 cm x 35 cm of a 15 MV photon beam is about 5.3 inches. There is just not enough space in the defining head for such a flattening filter. Also the shape of this filter is so steep that extremely small mechanical movements would considerably affect the symmetry of the dose distribution for small field sizes. So the best compromise for the choice of the material of the flattening filter is stainless steel.

Due to its shape the compensation filter is hardening the photon beam in the central axis considerably more than outside the central axis. In order to find out how this effect changes the energy distribution over the whole radiation volume central axis depth dose curves have been measured with and without flattening filter for different field sizes. (Fig. 6 and Fig. 7).

There is no significant shift of the maximum of the depth dose curves for both sets of curves. The change of the dose at 10 cm depth as a function of the field size with and without flattening filter is of the same amount. The hardening effect of the flattening filter is compensated by the influence of the larger effective field sizes. In the area close to the surface the favorable influence of the flattening filter can clearly be seen for the 5 cm x 5 cm and 10 cm x 10 cm field.

If the medium photon energy is degraded by photons which are scattered at the moveable collimators a measurable change in the central axis depth dose performance for different special collimator openings should be seen. A 5 cm x 5 cm depth dose curve has been compared against a curve of a 5 cm x 35 cm field with the collimator pair which is close to the focus is opened to 35 cm and the collimator pair which is at a larger distance from the focus is closed to 5 cm. Another pair of curves has been measured with the opposite arrangment of the collimator pairs. (Fig. 8 and Fig. 9). No measurable difference could be seen.

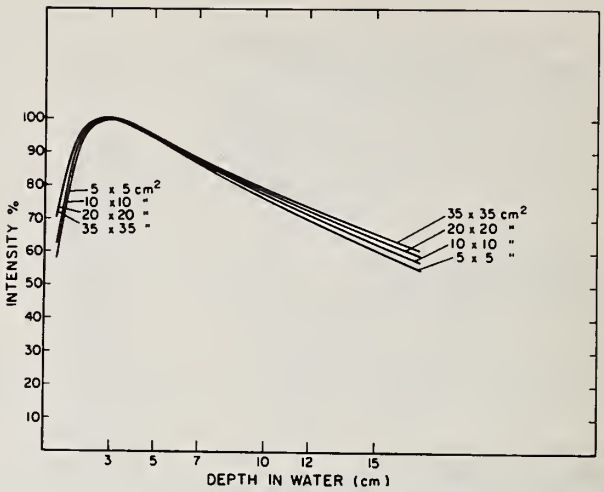

FIGURE 6

Central Axis Depth Curves for 15 MV X-Rays as Function of the Collimator Opening

SSD: 100 cm, Field Sizes: 5 x 5 cm^2
10 x 10 cm^2
20 x 20 cm^2
35 x 35 cm^2

Target, Electron Absorber and Compensation Filter Arrangement according to Figure 1

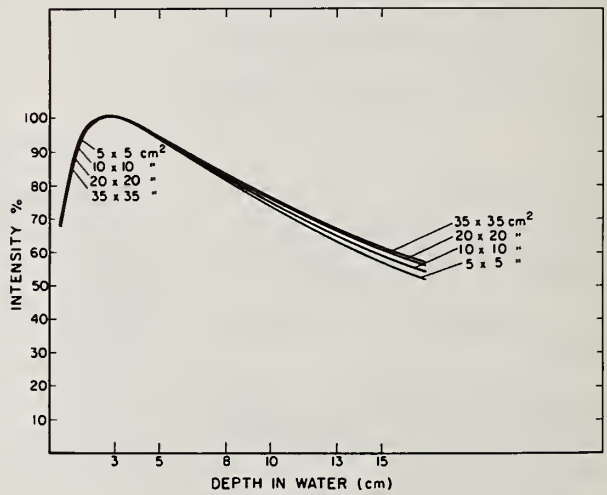

FIGURE 7

Central Axis Depth Dose Curves for 15 MV X-Rays as Function of the Collimator Opening

SSD: 100 cm, Field Sizes: 5 x 5 cm^2
10 x 10 cm^2
20 x 20 cm^2
35 x 35 cm^2

Without Compensation Filter
Target and Electron Absorber Arrangement according to Figure 1

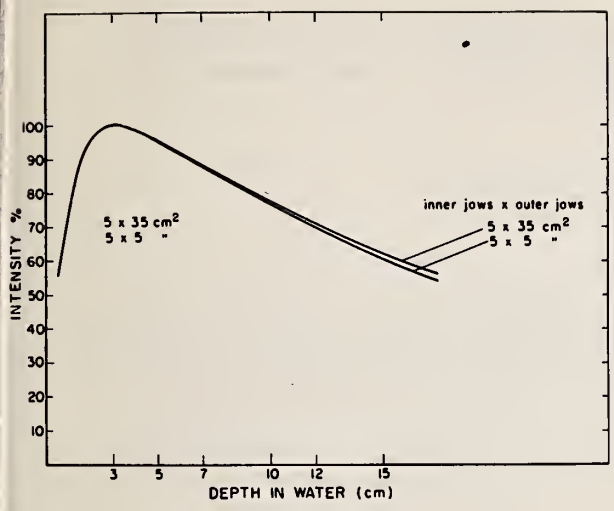

FIGURE 8

Central Axis Depth Dose Curves for 15 MV X-Rays as Function of Different Collimator Openings

SSD: 100 cm, Field Sizes:
5 x 5 cm^2 (inner jaws x outer jaws)
5 x 35 cm^2 (inner jaws x outer jaws)
X-Ray Exit according to Figure 1

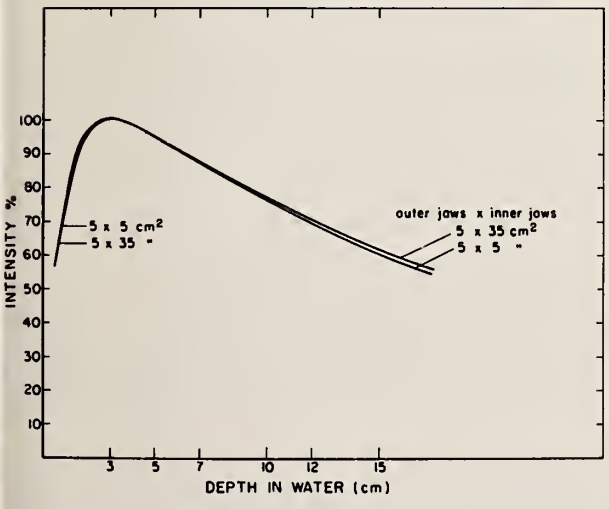

FIGURE 9

Central Axis Depth Dose Curves for 15 MV X-Rays as Function of Different Collimator Openings

SSD: 100 cm, Field Sizes:
5 x 5 cm^2 (outer jaws x inner jaws)
5 x 35 cm^2 (outer jaws x inner jaws)
X-Ray Exit according to Figure 1

The results are summerized in Table I. The carbon-aluminum absorber has the highest influence on the surface dose. This low z-material gives the thin tungsten target the chance to perform as a real target. The beam hardening effect of the stainless steel flattening filter can be seen over the whole depth. But the change in the energy distribution is within tolerable limits.

The neutron-production

1. The overall neutron production for the 15 MV photon beam of the Mevatron 20 is about .25 mrem per photon rad. No significant deviation could be found for all machines installed. The neutron distribution around the defining head is more or less isotrophic.

In order to find out how much the target contributes to the whole neutron production, measurements were done for three different target thicknesses. The extrapolation against zero target thickness shows that the neutron production in the target is in the order of only about 5%.

How much does the beam absorber and flattening filter contribute to the neutron production? Only 20% of the total photon intensity produced in the target is spread in the forward direction into the solid angle covered by the usefull beam. Considering the lower atomic number and the additional distance of the flattening filter from the focal spot the neutron production is insignificant.

Almost 95% of all the neutrons are produced in the shielding device of the head which is mainly tungsten. The neutron yield for tungsten in the energy range of 15 MV changes rapidly with energy.

Fig. 10 shows the relation between the bending magnet current and the electron energies at the exit window. These

electron energies were determined by measuring the extrapolated ranges. According to this curve the electron energy applied at the target is 13.9 MeV for producing a relative central axis depth dose of 77.5% at 10 cm depth for a field size 10 cm x 10 cm.

An increase of the electron energy of only one MEV would cause a higher neutron flux of a factor of about 1.7. Since also the medium energy of the neutrons penetrating the head is higher, another 20% has to be added to the dose equivalent.

Table: 1

Relative Central Axis Depth Dose Curve Numbers for Different Target- Beamabsorber- Compensation Filter Arrangements and Collimator Openings.

	Depth in Water (cm)											
	1				10				15			
	Field size (cm^2)				field size (cm^2)				Field size (cm^2)			
	5×5	10×10	20×20	35×35	5×5	10×10	20×20	35×35	5×5	10×10	20×20	35×35
Tungsten Target with Iron Absorber		91.3%				74.6%				59.7%		
Aluminium Target with Iron Absorber		91.6%				73.8%				59%		
Tungsten Target with Carbon-Aluminium Absorber	82.1%	83.4%	85.4%	86%	73.2%	74.8%	75.8%	76.5%	57.1%	59.5%	60.8%	61.6%
Tungsten Target with Iron Absorber + 1 inch Lead		88%				75.4%				60.9%		
Tungsten Target with Carbon-Aluminium Absorber and Iron Compensation Filter	76%	80%	85%	85.7%	76%	77.4%	78.4%	79.4%	60.5%	62.7%	64.4%	66%

This means that in this photon energy range one MeV change in the electron energy hitting the target is changing the neutron production within a factor of two. Therefore, an optimal beam hardening can considerably minimize the total neutron production.

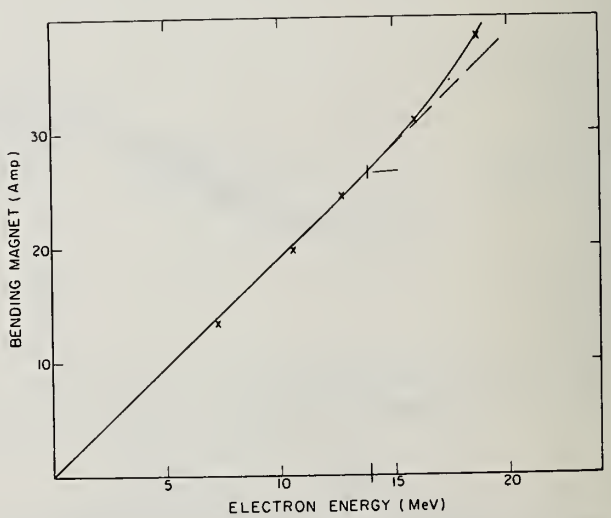

FIGURE 10

Electron Energy as a Function of the Bending Magnet Current

NEUTRON LEAKAGE CHARACTERISTICS RELATED TO ROOM SHIELDING

E. Tochilin

and

P. D. LaRiviere
Varian Associates, Inc.
Palo Alto, CA 94303

ABSTRACT

A systematic study of neutron leakage rates has been made over a range of x-ray energies 10-19 MeV in one of Varian's test cells. Leakage was evaluated at one meter and in the patient plane. Measurements were presented of neutron and gamma ray leakage in the concrete test cell, together with door shielding calculations. The information allows scaling of neutron leakage to other size rooms and x-ray energies extending to 25 MV. The neutron activation of concrete and its contribution to treatment room dose was investigated. Gamma rays from radiative capture in concrete and their influence on leakage through the exit door were also examined.

INTRODUCTION

Within the past few years considerable progress has been made in understanding the modifying effects of x-ray shielding material on the photoneutron spectrum from high energy medical accelerators. The mean energy of leakage neutrons is considerably lower than the values reported in some of the earlier literature. This leads to a lower rem dose and less neutron shielding material for the treatment room.

A considerable amount of neutron leakage data has been compiled at Varian on neutron leakage from a generic class of medical accelerators operating a x-ray energies from 10 MV to 19 MV. These include experimental measurements of neutron leakage vs. energy, both within and outside the patient plane, the average energy of leakage neutrons, radiation leakage at the entrance door to the treatment room, and room activation.

The broad objectives of the work reported here were to elucidate the mechanisms of neutron generation, shielding and interactions with the test cell environment so that machine design could be improved, and the production of capture and residual gamma radiation reduced in the most economical fashion.

Two accelerators were used in this study; namely, the Clinacs ® 18 and 20. The Clinac 18 produces a beam of electrons ranging in energy from 6 MeV to 18 MeV and a photon beam at 10 MV. The Clinac 20 produces electrons ranging from 6 MeV to 20 MeV and a single photon beam either at 15 MV (standard) or at 18 MV (optional). A systematic study of neutron leakage was also made with the photon beam energy increased to 19 MV. All measurements were made with the beam flattened to meet medical treatment specifications. Unless otherwise specified, the movable collimators were closed in order to eliminate neutron contamination from the primary beam.

The Clinac 20 medical accelerator is an upgraded version of the Clinac 18. One major modification has been the design of a new more efficient standing wave accelerator waveguide to allow the production of higher electron energies. Accelerator waveguides for both the 15 or 18 MV versions are approximately the same size.

By positioning the Clinacs at exactly the same location in the same cell we were able to determine the relative neutron leakage of 10, 15, 18 and 19 MV x rays under identical geometric conditions. The neutron leakage accompanying 25 MV x rays produced by the Clinac 35 in another test cell is also included.

INSTRUMENTATION

Two neutron detectors were used; namely, a neutron flux detector and a rem counter. Fast neutron flux inside the room was determined by measuring the activation of indium foils placed in the center of a cylindrical polyethylene shield 6.25 in. in diameter and 6.25 in. high. A cadmium outer cover surrounded the polyethylene moderator and absorbed any incident thermal neutrons. The detector measures neutron flux approximately independent of energy in the range from 20 keV to 10 MeV (1). The rem detector consisted of an Andersson-Braun counter (2) with a scaler readout and was used to measure neutron dose equivalent rate. Use of this instrument was primarily confined to leakage measurements at the door and within the maze leading into the test cell. A comparison between the neutron flux and rem detectors was also made in the room. In this case the rem counter readings were corrected for counting losses produced by the pulsed beam. Both neutron detectors were calibrated with a Pu-Be neutron source. Thermal neutron fluences were estimated with bare indium foils, but the results are not reported here because the dose equivalents were generally negligible.

X-ray leakage measurements were determined

by multiple dosimeters which included a pancake-type ionization chamber with a window area of 100 cm^2 and Keithley electrometer, LiF TLD dosimeters, Landsverk 2R ionization chamber dosimeters and Kodak Type AA 14x17 in. Ready Pack radiographic film. The Type AA film, ion chambers and TLD dosimeters were all calibrated against the 100 cm^2 ion chamber which was calibrated directly in the primary x-ray beam. Exposures were made on a one meter arc positioned around the Clinacs. The 14 in. x 17 in. film was sandwiched between two sheets of plastic each 0.10 in. thick. The outside of each plastic sheet contained a 1 in. x 2 in. lead strip 0.030" thick, duplicating the conditions used to calibrate the films. Two TLD dosimeters and two 2R ionization chambers were attached to the back plastic sheet next to the lead strips comprising the film dosimeter. This arrangement allowed 3 independent measurements of leakage radiation at each location, together with information on the possible existence of any significant gradients over the area of the film pack. The 100 cm^2 chamber was routinely affixed to a marked location on the back of the arc, thereby facilitating comparison of film and ion chamber readings.

The one meter arc allows simulataneous positioning of the films at a distance of one meter from the target as shown in Figure 1. The arc swings in azimuth about a vertical axis coincident with the central axis of the x-ray target.

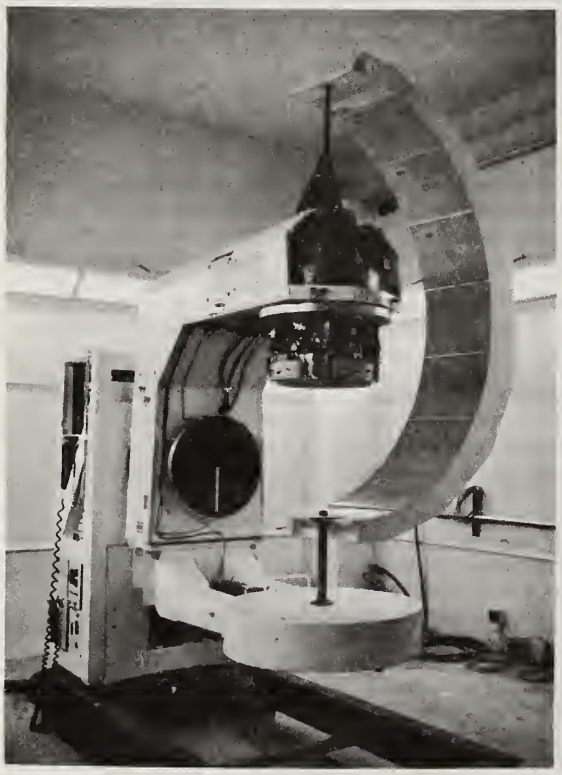

Fig. 1. The one meter arc mounted on the Clinac 6X.

The arc is swung in angular increments of 25^0 for each exposure, until virtually 4π coverage is obtained. The aximuth angles requisite for complete coverage are shown schematically in Figure 2, along with the vertical layout of the films.

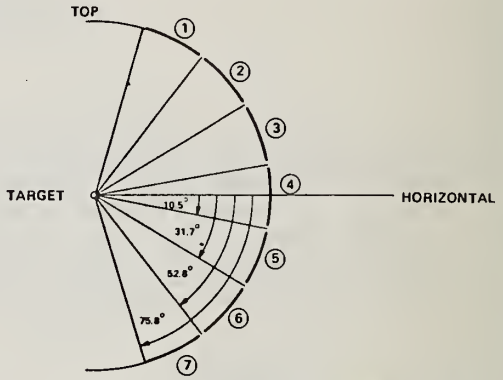

A. FILM LAYOUT ALONG ARC, VERTICAL PLANE. FILM NUMBERS IN CIRCLES.

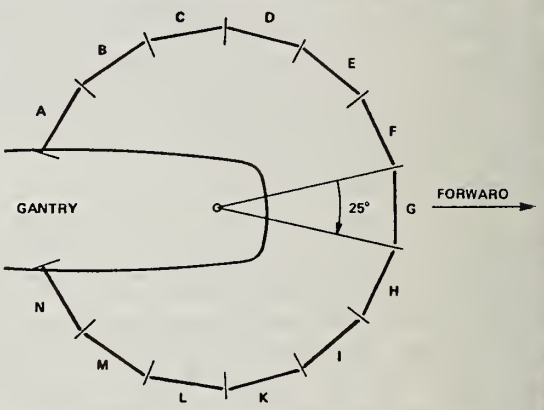

B. ARC POSITIONS, HORIZONTAL PLANE THROUGH TARGET – PLAN VIEW

Fig. 2. Arc positions and film locations on the one meter arc.

A horizontal angle of about 40^0 is excluded by the gantry, but supplementary measurements can be made in the patient plane and at the rear of the stand to close most of this excluded area. Calibration of the three dosimeters with ^{60}Co gamma rays have yielded consistent results for leakage radiation over an x-ray range of from 2 to 10 MV within $\pm$ 15%.

Neutron leakage can also be measured on the meter arc by securing the flux detectors at various locations. Because of their large physical size the flux detectors do not allow a high degree of spatial resolution. This requirement is less important for neutrons than for x rays since the neutron distribution is approximately isotropic.

LEAKAGE NEUTRON SPECTRA

The photoneutron spectrum has frequently been reported in the literature to closely resemble fission neutrons. While this approximation generally applies to the primary spectrum, inelastic scattering in the shielding material surrounding the target, normally lead and tungsten, results in a significant degradation of neutron energy. McCall et al. (3) have calculated the neutron leakage spectrum of photoneutrons from 15 MV photons, when shielded with tungsten. Figure 3 from their paper shows the integral spectra for a bare source and from one surrounded by a 4 in. thick tungsten shield placed in the center of a concrete room. A comparison is made with the ^{252}Cf fission neutron spectrum. The figure clearly shows that the fission spectrum is a poor approximation for leakage neutrons from a medical accelerator. The figure further illustrates the difficulties involved when threshold detectors are used to evaluate neutron leakage dose under these conditions, since most of them are completely insensitive to neutrons below 2 MeV.

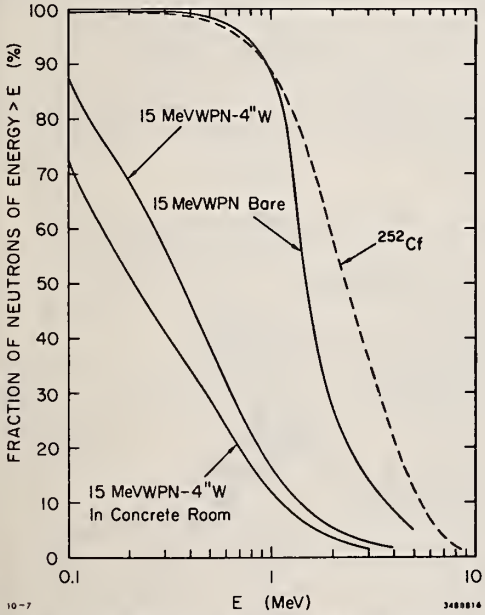

Fig. 3. Comparison of various neutron integral spectra: ^{252}Cf, 15 MeVWPN-Bare, 15 MeVWPN-4"W, 15 MeVWPN-4"W in a concrete room.

McCall has determined average neutron energies of 0.45 MeV and 0.64 MeV for 15 MV and 25 MV photoneutrons, respectively, degraded by transmission through 4 in. of tungsten shielding. He defines an effective neutron energy, E_{eff}, as the energy of a monoenergetic neutron beam which would have the same conversion factor from fluence to dose equivalent as the spectrum with an average energy, $\bar{E}$. It turns out, for calculations covering a wide range of typical conditions, that $E_{eff} = 0.59\ \bar{E}$.

Thus for 15 MV x rays from the Clinac 20, $E_{eff} = 0.27$ MeV, and the conversion factor derived from Figure 14 of ICRP Publication 15 and 21, (4) is 8×10^7 n cm^{-2} rem^{-1}. For 25 MV x rays, $E_{eff} = 0.38$ MeV and the factor is 6.2×10^7 n cm^{-2} rem^{-1}.

An independent check on the average photoneutron leakage energy was obtained from absorption curves in polyethylene. For these measurements, indium foil detectors were centrally interposed in a stack of 0.25 in. thick square polyethylene sheets 16 in. on a side. The surface of the stack, which was approximately 7 in. deep, was centered on the beam axis at the isocenter, and the jaws were adjusted as desired. The thermal activation of the foils, once equilibrium conditions are met, is proportional to the fast neutron fluence, thereby providing a convenient method of measuring fast neutron attenuation.

Energy calibration was obtained by reference to a family of curves obtained with monoenergetic neutrons from a 2 MeV positive ion accelerator utilizing the T $(p,n)^3$He and D $(d,n)^3$He nuclear reactions (5). Thermal neutron distributions with indium were obtained in a 15 in. diameter polyethylene cylinder for neutron energies ranging from 0.25 to 5.1 MeV. These curves are shown in Figure 4. Two trends are observed: first, the depth at which maximum thermalization occurs increases progressively with neutron energy; and, second, the slope in the descending region decreases exponentially with increasing energy.

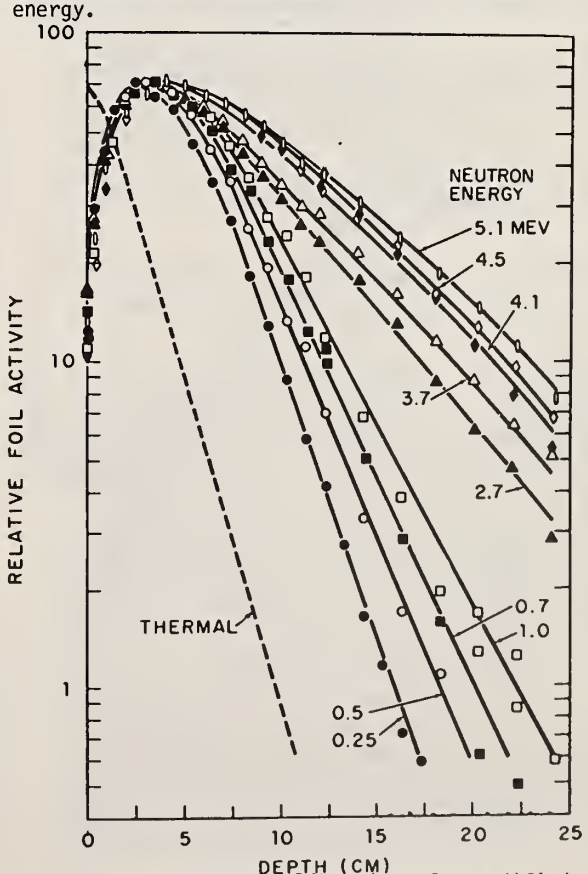

Fig. 4. Energy calibration of a modified long counter by indium foil activation.

ergy; and, second, the slope in the descending region decreases exponentially with increasing energy.

For the closed jaw condition, the average energy of the neutron leakage through the 6 in. of tungsten of the Clinac 20 was determined to be 0.37 MeV. This value is consistent with the average energy obtained by Monte Carlo calculations of 15 MV x-ray photoneutrons through 4 in. of tungsten, which was 0.45 MeV. The experiment was repeated with 15 MV photons. Within experimental error, the indium activation curves were identical to those obtained with 10 MV photons, indicating essentially no change in leakage neutron energy through tungsten for photoneutrons produced at the two energies.

The same measurements made in the primary 10 MV photon beam, for jaws open to a field size of 20 cm x 20 cm, gave an average neutron energy of 0.73 MeV.

One additional estimate of neutron leakage energy was obtained by shielding the head of a Clinac 20 with a 2.25 in. thick polyethylene box. This experimental structure was suspended over the accelerator head by means of a crane. The sides of the box extended down to the polyethylene shielding in the Clinac used to minimize neutron leakage in the patient plane. Measurements were made through the sides of the box by activation of indium in the fluence detectors. The geometry was essentially broad-beam with the sides of the box interposed between the target shielding material (primarily lead) and the detectors. For 19 MV photons the measured TVL was 3.2 in. $\pm$ 9%. NCRP 38 (6) gives a TVL of about 3 inches for 0.5 MeV neutrons normally incident on polyethylene slabs. It is quite evident that the average leakage neutron energy for the Clinac 20 does not exceed 0.5 MeV.

NEUTRON and X-RAY LEAKAGE FROM THE CLINAC 20

Leakage in the Patient Plane

Extensive neutron measurements have been made on the Clinac 20 at photon energies of 15, 18 and 19 MV. These included leakage at one meter from the target and leakage in the patient plane. Particular attention was given to minimizing leakage radiation to the patient. This region is defined as a circular plane of two meter radius (excluding the area covered by the primary beam) perpendicular to the central beam axis at the normal treatment distance. Neutron shielding was provided to insure that the combined x ray and neutron dose in the patient plane did not exceed 0.1% outside the useful beam area.

Neutron measurements were made with the flux detectors previously described. The neutron data were reduced to rem/rad percent using the dose equivalent conversion factors in ICRP 21 (4) and an effective energy of 0.27 MeV calculated for a 15 MV x-ray spectrum shielded with 4 in. of tungsten. An effective neutron energy of 0.31 MeV was used for leakage neutrons from 18 and 19 MV x rays. A typical set of measurements obtained with 15 MV photons will be used to illustrate the procedures used.

Neutron and x-ray measurements were made at a number of locations with shielding identical to that used on the Clinac 18. This allowed a direct comparison of neutron fluence per primary x-ray rad vs. energy. Neutron leakage in the patient plane was measured at 25 cm intervals from isocenter along two perpendicular axes, with and without neutron shielding. X-ray leakage was determined with the 100 cm^2 ion chamber and Type AA film packs. The combined neutron plus x-ray leakage is plotted in Figure 5 for 15 MV x rays. The points are the average of the observations obtained along the two perpendicular axes. Figure 5 shows the combined x ray plus neutron percentages as peaking at 25 cm, the critical radius just outside the useful beam. At this location the neutron leakage averaged 0.030 percent rem/rad and the x-ray leakage was 0.018%. The maximum total leakage was, therefore, 0.05 percent rem/rad.

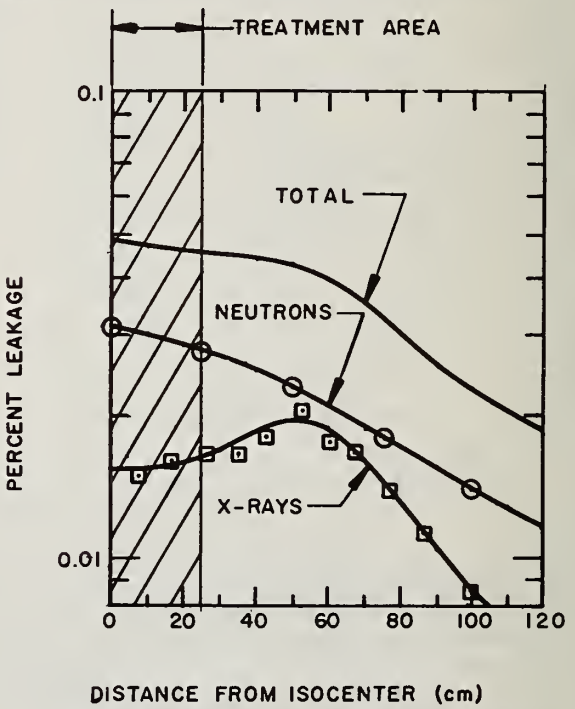

Fig. 5. Neutron and x-ray leakage measurements in the patient plane of a Clinac 20: 15 MV x rays, 100cm SSD.

The results of similar measurements made in the patient plane for 19 MV x rays are listed in Table I for distances 25 to 200 cm from isocenter. Once again, maximum leakage was obtained at 25 cm, decreasing rapidly at distances beyond 75 cm because of inverse square distance from the source. The neutron leakage at 200 cm is four times less than that at 25 cm. The critical measurement for determining maximum neutron

leakage in the patient plane would be just at the circular limit of the useful beam.

It is reiterated that these measurements were made with the jaws closed since the intent was to measure leakage. Much higher values would have been obtained, had the jaws been open, from neutrons scattered by the open collimator system. Analogously, Rawlinson and Johns have shown a similar increase in x-ray leakage with jaws open (7).

Leakage at One Meter

X-ray leakage for 10 and 15 MV photons was determined with the normal complement of dosimeters positioned on the meter arc. Both accelerators showed very low leakage, averaging just over 0.02%. The overall design objective was not to exceed 0.05%. Limited measurements with 18 MV photons gave similar results.

Neutron leakage measurements on the one meter arc were obtained with flux detectors at vertex angles of 0^0, 45^0, 90^0 and 135^0. Table 2 gives the neutron leakage obtained at these locations for 15 MV photons. The neutron dose equivalent was obtained assuming an effective energy of 0.27 MeV. X-ray leakage at the corresponding locations was not over 0.04%. It can be seen that the total leakage did not exceed 0.1% at any point.

TABLE I

FAST NEUTRON LEAKAGE IN PATIENT PLANE
DOSE RATE: 500 RADS/MINUTE

rem/rad (%) for 19 MV Photons

Location (cm)	Neutron Shielding on Clinac	No Neutron Shielding on Clinac
0	0.10	0.14
25	0.076	0.14
50	0.063	0.14
75	0.055	0.13
100	0.035	0.08
125	0.024	-
150	0.027	-
175	0.022	-
200	0.019	-

The accuracy of x-ray dosimeter leakage measurements is believed to be within ± 15%. The neutron values should probably be assigned a somewhat greater uncertainty since the effective energy is not precisely known and may differ from one location to the next. This uncertainty arises because of the amount of shielding material and its composition (lead, tungsten and a combination of both) varied with location.

From neutron measurements taken at one meter we have compiled the average neutron fluence at one meter for 10, 15, 18 and 19 MV photons taken with the accelerator located at identical positions in the test cell. The data has been extended to include neutron leakage from 25 MV photons, obtained with the same detectors from earlier measurements on a Clinac 35 in a somewhat different geometry. The neutron yield is plotted in Figure 6 in $n \cdot cm^{-2} \cdot rad^{-1}$ and in percent rem/rad. Conversion from n/cm^2 to neutron rem was obtained by our best estimate of effective neutron energy for each point.

TABLE 2

NEUTRON LEAKAGE AT 1 METER FROM TARGET
DOSE RATE: 500 RADS/MINUTE

rem/rad (%) for 15 MV Photons

Arc Setting	Angle from Zenith 0^0	45^0	90^0	135^0
A	-	0.050	0.031	0.028
N	-	0.052	0.029	0.030
C	-	0.053	0.054	0.029
L	-	0.052	0.055	0.030
E	-	0.035	0.037	0.024
I	-	0.039	0.043	0.026
G	0.022	0.030	0.028	0.025

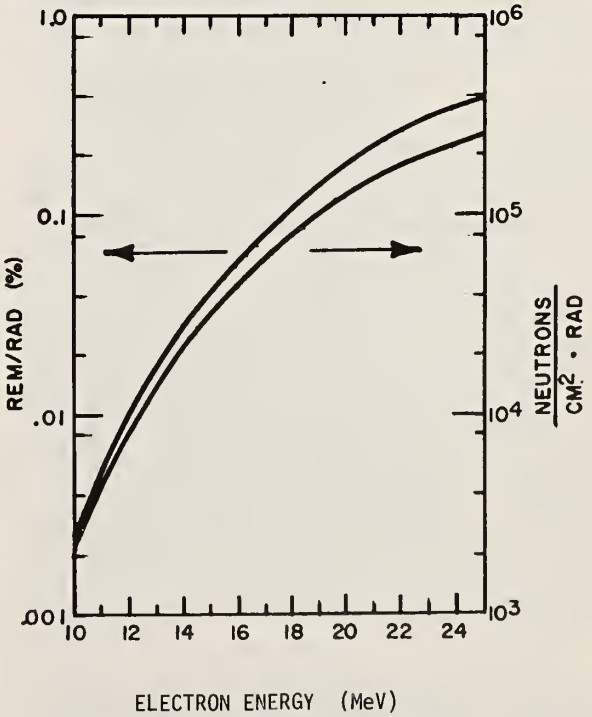

Fig. 6. Neutron leakage at one meter from a number of Clinacs with no neutron shielding.

All neutron flux measurements made on the Clinac 18 and 20 were accompanied by neutron leakage measurements made outside the entrance door with an Andersson-Braun rem meter. Door leakage in mrem/hr was found to be directly proportional to the neutron flux at one meter. This suggested that the neutron energy at the door after scattering down the maze was relatively constant.

Neutron Leakage Down the Maze

The engineering test cell partially shown in Figure 7, consists of a 20 ft x 20 ft test enclosure, 15 ft high. The entrance maze is 6.5 ft wide and 15 ft long with a 3.5 ft concrete wall between the maze passageway and the central room. The cell door consisted of 3/8 in. lead laminated between 4 in. of wood and an outer sheet of cadmium. The cadmium probably has a minimal influence on the neutron dose rate.

Initial measurements with the Clinac 20 indicated that the existing door provided insufficient neutron attenuation. Two 2 in. thick polyethylene doors were added in the maze at the location shown in Figure 7. The doors were displaced by two feet to allow easy personnel access. The doors were hinged to swing open for installation and removal of large equipment. All measurements were taken with the gantry positioned vertically down (180°). Measurement points numbered 1 through 11 were placed one meter apart except where noted otherwise.

Measurements made along the line including points 5A through 11 were made with the flux and rem counters and thermal neutron foils. The flux and rem values remained essentially constant at points 5, 5a, 3 and 6, all located within the treatment room. The dose rate at these locations was several times greater than that calculated by inverse square. This indicated that the fast neutron fluence and dose at these locations was principally from wall reflected neutrons, a finding in good agreement with McCall's calculations (3). The thermal neutron fluence was also constant over this region. At locations 7 and 8 (polyethylene doors open) the dose rate and fluence dropped markedly, decreasing at point 8 to approximately 0.2 the values obtained in the room. Beyond that point the dose rate decreased exponentially, decreasing by one-half for each 1.5 meters of maze length. On the other hand, the thermal neutron fluence decreased gradually with the thermal flux at point 6 only 2.5 times greater than at point 10, three meters away. These measurements indicate that the neutron energy is significantly degraded down the maze. NCRP 51 (8) states that for multi-leg mazes neutrons beyond the second leg may be considered to be completely thermalized.

Table 3 gives the neutron dose equivalent dose rates measured at the open doorway of the test cell for a primary dose rate of 500 rads/min or 3 x 10^4 rads/hr. The accompanying dose rates from scattered x rays and from capture gamma rays are also given. A further discussion of capture

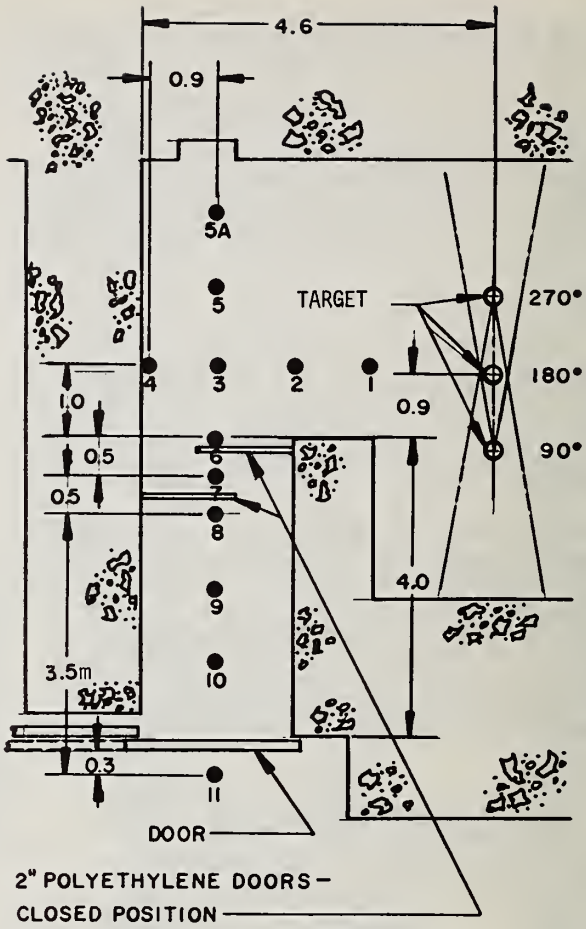

Fig. 7. Concrete test cell used for measurements and calculations.

TABLE 3

NEUTRON AND X+G DOSE EQUIVALENT RATES AT ENTRANCE TO CELL

(No neutron shielding on machine)

Photon Energy (MV)	mrem/hr Neutron	X + G	Total
10	6	3	9
15	54	23	77
19	162	48	210

gamma rays appears in the next section. The values in Table 3 may be scaled to rooms both larger and smaller than this cell, including rooms with shorter mazes.

Based on Clinac 20 measurements made at Varian, the following equations were developed to allow calculation of the door attenuation. Here we assume a built-in lead thickness of 3/8 in. in a polyethylene door.

XG: $I/I_o = 0.33 \times 10^{-t/32}$

N: $I/I_0 = 10^{-t/5.08}$

where t is the thickness of polyethylene in cm

Continuing the example above, for a door thickness of 3 in. (7.62 cm) of polyethylene in the cell and 15 MV x rays, we obtain

$XG = 23 \times 0.33 \times 10^{-7.62/32} = 4.4$ mR/hr

$N = 54 \times 10^{-7.62/5.08} = 1.7$ mrem/hr

6.1 mrem/hr

NEUTRON ACTIVATION AND GAMMA RAY PRODUCTION IN CONCRETE

Induced Radioactivity in Concrete

Upon initial operation of the Clinac 20 it was observed that the warning light on the radiation monitor inside the cell remained on after the accelerator was turned off. A radiation survey of the room showed the readings to be uniform throughout the room, with slightly higher readings in the immediate vicinity of the accelerator. This observation was in accord with expectation for an enclosure emitting gamma radiation uniformly from the walls; namely, that the dose rate is uniform throughout the room (9).

A decay curve of the gamma-ray dose rate was obtained by placing a survey meter in the treatment room immediately after a 10 minute irradiation. Readings were followed for a period of 40 minutes at which time the dose rate could no longer be measured. In order to obtain more precise results a small concrete disk was cut from a core sample obtained from a similar cell. This disk was exposed to accelerator produced neutrons and counted in a shielded beta counter. The disk was exposed on top of the accelerator head between two one-inch thick polyethylene slabs. Placing the sample 180° behind the direction of the primary beam virtually eliminated any possibility of photoneutron reactions; and the polyethylene moderators enhanced the thermal neutron fluence.

Part of the core sample was sent to a commercial laboratory for a chemical analysis of the major elements found in concrete. The analytical results are reproduced in Table 4 together with the composition of a typical concrete (10).

A resolution of half lives obtained from the decay measured in the laboratory counter isolated five components, three of which were gamma emitters; namely, ^{28}Al (T = 2.3 min), ^{49}Ca (T = 8.8 min) and ^{24}Na (T = 15 hr).

From the chemical abundance of these elements, their thermal neutron cross sections, half lives, and specific gamma-ray constants a gamma-ray curve was constructed simulating a ten-minute exposure to thermal neutrons. Good agreement was obtained between the experimental decay curve obtained in the cell and the calculations based on

TABLE 4

COMPOSITION OF CORE SAMPLE AND TYPICAL CONCRETE

Element	10^{22} atoms/cm^3 Typical Concrete	Core Sample
O	4.73	-
H	1.73	-
Si	1.57	1.477
Ca	0.26	0.261
Al	0.17	0.219
Fe	0.053	0.110
Na	0.028	0.109
K	0.028	-
Mg	0.013	0.076

core sample measurements.

Gamma Rays from Radiative Capture in Concrete

The energy released upon capture of a neutron is the binding energy of the neutron, on the order of 8 MeV, less the energy expended by any radioactive products that may be formed. This radiation ceases as soon as the accelerator is turned off. Its importance lies in the fact that this is the neutron-induced gamma radiation that is not only detectable at the cell door, but which overwhelms normal x-ray leakage by factors as large as 20, with 19 MV x rays.

By a process similar to that used to determine induced activity dose rates it was possible to determine a dose weighting factor, or R/capture, in concrete. This factor was derived from the measured gamma ray spectra for each element (11), and the specific gamma ray constant for each energy (12). With this information it was possible to calculate the approximate gamma ray spectrum for the core sample. The derived spectrum is plotted in Figure 8 together with a similar spectrum from "type 01 normal light concrete" (13). The two spectra agree very well in their major characteristics. The average energy of this spectrum was calculated as 3.6 MeV. The primary dose contribution was from the silicon and iron present in the concrete, followed by hydrogen and calcium. The relative dose from these materials was 30, 23, 22 and 14 percent, respectively.

Estimated Capture Gamma Radiation at the Cell Doorway

The Clinac 18 operating at 500 rads/ min typically produces x-ray leakage levels of 3 mR/hr and 0.8 mR/hr at the doorway of the cell with the door open and closed respectively. Since the production of neutrons at 10 MV is negligible, we may assume that these levels are due entirely to

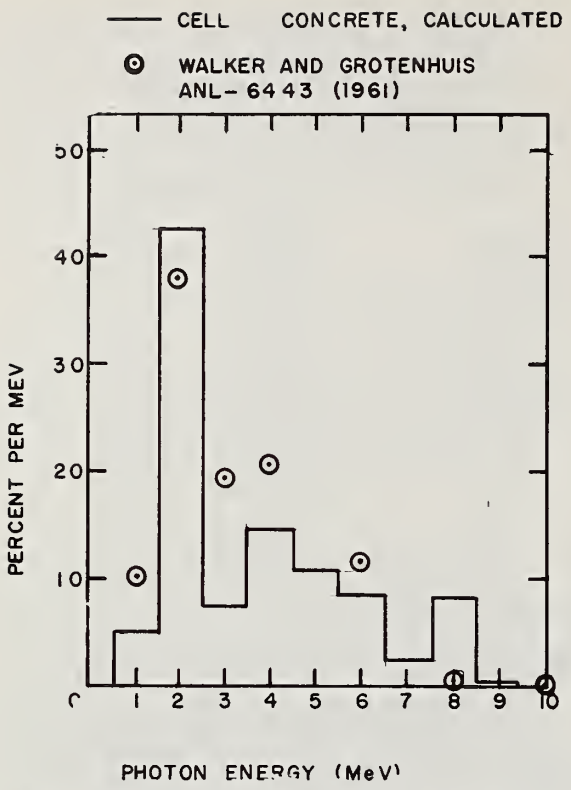

Fig. 8. Radiative capture gamma-ray spectrum from concrete.

leakage x rays scattered down the maze.

The Clinac 20, positioned at the same location and provided with the same shielding, produced 48 mR/hr and 18 mR/hr under similar conditions when operating at 19 MV. Since x-ray scattering conditions were identical, it is apparent that the greatly increased doorway leakage was due primarily to capture gamma rays resulting from thermal neutron captures in the concrete walls. The neutron dose equivalent at the open door was 162 mrem/hr, approximately three times greater than the gamma-ray dose rate. Neutron to gamma ray ratios obtained at the entrance maze of other installations operated at higher and lower energies ranged from values of two to three. While the observations were strictly empirical they did point out the additional shielding complications imposed by this high energy gamma-ray component.

It should be recognized that prescribing lead for gamma shielding has severe limitations. Usually the door becomes so massive that motor assistance becomes mandatory and a host of potential mechanical problems are generated.

In summary, it was estimated that the capture gamma-dose rate in the cell was about 270 mrem/hr under typical operating conditions. For comparison, the leakage x-ray dose was ~6000 mrem/hr at 1 meter, for the same conditions, and the residual initial radiation level was 1 to 2 mR/hr, for operation at 18 MV.

Treatment Room Dose due to Activated Concrete

Since 10 mrem per week is the allowable limit for non-radiation workers, initial activation levels on the order of 1 mrem/hr will produce measurable exposures of technologists who might go in and out of a treatment room some 40 to 50 times a day. As a preliminary to calculation of doses incurred inside a room by hospital personnel, Figure 9 was prepared illustrating the dose rates to be expected following 500 rad/min irradiations for 1, 5, 10, 50, 100 and 500 min at 18 MV. The activation products are ^{28}Al and ^{24}Na. The contribution from ^{49}Ca was negligible. These curves clearly show the influence of irradiation time. At 1 min, the initial decay is governed by the 2.3 min half-life of ^{28}Al. As the irradiation time is increased there is a progressive increase in the importance of the 15 hr ^{24}Na.

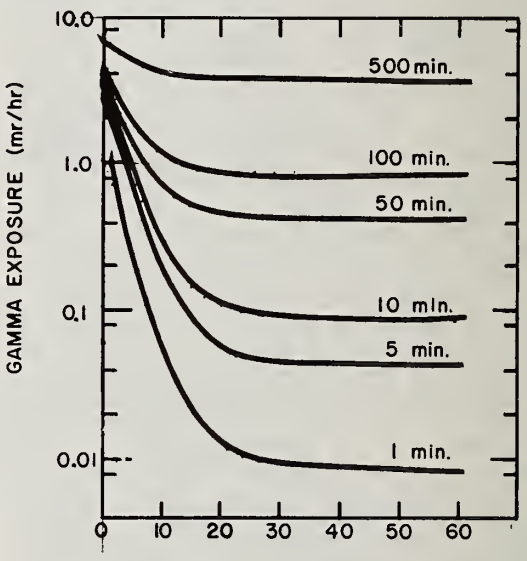

Fig. 9. Calculated residual radiation from a concrete room after several running times: 18 MV x rays, 500 rads/min.

We have used a simplified calculational model of a single one-minute treatment dose of 300 rad, followed by a maximum of 9 min room exposure, repeated 48 times a day for a weekly x-ray workload of 7×10^4 rad. The doses from room activation by a Clinac 20 operating at 18 MV were compared for varying stay times of from five to 9 min as shown in Table 5. In this calculation, it was assumed that the technologists would enter the room as soon as possible. It is evident that potential doses from activated concrete are the order of 10 mR/week. It, therefore, appears desirable to limit concrete activation to about the levels shown.

TABLE 5

WEEKLY TECHNOLOGIST DOSE FOR INDICATED STAY TIMES FOR 18 MV PHOTONS

Stay Time (min)	mR		
	^{28}Al	^{24}Na	Total
9	8.57	5.82	14.4
8	8.35	5.18	13.5
7	8.07	4.53	12.6
6	7.67	3.88	11.6
5	7.14	3.24	10.4

SUMMARY

The practice of installing and testing different energy Clinacs at the same location in the engineering test cell has provided an unique opportunity for systemization of a wide variety of x-ray and neutron leakage data. This practice, combined with the fact that the Clinacs 18/20 are equipped with identical x-ray shielding, provided experimenters with the equivalent of a single machine with multiple x-ray energies of 10, 15, 18 and 19 MV. The more important findings obtained during these investigations are the following:

1. The calculations presented by McCall and his collaborators (3) that we have been able to check experimentally have proved to be reliable. Two of these, for example, are a) the effective energy of the photoneutrons after degradation in lead and tungsten x-ray shielding, and b) the neutron dose equivalent per x-ray rad in the test cell proper and in the maze.

2. The maximum leakage in the patient plane for the Clinac 20 at 15 MV was 0.030% rem/rad for neutrons and 0.018% for photons. The total leakage was, therefore, just under 0.05% rem/rad. Maximum leakage occurred at the periphery of the useful beam. The adjustable collimators were closed for these measurements in order to insure that only leakage radiation was being measured. Higher values were obtained at 19 MV, where the maximum x and neutron leakage just outside the useful beam in the patient plane approached 0.1% rem/rad. For both energies, the neutron leakage in other (unshielded) directions was higher than in the patient plane.

3. At 15 MV, activation of ordinary concrete became easily detectable, producing radiation levels of approximately 1 mR/hr immediately after a few minutes of irradiation at 500 rad/min. The most important sources were tentatively identified as 2.3 min ^{28}Al and 15 hr ^{24}Na resulting from thermal neutron capture.

An estimate of technologist dosage from this residual radiation in the treatment room was ~10 mR/wk for a workload of 7×10^4 rad/wk for 18 MV x rays.

4. Gamma radiation from radiative capture reactions in concrete was identified as responsible for a 20-fold increase in the apparent x-ray leakage between 10 MV and 19 MV at the cell doorway. The principal dose contributors were calculated to be elemental silicon (30%), iron (23%) and hydrogen (22%). The average energy of the gamma-ray source spectrum was 3.6 MeV, which is of course degraded by multiple scattering in the concrete.

5. The weakest link in cell shielding is the doorway. The information available indicates the major problem is suppressing capture gamma radiation, rather than neutrons. An alternate to applying massive amounts of lead to the door is to exclude neutrons from the maze, thereby increasing the distance between the gamma emitters and the door. This approach has been tested successfully in the Varian engineering test cell.

REFERENCES

1. A. R. Smith, "A Cobalt Neutron-Flux Integrator," UCRL-9212 (1960), and L. D. Stephens and A. R. Smith, "Fast Neutron Survey Using Indium-Foil Activation," UCRL-8418 (1958).

2. I. O. Andersson and J. Braun, Neutron Dosimetry, Vol 2, 87, IAEA, Vienna (1963).

3. R. C. McCall, T. M. Jenkins and R. A. Shore, "Transport of Accelerator Produced Neutrons in a Concrete Room," IEEE Transactions on Nuclear Science, Vol. NS-26, No. 1 (1979).

4. International Commission on Radiological Protection "Protection Against Ionizing Radiation From External Sources," ICRP 15 and 21 (1971).

5. E. Tochilin and B. W. Shumway, "Flux and Spectrum of Simulated Fission Neutrons," NRDL TR-448 (1960).

6. National Council on Radiation Protection and Measurements, "Protection Against Neutron Radiation," NCRP 38 (1971).

7. J. A. Rawlinson and H. E. Johns, "Communications", Medical Physics, 4, 456 (1977).

8. National Council on Radiation Protection and Measurements, "Radiation Protection Design Guidelines for 0.1-100 MeV Particle Accelerator Facilities," NCRP 51 (1977).

9. W. S. Gilbert, K. Goebel, H. W. Patterson, and A. R. Smith, "Concrete Activation Experiment at the Bevatron," UCRL-19368 (1969) (unpublished).

10. H. W. Patterson and R. H. Thomas, Accelerator Health Physics, Academic Press, New York (1973).

11. R. E. Maerker and F. J. Muckenthaler, "Gamma Ray Spectra Arising from Thermal Neutron Capture in Elements Found in Soils, Concretes and Structural Materials," ORNL-4382 (1969).

12. M. Barbier, Induced Radioactivity, John Wiley & Sons, New York (1969).

13. Private communication R.C. McCall 9/13/78 Data from Walker and Grotenhuis, ANL-6443 (1967).

SUMMARY PANEL DISCUSSION

Moderator: J. S. Laughlin - Memorial Sloan-Kettering Cancer Center

Members:

L. M. Bates, American Association of Physicists in Medicine
R. S. Caswell, National Bureau of Standards
J. A. Devanney, Bureau of Radiological Health
G. R. Holeman, Yale University
H. E. Johns, Ontario Cancer Institute
C. S. Nunan, Varian
W. R. Swanson, Stanford Linear Accelerator Center

This panel discussion was recorded and slightly edited, but retains the flavor and intent of the speakers and questions alike.

Panel Session: Neutrons from Electron Medical Accelerators.

J. Laughlin: At this time we would like to collect the views of those on this panel and those in the audience. I suggest that we rotate around and take comments, first here from the panel members, and then throw it open to the audience.

To start things off I have put on the board a few of the points which I suggest for discussion-

I. Patient protection in radiation room
II. Operator protection outside radiation room

Machine design
- target
- filter
- collimator
- shielding

Room Shielding
Quality Factor

we'll direct our remarks either towards patient protection in the room, or operator protection outside the room. The role of quality factor is important for operator protection. With regard to machine design, these (pointing) are various topics which have already been covered which may deserve additional comment. I've also put on the board (Table 1) some values of dose - all in rads and which are approximate for a 20 MeV accelerator and approximately a 20 x 20 cm field. I've also indicated at the lower part of the board what I understand to be the IEC recommendations in the patient plane (2 meters in radius normal to the beam axis 1 meter from the target), and calling for leakage radiation as far as x-rays are concerned 1/10 of 1 percent (indicated there as .001) and for neutrons two-hundreths of one-percent, in rads.

I can't help but note that these values, measurement of neutron dose in the x-ray beam and also outside, have not essentially changed in the 20 MeV range over the last quarter of a century. The sophistication of measurement has

TABLE I

Patient Dose Due to Neutrons From Megavoltage X-Ray Treatment
(approx. 20 MV x-rays, 20 cm x 20 cm field size; all in rad)

	in irradiated field		out of target volume			
X-ray	neutron	heavy particle	x-ray leakage	x-ray scatter	neutron leakage	neutron internal
1	4×10^{-4}	3×10^{-3}	1×10^{-3}	5×10^{-2} (5 cm) 4×10^{-3} (20 cm) 2×10^{-4} (70 cm)	2×10^{-4}	2×10^{-7} (20MV) 9×10^{-6} (30MV) 2×10^{-5} (40MV) 3×10^{-5} (50MV)

Column 1: dose of 1 rad at depth of maximum dose in irradiated field
Column 2: dose in irradiated region due to absorption of neutron[1] contamination in x-ray beam
Column 3: maximum dose in irradiated field due to photo nuclear reactions[2] (assume all of photo neutrons locally absorbed)
Column 4: permissible dose due to leakage x-rays
Column 5: dose at indicated distance from x-ray field due to internal x-ray scatter[3]
Column 6: average dose produced by neutrons penetrating accelerator shielding[4]
Column 7: average dose produced by absorption of those photo neutrons internally produced[1]

IEC Recommendations

2 m radius plane at patient position
Percentage of maximum x-ray dose

	X-Rays	Neutrons
Average	0.1%	.02%
Maximum	0.2%	.05%

generally increased and for my part, I have found this meeting very stimulating. With these comments I will start at one end of the table and proceed along the entire panel.

G. Holeman: I will make my comments very brief so we can be sure and get around the table in the time allotted. In the measurements section that we held this morning, several problems were identified. The problems include: identifying the various sources that are generating the neutrons, the photon interference of the various measurement techniques, calibration problems, calculation problems; and treatment room layout. All of these are problems that we are having to deal with in this area. It seems like we all agree on some of the desired end results: information about beam contamination; information about leakage; and, information about occupational exposure. One inconsistency seems to be in the way data have been presented in the literature up to this time, and the various units used; fluence, absorbed dose, dose equivalent and various other units. The problem of photon interference has not always been addressed completely in the past.

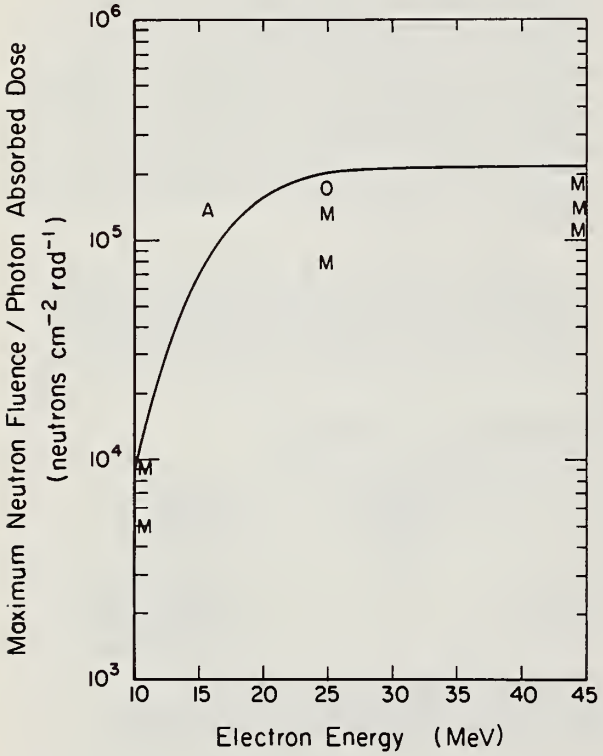

Figure 1. Comparison of Measured Neutron Fluence per rad of Use Beam with the Theoretical Curve of McCall and Swanson (solid line). O= Nath, Price and Holeman, M=McGinley and Sohrabi, and A=Axton and Bardell.

In the future it will be better addressed. Information about spectrum and beam sizes has not always been available in assessing information in the literature. I will not try to summarize Peter Almond's excellent paper as it will be in the proceedings, but I will attempt to summarize the percentage of neutron beam contamination that were given this morning by other authors. The in-beam dose equivalent per photon rad involved percentages all the way from .02 for the lower energy machines up to 0.8. In the patient plane the neutron contamination varied from .01 for the lower energy machines up to about 0.4. These are percent dose equivalent per photon rad. I will show one slide (Figure 1). Bill Swanson will use this Figure too, but I will get to use it first. Seven points are from McGinley's work (M) one from Axton's (A) and one from Nath's (O) there is good agreement with the theoretical curve.

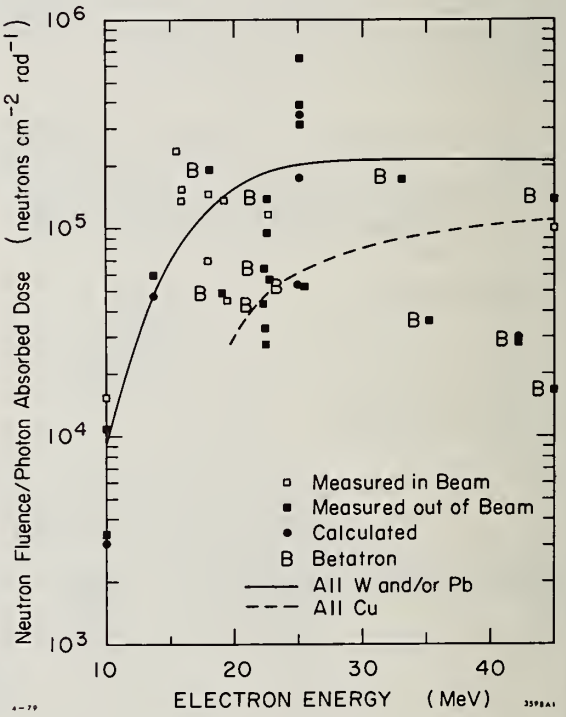

Figure 2: Neutron fluence per treatment dose Upper curve in maximum amount for all-w treatment head; lower curve us for all-c system. See McCall and Swanson paper for explanation of curves.

W. Swanson: One of the things that struck me by the conference is that while there is an awfully lot of data on the physical aspect - that is the neutron production of fluences and doses, and also a considerable amount of radiobiological input, there's not been an estimate of the actual risk in an absolute sense to the patient. Since I've never worked with radiobiology I am bold enough to attempt to make an assessment of sorts.

This slide (Figure 2) shows that we can believe that the fluence is a constant thing after about 25 MeV electron energy and this upper curve is undoubtedly an overestimate. I think Peter Almond's figure which is better than mine shows that better. My curve is probably an overestimate by a factor of 2 for the average accelerator.

This is Table 2 - that I showed just before the break this morning - that shows integral dose to the patient in gram·rads including 25 MeV treatment rad at 1 meter, divided up into portions within and without the useful beam. They are ranked in order of importance in terms of integral dose to the patient in gram·rads including 25 MeV per treatment rad at 1 meter, divided up portions within and without the useful beam. They are ranked in order of importance in terms of integral absorbed dose in gram·rads. By far, the largest term is the photon scattering within the patient. This was proved by Rawlinson and Johns in 1977. This is the most important thing: 500-1400 gram·rads. Second to that is the 0.1% photon leakage which contributes 40-50 gram·rads. Then we have 8 rad·grams of neutron leakage which I calculated myself. This result should be critically looked at by other people. It is surprisingly small, partly because of the rapid degradation of energy neutrons as they come through the tungsten or lead of the head shielding. Now let's see if I can figure what that means - if you

TABLE II

Integral Dose to Patient (g · rad) at 25 MeV (per rad at 100 cm SSD)

With Useful Beam			Outside Useful Beam		
Photons of Useful Beam		Neutrons Produced Within Patient	Photons Scattered Within Patient	Photon Leakage (0.1 %)	Neutron Leakage
1800	(100 cm^2)	5**	500	41	8.0
16200	(900 cm^2)	*50**	1390*	52*	

* Rawlinson and Johns, 1977.

**Horsely, et al. (03%), 1953

TABLE III

AVERAGE LEAKAGE NEUTRON DOSE

Averaged over 70-kg patient	$1.1\ 10^{-4}$	rad average dose per treatment rad
For 5000-rad treatment course	0.58	rad average dose per treatment course
** Times 28×10^{-6} leukemias yr^{-1} rad^{-1}	$16\ 10^{-6}$	leukemias/yr following treatment course
** Times 5 for all fatal malignancies	$80\ 10^{-6}$	all malignancies/yr following " "

** Rossi and Mays, 1977.

** Natural occurrence $43\text{-}48\ 10^{-6}$ leukemias / yr

divide by the average size of the patient, 70,000 grams, that gives only about 10^{-4} rads (averaged over the full body volume) per treatment rad (See Table 3). If a typical treatment of course is 5,000 rads, we only get about half a rad of neutron dose to the treatment of course. Now refer to a paper by Rossi and Mays (1977) and assuming for the moment that the bone marrow is distributed uniformly within the body, (which it is not, we just assume that) we multiply by the risk coefficient 28 x 10^{-6} leukemia's per year, per neutron rad, and we get this leukemia induction about 16 x 10^{-6} per year, following the treatment course. Still referring to Table 3, if we follow Rossi and Mays further and multiply by 5 we obtain about 80 x 10^{-6} fatal malignancies per year following the treatment course. This could be compared to the natural occurrence for leukemia which is given in the same paper as being in the range of 40-50 x 10^{-5} leukemia's per year.

You see the increase in leukemia is less than the natural occurrence and the increase of all types of malignancies is somewhat bigger than the natural occurrence of leukemia. Now, these figures are obtained by averaging the dose over the entire patient, and some people say that that is not the right thing to do; one should perhaps look at the maximum dose and find out the risk to the patient from that. I can't argue one way or the other about this point but I think that it should be addressed by others who are experts and by the agencies who will make up the rules concerning neutron leakage.

J. Laughlin: I have on the board the IEC values proposed for neutron leakage on the lower line. I wonder if Higson or associate could check me on the accuracy of those values, which are supposed to be in rads.

G. Higson: Yes, they are correct. The smaller figure in each case should be the average and the larger one the maximum.

R. Caswell: I have a few observations I'd like to make. I think that this is an appropriate time to review the regulations of the neutron production from medical electron linacs. I think that these regulations and recommendations should reflect the best concensus of scientific thinking as of now, and therefore the historical values which may have related actually to different situations and different types of machines should logically be replaced. We should be very grateful for the leadership of the IEC in working on this field, and I think that within the United States probably an NCRP type of committee with representation from medical physics is a reasonable way to try to find these scientific opinions and come out with a set of recommendations. These recommendations should include presentations on how to make this radiation as well as what might be reasonable levels. One problem that I don't know the answer to is: these committees usually work rather slowly, carefully and deliberately and if you want these regulations done before the committee report then it's very possible that regulation might be made before the committee has reported. Maybe someone else has a suggestiong on that.

One other comment that might be a little controversial-because discussion on quantities and units always seems to be controversial-it seems to me that we should try to have a common unit for a quantity for recording and comparing our data even if people have measured in different quantities. The three main quantities that have been reported here are neutron fluence, absorbed dose, and dose equivalent. It seems to me that fluence is probably not too good for the final answer, because effects are dependent on neutron energy. Either the dose equivalent or the dose absorbed per neutron per square centimeter could be off by a factor of 100. It would seem to me that the quantity should probably be either rads or rems. Of the two, it would be nice if it could be rads because that's really a physical quality without the committee-selected "quality factor". On the other hand, I can see someone running around with an Andersson-Braun rem-meter or Sievert meter, or whatever and saying, "I don't know how to get from the measurements I made in rems back to rads". However, I think that ever worse will be to have someone trying to assign a quality factor at a later date. The other argument is that the quality factor itself is likely to change with time.

It seems to me that rads would be the best way to report the data. Then you can always reconstruct. Therefore, the paper should report dose equivalent or whatever was measured, and then try to convert the result into rads. One other remark that I would like to make is that this question of whether the quality factor needs to be increased by perhaps a factor of 10 seems to me quite crucial to considerations of what is a reasonable neutron level. I think that this problem should be resolved.

H. Johns: I'd like to reiterate what I tried to say yesterday that I think it would be too bad if we create restrictive legistlation involving high energy machines especially if we deal only with neutrons. It seems to me that neutrons are only one of the problems. For example, if I understood the example of a moment ago, you can calculate the number of extra leukemias becuase of stray neutrons, you could also cause leukemia from the extra radiation within the radiation fields because you did not use a good beam. I suspect that the latter calculation would yeild many more leukemias. We still have not found a good way to handle large fields of radiation, maybe we need to line the inside of thses collimators with a material which can remove scattered electrons, as these are certainly a problem. It seems to me that if you replace the tungsten target with aluminum or copper we would get a 5-fold reduction of neutrons. Is that about right?

W. Swanson: If all of the internal shielding and the target were copper the neutrons would go down by about a factor of 5 at 20 MeV and about 3 at 25 MeV.

H. Johns: I think you have to remember we are dealing with very sick patients, and the leukemia calculations may be irrelevant. I was worried this morning that I would learn that

the machines we have been using all these years were really neutron machines. They are useful, they do cure cancer, but they can be made better and I think that our efforts should be along this line - to make them better and not worry about neutrons. By better I mean we should seek beams with very small entrance dose and beams for which the maximum dose is as far below the surface of the skin as possible. Having achieved these ends we might then feel there was some advantage in looking at neutrons.

C. Nunan: As far as the manufacturers are concerned they are selecting materials, adding permissible neutron shielding in the radiation head of their machines making more thorough measurements in an effort to achieve the maximum operating x-ray energy that would be within the suggested state regulation of 0.1% combined x-ray plus neutrons in rems per primary x-ray rad. The manufacturers are presently limited to the region of something like 15 to 19 MeV x-ray energy by that regulation. The radiotherapists say that patients fare better with high energy x-rays - they want 20 to 25 MeV x-rays. If these suggested state regulations are implemented by the state then we won't be able to furnish the radiotherapist with the machine that they want unless we go to very cumbersome radiation heads which the radiotherapist wouldn't buy, so the manufacturers hope that an NCRP committee will resolve the difficulty because we feel that the states are unable to resolve the difficulty. As far as the risk is concerned, the only risk that I've heard the radiotherapists mention is potential carcenogenesis, nothing else, and if you do the kind of calculations where the whole body, or at a point 10 centimeters from the field edge in bone marrow, and then calculate the compensating reduction in cure rate you find some very small fraction of a percent drop in cure rate would be equivalent, so we're talking about very, very small risks relative to the potential gains in cure rate by designing good machinery. The thing is complicated by this possible change in quality factor, and I understand the NCRP is studying this, the NCRP has convened a committee, I understand to recommend measurements techniques - it isn't clear whather this committee is to also recommend an allowable neutron leakage - I think it should be given that mission - I don't know how to get that accomplished but somebody ought to do it.

L. Bates: This is the fun thing of sitting at this end of the table is that by the time they get here everybody has said anything you've thought that you could possibly say - except for the panelist on my right.

Dr. Swanson has been a radiobiologist 10 seconds and already one wants to argue with him. He talked in terms of the carcinogenisis compared to the natural occurence and I don't really think this can be done for radiotherapy patients. I think that you have to look at this as an increase in late complications from the treatment and I think the proper value below the line is the number of complications arising from radiotherapy. The other thing: there was a question earlier on today about integral dose versus maximum dose. If my logic is correct when you're talking about carcinogenisis you're talking about a risk or a certain probability of a cell becoming malignant. In this case, the dose you should be considering is the average or the integral (which is always related with the constant) to the particular organ in question and, of course, the radiosensitivity of the particular organs.

J. Devanney: Before I start, I'd like to thank Tom Heaton and Bob Jacobs for putting together a very good meeting - I think it is something that has been needed for a long time. Several people have asked what we're going to do with the information that has come out of this meeting. Some people think that we will be able to generate some numbers and come up with neutron leakage levels and the like. I do not feel that way. I feel like the meeting has served as a very good data base on which BRH and other regulatory agencies can use as a jumping off point with which to develop a risk/benefit type study of leakage levels. It has been pointed out that there is no unified method or accepted method of measuring the neutron contamination or even the depth-dose for high energy therapy beams. I feel that we need more input from the Bureau of Standards in developing absorbed dose standards for the high energy beams. In December I had the pleasure of attending and working with one of the working groups of the IEC and I was very delighted because I hadn't realized how much the manufacturers had the concern of the patients at heart and how they didn't really wear the manufacturer's hat at these meetings.

There is one thing I would like to say concerning the suggested state regulations - they're passing out F-9 - if you'll look at F-9 you'll find some brackets in the first few paragraphs. You will have to read the preface of the suggested state regulations to understand what these brackets mean. These bracketted paragraphs address the area of leakage radiation and the brackets are there to show that this is a very controversial area, and it is not clear how far the stated values can be accepted, so I suggest that you read the preface of the suggested state regulations to see how to interpret the bracketted paragraphs.

H. Wyckoff: I have just a couple or three statements rather than questions. It always surprises me that when we talk about deaths from automobile accidents, deaths from airplane travel we don't say that the automobile accident death rate is so many time the rate from aircraft accidents. I think that we're getting into that kind of a thing here when we compare the presumed leukemia death rate from a given irradiation with that from natural causes. I think you forget that actual chances of death in any one year are about 10^{-2} from all causes. Second point, I think that the quality factor you should worry a little bit about because you must remember that the quality factors that we now have were developed back about 1950 at the time when you could almost count on your fingers the amount of data that you had, and primarily the factor of ten for neutrons were taken from some experimental data that was available then

for cataractogenesis. Now I think we have some evidence that for breast cancer the quality factor may be closer to one, so I think you should think in terms of 10 as being about right for some things, but let's not worry about changing it immediately. The third point I think is that the factor of 5 that Rossi gave, and I'm sorry that he's not here to hear me say this - if you take the ICRP risk coefficients, that for leukemia is about a sixth of the total rather than a fifth of the total. Thank you.

A. Jacobson: One number that did surface out of this meeting is the figure 1.6 rads for the neutron dose at the central axis of patients receiving 5,000 rads tumor dose. I want to be sure there is reasonable agreement amongst the panel on that figure. It seems very low and I'm happy to hear it.

H. Johns: I'm not sure, but I think they're not at the same place in space. The 5,000 was for the center of the body, the other figure I believe was 2 cm below the skin - Who gave that figure?

P. McGinley: I gave that figure - and that's right.

N. Suntharalingam: Craig, you made a statement that you think that the manufacturers will not be able to meet the current leakage specifications - is that right?

C. Nunan: The state proposed regulations at energies above 20 MeV.

N. Suntharalingam: Is the requirement for leakage 0.1% of the absorbed dose?

C. Nunan: Yes, 0.1% combined x and neutron on a rem basis, 0.1% of the primary x-ray rad.

N. Suntharalingam: Is this now on a rem basis putting in the quality factor?

C. Nunan: Yes

N. Suntharalingam: From the data which has been presented here it would not be difficult to satisfy the 0.1% of absorbed dose.

C. Nunan: No, no you have to read the suggested state regulations, they refer to a source for the quality factor.

N. Suntharalingam: The old NCRP requirement was 0.1% of absorbed dose. The numbers that I have here, that is, 0.02% for x-rays and about 0.03% for neutrons at 20 MeV. The data that has been presented by many of the speakers here, including the last speaker, was that the measurements indicate 0.02% for x-rays and about 0.08% for neutrons at 19 MeV and other data indicates that beyond 20 MeV it is reasonable flat, so that one could probably say that all machines in current use and in manufacture at 25 MeV energy will meet the current NCRP leakage requirements or recommendations which is 0.1% of the absorbed dose in the primary beam.

C. Nunan: The NCRP is rad or rem? I'm confused?

H. Wyckoff: The unit of absorbed dose is rad.

J. Laughlin: To clarify a point that's been made here I did place on the board what I understood to be the IEC recommendations which included this 0.02%, Craig, in rads per neutrons going up to a maximum of 0.05%. As has been observed over 20 MeV, the indicated levels level off - now do you find any difficulty with the proposed IEC recommendations?

C. Nunan: We believe that we will be able to meet the IEC proposed standard.

M. Cohen: When I came to this meeting two days ago I was under the impression that the main reason why we were interested in neutrons from medical accelerators is in order to protect the operators and the general public. As far as the patient is concerned, the philosophy up to now has been to design the machine so as to optimize the treatment and not to worry too much about the neutron dose to the patient which was considered of secondary importance and has not proved in the past to be of overwhelming significance. I've been a little surprised that the emphasis in this conference, unless I've midjudged it, has been on the whole body dose to the patient and possible consequences of that dose, with only perhaps a secondary consideration of the doses to the public and theoperator. I'd like to know where this new emphasis has come from - has it derived from the regulatory agencies, or if not, where has it come from?

J. Laughlin: I think several will respond to that - I think that is a very perceptive comment - we've gone along quite satisfactorily for a couple of decades and with the interest recently in the quality factor which would appear to pertain more to the operators the questions is why have the regulatory agencies suddenly become much more interested inside the radiation room. I don't know whether John Devanney wants to respond to that.

J. Devanney: We're interested mainly in reducing the dose to any one person, whether it be a patient or a operator, or the staff member, and if design of the medical accelerator could reduce the leakage radiation to the patient then I think that it should be done. I think that the regulatory agencies have always been concerned about the exposure to anybody.

P. Almond: I'd like to reply about Dr. Cohen's inquiries as to where the emphasis has come from. The people who are installing medical linear accelerators in this energy range are aware of what the regulations say, and that you have to satisfy them. I know that is where we are. You have to make these leakage measurement, but the regulations themselves are not at all clear as to whether it's total x-ray plus neutron or just x-ray, or whether it's rad dose or whether it's rem dose and there'e a lot of confusion in some of the regulations as to how the measurements are done, whether it is done with the jaws closed or open, in the plane of

the patient or elsewhere. We are having to satisfy the state health departments. That is where our emphasis is. It is not just the dose to the operator, it is also leakage around the machine in the treatment room.

A. Chung-Bin: I would like to make a comment as to whether those people who work in the regulatory agencies realize that, if you look at the trend in radiation therapy there is a tendency to make the field size larger and larger, i.e., using mantle field for radical treatment of Hodgkin's Disease and large field hemi-body treatment of leukemia and other metastasis. Many radiotherapists have stated one would prefer to give patients total body radiation, if possible, because the disease that will eventually kill the patients is probably the microscopic cancer cell diffusely distributed in the body. Therefore, we really should not be overly concerned about a neutron dose delivered to the patients.

D. Rogers: I would like to ask the panel to take a stand on the major issues facing us and tell the regulatory agencies our views on what the leakage limit should be while we've got some of them here. The statement was made that we're going to have to do cost/benefit analysis, and I think we've wasted a good deal of this conference by not addressing the real question which is what are the elements which must be considered in a proper cost/benefit or risk/benefit analysis. I would like the people in the audience to try to enumerate what are the costs and the benefits which we want the regulatory agencies to take into account when they to the calculations. In my opinion we are currently being forced to meet a set of essentially unjustifiable regulations, and I think it's time we should try to point out why we think these are dumb. The only talks which really dealt with this area were the first few lectures yesterday which were very suggestive but didn't really address the specific questions of justifying a proper limit. I would like to have people start enumerating the risks and the benefits that we want in the calculations.

J. Laughlin: Well, does anyone wish to respond to that particular challenge at this time? I'll have to say that we have only a couple more minutes.

W. Swanson: Yes, one reason for my standing up and giving this estimate of risk to the patient was to kind of start this thing in motion, and one reason for my doing this was to emphasize the smallness of the risk of these leakage neutrons- the smallness. In fact from this you could probably formulate some cost/benefit ratio in terms of cancers cured per cancers induced. Now I know my figures could be improved by experts who should review them, but what I have in my notes here is that the benefit/cost ratio of cancers cures to those induced, within say ten years, is about 1,000 to 1. That's one suggestion of a figure that should be looked at and reviewed and improved by others, then it could be an ingredient of an overall cost/benefit analysis for the regulatory agencies to use. Furthermore, I think that that is such a good cost benefit ratio, and the overall risk is so small that the wholematter could be left between the doctors, their patients and the manufacturers, and the government need not say anything further about it - that's my personal feeling about it.

J. Laughlin: Are there any other comments or questions?

We want to thank Tom Heaton and the National Bureau of Standards, Bob Jacobs and those of BRH very much for a very stimulating and important conference.

CONFERENCE ON NEUTRONS FROM ELECTRON MEDICAL ACCELERATORS

National Bureau of Standards
Gaithersburg, Maryland
April 9-10, 1979

List of Attendees

Robert B. Adams
Univ. Hospital of Cleveland
2065 Adelbert Road
Cleveland, OH 44106

Suresh K. Agarwal
Univ. of Virginia
Department of Radiology
1604 Cedar Hill Road
Charlottesville, VA 22901

Devendra K. Agrawal
Loyola University Medical Center
2160 S. First Avenue
Maywood, IL 60153

David P. Alberth
School of Hygiene & Public Health
Johns Hopkins Univ.
615 North Wolfe Street
Baltimore, MD 20215

Peter R. Almond
M.D. Anderson Hospital & Tumor Inst.
Texas Medical Center
6723 Bertner Ave.
Houston, TX 77030

Melvyn Altman
DHEW/Bureau of Radiological Health
5600 Fishers Lane
Rockville, MD 20857

Lee S. Anthony
Physics Associates
1229 Forest Lawn Drive
Salem, VA 24153

L. Armstrong
Atomic Energy of Canada Ltd.
P.O. Box 6300
Ottawa, Ontario
CANADA K2A 3W3

L. Atherton
M.E.L.
Manor Royal
Crawley, Sussex
ENGLAND RH10 9PZ

John A. Auxier
Oak Ridge National Laboratory
Post Office Box X
Oak Ridge, TN 37830

E. J. Axton
National Physical Laboratory
Queens Road
Teddington, Middlesex
ENGLAND

Farideh Bagne
Duke Univ. Medical Center
P.O. Box 3295, Edwin Morris Bldg.
Durham, NC 27710

Morris Bank
Hurley Medical Center, Dept. of
Radiology
6th & Begole
Flint, MI 48502

Lloyd M. Bates
American Assoc. of Physics in Medicine
Suite 307, 6900 Wisconsin Avenue
Chevy Chase, MD 20015

L. B. Beentjes
Katholieke Universiteit Nymegen
Toernooiveld
6525 ED Nymegen
NETHERLANDS

F. Behmann
McGill Univ. Radiotherapy Centre
1650 Cedar Ave.
Montreal, Quebec
CANADA H3G IA4

James W. Behrens
National Bureau of Standards
Washington, DC 20234

J. P. Bhatnagar
Mercy Hospital
1400 Locust St.
Pittsburgh, PA 15219

Peter J. Biggs
Massachusetts General Hosp.
Fruit Street
Boston, MA 02114

Joseph S. Blinick
Maine Med. Center
22 Bramhall St.
Portland, ME 04102

Frank J. Bova
J. Hillis Miller Health Ctr.
Univ. of Florida
Box J-385
Gainesville, FL 32610

Allen Brodsky
U.S. Nuclear Regulatory Commission
Washington, DC 20555

David Brown
DHEW/Bureau of Radiological Health
5600 Fishers Lane
Rockville, MD 20857

Joseph M. Brown, Jr.
U.S. Nuclear Regulatory Commission
5903 Greentree Road
Bethesda, MD 20034

Roger Budd
DHEW/Bureau of Radiological Health
5600 Fishers Lane
Rockville, MD 20857

Jan J. Buitendag
South African Dept. of Health
658 Sak Street
Pretoria, SOUTH AFRICA 0181

Dale W. Campbell
Richland Memorial Hosp.
Radiation Therapy
3301 Harden St.
Columbia, SC 29203

Allan David Carlson
National Bureau of Standards
Washington, DC 20234

Wayne Cassatt
National Bureau of Standards
Center for Radiation Research
Washington, DC 20234

Victoria G. Castro
Abington Memorial Hospital
1200 Old Fork Road
Abington, PA 19001

Randall S. Caswell
National Bureau of Standards
Washington, DC 20234

Frank Cerra
DHEW/Bureau of Radiological Health
5600 Fishers Lane
Rockville, MD 20857

Myung C. Choi
Washington Univ. Medical School
10225 Canter Way
Overland, MO 63114

Jim Chu
Hosp. of the Univ. of Pennsylvania
Dept. of Radiation Therapy
3400 Spruce Street, Box 522
Philadelphia, PA 19104

William T. Chu
Loma Linda Univ. Medical Ctr.
Radiation Oncology
Loma Linda, CA 92350

Anthony Chung-Bin
Rush Medical College
1753 W. Congress Street
Chicago, IL 60612

Lionel Cohen
Michael Reese Medical Ctr.
29th St. & Ellis Avenue
Chicago, IL 60616

Montague Cohen
Montreal General Hospital
McGill Univ. Radiotheraphy Centre
1650 Cedar Ave.
Montreal, Quebec
CANADA H3G 1A4

Alan Cohler
Abington Memorial Hospital
Laurel Road
Solebury, PA 18963

J. Joseph Coyne
National Bureau of Standards
Washington, DC 20234

Wilber Cyr
DHEW/Bureau of Radiological Health
5600 Fishers Lane
Rockville, MD 20857

Arne Dahler
Haukeland Hospital
5016 Hankeland Sykehus
Bergen, NORWAY

John Day
Hahnemann Hospital
230 N. Broad St.
Philadelphia, PA 19102

William H. Dederichs
The Radiation Center
1425 E. Enderly Place
Fort Worth, TX 76104

Paul M. DeLuca, Jr.
Univ. of Wisconsin
3321 Sterling Hall
475 North Charter Street
Madison, WI 53706

John DePangher
Stanford University
67 Encina Hall, Health Physics
Stanford, CA 94305

Nicholas A. Detorie
SIU - School of Medicine
Memorial Medical Center
800 North Rutledge St.
Springfield, IL 62702

John A. Devanney
Bureau of Radiological Health
12720 Twinbrook Pkwy
Rockville, MD 20857

Robert L. Dixon
Bowman Gray School of Medicine
Dept. of Radiology
Winston-Salem, NC 27103

Jack Dobson
WSA Inc.
5053 San Joaquin Drive
San Diego, CA 92109

Walter E. Downs
Atomic Energy oc Can. Ltd.
Commericial Products
P.O. Box 6300
Postal Stat. J. Ottawa, Ontario
CANADA K2A 3W3

Kenneth C. Duvall
National Bureau of Standards
1436 18th Street SE
Washington, DC 20234

Pavel Dvorak
Radiation Protection Bureau
Brookfield Road
Ottawa, CANADA K1A 1C1

Paul D. Eastvold
Illinois Dept. of Public Health
535 West Jefferson Street
Springfield, IL 62702

William Eden
Florida State Dept. of Health
2812 Duffton Loop
Tallahassee, FL 32303

Bradley D. Eichorst
BRH/FDA/HEW
5600 Fishers Lane
Rockville, MD 20857

Charles Eisenhauer
National Bureau of Standards
Washington, DC 20234

Elmer H. Eisenhower
National Bureau of Standards
Bldg. 245, Room C229
Washington, DC 20234

Melvin J. Ely, Jr.
National Naval Medical Center
Radiology Service
Bethesda, MD 20014

Harold Eriksen
Liberty Mutual Res. Ctr.
71 Frankland Road
Hopkinton, MA 01748

David Espejo-Villalobos
Hospitol Universitario
Calzada Madreno Pte.
Monterrey, N.L.
MEXICO 47-10-10, Ext 120

Fred Faw
Armot-Ogden Memorial Hospital
Radiology Dept.
Elmira, NY 14801

Thomas Fearon
National Council on Radiation
Protection and Measurements
7910 Woodmont Ave., Suite 1016
Bethesda, MD 20014

Kenneth P. Ferlic
Defense Nuclear Agency
Armed Forces Radiobiology Res. Inst.
Bethesda, MD 20014

Lawrence T. Fitzgerald
Univ. of Florida
Div. of Radiation Physics
Box J-385, JHM Health Center
Gainesville, FL 32610

Claude Flory
Defense Nuclear Agency
Armed Forces Radiobiology Res. Inst.
Bethesda, MD 20014

John G. Fox
Carnegie-Mellon Univ. and St. Francis
General Hospital
Schenley Park, 45th & Penn
Pittsburgh, PA 15213

John Frazier
DHEW/Bureau of Radiological Health
5600 Fishers Lane
Rockville, MD 20857

Elroy J. Friesen
University of Virginia Hosp.
Box 375
Charlottesville, VA 22923

Stephanie V. Frost
Methodist Hosp. of Indianapolis
1604 N. Capitol Ave.
Indianapolis, IN 46202

E. G. Fuller
Photonuclear Data Center
National Bureau of Standards
Washington, DC 20234

L. David Gager
Baylor College of Medicine
The Methodist Hospital
1200 Moursund
Houston, TX 77030

Benjamin M. Galkin
Thomas Jefferson Univ.
920 Chancellor St.
Philadelphia, PA 19107

Dwight W. Glenn
Mid-Atlantic Radiation Physics, Inc.
10408 Truxton Road
Adelphi, MD 20783

John C. Goble
NIH
Bldg. 21, Rm. 116
Bethesda, MD 20014

Donald A. Goer
Varian Associates
611 Hansen Way
Palo Alto, CA 94303

Robert Golden
Walter Reed Army Medical Ctr.
Radiation Therapy Service
Washington, DC 20012

Richard C. Granke
Private Practice of Medical
Radiological Physics
1311 Downs Drive
Silver Spring, MD 20904

Lance Green
Dosimeter Corporation of America
11286 Grooms Road
Cincinnati, OH 45242

Michael P. Grissom
Defense Nuclear Agency
Armed Forces Radiobiology Res. Inst.
Bethesda, MD 20014

James A. Grolten
Georgetown Univ. Medical Ctr.
Kober Cogan Bldg., Rm. 305
3750 Reservoir Road, NW
Washington, DC

Zygmunt C. Gromadzki
Georgetown Univ. Hospital
Radiation Oncology Dept.
3800 Reservoir Road, NW
Washington, DC 20007

Walter Gundaker
DHEW/Bureau of Radiological Health
5600 Fishers Lane
Rockville, MD 20857

David Gur
Graduate School of Public Health
Univ. of Pittsburgh
Pittsburgh, PA 15261

Richard Haas
Univ. of Illinois
840 S. Wood Street
Chicago, IL 60612

David Hammond
Baylor Univ. Medical Center
Charles A. Sammons Cancer Ctr.
3500 Gaston Ave.
Dallas, TX 75246

Antun Han
Argonne National Laboratory
9700 S. Cass Ave.
Argonne, IL 60439

Lawrence F. Hans, Jr.
Mercy Hospital
2500 7th Avenue
Altoona, PA 16603

George H. Harrison
University of MD Medical Sch.
Radiation Research Div.
660 W. Redwood St.
Baltimore, MD 21201

H. T. Heaton
National Bureau of Standards
Center for Radiation Research
Washington, DC 20234

William N. Herrington
M.D. Anderson Hosp. and Tumor Inst.
6723 Bertner Ave.
Houston, TX 77025

G. R. Higson
Dept. of Health & Social Security
14 Russell Square
London, ENGLAND WC1B 5EP

George R. Holeman
Yale University - Health Physics
314 Wright Nuclear Structure Lab.
West - 260 Whitney Ave.
New Haven, CT 06520

Carolyn Holman
Orlando Regional Medical Center
Radiation Division
50 West Sturtevant
Orlando, FL 32806

John R. Howley
NIH
Bldg. 21, Rm. 116
Bethesda, MD 20014

Jen-Shu Hsieh
Defense Nuclear Agency
Armed Forces Radiobiology Res. Inst.
Bethesda, MD 20014

Geoffrey S. Ibbott
Univ. of Colo. Med. Center
4200 E. Ninth Ave. (A-031)
Denver, CO 80262

Barrie J. Jackson
Atomic Energy of Canada Ltd.
P.O. Box 6300, Postal Station "J"
Ottawa, Ontario
CANADA K2A 3W3

Robert Jacobs
DHEW/Bureau of Radiological Health
5600 Fishers Lane
Rockville, MD 20857

Ahren Jacobson
Univ. of Louisville
Radiation Center
500 S. Floyd St.
Louisville, KY 40201

John P. Jacobus
Defense Nuclear Agency
Armed Forces Radiobiology Res. Inst.
Bethesda, MD 20014

Stan Jaeger
Bishop Clarkson Memorial Hosp.
Dewey Ave. at Forty-Fourth St.
Omaha, Nebraska 68105

Michael F. James
Atomic Energy Control Board
270 Albert St.
Ottawa, Ontario
CANADA

Mitchell J. Jarosz, Jr.
St. Francis General Hospital
45th St. and Penn Ave.
Pittsburgh, PA 15201

Roger M. Jean
CGR MeV
BP 34
78530 BUC, FRANCE 356 8002

Harold E. Johns
Ontario Cancer Institute
500 Sherbourne Street
Toronto, Ontario
CANADA M4X 1K9

Joel D. Johnson
Defense Nuclear Agency
Armed Forces Radiobiology Res. Inst.
Bethesda, MD 20014

Troyce D. Jones
Oak Ridge National Laboratory
P.O. Box X
Oak Ridge, TN 37830

D. M. Joseph
Lutheran General Hospital
1775 W. Dempster Ave.
Park Ridge, IN 60068

Jae Shik Jun
Korea Standards Research Inst.
P. O. Box 333
Dae Jeon, KOREA

Christos Kanellitsas
Universsity Hospital
1405 E. Ann Street
Ann Arbor, MI 48109

C. J. Karzmark
Stanford Univ. School of Med.
Dept. of Radiology
300 Pasteur Dr.
Stanford, CA 94305

Frank E. Kearly
Bur. of Radiological Health (HFX-70)
5600 Fishers Lane
Rockville, MD 20857

David R. Kneeland
Nucletronix
Birch Road
Middleton, MA 01949

George Komada
DHEW/Bureau of Radiological Health
5600 Fishers Lane
Rockeville, MD 20857

Max R. Kubik
Baptist Medical Center
800 Prudential Drive
Jacksonville, FL 32207

Chris K. Kuyatt
National Bureau of Standards
Center for Radiation Research
Bldg. 220, Rm. B206
Washington, DC 20234

Wing-Schee Lam
Johns Hopkins University
601 N. Broadway
Baltimore, MD 21205

Philip D. LaRiviere
Varian Associates, Inc.
611 Hansen Way
Palo Alto, CA 94303

John S. Laughlin
Memorial Sloan-Kettering Cancer Ctr.
1275 York Ave.
New York, NY 10021

Dennis D. Leavitt
Univ. of Utah Medical Center
Dept. of Radiology
50 N. Medical Drive
Salt Lake City, UT 84132

Paul Leggett, Jr.
FDA/BRH
9917 Shrewsbury Ct.
Gaithersburg, MD 20760

David Lightfoot
Hahnemann Hospital
230 N. Broad St.
Philadelphia, PA 19102

Shin S. Liu
Rush-Presbyterial-St. Luke Med. Ctr.
1753 W. Congress Parkway
Chicago, IL 60612

Salmen Loksen
Georgetown University Hospital
3800 Reservoir Rd., NW
Washington, DC 20007

Robert Loevinger
National Bureau of Standards
Radiation Phys. C210
Washington, DC 20234

Richard C. McCall
Stanford University
Stanford Linear Accelerator Center
P.O. Box 4349
Stanford, CA 94305

Joseph McDonald
Memorial-Sloan Kettering Cancer Ctr.
1275 York Avenue
New York, NY 10021

Patton H. McGinley
Emory University Clinic
1365 Clifton Road
Atlanta, GA 30322

Philip McHugh
Atomic Energy of Canada Ltd.
P.O. Box 6300
Ottawa, Canada K2A 3W3

Lou Milavickas
Univ. of Illinois
214 Nuclear Engineering Lab
Urbana, IL 61801

David W. Minnaar
Michigan Dept. of Public Health
Div. of Radiological Health
3500 N. Lorgan St.
P.O. Box 30035
Lansing, MI 48909

Robert Morton
Bureau of Radiological Health (HFX-70)
5600 Fishers Lane
Rockville, MD 20857

Ravinder Nath
Yale Medical School
333 Cedar St.
New Haven, CT 06510

J. Rao Nibhanupudy
Howard Univ. Hospital
2041 Goergia Ave., NW
Washington, DC 20060

Brian Noriega
Radiation Services
1404 N. Wheeler St.
Plant City, FL 33566

Craig Nunan
Varian
611 Hansen Way
Palo Alto, CA 94303

Michael P. Nunno
Albert Einstein Medical Center
Radiology Associates
York & Tabor Roads
Philadelphia, PA 19144

Thomas Ohlhaber
DHEW/Bureau of Radiological Health
5600 Fishers Lane
Rockville, MD 20857

H. M. Omar
Univ. of Tennessee
Radiation Oncology Dept.
865 Jefferson Ave.
Memphis, TN 38163

F. E. Owens
Defense Nuclear Agency
Armed Forces Radiobiology Res. Inst.
Bethesda, MD 20014

Peter Paras
DHEW/Bureau of Radiological Health
5600 Fishers Lane
Rockville, MD 20857

Mahendra Patel
Capintec, Inc.
540 Alpha Drive
Pittsburgh, PA 15238

John I. Pearce
Roswell Park Memorial Inst.
666 Elm St.
Buffalo, NY 14263

Harry Pettengill
U.S.N.R.C.
Nicholson Lane
Rockville, MD 20852

Jean-Louis Pourre
CGR MeV
420 Babylon Road
Horhsam, PA 19044

William E. Powers
Wayne State Univ. Medical School
3990 John R. St.
Detroit, MI 48201

Frederick Prevo
DHEW/Bureau of Radiological Health
5600 Fishers Lane
Rockville, MD 20857

Kenneth Price
Yale University
Health Physics Div.
Whitney Ave.
New Haven, CT

Vincent L. Rauaschieri
Seimens Corporation
449 Old Orchard Circle
Millersville, MD 21108

Alan Rawlinson
Ontario Cancer Institute
500 Sherbourne Street
Toronto, Ontario
CANADA M4X 1K9

Henry Rechen
DHEW/Bureau of Radiological Health
5600 Fishers Lane
Rockville, MD 20857

Don W. Reid
EMI Therapy Systems
570 Del Rey
Sunnyvale, CA 94086

Robert E. Rice
Hartford Hospital
80 Seymour St.
Hartford, CT 06115

Gordon Riel
NSWC
White Oak, MD 20910

Karim Rimawi
NY State Dept. of Health
15 Snellen Road, Apt. A-2
Schenectady, NY 12309

David W. O. Rogers
National Res. Council of Canada
Montreal Road., Bldg. M-35
Ottawa, Ontario
CANADA K1A 0R6

Joseph A. Rose
Wilmington Medical Ctr.
Dept. of Radiation Therapy
201 S. Broom St., P.O. Box 2850
Wilmington, DE 19805

Carl K. Ross
National Res. Council of Canada
Div. of Physics, Bldg. M-35
Ottawa, Ontario
CANADA K1A OR6

Harald H. Rossi
Radiological Res. Lab.
Columbia University
630 West 168th Street
New York, NY 10032

Donald R. Ruegsegger
Miami Valley Hospital
Radiation Therapy Dept.
1 Wyoming Street
Dayton, OH 45409

Joseph A. Sayeq
University of Kentucky
Dept. of Radiation Medicine
800 Rose Street
Lexington, KY 40506

Roger Schneider
DHEW/Bureau of Radiological Health
5600 Fishers Lane
Rockville, MD 20857

Michael C. Schell
GWUMC
Middle Atlantic Neutron Therapy Assoc.
Washington, DC 20375

Roald A. Schrack
National Bureau of Standards
Washington, DC 20234

Robert J. Schulz
Yale University School of Medicine
333 Cedar Street
New Haven, CT 06510

Robert Schwartz
National Bureau of Standards
Washington, DC 20234

Ralph Severance
Defense Nuclear Agency
Armed Forces Radiobiology Res. Inst.
Bethesda, MD 20014

S. Shalev
Dept. of Biomedical Engrs.
Technion
Haifa, ISRAEL

Jeffrey Silberberg
DHEW/Bureau of Radiological Health
5600 Fishers Lane
Rockville, MD 20857

Theodore N. Simmons
Sandia Laboratories
Health Physics Div., 3312
P.O. Box 5800
Albuquerque, NM 87185

Bill Simon
Victoreen Inc.
10101 Woodland Ave.
Cleveland, OH 44104

Lester A. Slaback, Jr.
Defense Nuclear Agency
Armed Forces Radiobiology Res. Inst.
Bethesda, MD 20014

C. Smith
Oklahoma St. Dept. of Health
Oklahoma City, OK

George Snyder
Student Johns Hopkins Univ.
8900 Centerway Road
Gaithersburg, MD 20760

Robert Stanton
Cooper Medical Center
One Cooper Plaza
Camden, NJ 08103

Edward S. Sternick
Tufts-New England Med. Ctr.
Dept. Therapeutic Radiology
171 Harrison Ave.
Boston, MA 02111

N. Suntharalingam
Thomas Jefferson Univ. Hospital
11th & Walnut Sts.
Philadelphia, PA 19107

Roy E. Summers, Jr.
Allepheny General Hospital
320 E. North Ave.
Pittsburgh, PA 15212

Goran K. Svensson
Harvard Medical School
Joint Ctr. for Radiation Therapy
50 Binney Street
Boston, MA 02115

Robert W. Swain
NIH
6010 Walton Road
Bethesda, MD 20034

William P. Swanson
Stanford Linear Accelerator Ctr.
P.O. Box 4349
Stanford, CA 94305

Leonhard Taumann
Siemens Medical Laboratories, Inc.
2404 N. Main Street
Walnut Creek, CA 94596

Paul Thiess
Catholic University
P. O. Box 951, Cardinal Station
Washington, DC 20064

Jerry A. Thomas
National Naval Medical Center
13122 Pelfrey Lane
Fairfax, VA 22030

Othniel Thompson
MD. State Dept. of Health EHA
201 W. Preston Street
Baltimore, MD 21050

Winston L. Thompson
Howard University
College of Allied Health
Washington, DC 20059

Joseph Y. Ting
Our Lady of Lourdes Hospital
169 Riverside Dr.
Binghamton, NY 13905

Eugene Tochilin
Varian Associates
611 Hansen Way
Palo Alto, CA 94303

Neil VanHooydonk
Philips Medical Systems, Inc.
710 Bridgeport Avenue
Shelton, CT 06484

David L. Vassy, Jr.
Mid-Atlantic Radiation Physics, Inc.
10408 Truxton Road
Adelphi, MD 20783

Donald E. Velkey
Div. of Radiation Oncology
M.S. Hershey Medical Ctr. of the
Pennsylvania State Univ.
Hershey, PA 17033

Lorne Vernon
Defense Nuclear Agency
Armed Forces Radiobiology Res. Inst.
Bethesda, MD 20014

Paul Wagner
Bur. of Radiological Health (HFX-70)
5600 Fishers Lane
Rockville, MD 20857

Ray Walehle
DHEW/Bureau of Radiological Health
5600 Fishers Lane
Rockville, MD 20857

Joseph Wang
BRH
5600 Fishers Lane
Rockville, MD 20857

A. Carl Warner
Dept. of Radiation Oncology
Indiana Univ. Sch. of Medicine
1100 West Michigan Street
Indianapolis, IN 46223

Oren Wasson
National Bureau of Standards
Washington, DC 20234

William R. Webber
Defense Nuclear Agency
Armed Forces Radiobiology Res. Inst.
Bethesda, MD 20014

Robert V. Wheeler
R.S. Landauer, Jr. & Co.
Science Road
Glenwood, IL 60425

Ralph Worsnop
Medical Physics
1250 Godetia Drive
Woodside, CA 940062

Ann E. Wright
Univ. of Texas Medical Branch
18635 Point Lookout
Houston, TX 77058

John Wright
Geisinger Medical Center
Danville, PA 17821

Kenneth A. Wright
Mass. Inst. of Tech.
Bldg. N-10, M.I.T.
Cambridge, MA 02139

Raymond K. Wu
Temple University Hospital
3401 N. Broad St.
Philadephia, PA 19140

Harold Wyckoff
4108 Montpelier Road
Rockville, MD 20853

Harry Youmans
DHEW/Bureau of Radiological Health
5600 Fishers Lane
Rockville, MD 20857

Gary H. Zeman
National Naval Medical Center
Bethesda, MD 20014

AUTHOR INDEX

NBS-114A (REV. 9-78)

U.S. DEPT. OF COMM. BIBLIOGRAPHIC DATA SHEET	1. PUBLICATION OR REPORT NO. SP 554	2. Gov't. Accession No.	3. Recipient's Accession No.

4. TITLE AND SUBTITLE

Proceedings of a Conference on Neutrons from Electron Medical Accelerators

5. Publication Date

September 1979

6. Performing Organization Code

7. AUTHOR(S)

H. T. Heaton, II and R. Jacobs

8. Performing Organ. Report No.

9. PERFORMING ORGANIZATION NAME AND ADDRESS

NATIONAL BUREAU OF STANDARDS
DEPARTMENT OF COMMERCE
WASHINGTON, DC 20234

10. Project/Task/Work Unit No.

11. Contract/Grant No.

12. SPONSORING ORGANIZATION NAME AND COMPLETE ADDRESS *(Street, City, State, ZIP)*

Sponsored in part by:
Bureau of Radiological Health
Food and Drug Administration
Rockville, Maryland 20857

With cooperation from:
American Association of
Physicists in Medicine
Bethesda, Maryland 20014

13. Type of Report & Period Covered

N/A

14. Sponsoring Agency Code

15. SUPPLEMENTARY NOTES

Library of Congress Catalog Number 79-600-33

☐ Document describes a computer program; SF-185, FIPS Software Summary, is attached.

16. ABSTRACT *(A 200-word or less factual summary of most significant information. If document includes a significant bibliography or literature survey, mention it here.)*

These proceedings are the compilation of 18 papers presented at the Conference on Neutrons from Electron Medical Accelerators held in Gaithersburg, MD on April 9 and 10, 1979. The topics addressed include: properties of high energy beams for radiotherapy, regulations, biological interpretation, physical measurements and calculations, and neutron reduction techniques.

17. KEY WORDS *(six to twelve entries; alphabetical order; capitalize only the first letter of the first key word unless a proper name; separated by semicolons)*

Dosimetry, high energy radiotherapy beams, leakage, measurement techniques, medical accelerators, neutrons, relative biological effect, standards, shielding techniques.

18. AVAILABILITY

☒ Unlimited

☐ For Official Distribution. Do Not Release to NTIS

☒ Order From Sup. of Doc., U.S. Government Printing Office, Washington, DC 20402, SD Stock No. SN003-003-02115-6

☐ Order From National Technical Information Service (NTIS), Springfield, VA. 22161

19. SECURITY CLASS (THIS REPORT)	21. NO. OF PRINTED PAGES
UNCLASSIFIED	172
20. SECURITY CLASS (THIS PAGE)	**22. Price**
UNCLASSIFIED	$4.75

OMM-DC

☆ U.S. GOVERNMENT PRINTING OFFICE : 1979 O—281-067 (245)

NBS TECHNICAL PUBLICATIONS

PERIODICALS

JOURNAL OF RESEARCH—The Journal of Research of the National Bureau of Standards reports NBS research and development in those disciplines of the physical and engineering sciences in which the Bureau is active. These include physics, chemistry, engineering, mathematics, and computer sciences. Papers cover a broad range of subjects, with major emphasis on measurement methodology, and the basic technology underlying standardization. Also included from time to time are survey articles on topics closely related to the Bureau's technical and scientific programs. As a special service to subscribers each issue contains complete citations to all recent NBS publications in NBS and non-NBS media. Issued six times a year. Annual subscription: domestic $17.00; foreign $21.25. Single copy, $3.00 domestic; $3.75 foreign.

Note: The Journal was formerly published in two sections: Section A "Physics and Chemistry" and Section B "Mathematical Sciences."

DIMENSIONS/NBS

This monthly magazine is published to inform scientists, engineers, businessmen, industry, teachers, students, and consumers of the latest advances in science and technology, with primary emphasis on the work at NBS. The magazine highlights and reviews such issues as energy research, fire protection, building technology, metric conversion, pollution abatement, health and safety, and consumer product performance. In addition, it reports the results of Bureau programs in measurement standards and techniques, properties of matter and materials, engineering standards and services, instrumentation, and automatic data processing.

Annual subscription: Domestic, $11.00; Foreign $13.75

NONPERIODICALS

Monographs—Major contributions to the technical literature on various subjects related to the Bureau's scientific and technical activities.

Handbooks—Recommended codes of engineering and industrial practice (including safety codes) developed in cooperation with interested industries, professional organizations, and regulatory bodies.

Special Publications—Include proceedings of conferences sponsored by NBS, NBS annual reports, and other special publications appropriate to this grouping such as wall charts, pocket cards, and bibliographies.

Applied Mathematics Series—Mathematical tables, manuals, and studies of special interest to physicists, engineers, chemists, biologists, mathematicians, computer programmers, and others engaged in scientific and technical work.

National Standard Reference Data Series—Provides quantitative data on the physical and chemical properties of materials, compiled from the world's literature and critically evaluated. Developed under a world-wide program coordinated by NBS. Program under authority of National Standard Data Act (Public Law 90-396).

NOTE: At present the principal publication outlet for these data is the Journal of Physical and Chemical Reference Data (JPCRD) published quarterly for NBS by the American Chemical Society (ACS) and the American Institute of Physics (AIP). Subscriptions, reprints, and supplements available from ACS, 1155 Sixteenth St. N.W., Wash., D.C. 20056.

Building Science Series—Disseminates technical information developed at the Bureau on building materials, components, systems, and whole structures. The series presents research results, test methods, and performance criteria related to the structural and environmental functions and the durability and safety characteristics of building elements and systems.

Technical Notes—Studies or reports which are complete in themselves but restrictive in their treatment of a subject. Analogous to monographs but not so comprehensive in scope or definitive in treatment of the subject area. Often serve as a vehicle for final reports of work performed at NBS under the sponsorship of other government agencies.

Voluntary Product Standards—Developed under procedures published by the Department of Commerce in Part 10, Title 15, of the Code of Federal Regulations. The purpose of the standards is to establish nationally recognized requirements for products, and to provide all concerned interests with a basis for common understanding of the characteristics of the products. NBS administers this program as a supplement to the activities of the private sector standardizing organizations.

Consumer Information Series—Practical information, based on NBS research and experience, covering areas of interest to the consumer. Easily understandable language and illustrations provide useful background knowledge for shopping in today's technological marketplace.

Order **above** *NBS publications from: Superintendent of Documents, Government Printing Office, Washington, D.C. 20402.*

Order **following** *NBS publications—NBSIR's and FIPS from the National Technical Information Services, Springfield, Va. 22161.*

Federal Information Processing Standards Publications (FIPS PUB)—Publications in this series collectively constitute the Federal Information Processing Standards Register. Register serves as the official source of information in the Federal Government regarding standards issued by NBS pursuant to the Federal Property and Administrative Services Act of 1949 as amended, Public Law 89-306 (79 Stat. 1127), and as implemented by Executive Order 11717 (38 FR 12315, dated May 11, 1973) and Part 6 of Title 15 CFR (Code of Federal Regulations).

NBS Interagency Reports (NBSIR)—A special series of interim or final reports on work performed by NBS for outside sponsors (both government and non-government). In general, initial distribution is handled by the sponsor; public distribution is by the National Technical Information Services (Springfield, Va. 22161) in paper copy or microfiche form.

BIBLIOGRAPHIC SUBSCRIPTION SERVICES

The following current-awareness and literature-survey bibliographies are issued periodically by the Bureau:

Cryogenic Data Center Current Awareness Service. A literature survey issued biweekly. Annual subscription: Domestic, $25.00; Foreign, $30.00.

Liquefied Natural Gas. A literature survey issued quarterly. Annual subscription: $20.00.

Superconducting Devices and Materials. A literature survey issued quarterly. Annual subscription: $30.00. Send subscription orders and remittances for the preceding bibliographic services to National Bureau of Standards, Cryogenic Data Center (736.00) Boulder, Colorado 80303.

U.S. DEPARTMENT OF COMMERCE
National Bureau of Standards
Washington, D.C. 20234

OFFICIAL BUSINESS

Penalty for Private Use, $300

POSTAGE AND FEES PAID
U.S. DEPARTMENT OF COMMERCE
COM-215

U.S.MAIL

SPECIAL FOURTH-CLASS RATE
BOOK